INEEL/EXT-04-02245

Advanced Core Design And Fuel Management For Pebble-Bed Reactors

Hans D. Gougar
Abderrafi M. Ougouag
William K. Terry

October 2004

Idaho National Engineering and Environmental Laboratory
Bechtel BWXT Idaho, LLC

INEEL/EXT-04-02245

Advanced Core Design And Fuel Management For Pebble-Bed Reactors

Hans D. Gougar
Abderrafi M. Ougouag
William K. Terry

October 2004

Idaho National Engineering and Environmental Laboratory

Idaho Falls, Idaho 83415

Prepared for the
U.S. Department of Energy
Office of Nuclear Science and Engineering
Under DOE Idaho Operations Office
Contract DE-AC07-99ID13727

ABSTRACT

A method for designing and optimizing recirculating pebble-bed reactor cores is presented. At the heart of the method is a new reactor physics computer code, PEBBED, which accurately and efficiently computes the neutronic and material properties of the asymptotic (equilibrium) fuel cycle. This core state is shown to be unique for a given core geometry, power level, discharge burnup, and fuel circulation policy. Fuel circulation in the pebble-bed can be described in terms of a few well-defined parameters and expressed as a *recirculation matrix*. The implementation of a few heat-transfer relations suitable for high-temperature gas-cooled reactors allows for the rapid estimation of thermal properties critical for safe operation. Thus, modeling and design optimization of a given pebble-bed core can be performed quickly and efficiently via the manipulation of a limited number key parameters. Automation of the optimization process is achieved by manipulation of these parameters using a genetic algorithm. The end result is an economical, passively safe, proliferation-resistant nuclear power plant.

TABLE OF CONTENTS

LIST OF FIGURES

LIST OF TABLES

FORWARD

A number of people contributed to the development and analysis of the models contained herein. Dr. Eben Mulder and Frank Emslie of PBMR (Pty), Ltd. of the Republic of South Africa (RSA) graciously volunteered design information on the Pebble Bed Modular Reactor. Ramatsemela Mphahlele, fellow Penn State graduate student and analyst for the National Nuclear Regulator of the RSA, donated a considerable number of hours running MICROX to generate cross-sections for use in this work. Richard L. Moore of the INEEL constructed and ran reactor models using MELCOR. This provided the confirmation of the heat transfer models exploited in PEBBED.

Drs. William Terry and Abderrafi Ougouag offered guidance and feedback on a daily basis at the INEEL. Much of this research is a product of the exceptional synergy developed between the three of us. Dr. Terry is the creator of the PEBBED algorithm. Dr. Ougouag laid the foundation for the work on non-proliferation, optimal moderation, and hot spot analysis. Both of them contributed substantially to this effort.

Chapter 1

Introduction

1.1 Objective of this Research

Decades of research and development into light water reactor in-core fuel have contributed to an impressive increase in the amount of energy that can be safely extracted from uranium fuel. Recently, the *pebble-bed reactor* (PBR) with recirculating fuel is attracting interest as a viable alternative. Passive safety features, simplicity of operations, a stable waste form, high outlet temperature, and more efficient use of fuel are causing some utilities to take a closer look at the helium-cooled thermal reactor. In some ways, the pebble-bed is an established technology; two pebble-bed reactors successfully generated power in Germany [1], a 10 MW pebble-bed achieved criticality in China in 2000 [2], and a number of critical facilities have been built to conduct physics experiments [3]. Yet this reactor concept has yet to mature, particularly with regard to fuel design and in-core fuel management. With regard to the latter, the fact that the fuel physically moves through the core during operation poses both interesting challenges and opportunities. The sophisticated optimization techniques that have been applied to light water reactor designs cannot be similarly applied to pebble-bed cores without new analysis tools.

This work introduces new techniques for PBR design and fuel management. These techniques have been incorporated into a new PBR analysis code called PEBBED.

1.2 Next-Generation Nuclear Power Plants – Greater Demands on Design and Operation

In 2000 William Magwood IV, Director of the U.S. Department of Energy's Office of Nuclear Energy, Science and Technology, called for a new generation of nuclear power plant [4]. The Department of Energy has since engaged governments, industry, and the research community worldwide in a wide-ranging discussion on the development of next-generation nuclear energy systems known as “Generation IV.” The Generation IV roadmap calls for the development and demonstration of one or more advanced nuclear energy systems that offer advantages in the areas of sustainability, safety and reliability, and economics, and that could be deployed commercially by 2030. Concepts are identified as “Generation IV” if they may satisfy most or all of eight goals pertaining to these areas as identified by the Generation IV NERAC Subcommittee. These goals are:

Goal 1 – Generation IV systems (including fuel cycles) will provide sustainable energy generation that meets clean air objectives and promotes long-term availability of systems and effective fuel utilization for worldwide energy production,

Goal 2 – Generation IV nuclear energy systems will minimize and manage their nuclear waste and notably reduce the long-term stewardship burden in the future, thereby improving protection for the public health and the environment,

Goal 3 – Generation IV nuclear energy systems including fuel cycles will increase the assurance that they are a very unattractive and least desirable route for diversion of theft of weapons-usable materials,

Goal 4 – Generation IV nuclear energy systems operations will excel in safety and reliability,

Goal 5 – Generation IV nuclear energy systems will have a very low likelihood and degree of reactor core damage,

Goal 6 – Generation IV nuclear energy systems will eliminate the need for off-site emergency response,

Goal 7 – Generation IV nuclear energy systems will have a clear life-cycle cost advantage,

Goal 8 – Generation IV nuclear energy systems will have a level of financial risk comparable to other energy projects.

Though no specific cost targets were identified by the Generation IV Roadmap group, a target of $1,000 per KWe of installed electrical power was identified by a Generation IV Working Group as a value under which new nuclear plants may compete with other energy sources. A busbar cost of 3¢/KWh wholesale electricity from a new plant is also considered a maximum value if nuclear plants are to compete with natural gas-fired units.

One concept identified as a Generation IV candidate, the Very High Temperature Reactor (VHTR), is distinguished by its graphite-moderated core, helium coolant, and high outlet temperature (1,000℃) [5]. This high outlet temperature makes the VHTR a leading candidate for hydrogen as well as electricity production. The VHTR is the successor to the high temperature gas reactor (HTGR), of which many versions have been designed and few actually built and operated. Pebble fuel can be used in either to enhance fuel efficiency and safety. Modular construction may also reduce the capital cost of the plants. The attributes of a modular pebble-bed HTGR/VHTR (henceforth referred to as a Modular Pebble-Bed Reactor [MPBR]) are summarized in the next chapter.

In order for the MPBR to compete successfully as an advanced power plant, however, advanced design and analysis methods must be applied. Such methods have heretofore not existed. Because the fuel elements in these reactors is actually in motion

during operation, the techniques developed for other reactor types are not valid. Genetic algorithms, neural networks, and other modern optimization tools that have been successfully applied to light water reactors have not been adapted for the MPBR. The principal obstacle has been the lack of an efficient analysis method that can treat moving fuel. Such a method has recently been developed and incorporated into PEBBED [6]. This code solves the coupled diffusion and depletion equations for cores in which fuel flows in a predictable pattern. The current version converges directly upon the asymptotic or equilibrium core burnup distribution but can analyze static cores as well.

A boundary condition for the solution to the asymptotic core profile is the *entry plane burnup*, a spatially dependent quantity that is determined by the method in which pebbles are loaded and reloaded in the core. In this work, a formulation for the entry plane burnup is developed that describes arbitrary, user-defined pebble flow patterns in terms of a multi-dimensional *recirculation matrix*, the elements of which are functions of a few easily computed coefficients. Thus, PBR core design and fuel management are reduced to the manipulation of a small number of variables readily amenable to optimization techniques. This is demonstrated by applying one such technique, a *genetic algorithm*, to optimize a number of proposed MPBRs designs. The utility of the recirculation matrix is also used to address other issues that are common to pebble-bed reactors.

The techniques introduced in this work provide a framework for advanced core design and fuel management of pebble-bed reactors that will allow them to achieve ever more stringent standards of safety and performance.

1.3 Organization of this Thesis

Chapter 2 provides a brief overview of the high-temperature, gas-cooled reactor followed by a description of the pebble-bed reactor and the properties of pebble flow. Methods for physics analysis are discussed including an introduction of the technique used in PEBBED.

Chapter 3 provides an overview of the PEBBED code followed by the derivation of the recirculation matrix, the method by which entry plane burnup is computed in PEBBED. Special cases of the matrix are discussed. Also described are the correlations and equations that are used in PEBBED to estimate fuel temperatures under normal and accident conditions.

Chapter 4 describes applications of the code to various reactor designs in the literature. Comparisons to results of previous analyses are made when possible.

Chapter 5 shows how the code is used to address important issues in the design and safe operation of the modular pebble-bed reactor.

Chapter 6 describes the conceptual design of a VHTR using a manual search.

Chapter 7 introduces the genetic algorithm and how it is used for efficient MPBR design. Optimization is performed on three different MPBR concepts. Chapter 8 summarizes the work and discusses future research needs.

Chapter 2

The Pebble-Bed Reactor and Analysis Methods

2.1 Summary of High-Temperature Reactor Design Efforts

The history of graphite-moderated thermal reactors goes back to the first man-made critical assembly, CP-1. A *high temperature* graphite reactor with a prismatic core was first investigated in 1956 at the Atomic Energy Research Establishment in Harwell, England. The 20 MWt DRAGON reactor was built in the United Kingdom and began operation in 1966 with cooperation and support from a number of countries in Europe [1]. General Atomics picked up on the prismatic HTGR concept and built the 40 MWe Peach Bottom power station in 1967 near Philadelphia. Using the particle fuel concept invented in the U.S., Schulten proposed the alternative concept of the pebble-bed in Germany in the late 1950's [7]. The pebble-bed was (and is) unique in that it uses solid, spherically-shaped fuel elements that trickle through the core vessel during operation. Details of the fuel and core are described in the next section. Design and construction began on the *Arbeitsgemeinschaft Versuchs Reaktor* (AVR,

Figure 2-1: AVR – the first pebble-bed reactor.

Figure **2-2**: THTR

Figure **2-1**) with initial criticality in 1967 [8]. The success of the AVR led to larger pebble-bed designs and the construction of the *Thorium Hochtemperatur Reaktor* (THTR) [1]. This thorium-fueled power plant (Figure **Figure 2-2**) ran from 1986 until 1988 when, during a planned maintenance outage, some bolt heads from the hot duct cover plates were found inside the gas ducts. In isolation such a technical setback would not have prevented eventual restart but the combination of public safety concerns (Chernobyl was still a recent memory) and the growing strength of the PWR in Germany led to the decision not to restart. In the U.S., General Atomics built the Fort St. Vrain 300 MWe HTGR power plant in Colorado, again with a prismatic core, based on its success with the Peach Bottom plant, which shut down in 1975. The Fort St. Vrain reactor operated from 1974 to 1989.

The *modular* HTGR concept gathered technical momentum in the early 1980's with the design of the *HTR Modul 200* by Kraftwerk Union and Siemens/Interatom [9], [10]. The design stressed simplicity and inherent safety even in the most severe of accidents. The HTR Modul 200 (Figure **2-3)** features a recirculating core with a single discharge tube and a single central loading tube for pebbles. Large electricity demands could be met by building multiple copies of the same 200 MWt plant on the same site. Although this plant was designed to drive a steam cycle, many of the basic design features have been adapted for the gas-turbine PBRs under consideration today.

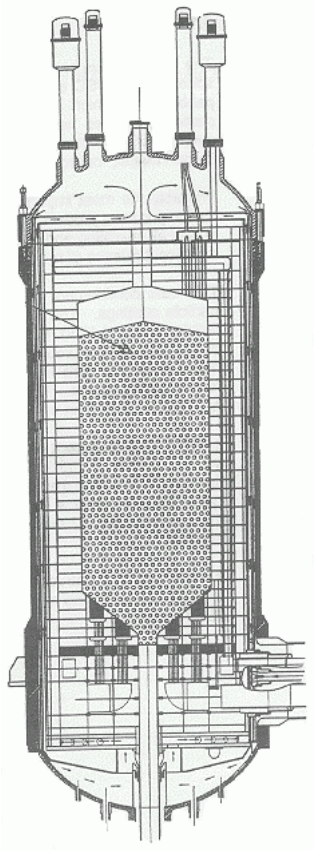

Figure **2-3**: Core vessel of the HTR Modul 200.

At the same time in the United States, General Atomics was developing its own modular HTGR efforts with support from the Department of Energy (DOE) [11], [12]. In addition to power generation, variants of the basic General Atomics design have been proposed for both weapons material production (MHTGR-NPR or New Production Reactor), weapons material destruction [13], and even submarine propulsion [14]. More recently, the DOE has supported development of a modular pebble-bed reactor power plant via a research grant to the Idaho National Engineering and Environmental Laboratory (INEEL) with support from the Massachusetts Institute of Technology [15].

Elsewhere in the world the HTGR has also received some attention and development. Critical PBR facilities have been built in Germany [16], Switzerland [3],

and Russia [17]. Japan began fuel and materials testing for its HTGR program in 1976 and the 30 MWt High Temperature Test Reactor (HTTR) began operation in 1998 [18]. It uses a prismatic core to drive a steam generator. An experimental hydrogen production unit recently began operation and gas-turbine power conversion unit is under development.

In the Netherlands, the research consortium NRG is developing a 40 MWt pebble-bed reactor for cogeneration [19], [20]. The same power plant has been proposed for ship propulsion [21].

The People's Republic of China purchased technology and equipment from Germany to build a 10 MWt experimental pebble-bed reactor, the HTR-10. This reactor went critical in December 2000 [22]. The HTR-10 is the only pebble-bed reactor in operation in 2003.

The South African state utility ESKOM directed an analysis of the technical, commercial, and economic feasibility of the modular PBR in the late 1990s. It has recently received preliminary approval for construction [23] [24]. The ESKOM PBMR has backing from the energy firm BNFL and its American partner Westinghouse. The power plant would be built on the site of South Africa's only other nuclear power plant, a PWR at Koeberg. The PBMR borrows heavily from the German designs but uses a gas-turbine cycle for improved thermodynamic efficiency.

2.2 Characteristics of the Pebble-Bed Reactor

The MPBR's safety and economic basis is the fuel element. Fuel kernels coated with pyrolytic layers and encased in a graphite matrix, PBR fuel can be burned safely to a high degree.

2.2.1 Fuel Design

Modern gas-reactor fuel elements are composed of small (0.5 mm diameter) uranium oxide (UO_2) kernels surrounded by various layers of pyrolytic carbon, silicon carbide, and buffer graphite (Figure **2-4**). Kernels composed of uranium carbide (UC_2) or a mixture of UO_2 and UC_2 have also been designed and fabricated. The pyrolytic carbon layers are applied in a chemical vapor deposition process to form a fuel *particle* of just under 1 mm diameter. The layers serve as a pressure boundary and retention zone for fission products. Many thousands of these so-called TRISO particles are then mixed with graphite and a binder. The mixture is formed into a sphere of about 5 cm in diameter (or a cylindrical compact for use in a prismatic core).

A 0.5 cm layer of pure graphite surrounds the fuel zone to form the 6 cm *pebble*. In most current designs, each pebble contains between 7 to 9 grams of uranium enriched to about 8%. The Dutch research consortium NRG has developed a small 40 MWt design for co-generation applications that would use 19.7% enriched uranium in its pebbles [20].

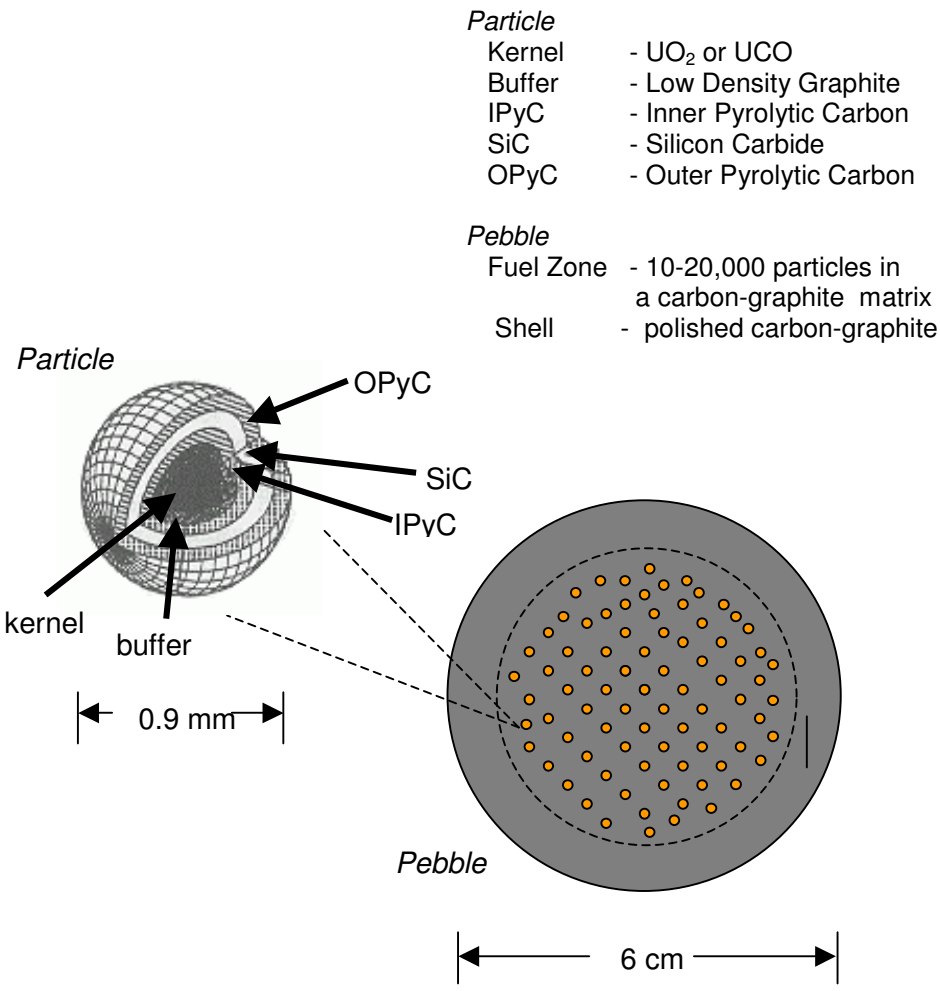

Figure **2-4**: A typical PBR fuel element with embedded fuel particles.

2.2.2 Core Safety

The potential safety characteristics of the modular pebble-bed reactor are the result of a number of design features, the most important of which is the TRISO-coated fuel particle described above. Other factors contribute to safe operation as well. The active core of the pebble-bed is much larger than a LWR of the same power. The HTR-Modul 200 produces 200 MW of thermal power in a core of about 9.4 m in height and 3 m in diameter (66.4 m^3 volume). This core has an average thermal power density of 3.0 W/cm.

By contrast a 3,400 MWth Westinghouse PWR has an active core volume of about 32.8 m^3 and thus generates an average power density of 104 W/cm^3. The lower power density of the pebble-bed means that the fuel is less likely to attain a high enough temperature to induce failure. The relatively high thermal conductivity of graphite (30-50 W/mK) compared to pure UO_2 (3 W/mK) ensures that heat is transferred quickly away from the fuel and out of the core even in the event of a loss of forced cooling or depressurization. Computational analysis and experiments performed on the AVR confirm that fuel failure temperatures are avoided in these extreme cases [25], [26], [27], [28], [29], [30]. The strong negative feedback coefficient in the fuel also limits the amount of fission power that is generated in the fuel elements in the event of a reactivity excursion.

In addition to the core features that limit achievable core temperatures, the confinement of radioactive fission products is assured by the design of the fuel particle coatings. Extensive studies of the behavior of coated fuel particles have been conducted under various temperature and fluence conditions. These studies will not be described here but some of the conclusions are important for fuel cycle optimization. For example,

the silicon carbide layer is such that that no radiologically significant quantities of gaseous or metallic fission products are released from the fuel elements at temperatures of up to 1,650 ℃ (3,000 ℉).

Figure **2-5** illustrates the results of krypton release tests performed on pebbles using various particle designs.

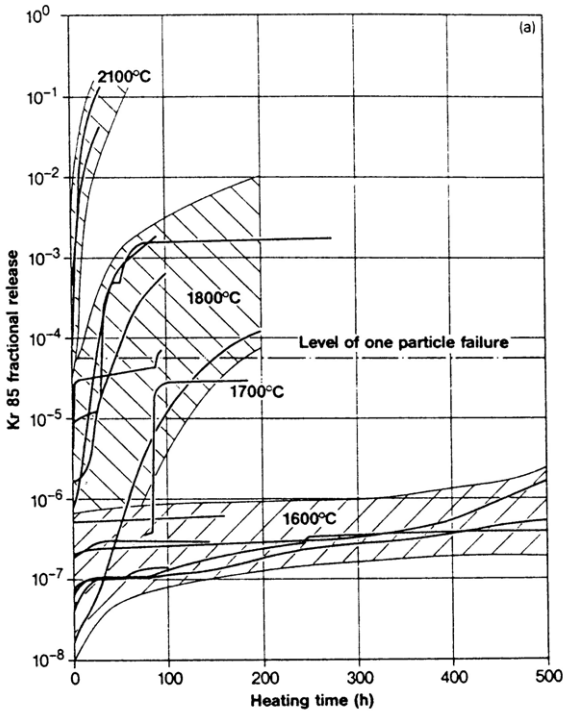

Figure **2-5**: Krypton release during tests with irradiated spherical fuel elements at 1,600 ℃ to 2,100 ℃ [31].

A number of such tests were conducted in Germany in support of the pebble-bed reactor programs. The plot shows the release fraction of krypton-86, a fission product, which can be detected after the failure of the silicon carbide boundary in a particle [31]. In essence it shows the fraction of particles in a pebble that fail after a certain time at temperature. A substantial amount of data exists for 1,600 ℃ tests and the results clearly

indicate that, on average, less than one particle per pebble will fail as long as the temperature remains below this value. A few tests showed that, for some particle designs, no failed particles were detected for heating times of less than 100 hours at this temperature. Particle failures on the order of 10 to 20 per pebble (about 0.1% of the total) were observed when pebbles were heated for more than 50 hours above 1,800℃. Bulk failure of particles is observed at temperatures exceeding 2,000℃, the temperature above which silicon carbide begins to decompose.

Fuel integrity was also confirmed in loss of forced flow experiments on the AVR [30]. The peak fuel temperature, presented in Figure **2-6**, rose to a peak value of 1,400℃ then decreased as decay heat transferred out of the core. This favorable outcome is the results of a combination of proper pebble and core design.

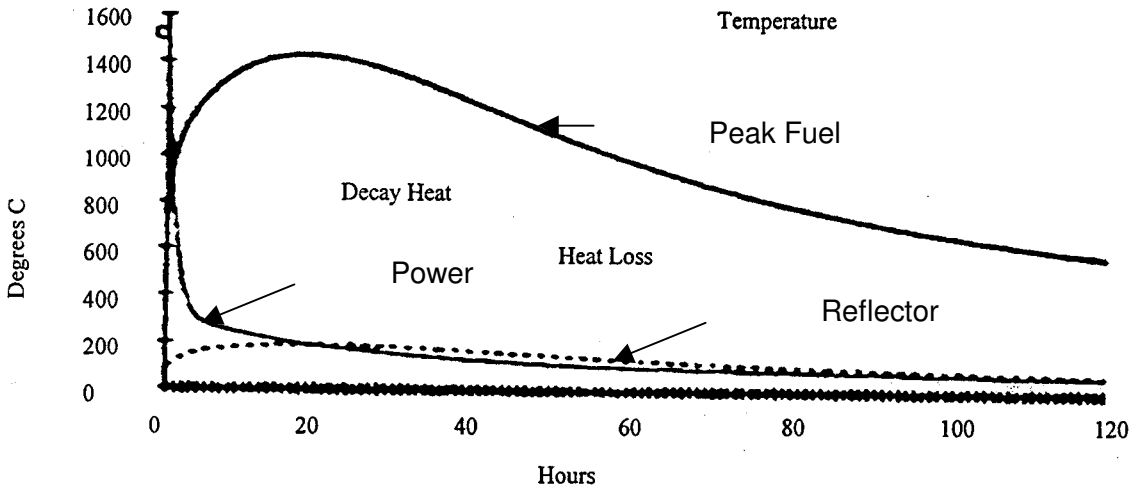

Figure **2-6**: Peak fuel temperature in AVR during loss-of-forced-cooling tests.

In the AVR experiment, primary system helium pumps were turned off and the control system that would respond with the insertion of control elements was disabled. The strong negative fuel temperature feedback quickly shut down the reactor. The fuel

temperature peaked at a level well below the value at which fuel failure is expected to start occurring (1,650°C). Radiation monitors detected no fission product release.

The South African PBMR and Kraftwerk Union HTR-Modul 200 possess such characteristics. Future designs will be expected to do so as well.

The extremely low probability (<once per 10^6 reactor years of operation) of fuel damage and subsequent release of fission products puts the risk of off-site consequences at a level far lower than other accepted hazards of modern living and LWRs. Thus, off-site emergency response is not required.

2.2.3 Fuel Economy

Most MPBR designs assume a spent fuel discharge burnup of 80 megawatt-days per kilogram of initial loaded heavy metal (MWd/kg_{ihm}), considerably higher than is currently achieved in light water reactors (LWR). Experiments conducted in Germany extended the burnup of some fuel pebbles up to 160 MWd/kg_{ihm} [32]. If a recirculating fuel system is used, *each* fuel element loaded into the core will achieve a minimum specified burnup before discharge in contrast to fixed fuel reactors in which the burnup of individual fuel units is a function of their location in the core. Furthermore, the fact the pebbles are loaded at intervals measured in minutes, sufficient excess reactivity is needed only for control and restart. The need for burnable poisons to hold down fresh fuel reactivity is eliminated. Semi-continuous refueling also means that the core can operate in an *optimally-moderated* state during most of its operating life. A study was performed by the author and colleagues to demonstrate this effect and will be described in Chapter 4.

The PBR can thus operate with very high neutron economy. This advantage of the MPBR is somewhat offset by the higher enrichment required of most high temperature gas reactor designs. Nonetheless, significant overall savings in fuel costs can be realized with a properly designed MPBR and fuel cycle [33]. Improved fuel economy also results in reduced waste volume.

The fuel form itself is a robust waste form. The silicon carbide pressure boundary and the graphite matrix are thermodynamically stable on a geologic time scale. Spent pebbles can be released directly to a repository.

2.2.4 Proliferation

Graphite-moderated thermal reactors fueled with low enriched uranium (LEU) generate significant amounts of plutonium and other actinides within the fuel pebbles during operation [34]. The on-line refueling mechanism in a recirculating MPBR allows for the extraction of pebbles at various stages of burnup. Considered in isolation, these two factors would imply that the danger of weapons material proliferation might be greater in the MPBR than in other reactor types. In fact, on-line refueling capability in the pebble-bed reactor allows for a mode of operation that greatly decreases the likelihood that the power plant will be co-opted for weapons production. Studies [35], [36], [37] have been performed by the author and colleagues to demonstrate this effect and will be described in more detail in later chapters. By allowing the addition of fuel only as needed to maintain criticality, the MPBR can operate with a very small amount of excess reactivity. The diversion of neutrons toward illicit weapons material production would result in a drop in reactivity that would require either higher enrichment in the fresh fuel or an easily detected change in the operation of the reactor (lower power, frequent

shutdown, etc.). In a batch-fueled reactor loaded on an 18- to 24-month cycle (PBR or LWR), this reactivity penalty could be avoided by lowering the concentration of burnable poison in the fresh fuel. Thus, with reasonable oversight on the part of a safeguards agency, the proliferation threat posed by a nation possessing a pebble-bed reactor is comparable to or less than that of one operating a LWR, provided that the nation does not possess an indigenous enrichment capability. Reduction of the rate of weapons-material production can be considered a goal of an optimization calculation.

2.3 HTGR Physics

The use of graphite as both moderator and structural material distinguishes the HTGR from other thermal reactor designs. It also eliminates the need for metal cladding and other structure material in the core assembly. Coated fuel particles in either prismatic or pebble-bed cores distinguish the HTGR from other graphite-moderated reactors such as the British Magnox and AGR (Advanced Gas-Cooled Reactor). Although very high coolant temperatures are normal (>1,000℃ at the outlet of hot channels), the structural integrity of the particle coating keeps the fuel confined even under loss-of-flow or loss-of-pressure conditions. Heavy metal kernels of 0.5 mm diameter mixed with graphite in either pebbles or fuel compacts results in a tight coupling between the moderator and fuel and a strong negative temperature feedback coefficient [38].

The use of helium as coolant is also a unique feature. The chemical inertness and transparency to neutrons means that direct void reactivity feedback effects are negligible. The high coolant outlet temperatures make the HTGR a potential power source for process heat applications [39].

The modular pebble-bed core consists of a cylindrical graphite vessel/reflector that contains upwards of 450,000 pebbles. The pebbles are randomly packed in the vessel with a packing density that varies between 0.61 and 0.64. Helium gas is blown in from the top and is forced through the packed bed to carry off heat. Table **2-1** contains a comparison of the more important core parameters in the HTR Modul-200 and an early version of the South African PBMR.

Table **2-1**: Key parameters for two PBR designs [9]

	HTR Modul 200	PBMR (dynamic core)
Thermal Power (MW)	200	268
Core Diameter (m)	3.0	3.5
Core Height (m)	9.4	8.5
Mean Power Density (W/cc)	3.0	3.25
Diameter of Inner Reflector (m)	N/A	0.8m
Number of Pebbles (fuel/graphite)	360,000/0	330,000/110,000
System Pressure (MPa)	6	7.0
Helium Temperature (℃ inlet/outlet)	250/700	530/900
Number of control rods	6	6
Number of Absorber ball systems	18	18
Average No. of Passes per Pebble	15	10
No. of Particles per Pebble	11,200	15,000
Heavy Metal Loading (g/pebble)	~7	~9
Enrichment	7%	8%
Fresh Fuel Injection Rate (pebbles/day)	347	372
Discharge Burnup (MWD/kg)	80	80
Fuel Residence Time (days)	~1,000	~850

Nominal reactor control is achieved with control rods inserted into the outer reflector. The small diameter of the modular pebble-bed results in sufficient reactivity worth of these radial absorbers so that in-core absorption is not necessary. A secondary

shutdown system (KLAK) consisting of absorber balls blown into reflector channels is also available but these are not used for power shaping or ramping. Load following is also achievable through manipulation of the helium inventory of the primary loop [40], [41].

The use of graphite as moderator has both advantages and disadvantages. The low absorption cross-section means a higher moderating ratio but the crystalline properties also necessitate a detailed treatment of the scattering law in physics calculations. The low parasitic absorption rate in the overall core and reflector allows the fuel to achieve high burnup at low fuel cost. Taking the fuel to these levels also requires higher enrichment. A higher moderating ratio (moderator atom per fuel atom) results in more neutron absorptions by the fuel in the thermal energy range (85% vs. 70% in a PWR). However, the high temperature promotes upscattering and pushes the thermal energy peak into a range populated by a number of plutonium resonances (Figure **2-7**). The effect is particularly evident at high burnups with the significant buildup of plutonium isotopes.

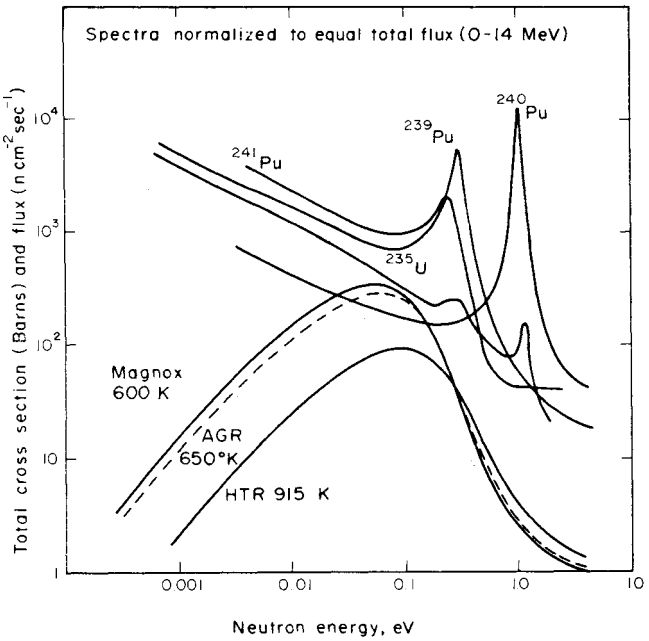

Figure **2-7**: Moderator spectrum and absorption cross-section in a graphite-moderated reactor.

Helium is essentially transparent to neutrons and thus coolant temperature and voiding effects have a negligible effect on reactivity.

Although HTGR fuel is rather homogeneously dispersed in the graphite matrix, heterogeneity effects cannot be ignored [42]. Traditionally, the effect of the irregular pebble lattice is addressed through the use of Dancoff correction factors in the resonance treatment. Closed-form expressions for Dancoff factors in spherical-element lattices do not exist but an approximation can be made [43]. More recently, Monte Carlo calculations of Dancoff factors for both pebble and particle lattices have been performed for a variety of geometries and packing densities [44]. The Dancoff factor, however, is still an approximation to the resonance absorption calculation. An explicit treatment of randomly packed spherical fuel lattices would require a three-dimensional deterministic

transport treatment of a homogeneous infinite-cell cross-section calculation. Such work is underway with support from the INEEL [45].

With an appropriate method for generating cross-sections, HTGR cores with stationary (prismatic or pebble-bed) fuel elements can be analyzed with a number of existing few-group diffusion-depletion codes. If the fuel is allowed to flow through the core during operation, the set of applicable analysis tools shrinks considerably. Before surveying the set of PBR analysis tools, it is useful to understand the nature of the flow of pebbles in a cylindrical vessel.

2.3.1 Pebble Flow – Studies and Relevance

Soon after Schulten proposed the concept of spherical fuel elements flowing through a core, a detailed study of the characteristics of pebble flow was undertaken by Bedenig, et al., in support of AVR operation and THTR design [46], [47]. Two techniques were used in this effort; one to determine the paths followed by fuel in the core and one to determine the velocity distribution.

In a cylindrical core with single or multiple discharge tubes, the flow of pebbles is observed to follow *streamlines*. These streamlines were first investigated using a transparent core model with glass spheres some of which were rendered opaque. The core was filled with a liquid with an index of refraction identical to that of the transparent spheres. As the clear pebbles were circulated, opaque pebbles were inserted at fixed locations on the top of the pebble-bed (see Figure **2-8**).

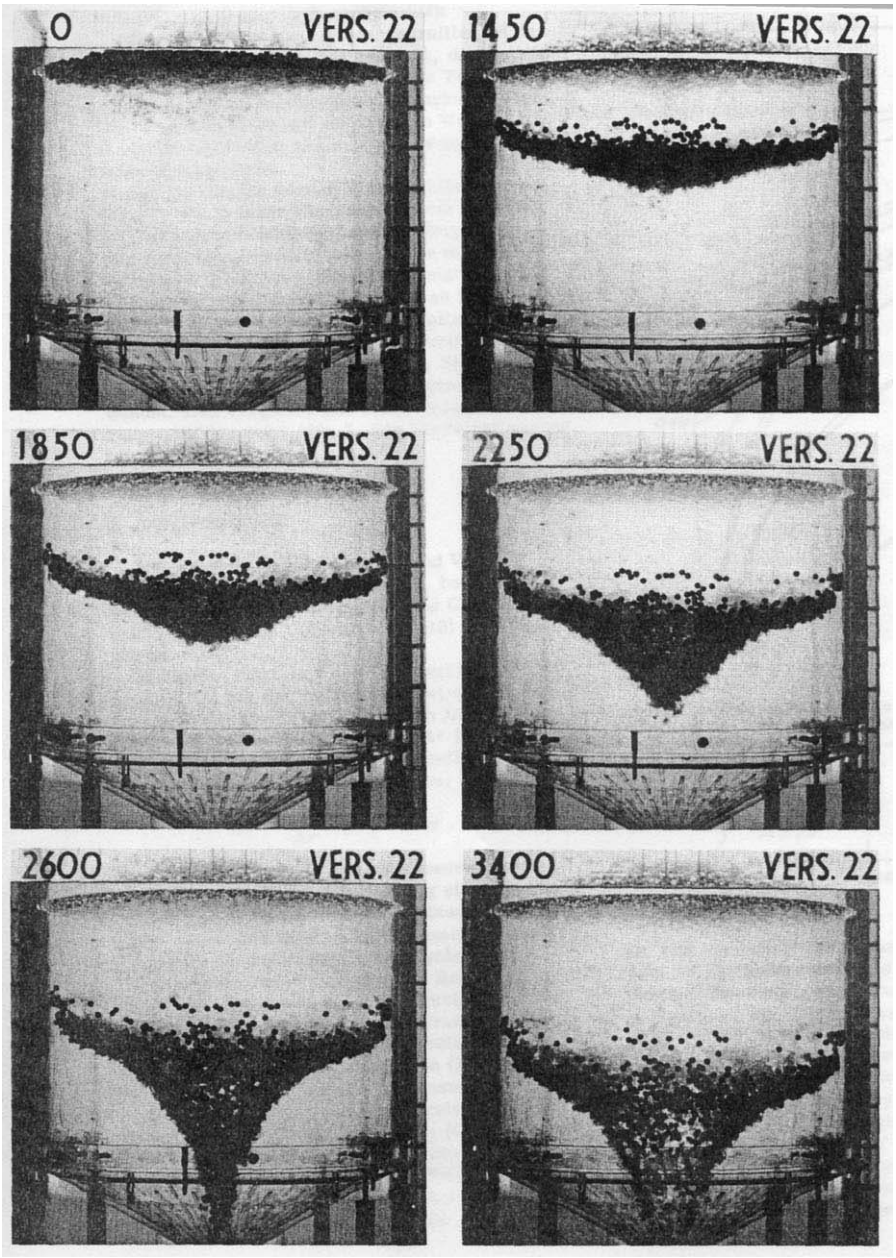

Figure 2-8: Photographs of pebbles in recirculating pebble-bed.

The principal conclusion from these studies was that pebble flow could be considered “laminar,” i.e., streamlines do not cross. This fact is crucial to the development of valid nuclide distribution models.

The other study did not require the visualization of pebble flow. A single layer of pebbles distinguishable by a subtle difference in diameter or the presence of radioactive tracer was placed on a surface of a pebble-bed. The pebbles were allowed to circulate and the appearance of pebbles at the core outlet was recorded as a function of the total number of recirculated pebbles. The results are plotted as a *residence spectrum*, which illustrates the distribution of the time for a fraction of the pebbles to traverse the core relative to the recirculation of the entire core. A schematic drawing of residence spectra is shown in Figure **2-9**.

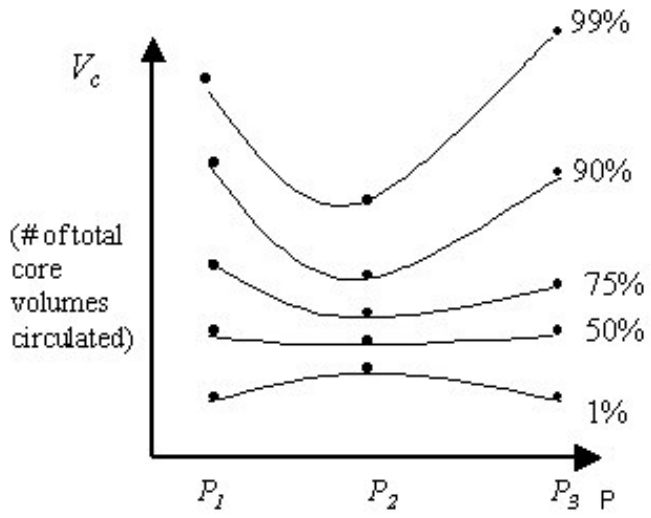

Figure **2-9**: Qualitative drawing of residence spectra vs. an arbitrary parameter [47].

Each curve represents a percentage of the total number of pebbles that traverse the core in a specified time interval as a function of the parameter of interest (*P*). The effect of that parameter on pebble flow rate is thus inferred.

Because of the streamline flow confirmed in the first study, a relation between the distance from the core axis and the *residence time* in the core can be inferred. In other words, the farther from the core axis, the longer a pebble takes to traverse the core.

Residence spectra were measured for test cores with varying values of parameters such as; the ratio of the core height to its diameter, the angle of inclination of the discharge conus, the diameter of the discharge tube, friction on the pebble surface, pebble specific weight, and so on. With knowledge of the residence spectra and the assumption of streamline flow the velocity distribution in a pebble-bed core can be computed.

Among other findings, Bedenig concluded the following:

1. With increasing core height, the flow becomes more uniform,
2. Above core height-to-diameter ratios of 0.8, the ratio of residence time for the first and last pebble is unity (slug flow).

Most of the PBR designs under consideration today have height-to-diameter ratios around 3.0. The uniform velocity (slug flow) assumption is valid for purposes of computing nuclide flow distribution in the core. The flow rate of pebbles as a function of radial location *r* and axial velocity *v* at the entry plane is expressed simply as in Eq. **2.1**.

$$F(r,v) = 2\pi rv \qquad \textbf{2.1}$$

More recently, computational methods have been applied to the flow of pebbles [48]. Discrete element codes running on fast computers model the motion of individual pebbles as they are dropped into the core (Figure **2-10)** and flow through it. The PFC^{3D} code has been used to model the flow in the early PBMR design featuring graphite and fuel pebbles in an annular configuration.

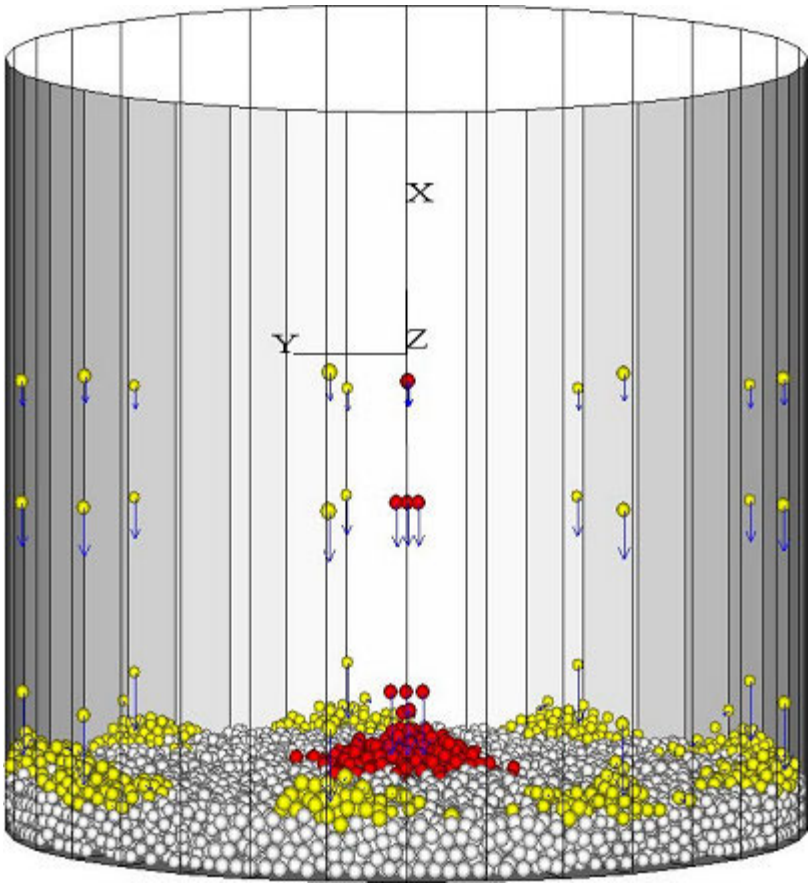

Figure **2-10**: Drop zone above core as modeled by PFC^{3D} [48].

Also of interest is the stochastic radial motion of pebbles particularly with regard to the mixing of two major pebble zones such as in the original PBMR design. This effect is illustrated in Figure **2-11** and quantified in Figure **2-12**.

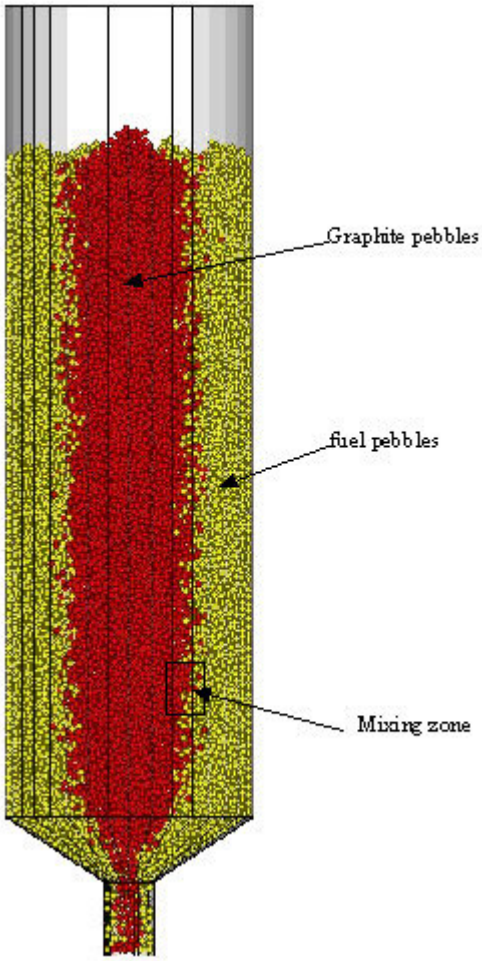

Figure 2-11: PBMR core with mixing of graphite and fuel pebbles [48].

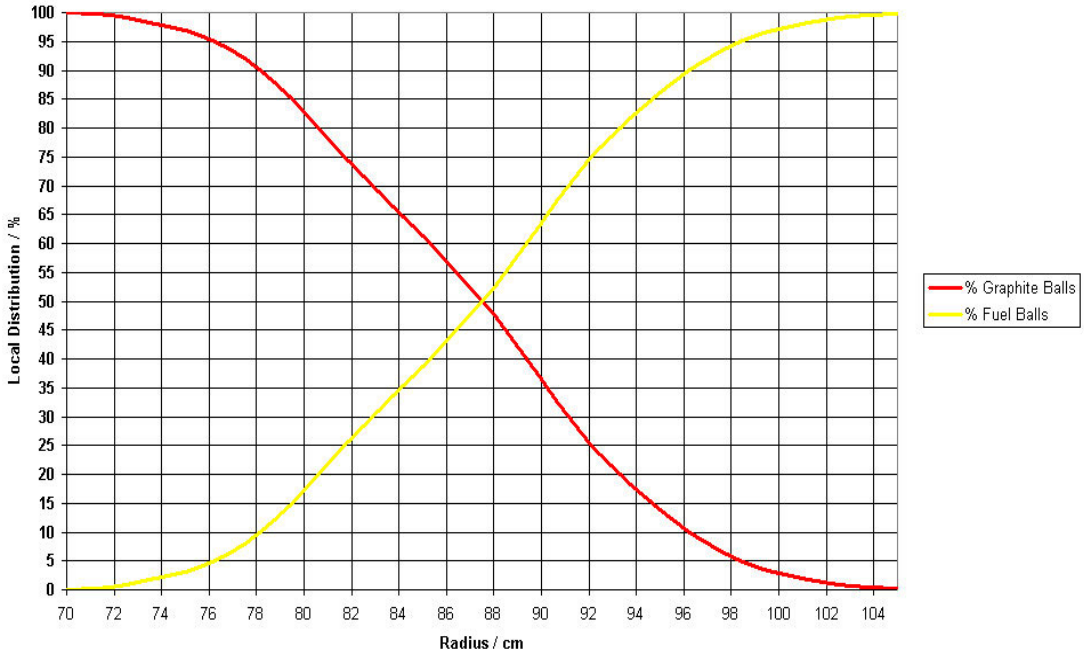

Figure **2-12**: Local distribution vs. core radius.

The distribution of fuel pebbles increases smoothly from the inner boundary of the mixing region to the outer. Agreement between experimental results and these computations is within 10% [49].

These results are important for modeling the burnup distribution in the recirculating core.

2.4 Existing PBR Neutronics Analysis Methods

2.4.1 Neutronics of Cores with Moving Fuel

The movement of fuel through the PBR core is orders of magnitude slower than the change in power level under normal and accident conditions. For safety analysis and reactor control, core dynamics models and codes that assume stationary fuel are no doubt adequate provided that reasonable estimates of the power and nuclide distributions can be supplied. These distributions, however, must be obtained from a code that solves the balance equation for nuclide *k* expressed as Eq. **2.2** [38],

$$\frac{\partial N_k(\vec{r},t)}{\partial t}+\frac{\partial N_k(\vec{r},t)}{\partial z}v(\vec{r})=\phi(\vec{r},t)\sum_{i=l}^{m}N_i(\vec{r},t)\sigma_{fi}y_{ik}+\phi(\vec{r},t)\sum_{s=r}^{q}N_s(\vec{r},t)\sigma_{asi}\gamma_{sk}+\sum_{j=n}^{p}N_i(\vec{r},t)\lambda_j\alpha_{jk}-\lambda_k N_k(\vec{r},t)-\phi(\vec{r},t)N_k(\vec{r},t)\sigma_{ak} \qquad \textbf{2.2}$$

in which

$N_k(\vec{r},t)$ = atomic concentration of isotope k

$v(\vec{r})$ = $v(\vec{r})\hat{z}$ axial velocity of pebble at location $\vec{r}$

$\phi(\vec{r},t)$ = neutron flux

σ_{fi} = fission cross section of isotope i

σ_{ai} = absorption cross section of isotope i

y_{ik} = yield of isotope k due to fission of isotope i

λ_i = decay constant of isotope i

γ_{sk} = probability that absorption in isotope s produces isotope k

α_{jk} = probability that the decay of isotope j produces isotope k

Equation **2.2** assumes that pebble flow is strictly axial. All current PBR designs have one or two discharge tubes so that radial movement of fuel is a fact. However, the axial flow assumption is generally valid because most of the radial movement occurs in the bottom *conus* in which a relatively low flux exists. Equation **2.2** can be generalized to track nuclide variations along *streamlines* with a modest increase in input specifications and computation.

Depletion codes used in LWR analysis justifiably set the spatial derivative on the left-hand side of equation **2.3** to zero. Detailed treatment of the effects of azimuthally-dependent core elements such as control rods requires the full three-dimensional representation. For many applications, however, azimuthal symmetry may be assumed with little loss in accuracy. Eq. **2.2** then reduces to Eq. **2.3.**

$$\frac{\partial N_k(r,z,t)}{\partial t}+\frac{\partial N_k(r,z,t)}{\partial z}v(r,z)=\phi(r,z,t)\sum_{i=l}^{m}N_i(r,z,t)\sigma_{fi}y_{ik}+\phi(r,z,t)\sum_{s=r}^{q}N_s(r,z,t)\sigma_{asi}\gamma_{sk} + \sum_{j=n}^{p}N_i(r,z,t)\lambda_j\alpha_{jk}-\lambda_k N_k(r,z,t)-\phi(\vec{r},t)N_k(r,z,t)\sigma_{ak} \quad \textbf{2.3}$$

in which *r* is the distance from the core centerline and *z* is the distance from the *entry plane* or top of the pebble-bed core.

The inter-dependence of neutron flux and nuclide density requires that Eq. **2.3** and the neutron diffusion equation be solved simultaneously. The first code to do this was VSOP (Very Superior Old Programs) [50], developed in Germany with the HTGR program. VSOP consists of cross-section libraries and processing routines and neutron spectrum evaluation based upon the GAM-GATHER-THERMOS system, 2-D diffusion and depletion routines, in-core and out-of-pile fuel management, fuel cycle cost analysis, and thermal hydraulics for pebble-bed reactors. Until recently, it was the only code available for life-cycle analysis of PBRs. The diffusion module, based on the CITATION

finite difference method, synthesizes the R-Z flux distribution in four energy groups from one-dimensional (axial) calculations. Forty isotopes can be tracked explicitly in up to 200 compositions and the spectrum calculation is repeated when a significant change in the spectrum is expected. The fuel management module tracks 'batches' of pebble from the moment of entry into the core, through recycling, and to eventual discharge. The batches are treated as though they reside in a stationary manner in assigned sections of fuel streamlines so that the second term in Eq. **2.3** vanishes. The equation can be solved using standard depletion techniques (Appendix B). After each time step, they are moved discontinuously to the next region in the streamline. The module simulates shuffling (recirculation) in this manner for currently known PBR designs. It has been extended to include burnup-dependent optional re-loading of pebbles and different fuel streams. Optimization with VSOP was even performed to a limited extent on an azimuthally-varying core for the design of a 500 MWt PBR [51]. The time-dependent capability allows VSOP to model changes in the fueling scheme in mid-cycle.

VSOP is widely accepted as the most appropriate suite of codes for fuel cycle analysis of PBRs. Though effective for many situations (in particular the pre-equilibrium or *running-in* phase of operations), it is two generations of codes and methods older than the state of the art in neutronics solvers. Because the finite difference method requires a very fine spatial mesh for accuracy, it is significantly slower than one that uses a nodal diffusion solver, and it is thus a less effective tool for frequent repetitive calculations needed for design and optimization.

The BURNER/VENTURE codes [52] use a similar approach as VSOP. Werner [34] very briefly describes a method that appears similar to VSOP. Jung [53] presents a formal time-dependent solution in one spatial dimension, but he leaves it to the reader to

determine the boundary conditions, i.e., the nuclide concentrations at the entry plane, which are a function of the way pebbles, are recirculated.

More recently, the PANTHERMIX [54] code has been developed to compute combined neutronic and thermal-hydraulic data for pebble-bed cores. It also solves the time-dependent nuclide balance equation in a batch manner like VSOP and can analyze non-equilibrium conditions. Like VSOP, it tracks nuclide density along streamlines so is not restricted to axial flow models. PANTHERMIX is a combination of the PANTHER neutronics analysis code (hexagonal finite-difference) with the THERMIX/DIREKT thermal-hydraulics codes (the PANTHER thermal-hydraulics module does not cover pebble-bed cores). Nuclide contributions from batches leaving the core with various stages of burnup are used to compose new batches at the entry plane. Discrete changes in burnup per time step are distributed over the different fuel types and burnup classes according to a specified distribution function of the heavy metal mass.

2.4.2 Equilibrium Cycle Analysis

After a pebble-bed core has been operating for some time (e.g., three years for the ESKOM PBMR) with new fuel elements of constant composition being added to maintain criticality, the average nuclide distribution converges to a steady value. The reactor may then run indefinitely with this *equilibrium* or *asymptotic* nuclide and flux distribution. Some approaches attempt to find this steady-state configuration directly. The KUGEL code [55] treats the distribution of fuel pebbles statistically, assuming that their composition is a function of irradiation only, and then calculates the probability of finding a pebble with a given irradiation at any point in the core. A zero-dimensional depletion code (MUPO/BO) computes the burnup of pebbles as a function of irradiation

and tabulates the results for lookup so that the burnup equations do not explicitly appear in KUGEL. Simple reshuffling schemes can be approximately modeled in this manner [56]. Izenson [57] also used a statistical approach, coupled with VSOP for the flux calculations, to find a steady state and evaluate the probability of finding "hot spots" in which groups of pebbles of higher-than-average power are clumped together. The PREC [58] and PREC2 [59] codes obtain a steady state directly for the *once-through-then-out* (OTTO) cycle in which pebbles are discharged after one pass through the core, i.e., no recirculation. These codes allow tracking of pebbles along curved streamlines. PREC converts the nuclide balance equation to discretized differential form and solves iteratively the resulting system of algebraic equations. The finite difference neutron diffusion equation with direct-coupled scattering law is solved simultaneously with this system.

The time-dependent codes and the statistical methods require extensive calculations, and the OTTO cycle is not general enough for design optimization of most PBRs. Liem [60] proposed a code (BATAN-MPASS) that solves the discretized burnup equation and computes the entry plane burnup from prescribed mixing of contributions from exit plane pebbles. Streamline flow and various recirculation strategies can be modeled. The extent to which this code can model complex recirculation schemes is not described in the reference. However, Liem also incorporated thermal-hydraulic calculations of accident temperature with the BATAN-MPASS burnup analysis in order to assess the ability to design passively safe cores [61]. Although no advanced optimization technique was used, Liem’s work was the first to use a combined neutronic and thermal-hydraulic calculation in the design of a modern pebble-bed reactor.

2.5 Direct, Deterministic Analysis and Optimization of the Asymptotic Core

Terry, Ougouag, and Gougar [6] developed a new method for solving the coupled neutron diffusion and nuclide depletion equations. The exact solution to the nuclide balance equation in a small region of the core is solved assuming constant flux across the region. One way to express the change in nuclide density is to treat burnup as an incompressible fluid and solve a continuity equation (Eq. **2.4).**

$$\frac{\partial B(\vec{r},t)}{\partial t} = F(\vec{r},t) - \nabla \bullet \left(B(\vec{r},t)\cdot \vec{u}(\vec{r},t)\right) \qquad \textbf{2.4}$$

The partial derivative of burnup (*B*) with respect to time is the rate at which burnup is generated in the volume, *F*, minus the net rate at which it flows from the volume given by the divergence of the product of the burnup and the flow rate vector $\vec{u}$. The relationship between the burnup variable *B* and nuclide density *N* is given in Appendix B.

In the asymptotic limit, the time derivative in Eq. **2.4** vanishes. By assuming incompressibility (a valid assumption for pebble-beds in which the packing fraction does not vary considerably) and strictly axial pebble flow, Eq. **2.4** is integrated to obtain the following expression for the burnup distribution, Eq. **2.5**,

$$B(x,y,z) = B_0(x,y) + \frac{A}{w(x,y)} \int_{z'=0}^{z} \Sigma_f(x,y,z')\phi(x,y,z')dz' \qquad \textbf{2.5}$$

in which

B_o is the distribution of burnup at the entry plane (top of core),

A is a normalization factor,

w is the axial pebble speed such that $\vec{u} = w\hat{z}$,

Σ_f is the macroscopic fission cross section, and

ϕ is the average flux in the volume.

Because the flux is a function of the cross sections and the nuclide density, the burnup distribution expressed in Eq. **2.5** must be solved in an iterative fashion after assuming an initial burnup distribution.

An important boundary condition in Eq. **2.5** is the entry plane burnup, B_o. In an OTTO cycle fed with fresh fuel, the entry-plane burnup is identically zero. When pebbles are recirculated, however, the entry-plane burnup depends on the procedure governing the recirculation process and on the burnup increments accrued by pebbles on successive passes through the core. So the entry-plane burnup becomes another unknown quantity to be determined in the iteration scheme; the rule for the recirculation procedure (e.g., cutoff burnup for recirculation) provides the extra information needed for finding the additional unknown quantity.

The solution is started by assuming that the burnup is zero throughout the core and calculating the neutron flux distribution with the diffusion or transport solver. Then the burnup and associated composition are found from Eq. **2.5** under the assumption that the entry plane burnup is still zero. The solution is still not self-consistent, because the neutron flux was not obtained from the compositions calculated in the last step. Furthermore, except in the OTTO cycle, the entry-plane burnup is still not determined.

Next, a double iteration loop is begun in which the inner iteration converges on the neutron flux and the burnup below the entry plane, and the outer iteration converges on the entry-plane burnup. The algorithm for the outer iteration depends on the rule governing pebble recirculation and will be covered more thoroughly in the next section.

The method does not require the solution variables to follow a physically meaningful sequence of states, but only to converge to a physically meaningful configuration. The solution is guaranteed to converge for any initial value of the burnup

(nuclide) distribution. Thus convergence is obtained in a few outer iterations. This behavior permits the new method to calculate steady states much more rapidly than methods that follow actual sequences of transient states to asymptotic steady states.

The early version of the PEBBED code adopted this approach for two simple recirculation schemes: 1) partially burned pebbles exiting the core are randomly distributed at the entry plane, and 2) partially burned pebbles are reloaded into their original radial locations. Under these conditions, entry plane nuclide densities are simple functions of the values at the exit plane with fresh fuel densities replacing those of pebbles to be discharged. The entry plane burnup for a randomly-reloaded core can be approximated using the following one-dimensional treatment.

The equation for the entry-plane burnup is found by following the accumulation of burnup in a single pebble as it makes repeated trips through the core. If a pebble is removed when its burnup exceeds the cutoff value B_{max}, and m_{max} trips through the core are required for this, then it is found that the average burnup of the mixture of recirculated and new pebbles at the entry plane is

$$\overline{B}_o = \frac{1}{m_{\max}} \sum_{m=1}^{m_{\max}-1} B_H^m \qquad \textbf{2.6}$$

where B_H^m is the burnup of an individual pebble at the end of its m^{th} pass (after traversing a core of height H). This equation relies on the observation that the number of pebbles in any core layer which are making their m^{th} pass is the same for all m less than or equal to m_{max}.

An approximate value for m_{max} can be found from the core thermal power, P, and the number of pebbles in the core, n_p, as Eq. **2.7**,

$$m_{\max} \geq \frac{B_{\max} v m_p n_p}{PH}, \qquad \textbf{2.7}$$

where

B_d is the threshold discharge burnup (MWD/kg_{ihm}),

v = the mean axial pebble speed (m/day),

m_p = the mass (kg) of heavy metal in a fresh pebble,

n_p = the number of such pebbles in the core,

P = the core power (MW), and

H = the height (m) of the core.

Because pebbles can only be extracted from the core at the exit plane, the value computed by Eq. **2.7** must be rounded up to the next integer.

The values of $B^{(m)}$ are found in terms of the number density, N, of fuel nuclei:

$$B = (N_o - N)A \quad . \tag{2.8}$$

By following the consumption of fuel nuclei in a pebble during successive passes through the core, and applying Eq. **2.8,** one finds that

$$B^m(H) = N_o A\left\{1-\exp\left[\frac{-m\sigma_f}{w}\int_{z=0}^{H}\phi(z)dz\right]\right\} \tag{2.9}$$

and

$$\overline{B}_o = \frac{N_o A}{m_{\max}}\sum_{m=1}^{m_{\max}-1}\left\{1-\exp\left[\frac{-m\sigma_f}{w}\int_{z=0}^{H}\phi(z)dz\right]\right\} \tag{2.10}$$

The random reloading pattern is actually a good approximation of the HTR Modul 200 design in which there is only one path for discharge and loading of pebbles into the core. However, if multiple pathways for loading and discharge are present, radially-dependent reloading of pebbles of various types and various stages of burnup is

possible. A more general method for the computing radially-dependent entry-plane burnup is needed. Such a method is introduced in Chapter 3.

2.6 PBR Design and Optimization Considerations

Powerful tools have been developed for performing optimization of nuclear reactor fuel cycles. Such methods and tools will not be described here because they are generally not applicable to the PBR. Fuel cycle optimization in a light water reactor involves finding the most effective distribution of fuel assemblies and burnable poisons within those assemblies to safely maximize the length of a cycle. The fundamental goal of PBR optimization is similar: minimize the cost of the fresh fuel required to safely operate the power plant at the desired power level. In a nutshell, this means either reducing the enrichment or mass of the fuel to be loaded, and to load it in such a manner as to keep the fuel temperature within an acceptable range. Particle degradation and fission product release becomes significant at temperatures above 1,800℃ [62] so the distribution of the fissile inventory, flux, and coolant must be tuned to avoid local fuel temperature peaks [63].

In the recirculating PBR, fuel is loaded while the reactor is operating and in such small increments that for all practical purposes it can truly be considered continuous. There is no need to build in excess reactivity into the fresh fuel and thus no need to use burnable poisons or control rods to hold down this reactivity. Because each fuel element spends roughly equal amounts of time in all axial zones, the need to use burnable poisons to shape the axial power profile, as is done in PWR fuel assemblies, is also eliminated.

Burnable poisons have been proposed for PBRs, particularly for OTTO [64] or so-called peu-à-peu cycles. In OTTO (once-through-then-out) cores, the fuel must move an order of magnitude more slowly than in recirculating cores in order to extract an economically feasible amount of energy from each pebble. In the peu-à-peu core, a very tall reactor vessel is partially loaded with pebbles. Fresh pebbles are simply added to the top of the bed to maintain power and criticality. This continues until the vessel is filled. In both cases, the difference in the average burnup between pebbles at the top and bottom of the core is so great that the axial power peak is amplified and shifted toward the top. Burnable poisons have been proposed to push this peak down and back toward the center. The use of these poisons necessarily reduces the neutron economy of the core. They do represent an interesting option for PBRs but will not be examined in this study.

The graphite blocks that serve as both a container for the pebbles and as a neutron reflector also protect the outer pressure vessel from excessive damage caused by fast neutrons. This reduces the need to load fuel in such a way as to reduce fast fluence at the periphery. The blocks also act as a large heat sink that is able to absorb much of the decay heat of the core during an accident.

Unlike light water reactors, options for loading fuel in a PBR are strongly dependent upon the fuel loading mechanism itself. In the LWR, the vessel head is removed providing access to each fuel assembly in its entirety. In theory, each fuel assembly can be transposed with any other or replaced with a new assembly. In the PBR, fuel elements are dropped onto the top surface of the pebble-bed through one or more loading tubes. In the simplest designs, a single centrally located tube is used so that the dropped pebbles form a cone throughout which they are randomly distributed. Not much ‘in-core’ fuel management can be performed. Fuel elements are not accessible until they drop out of the bottom discharge tube(s). Because of this feature,

the complexity of the fuel management problem in PBRs is very much a function of the design of the pebble handling mechanism.

In a recirculating core, partially-burned pebbles are reintroduced to the top of the pebble-bed along with fresh pebbles. Any local region of the core contains pebbles at various stages of burnup. This novel approach to fuel management lends itself to optimization in a way that is very different than what can be accomplished with batch-loaded cores. Figure **2-13** shows three different fueling schemes that have been proposed for PBRs. The left figure shows a simple single-zone, single-pebble-type core. The central figure shows a two-zone core in which pebbles of one type are loaded into a central column while pebbles of the other type are loaded into the surrounding annulus. In the right figure, only one pebble type is used but its recirculation is burnup-dependent. Fresh pebbles are loaded into the outer annulus for one or more passes before being transferred to the central zone to finish out the remainder of their lives.

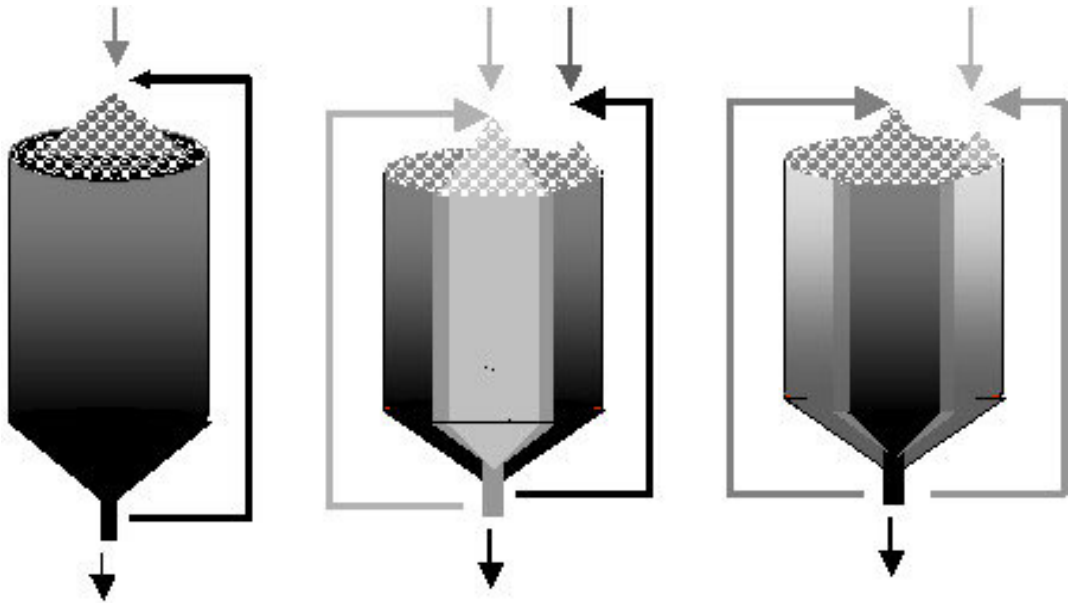

Figure **2-13**: Some fuel loading options in a PBR.

The local population of pebbles within a given burnup range is a function of the flexibility of the loading mechanism and the desired fuel recirculation policy. For this reason, a PBR fuel management/core analysis code system must possess a means of prescribing the pebble flow scheme in a way that is amenable to optimization routines.

Once this has been achieved, any one of a number of sophisticated optimization methods can be applied. The one chosen for this work is the *Genetic Algorithm*.

2.7 Genetic Algorithm Optimization

2.7.1 Stochastic Optimization

Genetic algorithms [65] are a type of *stochastic* optimization. Stochastic methods sample a wide variety of solutions and then focus on ones that satisfy increasingly stringent criteria. Simulated Annealing is another type of stochastic approach. Traditional linear optimization techniques rely on local gradients to minimize or maximize a function and thus may yield only a local optimum. Stochastic methods by contrast possess a random search component that allows the search to explore other regions of the variable space. This random search component greatly increases the chance of locating the global optimum.

A major drawback with stochastic methods is the significant number of calculations that must be performed in order to locate the global optimum with reasonable confidence. Each sampled solution requires running a core analysis code to evaluate the objective function (k_{eff}, power peaking, etc.) and can mean prohibitively long computer time. One way around this obstacle is to bias the search by eliminating known sub-optimal regions from the searchable space (heuristics or expert knowledge). Parks

[66] used the former when applying the simulated annealing approach to optimize a fuel stringer in a British Advanced Gas Reactor (AGR). An AGR typically contains over 300 such stringers that are replaced regularly while the reactor is running. Optimization means reducing the net cost of the assembly by adjusting, among other parameters, the enrichment and burnable poison loading. Knowledge acquired from previous AGR experience was used to filter out poor solutions before the simulated annealing routine had a chance to sample them. Mahlers [67] used simulated annealing to place assemblies then used linear programming to place burnable poisons.

Kropaczek and Turinsky [68] developed a fuel management procedure based upon a method known as *simulated annealing*. This method is modeled upon the process of a slowly cooling solid in which particles in the solid attempt to reach the lowest energy state. The method works by starting at an initial state and moving in small random steps until an optimum state is reached as measured by the value of an objective function. If the step improves the value, the step is accepted. If not, there is a chance that the step may still be accepted. The probability of acceptance depends upon the system *temperature*, an analog of the actual temperature of a cooling solid (Eq. **2.11**).

$$\text{Prob}(E) \propto \exp(-E / kT) \qquad \textbf{2.11}$$

This probabilistic element allows the system to climb away from a local minimum and continue towards a global minimum. In the algorithm, the initial temperature is high, allowing the system to freely sample a number of possible states. As the calculation progresses, then temperature is lowered so that the solution converges to a (hopefully) global minimum.

A full discussion and application of the various stochastic methods is beyond the scope of this work. Rather, it is the objective of this research to demonstrate how such methods can be used successfully in PBR core design. Future studies can and should explore the merits of different optimization schemes. As genetic algorithms are the method employed in this work, some background information is necessary.

2.7.2 Genetic Algorithm Basics

Genetic Algorithms have been used for a wide variety of optimization applications, including LWR fuel cycle optimization. Genetic Algorithms (GAs) differ from simulated annealing in that while both incorporate small random perturbations (mutations) in searching for better solutions, GAs retain information about a solution that can direct the next step. The problem starts by coding the important attributes (genes) of the system either as a binary word (i.e., a series of zeros and ones) or as real numbers. A ‘net’ is cast over the domain of the solution space by randomly generating the genes for a specified number (population) of ‘individuals’. Genotypes (e.g., core attributes) that produce favorable ‘traits’ (e.g., acceptable peak fuel temperature and/or fast fluence near the pressure vessel) are passed along to the next generation. An overall fitness value is generated for each individual core design based upon a user-specified function of the traits. In a process called *selection*, a specified fraction of the population with the highest fitness values are allowed to ‘survive’ and form the gene pool for the next generation. Attributes of two randomly chosen survivors are mixed to form two new individuals in a *crossover* process that is mathematically analogous to genetic breeding. The population is thus rebuilt from the fittest individuals and the process is repeated. The selection and crossover processes alone may, however, lead to a loss in population

diversity and converge to a local fitness maximum. Therefore, a third process, *mutation* is employed. This low probability event involves changing the gene of an individual to a randomly chosen new value within the variable domain. In this way, the search is directed toward previously unexplored regions of the solution space that may yield better local, and hopefully a global, optima.

Finding a global optimum nestled within a large number of local optima more than a brute force random search. In a genetic algorithm, search refinement is achieved using 'mutation' and 'cross-over' processes. In mutation, there is a small (say, 1 in 10^4) possibility that a bit in the string will be arbitrarily changed to the opposing value. This does not advance the search for a solution but it does prevent the development of a uniform population unable to 'evolve'. Crossover refers to the exchange of subsets of two strings in which the favorable parts of two parent strings are combined to produce an offspring that contains both, as illustrated in Figure **2-14**.

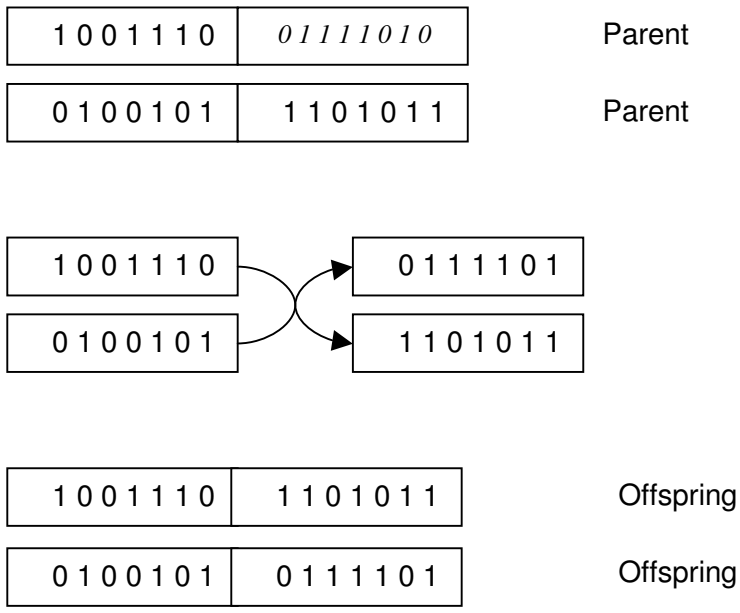

Figure **2-14**: 8-bit binary crossover operation.

In real-coded genetic algorithms, population characteristics are stored as real variables rather than binary words. Crossover may result in the direct transposition of genes from the parents but it also may result in a hybrid, i.e., a weighted average of the genes of the parents. A wide variety of “crossover operators” have been proposed and employed in different optimization routines.

Crossover does not guarantee that the offspring solution will be superior but it does focus the search algorithm on regions that have a higher concentration of favorable attributes. The three attributes of selection, mutation, and crossover are direct analogs of biological reproduction with recombinant DNA.

Because of the ease of use and effectiveness, genetic algorithms have been the subject of much study and broad application. A full review of these efforts is beyond the scope of this thesis and would not improve upon some definitive work already completed. Goldberg [70] in particular provides a comprehensive text on the theory and practice of genetic algorithms as well as a list of authors of many of the early developments in the field.

2.7.3 Genetic Algorithms in LWR Fuel Management

Poon and Parks [71] replaced a simulated annealing routine in the FORMOSA code with a genetic algorithm. They observed that the GA was superior in narrowing down the initial global search but that the simulated annealing algorithm converged on the local solution more quickly. This conclusion was consistent with belief that GAs are efficient for locating the region in which a global solution resides, but other techniques are better for ‘pin-pointing’ the exact optimal point. The authors did conclude that the Generalized Perturbation Theory they used to accelerate the GA process effectively (in

place of a full core analysis) limited the ability of the algorithm to converge quickly on the optimum.

Initial work with GAs indicated the promise of the technique even though not all of these attempts yielded success. Parks extended the work to multi-objective optimization to simultaneously maximize EOC boron concentration and discharge burnup while minimizing power peaking. DeChaine and Feltus developed a bit-base GA system (CIGARO) to represent the k_∞ map in a $1/8^{th}$ core model that is able to work with any reactor physics code [72]. They then accelerated the search by incorporating expert knowledge to bias the 'genotype encoding' in a PWR optimization problem [73]. Yamamoto used a hybrid GA search for the global optimal fuel and burnable poison loading then performed local optimization on fuel assembly rotations [74]. Martín del Campo applied the system to BWR fuel assembly axial optimization [75].

The GA technique has emerged as a powerful tool for LWR in-core fuel management. In this work, it is applied to the problem of pebble-bed reactor core design and fuel management

Chapter 3

Modeling Pebble Bed Cores with PEBBED

3.1 PEBBED

The PEBBED code was developed by the author to solve for the asymptotic loading pattern in a pebble-bed reactor using the method proposed by Terry, et al. [6] For the flux distribution, PEBBED solves the one, two, and three-dimensional finite difference approximations to the diffusion equation (Appendix A). The outer boundary condition is that of non-re-entrant current in the formulation described by Stamm'ler and Abbate [76]. Work is underway at the INEEL to replace this solver with a three-dimensional analytical nodal solution [77]. The semi-analytical solution to the depletion equations used in PEBBED is detailed in Appendix B and is based upon the formulation presented by Benedict, et al. [78]. The neutronics solver was tested using simple reactor models for which analytical solutions exist. These solutions and a comparison of computational and analytical results are given in Appendix D.

Currently, PEBBED assumes that pebble flow is strictly axial so that the mesh cells over which the depletion equation is solved are the same as the diffusion equation cells. The algorithm does allow for radially varying pebble velocities.

The computational flow of the code is illustrated in Figure 3-1.

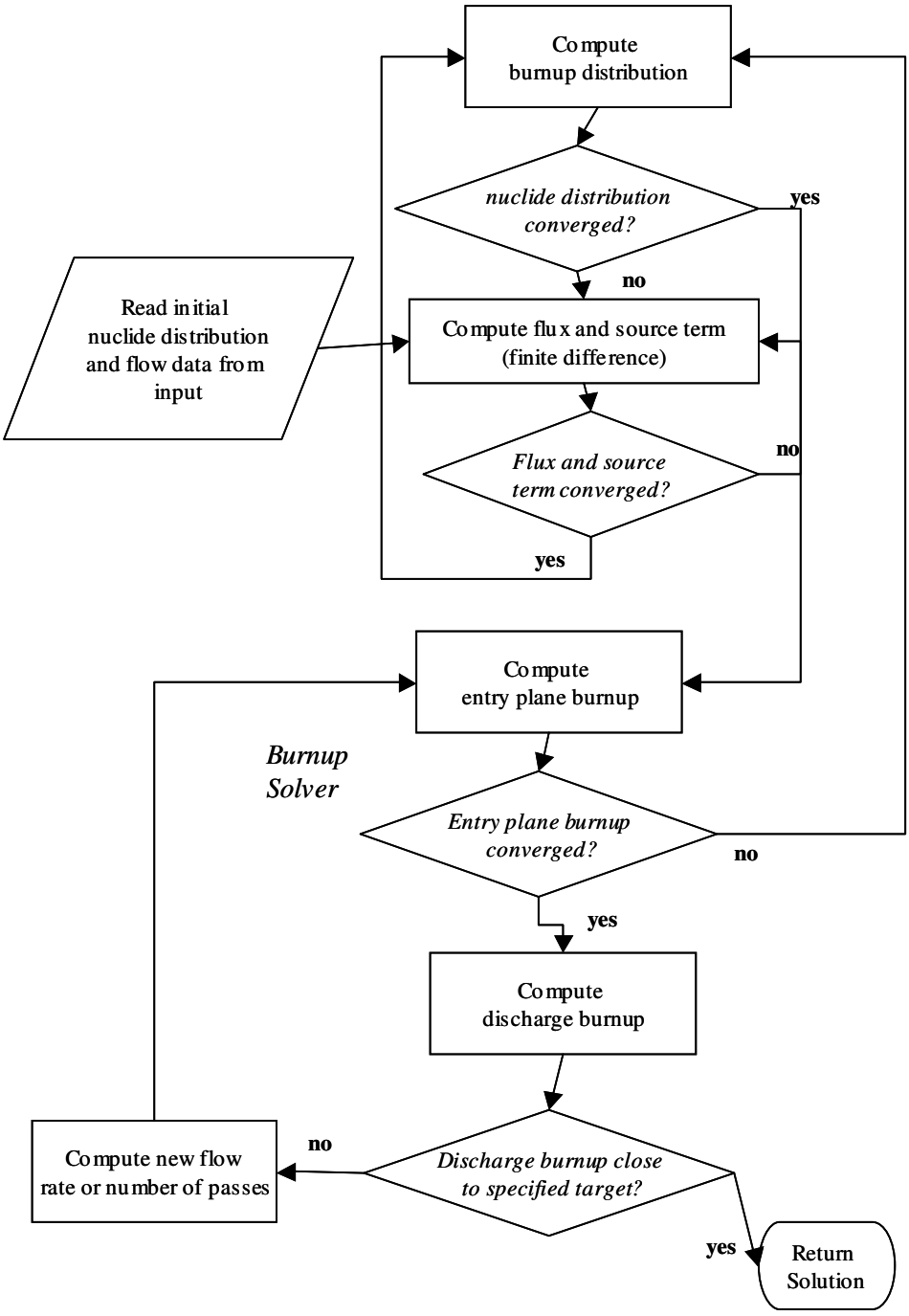

Figure 3-1: Computational flow in PEBBED version 3.

A key feature of the code is its ability to solve for the entry plane burnup for an arbitrary, user-defined recirculation pattern. It achieves this solution through the use of a matrix formulation for the recirculation of pebbles. This formulation was introduced by the author in reference [79] is described in detail below.

3.2 Matrix Representation of Recirculation in PEBBED

The PEBBED code currently assumes axial flow and thus the streamlines correspond to concentric cylinders or flow *zones* (Figure **3-2)**.

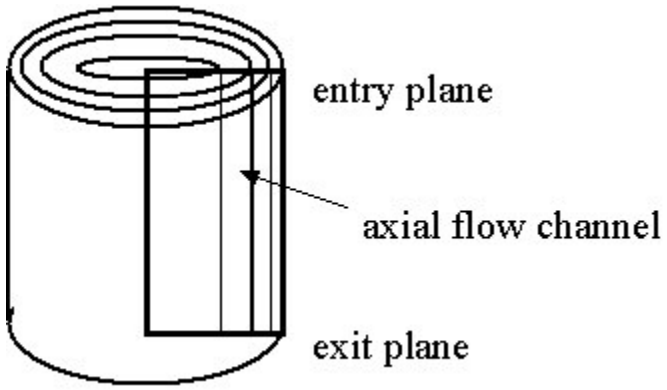

Figure **3-2**: Radial zoning of pebble flow.

The average value for the density of a nuclide at the entry plane of a zone is computed from the densities in each of the pebbles that are loaded into that zone. These pebbles will differ in composition based upon the initial material loading (pebble type) and previous history (trajectory) in the core. The rate at which pebbles of different types and burnups are loaded into a zone is a function of the recirculation scheme.

3.2.1 Recirculation Matrix Nomenclature

Before proceeding with the derivation, it is helpful to define some of the variables to be used.

General

- A curved "hat" (^) over an *N* refers to a *pebble* nuclide density
- No hat refers to a *zone average* nuclide density
- A ~~strike~~ through *N* refers to an *exit* plane value (leaving the core)
- No strike refers to an *entry* plane value (entering the core).

Specific

$\dot{n}_i$ Nuclide flow rate (atoms/sec) into zone *I*

N_i Mean entry plane density in *i*th zone

${}^m\widehat{\bar{N}}_j^p$ Exit plane nuclide density in pebble of type type *p*, on pass *m*, in zone *j*

${}^mN_j^p$ Zone—averaged entry plane nuclide density in pebble of type type *p*, on pass *m*, in zone *j*

N_j^p Zone—averaged entry plane nuclide density in pebble of type type *p*, in zone *j*, from all passes

M Maximum number of passes per pebble (core mean)

P Total number of pebble types

J Total number of zones

F Total core pebble flow rate (cm^3/sec)

f_i Flow rate in zone *i* (cm^3/sec)

f_i^p Flow rate of type *p* in zone *i*

${}^{m}f_i$ Flow rate of pebbles on pass *m* on zone *i*

${}^{m}f_i^{p}$ Flow rate of pebbles of type *p,* on pass *m* in zone *i.*

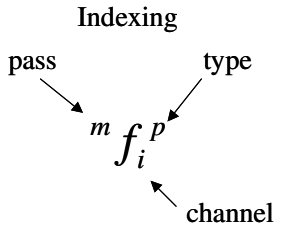

If a quantity is missing one or more indices, then it is assumed that the quantity indicates the *sum over all units* specified by the missing index; e.g., ${}^{m}f_i$ refers to the flow rate into zone *i* of *m*th pass pebbles of *all* pebble types.

The flow of nuclide units (e.g., atoms) into a zone is denoted as:

${}^{m}\dot{n}_i^{p}$ = atoms/sec of a nuclide flowing into zone *I* that are constituents of pebbles of type *p* and are starting their *m*th pass.

This is a *zone* flow rate. It is related to the nuclide density in the *pebbles* (smeared over the effective pebble volume). To relate the zone flow rate to the atom density of the nuclide within a pebble, one must account for the fact that only a fraction of the flow in zone *i* may be of type *p*, and only a fraction of the flow is undergoing its *m*th pass. Define the *partition coefficients*:

$\alpha_i = \frac{f_i}{F}$ (fraction of core flow in that is in zone *I*)

$\alpha_i^{p} = \frac{f_i^{p}}{f_i}$ (fraction of flow in *I* that consists of type *p* pebbles)

${}^{m}\alpha_i^{p} = \frac{{}^{m}f_i^{p}}{f_i^{p}}$ (fraction of type *p* flow in *i* that consists of pebbles on pass *m*)

${}^{m}\alpha_{ij}^{p} = \frac{{}^{m}f_{i\leftarrow j}^{p}}{{}^{m}f_{j}^{P}}$ (fraction of flow of pebbles of type *p*, on pass *m*, in zone *j* that is diverted to *i*).

3.2.2 Pebble Flow in a Channel

The flow rate of a nuclide into zone *i* due to pebbles of type *p* starting their *m*th pass is related to the nuclide density in the pebble by Eq. **3.1:**

$$\begin{aligned} {}^{m}\dot{n}_{i}^{p} &= {}^{m}\widehat{N}_{i}^{p} \cdot f_{i} \cdot \frac{f_{i}^{p}}{f_{i}} \cdot \frac{{}^{m}f_{i}^{p}}{f_{i}^{p}} \\ &= {}^{m}\widehat{N}_{i}^{p} \cdot f_{i} \cdot \alpha_{i}^{p} \cdot {}^{m}\alpha_{i}^{p} \end{aligned} \qquad \textbf{3.1}$$

To obtain the total flow of a nuclide into zone I, sum over *M* passes and *J* types (Eq. **3.2)**

$$\sum_{p=1}^{P}\sum_{m=1}^{M} {}^{m}\dot{n}_{i}^{p} = \dot{n}_{i} = N_{i} f_{i} \qquad \textbf{3.2}$$

Substitute Eq. **3.2** into Eq. **3.1** to obtain an expression for the total flow rate of the nuclide in terms of the contributions from all pebbles and passes (Eq. **3.3)**.

$$\dot{n}_{i} = \sum_{p=1}^{P}\sum_{m=1}^{M} {}^{m}\dot{n}_{i}^{p} = \sum_{p=1}^{P}\sum_{m=1}^{M} {}^{m}\widehat{N}_{i}^{p} f_{i} \cdot \alpha_{i}^{p} \cdot {}^{m}\alpha_{i}^{p} \qquad \textbf{3.3}$$

The flow of a nuclide into zone *i* is composed of contributions from the zone exit plane flows (except for the last pass) and the fresh pebble injection flow rate given by ${}^{1}n_{1}^{p} = {}^{1}\widehat{N}_{1}^{p\,1} f_{1}^{p}$,

$$
\begin{aligned}
{}^{m+1}\dot{n}_i^p &= \sum_{j=1}^{J} {}^{m}\dot{n}_j^p \cdot {}^{m}\alpha_{ij}^p \qquad (m = 1 \ldots M-1) \\
&= \sum_{j=1}^{J} \left({}^{m}\widehat{N}_j^p \cdot f_j \cdot \alpha_j^p \cdot {}^{m}\alpha_j^p \right) {}^{m}\alpha_{ij}^p
\end{aligned}
\tag{3.4}
$$

Now sum this over all passes *m* (except for the last pass), add the fresh flow contribution, and sum over all pebble types *p* to get the total flow of the nuclide into the zone:

$$
\sum_{p=1}^{P} \sum_{m=1}^{M} {}^{m}\dot{n}_i^p = \sum_{p=1}^{P} \left\{ {}^{1}\dot{n}_i^p + \sum_{j=1}^{J} \sum_{m=1}^{M-1} {}^{m}\widehat{N}_j^p \cdot f_j \cdot \alpha_j^p \cdot {}^{m}\alpha_j^p \cdot {}^{m}\alpha_{ij}^p \right\} \tag{3.5}
$$

Using Eq. **3.2** equate this to the RHS of Eq. **3.5** to get:

$$
N_i \cdot f_i = \sum_{p=1}^{P} \left\{ {}^{1}\widehat{N}_i^p \, {}^{1}f_i^p + \sum_{j=1}^{J} \sum_{m=1}^{M-1} {}^{m}\widehat{N}_j^p \cdot f_j \cdot \alpha_j^p \cdot {}^{m}\alpha_j^p \cdot {}^{m}\alpha_{ij}^p \right\} \tag{3.6}
$$

and thus

$$
N_i = \frac{1}{f_i} \sum_{p=1}^{P} \left\{ {}^{1}\widehat{N}_i^p \, {}^{1}f_i^p + \sum_{j=1}^{J} \sum_{m=1}^{M-1} {}^{m}\widehat{N}_j^p \cdot f_j \cdot \alpha_j^p \cdot {}^{m}\alpha_j^p \cdot {}^{m}\alpha_{ij}^p \right\} \tag{3.7}
$$

The denominator can be brought inside the sums and noting that

$$
{}^{1}f_i^p = {}^{1}\alpha_i^p \cdot \alpha_i^p \cdot f_i \tag{3.8}
$$

then

$$
N_i = \sum_{p=1}^{P} \left\{ \frac{{}^{1}\widehat{N}_i^p \, f_i \, {}^{1}\alpha_i^p \alpha_i^p}{f_i} + \sum_{j=1}^{J} \sum_{m=1}^{M-1} {}^{m}\widehat{N}_j^p \cdot \frac{f_j}{f_i} \cdot \alpha_j^p \cdot {}^{m}\alpha_j^p \cdot {}^{m}\alpha_{ij}^p \right\} \tag{3.9}
$$

Finally, given that

$$\frac{f_j}{f_i} = \frac{\frac{f_j}{F}}{\frac{f_i}{F}} = \frac{\alpha_j}{\alpha_i} \qquad \textbf{3.10}$$

one can write

$$N_i = \sum_{p=1}^{P} \left\{ {}^{1}\hat{N}_i^p \cdot {}^{1}\alpha_i^p \cdot \alpha_i^p + \sum_{j=1}^{J} \sum_{m=1}^{M-1} {}^{m}\hat{N}_j^p \cdot \frac{\alpha_j \cdot \alpha_j^p \cdot {}^{m}\alpha_j^p \cdot {}^{m}\alpha_{ij}^p}{\alpha_i} \right\} \qquad \textbf{3.11}$$

Eq. **3.11** is the expression relating the nuclide density in *pebbles* from zones *j*, passes *m*, and types *p*, to the overall *zone* nuclide density in zone *i*. The inner-bracketed term is thus the decomposed recirculation matrix element ${}^{m}r_{ij}^{p}$

$${}^{m}r_{ij}^{p} = \frac{\alpha_j \cdot \alpha_j^p \cdot {}^{m}\alpha_j^p \cdot {}^{m}\alpha_{ij}^p}{\alpha_i} \qquad \textbf{3.12}$$

This matrix element weights the contributions from the exit plane nuclide densities on zone, pebble type, and pass (burnup) basis to yield an overall entry plane zone nuclide density.

The partition coefficients, α_j, α_j^p, ${}^{m}\alpha_j^p$ and ${}^{m}\alpha_{ij}^p$, are functions of the core geometry and/or the pebble loading and recirculation policy. The fraction of total core flow in zone *j* (α_j) is a function of the total core dimensions and the mechanics of pebble motion which can be considered fixed for a given core design. The pebble type fraction per zone (α_j^p) and the transfer coefficient (${}^{m}\alpha_{ij}^p$) are both functions of the pebble loading mechanism. These may be considered to have user-specified values in that they can be altered either in the core design process or, if the design allows, during operation. The

remaining coefficient, the fraction of pebbles of type *p* on pass *m* ($^{m}\alpha_{j}^{p}$), is now shown to be a function of the other coefficients.

Except for $m = 1$ (fresh pebbles), the flow rate of pebbles of type *p* starting their m^{th} pass in zone *i* is given by:

$$
\begin{aligned}
{}^{m}f_{i}^{p} &= F \cdot \frac{f_i}{F} \cdot \frac{f_i^p}{f_i} \cdot \frac{{}^{m}f_i^p}{f_i^p} \\
&= F \cdot \alpha_i \cdot \alpha_i^p \cdot {}^{m}\alpha_i^p
\end{aligned}
\qquad \textbf{3.13}
$$

Here, f denotes the pebble flow rate (pebbles/sec) rather than the volumetric flow rate. Likewise, *F* denotes the total core pebble flow rate. The two rates are directly proportional if one assumes that the effective pebble volume (pebble plus surrounding coolant space) is constant.

Note that PEBBED assumes that the distribution of pebbles *within* a channel is homogeneous. This assumption may lead to error in cores that have radially-varying entry plane composition. For example, a core composed of an inner column of graphite pebbles surrounded by an outer annulus of fuel pebbles contains a narrow region (about 30 cm) that contains both. The distribution of graphite and fuel pebbles in this region varies smoothly from all graphite on the inner boundary to all fuel on the outer. By assuming that the mixing zone is a homogeneous mixture, the neutronic effect of this smooth transition is lost. Preliminary study by the author indicates that this effect is minor. Nonetheless, further study should be performed to confirm this.

3.2.3 Flow Contributions from Recirculated Pebbles

Eq. **3.13** reflects how the channel flow rate is evaluated from that of pebbles completing the *m-1*th pass:

$$ {}^{m}f_i^p = \sum_{j=1}^{J} F \cdot \alpha_j \cdot \alpha_j^{p\,\cdot m-1} \alpha_j^{p\,m-1} \alpha_{ij}^p \qquad \textbf{3.14} $$

Equating Eq. **3.13** and Eq. **3.14** and eliminating the total core flow rate *F* yields:

$$ \alpha_i \cdot \alpha_i^{p\,\cdot m} \alpha_i^p = \sum_{j=1}^{J} \alpha_j \cdot \alpha_j^{p\,\cdot m-1} \alpha_j^{p\,m-1} \alpha_{ij}^p \qquad \textbf{3.15} $$

Solve for ${}^{m}\alpha_j^p$ to get

$$ {}^{m}\alpha_i^p = \frac{\sum_{j=1}^{J} \alpha_j \cdot \alpha_j^{p\,\cdot m-1} \alpha_j^{p\,m-1} \alpha_{ij}^p}{\alpha_i \cdot \alpha_i^p} \qquad \textbf{3.16} $$

This indicates that each pass-type partition coefficient ${}^{m}\alpha_j^p$ is a function of ${}^{m-1}\alpha_j^p$ *(j*=1..*J)*. Equation Eq. **3.16** is valid for *m* = 2…*M*, i.e., all recirculated pebbles. To obtain a fully determined set of linear equations, one more expression involving these coefficients is needed. This expression is obtained from the fact that, by definition, the sum of ${}^{m}\alpha_j^p$ over all passes *m* is unity.

$$ \sum_{m=1}^{M} {}^{m}\alpha_j^p = 1 \quad \text{for all } j,p \qquad \textbf{3.17} $$

The system of equations is more obvious if one substitutes the following into Eq. **3.16**. Let

$$ {}^{m-1}K_{ij}^p = \frac{\alpha_j \cdot \alpha_j^{p\,\cdot m-1} \alpha_{ij}^p}{\alpha_i \cdot \alpha_i^p} \qquad \textbf{3.18} $$

so that

$$ {}^{m}\alpha_i^p = \sum_{j=1}^{J} {}^{m-1}K_{ij}^p \cdot {}^{m-1}\alpha_j^p \qquad \textbf{3.19} $$

Or, cast as a linear equation with constant coefficients,

$$ {}^{m}\alpha_i^p - {}^{m-1}K_{i1}^{p}\cdot{}^{m-1}\alpha_1^p - {}^{m-1}K_{i2}^{p}\cdot{}^{m-1}\alpha_2^p \ldots - {}^{m-1}K_{iJ}^{p}\cdot{}^{m-1}\alpha_J^p = 0 \quad . \qquad \textbf{3.20} $$

Combining Eq. **3.20** with Eq. **3.17** yields the following system of linear equations of order $J \bullet M_x$

$$
\begin{bmatrix}
1 & 1 & 1 & \cdots & 1 & 0 & \cdots & & & 0 & \cdots & 0 & \cdots & & & 0 \\
-{}^{1}K^{p}_{1,1} & 1 & 0 & \cdots & 0 & -{}^{1}K^{p}_{1,2} & & & & & & -{}^{1}K^{p}_{1,J} & & & & 0 \\
0 & -{}^{2}K^{p}_{1,1} & 1 & 0\cdots & 0 & 0 & \ddots & & & & & \vdots & \ddots & & & 0 \\
\vdots & & \cdots & \ddots & \vdots & \vdots & & & & & & & & & & 0 \\
0 & & \cdots & -{}^{M-1}K^{p}_{1,1} & 1 & 0 & \cdots & 0 & -{}^{M-1}K^{p}_{1,2} & 0 & \cdots & 0 & \cdots & 0 & -{}^{M-1}K^{p}_{1,J} & 0 \\
\hdashline
0 & 0 & \cdots & & 0 & 1 & 1 & 1 & \ldots & 1 & \cdots & 0 & \cdots & & & 0 \\
-{}^{1}K^{p}_{2,1} & 0 & \cdots & & 0 & -{}^{1}K^{p}_{2,2} & 1 & 0 & \ldots & 0 & & -{}^{1}K^{p}_{2,J} & & & & 0 \\
0 & -{}^{1}K^{p}_{2,1} & \cdots & & 0 & 0 & & 1 & & \vdots & & 0 & \ddots & & & 0 \\
\vdots & & \ddots & & & \vdots & & & \cdots & 0 & & \vdots & & & & 0 \\
0 & & \cdots & -{}^{M-1}K^{p}_{2,1} & 0 & 0 & \cdots & 0 & -{}^{M-1}K^{p}_{2,2} & 1 & \cdots & 0 & \cdots & 0 & -{}^{M-1}K^{p}_{2,J} & 0 \\
\hdashline
\vdots & & & & & \vdots & & & & & \vdots & \vdots & & & & \vdots \\
\hdashline
0 & 0 & \cdots & & & 0 & & \cdots & & 0 & \cdots & 1 & 1 & & \cdots & 1 \\
-{}^{1}K^{p}_{J,1} & & & & & -{}^{1}K^{p}_{J,2} & & & & \vdots & & -{}^{1}K^{p}_{J,J} & 1 & & & \\
0 & \ddots & & & & 0 & \ddots & & & & & 0 & & 1 & & \\
& & & & & \vdots & & & & & & \vdots & & & \ddots & \vdots \\
0 & & \cdots & -{}^{M-1}K^{p}_{J,1} & 0 & 0 & & \cdots & -{}^{M-1}K^{p}_{J,2} & 0 & \cdots & 0 & \cdots & 0 & -{}^{M-1}K^{p}_{J,J} & 1
\end{bmatrix}
\begin{bmatrix}
{}^{1}\alpha^{p}_{1} \\
{}^{2}\alpha^{p}_{1} \\
\vdots \\
\\
{}^{M}\alpha^{p}_{1} \\
{}^{1}\alpha^{p}_{2} \\
{}^{2}\alpha^{p}_{2} \\
\vdots \\
\\
{}^{M}\alpha^{p}_{2} \\
\vdots \\
{}^{1}\alpha^{p}_{J} \\
{}^{2}\alpha^{p}_{J} \\
\vdots \\
\\
{}^{M}\alpha^{p}_{J}
\end{bmatrix}
=
\begin{bmatrix}
1 \\ 0 \\ 0 \\ \vdots \\ 0 \\ 1 \\ 0 \\ 0 \\ \vdots \\ 0 \\ 1 \\ 0 \\ 0 \\ \vdots \\ 0
\end{bmatrix}
\qquad \textbf{3.21}
$$

3.2.4 Order of the Recirculation Matrix

The coefficients *K* are unique and known for a specified recirculation scheme. The pass-type partition coefficients, ${}^{m}\alpha_{j}^{p}$, can thus be computed off-line using a standard matrix inversion algorithm. This system is solved separately for each pebble type *p*. Because of this independence, different recirculation trajectories can be assigned to each pebble type. Sophisticated fuel management schemes not available to batch-loaded reactor cores are thus possible.

This fully decomposed expression for the recirculation matrix element indicates the sensitivity of entry plane density to various partitioning schemes (i.e., pebble recirculation rules). It also lends itself to sophisticated optimization algorithms. The partition coefficients, $\left(\alpha_{j}^{p}, {}^{m}\alpha_{ij}^{p}\right)$, may form part of the solution space over which the search is performed.

The number of partition coefficients to be computed depends upon the complexity of the fueling pattern. The number of flow partition coefficients is equal to the number of flow channels *J* specified by the user. The number of type partition coefficients is equal to the product of *J* and the number of pebble types specified, *P*. The number of pass partition coefficients for a given pebble type is equal to the product of *J* and the maximum number of passes *M* computed for that pebble type. The number of transfer partition coefficients for each pebble type is equal to J^2*M. For example, the HTR Modul 200 can be modeled with a single flow channel ($J = 1$) and uses only one type of pebble ($P = 1$). Each pebble traverses the core 15 times ($M = 15$). Thus, the number of flow partition coefficients is one, as is the number of type partition coefficients.

The number of pass partition coefficients is 1*1*15 = 15, and the number of transfer partition coefficients is 1*1*1*15 = 15.

The PBMR core model used extensively in this work contains five flow channels and two pebble types. Graphite pebbles are assumed to pass through the core only once (because they accrue no burnup a fresh graphite pebble is neutronically identical to a recirculated one) while the fuel pebbles each traverse the core ten times. Thus, the number of flow coefficients is 5, the number of type coefficients is 10, the number of pass coefficients for the graphite and fuel pebbles is 5 and 50, respectively. The number of transfer coefficients for the graphite and fuel pebbles is 25 and 250, respectively.

At first glance, the number of partition coefficients needed to accurately describe a given design may look unwieldy and not amenable to efficient design. In Chapter 4, however, a number of examples will be used to demonstrate that all of the coefficients can be generated easily from a handful of core parameters.

3.2.5 Validity of Values

The coefficients are all assumed to be real numbers on the closed interval [0,1] and thus there is an infinite number of possible values. However, only sets that conserve pebble flow are candidates for valid recirculation matrices. Regardless of the values chosen for the elements of the recirculation matrix, total recirculated nuclide flow into or out of a zone must sum to the fraction of the core flow in the zone less the fresh injection flow rate. The following relations must hold:

$$\sum_{m=1}^{M-1}\sum_{j=1}^{J} {}^{m}r_{ij}^{p} = \alpha_i^p\left(1-{}^{1}\alpha_i^p\right) \qquad \textbf{3.22}$$

which states that flow of type *p* diverted from all zones to *i* must sum to the fraction of the total flow of type *p* that is recirculated,

$$\sum_{p=1}^{P}\sum_{m=1}^{M-1}\sum_{j=1}^{J} {}^{m}r_{ij}^{p} = 1-\sum_{p=1}^{P} {}^{1}\alpha_{i}^{p} \qquad \textbf{3.23}$$

which states that the total flow diverted from all zones to *i* must sum to recirculated flow fraction of *i,*

$$\sum_{m=1}^{M-1}\sum_{i=1}^{J} {}^{m}r_{ij}^{p}\alpha_{i} = \alpha_{j}^{p}\alpha_{j}\left(1-{}^{1}\alpha_{j}^{p}\right) \qquad \textbf{3.24}$$

which states that the flow of type *p* diverted from zone *j* to other zones must sum to the recirculated flow fraction of *p* in *j,* with ${}^{1}\alpha_{j}^{p}$ being the fraction of *p*-type pebbles in channel *j* that are fresh (m = 1), and

$$\sum_{p=1}^{P}\sum_{m=1}^{M-1}\sum_{i=1}^{J} {}^{m}r_{ij}^{p}\alpha_{i} = \alpha_{j}\left(1-\sum_{p=1}^{P} {}^{1}\alpha_{j}^{p}\right) \qquad \textbf{3.25}$$

which states that the total pebble flow diverted from zone *j* to other zones must sum to *j* to other zones must sum to the fraction of core flow that is recirculated through *j.*

PEBBED performs a check on user-supplied partition coefficients by checking that these equalities hold for the supplied or computed sets of coefficients.

In the next chapter, partition coefficients are computed for a few proposed PBR designs that employ simple recirculation schemes. It will be shown that these partition coefficients are easily computed from a few parameters. For ease of use, these cases are “hard-wired” into PEBBED and may be invoked by setting the proper parameter in the input deck. These include:

3. Random recirculation – recirculated and fresh pebbles are distributed randomly over the entire entry plane (e.g., HTR Modul 200),

4. Pebble channeling – pebbles are restricted to a specific flow channel for their entire core lives,
5. Two-zone transfer – pebbles are introduced into either the inner or outer radial zone then transferred to the opposing zone at some point in their trajectory (OUT-IN or IN-OUT).

The partition coefficients for more complex schemes must be supplied by the user in an auxiliary input file. Examples of both will be provided in Chapters 4 and 5.

3.3 Temperature Calculations in PEBBED

Fuel temperature during both normal operation and severe accident conditions must be kept below specified limits. For a passively safe pebble bed reactor, heat is removed by the primary coolant during normal operation and by conduction and radiation during extreme loss-of-pressurized-flow events. A proper core design effort must include fuel temperature calculations to which a certain amount of conservatism is applied. Normally, sophisticated thermal-hydraulic and systems analysis models are constructed and run to determine fuel temperatures during normal and accident conditions. A fair amount of iteration between neutronics and thermal-hydraulics may occur during the design process; a potentially tedious and time-consuming process.

In a modular pebble-bed reactor, however, fuel temperatures can be estimated to first order using computationally quick one-dimensional heat transfer models. Heat transfer modules have been added to PEBBED to generate a fuel temperature profile during normal operation and the peak fuel temperature during a loss-of-pressurized flow event, also known as a *depressurized conduction cooldown* (DCC). The results of these calculations are used to evaluate core safety margins and are fed directly to the

objective function of the optimization algorithm. This procedure is sufficient for a conceptual design; a final design must be subjected to a multi-dimensional thermal-hydraulic analysis with valid correlations.

3.3.1 Fuel and Coolant Temperatures During Normal Operation

Estimation of Coolant Temperature Profile

Coolant and fuel temperatures during normal operation are estimated using a simple one-dimensional mass and heat balance. The inlet coolant temperature, T_c^i, and mass flow rate, $\dot{m}$, are provided by the user. The coolant flow is divided among the major pebble flow channels according to cross-sectional flow area. The helium flow model currently used in PEBBED assumes:

1. The coolant mass flow is divided among the pebble flow zones in proportion to the cross-sectional area of the flow zone, and
2. There is no flow between coolant channels.

The first of these assumptions is not conservative with regard to fuel temperatures. Regions of higher power density generally cause higher coolant temperatures and pressure, thus reducing the mass flow in the zone. A more sophisticated model incorporating a momentum balance would be needed to address this deficiency. The second assumption is conservative with regard to fuel temperatures but is generally considered reasonably valid for pebble-beds.

The power, *P*, generated in axial cell, *k*, of coolant zone, *i*, is related to the temperature rise across the cell by Eq. **2.5**

$$P_k^i = \dot{m}^i C_p \left(T_{k+1}^i - T_k^i \right) \qquad \textbf{3.26}$$

in which

$\dot{m}^i$ is the helium flow rate (kg/s) through zone I,

C_p is the temperature-dependent specific heat (J/kg-K) of helium,

T_k^i is the coolant temperature at the inlet side of cell *k*, zone *i,*

and

T_{k+1}^i is the coolant temperature at the outlet side of cell *k*, zone *i.*

The cell powers are provided by the neutronics solution.

Temperature Profile Inside a Pebble

The temperature distribution in the pebble is computed using a one-dimensional model of heat generation and conduction through a uniform sphere. The coolant temperature surrounding the pebble is assumed to be uniform. All the thermal power is assumed to be generated within the fueled region of the pebble, conducted through the graphite shell, and deposited into the coolant by convection. (In fact, some heat is generated by neutron thermalization and gamma heating in the graphite shell region but the error introduced by this omission is considered to be well within the accuracy limits of this model). There are three heat transfer regions modeled when computing pebble temperatures. These are illustrated in Figure **3-3**.

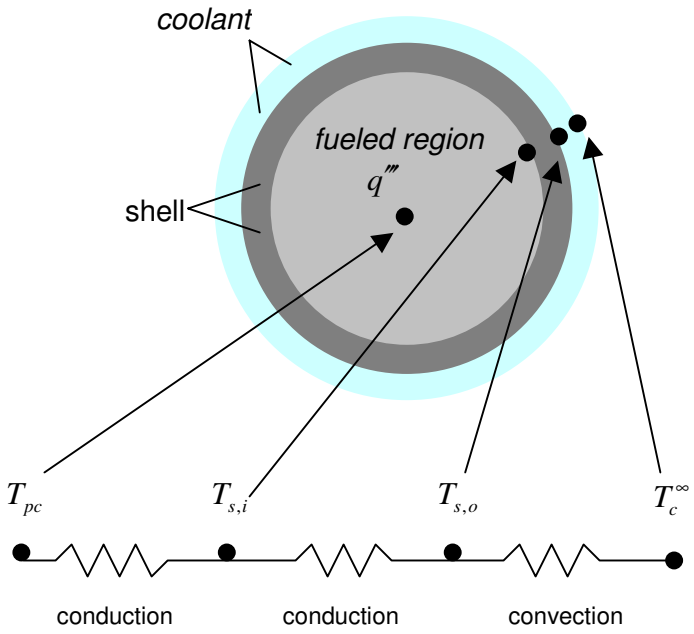

Figure 3-3: PEBBED heat transfer model of pebble cooling.

The convective heat transfer between the bulk coolant and the pebble surface is a function of the mass flow rate and temperature difference Eq. 3.27.

$$q = hA\left(T_{s,o} - T_c^{\infty}\right) \tag{3.27}$$

The convective heat transfer coefficient is given by Eq. 3.28

$$h = \frac{Nuk_{He}}{D_p} \tag{3.28}$$

in which

h = heat transfer coefficient (W/m^{2}K),

D_p = pebble diameter (m),

K_{He} = thermal conductivity (W/mK) of coolant,

and

Nu = Nusselt number.

Three correlations for the Nusselt number are available in PEBBED, one of which is detailed here. Gnielinski [81] evaluated the results of 20 authors to establish a relationship among the Nusselt, Prandtl, and Reynolds numbers and void fraction of helium cooled pebbled-bed systems. The theory is based upon the assumption that the heat transfer of spheres in a pebble-bed (Eq. **3.29)** can be related to that of a single sphere by introducing an arrangement factor, f_ε, dependent on the void fraction, ε:

$$Nu = f_\varepsilon Nu_s \qquad \textbf{3.29}$$

with

$$f_\varepsilon = 1+1.5(1-\varepsilon) \quad . \qquad \textbf{3.30}$$

The Nusselt number of a single sphere is given by Eq. **3.31**

$$Nu_s = 2+\sqrt{Nu_l^2 + Nu_t^2} \qquad \textbf{3.31}$$

with the Nusselt number for laminar flow given by

$$Nu_l = 0.664\left(\frac{\mathrm{Re}}{\varepsilon}\right)^{1/2}\mathrm{Pr}^{1/3} \qquad \textbf{3.32}$$

the Nusselt number for turbulent flow given by

$$Nu_t = \frac{0.037\left(\frac{\mathrm{Re}}{\varepsilon}\right)^{0.8}\mathrm{Pr}}{1+2.443\left(\frac{\mathrm{Re}}{\varepsilon}\right)^{-0.1}\left(\mathrm{Pr}^{2/3}-1\right)} \qquad \textbf{3.33}$$

and the Reynolds number given by Eq. **3.34**

$$\mathrm{Re} = \frac{vD_p}{\mu_c} \qquad \textbf{3.34}$$

with coolant velocity (m/s), v, and dynamic viscosity μ_c (Ns/m^2). This correlation is valid for the ranges 500 < Re < 10^4, Pr > 0.6, and 0.26 < e < 0.935. This covers the range of PBRs under consideration today and was used for the analyses described in this work.

Incropera [80] provides the steady-state heat balance between the inner and outer surfaces of the graphite shell, as

$$q = \frac{4\pi k_s \left(T_{s,i} - T_{s,o}\right)}{1/r_i - 1/r_o} \qquad \textbf{3.35}$$

in which

q is the power (W) generated within the pebble,

k_s is the thermal conductivity (W/mK) of the shell,

$T_{s,i}$ and $T_{s,o}$ are the inner and outer shell temperatures (°C),respectively,

and

r_i and r_o are the radii (m) of the inner and outer shell surfaces.

Within the heat-generating, uniform fueled region, the temperature at the center of the pebble is derived here. The steady-state heat balance for a uniform sphere is given by Eq. **3.36**

$$\frac{1}{r^2}\frac{d}{dr}\left(k_f r^2 \frac{dT}{dr}\right) + q''' = 0 \qquad \textbf{3.36}$$

in which

k_f, is the thermal conductivity of the fuel region,

and

q" is the thermal power density (W/m^3) within the sphere.

Assuming that the thermal conductivity throughout the sphere is constant, multiply both sides by r^2/k_f to get

$$\frac{d}{dr}\left(r^2\frac{dT}{dr}\right)=-\frac{q'''r^2}{k_f} \qquad \textbf{3.37}$$

Integrate both sides to obtain Eq. **3.38**

$$r^2\frac{dT}{dr}=-\frac{q'''r^3}{3k_f}+C_1 \qquad \textbf{3.38}$$

Divide by r^2 and integrate again to obtain Eq. **3.39**

$$T(r)=-\frac{q'''r^2}{6k_f}-\frac{C_1}{r}+C_2 \qquad \textbf{3.39}$$

The two integration constants are obtained by applying the boundary conditions:

BC#1: $\left.\frac{dT}{dr}\right|_{r=0}=0$ (spherical symmetry)

BC#2: $T(R)=T_s$ (known temperature at sphere surface, R).

Applying BC#1 to leads directly to $C_1 = 0$. Applying the second boundary condition yields Eq. **3.40.**

$$C_2=\frac{qR}{6k_f}+T_s \qquad \textbf{3.40}$$

Thus, the temperature distribution is given by Eq. **3.41.**

$$T(r)=-\frac{q'''}{6k_f}\left(r^2-R^2\right)+T_s \qquad \textbf{3.41}$$

The pebble centerpoint temperature is obtained by setting $r = 0$ to obtain

$$T_{pc}=\frac{q'''R^2}{6k_f}+T_s \qquad \textbf{3.42}$$

By assuming constant density and averaging the temperature in Eq. **3.41** over the mass of the fueled region, one can show that that mean fuel region temperature is related to the centerpoint and surface temperature by Eq. **3.43**

$$\overline{T} = T_s + \frac{6}{15}\left(T_{pc} - T_s\right). \qquad \textbf{3.43}$$

With the local pebble power provided by the neutronics solution and the inlet coolant temperature and mass flow rate provided by the user, these equations are used to generate a fuel and coolant temperature profile for the steady-state core.

Pebble- and Channel-Averaged Quantities

Using the partition coefficients defined in Section 3.2 to generate weighting factors, average quantities for each pebble type can be computed. For example, the bulk coolant temperature at a certain axial location surrounding pebbles of type *p* undergoing their *m*th pass through the core is obtained from a weighted average of the coolant temperatures in the different flow zones, T_i^c. The weight applied to the coolant temperature in zone *i* depends upon the fraction of total flow of pebbles through that zone, the fraction of the zone flow that is of type *p*, and the fraction of type *p* pebbles in that zone that are on their *m*th pass. The mean is thus obtained by summing over the weighted coolant temperatures, i.e., Eq. **3.44**.

$$\overline{T}^c = \frac{\sum_{i=1}^{N} \alpha_i \alpha_i^{p\ m} \alpha_i^p T_i^c}{\sum_{i=1}^{N} \alpha_i \alpha_i^{p\ m} \alpha_i^p} \qquad \textbf{3.44}$$

Of course, averaging over pebbles in all channels discards information about the extreme temperature to which a member of a given pebble type will be subjected. In the next chapter, a method for obtaining extreme values will be demonstrated.

3.3.2 Peak Accident Temperature

Core safety implies that fuel temperatures can never achieve a failure threshold during a design basis event. Passive safety implies that this is achieved without deliberate action on the part of engineered safety systems or operators. For modular pebble-bed reactors, a worst-case accident is the depressurized loss of coolant event, also known as the depressurized conduction cooldown (DCC). In such an event, the forced cooling of the pebbles ceases and the vessel depressurizes. A properly designed MPBR can withstand such events without significant core damage for two reasons:

3. Strong negative fuel temperature feedback inhibits the fission chain reaction with a modest increase in temperature, i.e., the reactor shuts itself down, and
4. Decay heat is transported from the core into the surrounding reflector and containment by conduction and radiation at a sufficiently high rate to prevent the fuel from ever reaching failure temperature.

Studies confirming this behavior are well documented [25], [26], [27], [28], [29], [30] and will not be discussed here. However, the robust characteristics of the fuel and core design also allow for rapid and reasonably accurate evaluation of passive safety during the design process itself. Specifically, the large height-to-diameter ratio of modular PBR cores means that the flow of thermal energy during a depressurized conduction cooldown is predominantly *radial* in direction. Ignoring axial and convective

heat transfer results in only a small but conservative error in the estimate of peak accident core temperature. This fortunate consequence of MPBR core design was confirmed with comparison to two-dimensional computational results [82], [83] and exploited in other studies [84]. It is again exploited in PEBBED to provide the means to assess the passive safety characteristics of the numerous designs that can be generated by the code.

The technique involves simply using the pebble power and temperature profile generated using the methods described above to compute the initial conditions for a subsequent transient heat conduction-radiation problem. One of the conclusions of the studies performed in Germany (cited above) was that the peak accident fuel temperature generally occurs at the location of the greatest local power density. In PEBBED, the radial profile of the core at the axial location of this peak provides the initial conditions for the one-dimensional radial heat transfer equation (Eq. **3.45)**.

$$\rho(T)C_p(T)\frac{\partial T(r,t))}{\partial t} = \nabla \bullet k(T)\nabla T(r,t) + q(r,t) = \frac{1}{r}\frac{\partial}{\partial r}\left(k(T)r\frac{\partial T(r,t)}{\partial r} \right) + q(r,t) \qquad \textbf{3.45}$$

Material and geometric details of the power plant outside of the outer reflector must be provided by the user to perform this calculation (the neutronics calculation only requires specification of the core out to the outer reflector.) The radially-dependent power density and core temperature profile provide part of the initial conditions. A constant outer boundary (containment wall) temperature is also provided by the user. Because no heat is generated outside of the core, the initial temperature profile outside of the core can be obtained by solving the steady-state version of Eq. **3.45** with the heat generation term set to zero and the boundary conditions obtained from the neutronics solution and this outer boundary temperature. The transient solution is then solved using a semi-implicit, finite-difference approximation to Eq. **3.45** with the spatial and temporal

mesh specified by the user. Radiant heat transfer between pebbles and across voids are subsumed by casting the radiant heat transfer equation in conduction equation form. This general approach was used successfully by Savage [83] in the stand-alone thermal-hydraulic code SHERLOC with the initial core power and temperature profiles provided by independent analysis. This method has also been adapted with some modification for use in PEBBED. The full derivation of the PEBBED one-dimensional transient calculation is given in Appendix C.

3.4 Summary of PEBBED Modeling Capability

Direct convergence on the asymptotic burnup solution, pebble recirculation described in terms of a few easily manipulated parameters, and one-dimensional heat transfer calculations for nominal and extreme accident conditions combine to yield an efficient and powerful approach to pebble-bed core design and sensitivity analysis. In the next two chapters, the utility of this approach will be demonstrated using documented and proposed PBR designs. In Chapter 7, the method will be augmented with an advanced optimization routine to automate the design process.

Chapter 4

Examples of PEBBED Reactor Models

In the previous chapter, a formulation was derived to compute the entry plane burnup of a recirculating pebble-bed reactor from the content of pebbles leaving the core. The elements of the recirculation matrix were shown to be simple functions of a few parameters easily computed in advance of the burnup calculation. In this chapter, examples of a few reactor concepts with different fuel management schemes are discussed. The utility of the recirculation matrix is further shown via application to generic issues associated with the PBR. Nominal and accident fuel temperatures will be computed and compared to data available in the literature.

4.1 HTR Modul 200

4.1.1 Model of the HTR-Modul 200

The Hochtemperaturreaktor-Modul 200 (HTR Modul 200) was developed in the mid 1980s by Kraftwerk Union and Interatom [9], [10] as the first modular high temperature reactor emphasizing passive safety under all design basis conditions. Its tall, thin pebble-bed core design allowed the removal of decay heat before fuel failure temperatures would be attained. Modularity implied the use of standardized reactor, heat transfer, and loop components. Although no HTR Modul 200 was ever built, this design set the standard for all subsequent modular pebble-bed reactors.

4.1.2 Recirculation Matrix Formulation for the HTR Modul 200

In Chapter 2, a formulation was introduced that described the flow of pebbles through a pebble-bed core in terms of a few easily computed parameters called partition coefficients (redefined below):

$\alpha_i = \frac{f_i}{F}$ (fraction of core flow in that is in zone i)

$\alpha_i^p = \frac{f_i^p}{f_i}$ (fraction of flow in i that consists of type p pebbles)

${}^m\alpha_i^p = \frac{{}^m f_i^p}{f_i^p}$ (fraction of type p flow in i that consists of pebbles on pass m)

${}^m\alpha_{ij}^p = \frac{{}^m f_{i\leftarrow j}^p}{{}^m f_j^P}$ (fraction of flow of pebbles of type p, on pass m, in zone j that is diverted to i).

These coefficients are used to relate the burnup of pebbles at the discharge point (exit plane) of the reactor to the burnup distribution at the entry plane (top). The variability of the coefficients is related to the flexibility of the core loading and discharge mechanism.

In terms of simplicity and flexibility, the HTR Modul 200 is an extreme. It features a single fuel loading tube centered above the core and a single discharge tube centered below. Only one type of pebble type (fuel) is circulated. These pebbles are dropped onto the top, forming a conus, and are distributed randomly over all radial and azimuthal zones, regardless of the accumulated burnup. Once the threshold burnup is achieved (about 15 passes through the core), the spent pebbles are discharged. This fuel loading policy may be described as type-independent, burnup-independent, and zone-independent recirculation.

The flow coefficient, α_i, is a function of the dynamics of the pebble-bed core. The subscript is the radial channel index, with *i* = 1, corresponding the innermost radial channel. Bedenig's experiments [46], [47] showed that for sufficiently high height-to-diameter ratios (H/D>0.8) that pebble flow is uniform, i.e., axial and largely constant as a function of radial distance. The downward velocity does decrease near the reactor wall as a result of wall friction but for the most part the 'slug flow' approximation yields reasonable results for typical PBR designs. Therefore, the flow fraction coefficients can be computed directly from the cross-sectional area of the specified flow zone. In PEBBED, the user specifies the zone boundaries and total core flow rate. The user may also specify the coefficients of a quadratic axial velocity profile (as a function of radial distance) for non-uniform pebble-flow. The flow fraction coefficients are computed directly from these values. Given the assumption of slug flow and zone-independent recirculation in the HTR Modul 200, the entire pebble-bed region may be modeled as a single flow zone for burnup purposes, i.e., $\alpha_i = 1$, (i = 1).

The type coefficient, α_i^p, is also equal to unity because there is only one pebble type in this design. Even if more than one radial flow zone were specified (i>1), these values would all be set to 1.

The pass coefficient, ${}^m\alpha_i^p$, indicates what fraction of pebbles of a certain type p in zone i are on their mth pass. As discussed in Chapter 3, the values of the pass coefficients are computed from the others. However, for the HTR Modul 200 the values can also be determined heuristically. Because the distribution of pebbles at the entry plane is completely random, all burnup stages (passes 1 through 15) are represented equally (on average) in any location in the core. Thus, for a single-zone core (i = 1) with one pebble type (p = 1),

$$ {}^{m}\alpha_i^p = {}^{m}\alpha = \frac{1}{15}, \qquad m = 1,15. \tag{4.1} $$

Finally, the transfer coefficient specifies what fraction of the pebbles of type p in zone j and completing their mth pass will be loaded into zone i at the entry plane. For the HTR Modul 200 with its single loading tube, there is no deterministic means of sorting the pebbles and they will be distributed randomly over all zones. Therefore the value of the transfer coefficient is just the probability of being dropped into the specified zone, i.e.,

$$ {}^{m}\alpha_{ij}^p = \alpha_i \text{ for all } p, m, j. \tag{4.2} $$

Thus, all partition coefficients are completely specified by the pebble flow characteristics (radial flow distribution) and the number of passes traversed by a pebble before discharge (*M*). No changes can be made to these values without radically changing the core design or fuel handling mechanism.

An estimate of the number of passes traversed by a pebble before discharge can be determined to first order from the core geometry, power level, and discharge burnup target using Equation 2.7.

Because the burnup accrued by a pebble flowing through the core is a function of the fissile content of the fuel as well as the overall mass, the discharge burnup of each pebble type in a core is computed and checked against the target burnup. If they do not match to within a specified tolerance, the number of passes or core flow rate is adjusted automatically.

Equivalent cylindrical volumes are computed for the top and bottom flow cones to obtain the effective core height. The cones are located in low flux regions of the core and thus the error introduced by this approximation is limited.

All of these factors can be determined in advance of the burnup-flux calculation and thus the recirculation matrix can be fully specified off-line. Table **4-1** includes these and thermal parameters used in the PEBBED model. A full description of the PEBBED computational model of the HTR Modul 200 is given in Appendix E. A detailed description of the HTR Modul fuel element is given in Appendix F.

Table **4-1**: Recirculation and thermal parameters for the HTR Modul 200 [9].

Height (m)	9.4
Core Radius (m)	1.50
Discharge Burnup (MWd/kg)	80
Core Thermal Power (MW)	200
Fresh Pebble Heavy Metal Content (kg)	0.007
Uranium Enrichment	7.8%
Coolant Inlet/Outlet Temperatures (°C)	250/700
System Pressure (MPa)	6
Mean Pebble Velocity (m/day)	0.14

Six group cross-sections for the fuel and reflector materials were generated using the MICROX-2 [85] cross-section code. The last two groups are in the thermal region in which upscattering does occur. PEBBED does treat upscattering (unlike VSOP, which is limited to four groups) but does not currently update cross-sections as functions of temperature or spectrum. A single set of values based on a unit cell calculation was used. A full description of the process by which these cross-sections were generated will be provided in Chapter 5. Control rods and absorber balls are generally withdrawn from the core during operation and thus were not modeled. Efforts are underway at the INEEL to develop an accurate control rod modeling method for PBRs.

4.1.3 Results of PEBBED Analysis

Some of the results of the analysis are shown in Table 4-2.

Table 4-2: PEBBED-computed characteristics of the HTR Modul 200.

Core Multiplication Factor (k_{eff})	1.0885
Mean Power Density (W/cm^3)	3.01
Peak Power Density (W/cm^3)	5.035
Peak Pebble Temperature (°C)	736
Mean Pebble Temperature (°C)	522
Fresh Fuel Rate (pebbles/day)	356
Total Pebble Flow Rate (pebbles/day)	5,335
Discharge Quantities (g/pebble)	
U-235	0.097
U-238	6.14
Pu-239	0.038
Pu-240	0.023
Pu-241	0.019

The core eigenvalue is high. This can be attributed to the fact that most fission product chains are not modeled in this case (only xenon and samarium). The actual HTR Modul may have control rods partially inserted from the top. Including these two effects would decrease the core multiplication factor to something closer to unity. The fast (<0.11MeV) flux is plotted in Figure 4-1.

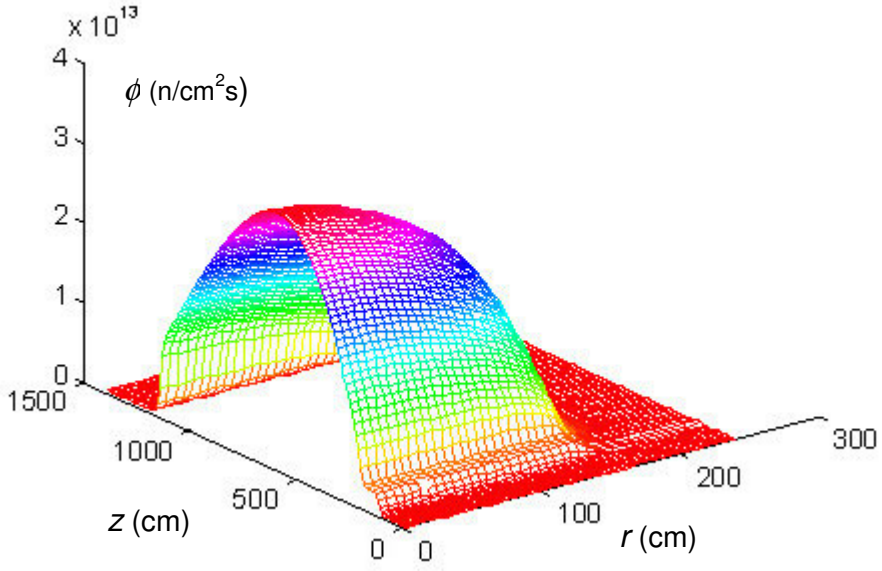

Figure 4-1: Fast (>0.11MeV) flux in the HTR Modul 200.

Calculations were performed to generate the peak fuel temperatures during normal operation and after a depressurized conduction cooldown (DCC). For the DCC, the structural components and dimensions are shown in Table 4-3.

Table 4-3: Structural components of HTR Modul 200 1D radial heat transfer model.

Radial Region	Outer Radius (cm)	Density (g/cm^3)	Emissivity
Pebble Bed	150	1.06	0.75
Outer Reflector (Graphite)	230	1.53	0.75
Carbon Brick Insulator	250	1.75	0.80
Gas Channel	265	0.0	N/A
Core Barrel (SSTL-304)	270	7.8	0.80
Gas Channel	295	0.0	N/A
Pressure Vessel (2.25Cr: 1 Mo Steel)	310	7.675	0.80
Gas Channel	430	0.0	N/A

A reactor cavity cooling system is assumed to be functional at the inner wall of the concrete containment vessel. This system provides an outer wall boundary temperature of a constant 50°C. The mathematics of the transient calculation and detailed material properties are described in Appendix C. Although material properties and correlations for the calculation performed by Frewer [9] are not included in their paper, enough detail is provided to re-create their model within reasonable accuracy. Frewer's calculation predicts a peak fuel temperature of 1,530°C at 32 hours after shutdown. This peak occurs at the core centerline 380 cm below the top of the core. PEBBED predicts a peak DCC temperature of 1,424°C at 32 hours, 390 cm below the core top. Part of the reason for the lower temperature is the lower initial fuel temperature estimated by PEBBED. Frewer reports a steady state temperature of about 600°C at this axial location while PEBBED computes a starting temperature of 465°C. The coolant temperature rise across the core for the specified inlet and outlet temperatures is 450°C. If half the power is produced and deposited into the coolant in the top 390 cm of the pebble bed, one would expect the coolant temperature to be roughly 250°C + 225°C = 475°C, similar to the PEBBED value. The value reported by Frewer no doubt reflects a fair amount of conservatism in the accident temperature calculation. Therefore, a second PEBBED computation was performed in which the inlet temperature was raised until the steady-state fuel temperature reached about 610°C. The peak accident temperature under these conditions is computed by PEBBED to be 1,465°C and occurs 27 hours after accident initiation.

Another run was performed in which the core power was raised to 250 MW. The authors surmised that the reactor could operate at this power under less stringent U.S. regulations. With the 250°C inlet temperature and same coolant flow rate, PEBBED computes a peak accident temperature of 1,589°C at 371 cm below the core top

occurring 34 hours after accident initiation. These results indicate that the peak accident temperature is more a function of local power density than initial temperature, as reported by Lutz [82].

4.2 PBMR with Dynamic Inner Reflector

4.2.1 Model of the PBMR-DIR

The first Pebble-Bed Modular Reactor proposed for construction in South Africa is a variation on the HTR Modul theme. The early design, the subject of study in this work, featured a 268 MWt core with a so-called dynamic inner reflector consisting of flowing graphite pebbles. The outer annulus would be fueled with fuel pebbles with a slightly higher enrichment and heavy metal content than the HTR Modul 200. The graphite and fuel pebbles are not physically separated and thus are free to mingle (see Figure 2-11). This mixing is limited, however, and a two-zone pebble-bed core is maintained, albeit with a ‘fuzzy’ boundary. The graphite pebbles are always loaded via the central loading tube while the fuel pebbles are loaded via the outer radial loading tubes. A single discharge tube is shared in this *type-dependent, burnup-independent* loading scheme. The overall radius of the active core is 175 cm and the approximate radius of the inner reflector is 87 m. Fuel pebbles traverse the core 10 times before discharge. Other parameters are specified in Table **4-4**.

Table 4-4: Operating parameters of the PBMR with dynamic inner reflector.

Height (m)	8.5
Core Radius (m)	1.75
Discharge Burnup (MWd/kg)	80
Core Thermal Power (MW)	268
Fresh Pebble Heavy Metal Content (kg)	0.009
Uranium Enrichment	8.0%
Coolant Inlet/Outlet Temperatures (℃)	503/900
System Pressure (MPa)	7
Mean Pebble Velocity (m/day)	0.099

4.2.2 Recirculation Matrix

The two-zone core requires multiple fuel loading tubes; a central tube for the graphite pebbles and a number of azimuthally-spaced fuel loading tubes set some distance from the core centerline. The partition coefficients are derived as follows.

The flow partition coefficients are dependent only upon the mechanics of pebble flow. It is reasonable approximate this flow as uniform (constant velocity across all channels) but for this model a second order polynomial was fitted to a flow distribution obtained from VSOP and also used in PANTHERMIX [54]. Equation 4.3 states the radial dependence of the flow velocity used in the PEBBED model as,

$$v(r) = v_o\left(-0.23x10^{-4}\,r^2 + 0.27x10^{-2} + 1\right), \qquad 4.3$$

in which v_o is the centerline pebble speed. The zone boundaries were chosen to divide the core flow into approximately equal parts so that the zone coefficients, α_i, are all roughly equal to 0.2 (Table **4-5).**

Table **4-5**: Flow Zone Boundaries and Flow Partition in the PBMR-DIR

Zone	Outer Radius (cm)	α_i
1	72.5	0.19
2	102.5	0.19
3	129.5	0.21
4	152.5	0.20
5	175.0	0.21

The boundary between the inner graphite column and outer fuel annulus lies about halfway through the second pebble flow channel and thus this channel contains both graphite and fuel. The location of this boundary is determined by the relative flow rates of pebbles loaded into these two major core zones. The other channels contain only one pebble type. The type partition coefficients, α_j^p, are easily computed from the user-supplied parameter that specifies the fraction of total pebble flow that is loaded into the outer zone. This parameter is defined in Eq. **4.4**.

$$\alpha^o = \frac{f^o}{F} \qquad \textbf{4.4}$$

For the PBMR, this value is about 0.75 which means that 75% of the total pebble flow in the core is in the outer annulus (and 75% of the flow consists of fuel while the

remaining 25% consists of graphite pebbles). The type coefficients are computed from this quantity and the flow coefficients using, for fuel, Eq. **4.5**.

$$\alpha_j^p = \begin{cases} 1 \quad \text{for} \dfrac{\alpha_o - \sum_{i=1}^{j} \alpha_i}{\alpha_j} > 1 \\ \max\left(0, \dfrac{\alpha_o - \sum_{i=1}^{j} \alpha_i}{\alpha_j}\right) \text{for} \dfrac{\alpha_o - \sum_{i=1}^{j} \alpha_i}{\alpha_j} \le 1 \end{cases} \quad (p = 1), \qquad \textbf{4.5}$$

and, for graphite pebbles (p = 2) going into the inner zone, Eq. 4.6.

$$\alpha_j^2 = 1 - \alpha_j^1. \qquad \textbf{4.6}$$

The transfer coefficients, ${}^m\alpha_{ij}^p$, are type-dependent. Graphite pebbles are distributed randomly among zones 1 and 2 while fuel pebbles are distributed randomly among zones 2 through 5. However, only about half of zone 2 is open to each pebble type. The transfer partition coefficients can be computed from Eq. **4.7**.

$${}^m\alpha_{ij}^p = \frac{\alpha_i^p \alpha_i}{\sum_{n=1} \alpha_n^p \alpha_n} \quad \text{for all } m \qquad \textbf{4.7}$$

For $p = 1$ (fuel), the summation in the denominator is just α^o because fuel pebbles are exclusively loaded into the outer zone. For graphite pebbles, the summation is 1- α^o. The numerator is the fraction of total core pebble flow that occurs in zone *i and* consists of type *p*.

The pass coefficients are computed by PEBBED from the other coefficients. Like the HTR Modul 200, however, the distribution of pebbles in not burnup-dependent and thus all burnup stages are equally represented at each location in the fueled zones, i.e.,

${}^{m}\alpha_i^1 = \frac{1}{10}$ for all passes *m*. The graphite pebbles are similarly distributed by pass but since no burnup is accrued in these pebbles, they can be circulated using an OTTO (once-through-then-out) policy without affecting the neutronic solution.

These relations are coded into PEBBED and can be invoked by flagging a two-zone, burnup-independent recirculation pattern in the input deck. The user supplies, in the input file, the coefficients of the velocity profile (Eq. **4.3)** and the fraction of core flow in the outer zone, α^o. PEBBED computes *all* of the partition coefficients from these parameters and the core geometry.

The resulting pebble flow distribution (by channel, type, and pass) is shown in Table **4-6**.

Table 4-6: Flow distribution in PBMR-DIR.

	Pebble Flow Rate (pebbles/hour)				
Channel	**1**	**2**	**3**	**4**	**5**
Pass	**Fuel**				
1	0	2.16	4.55	4.35	4.42
2	0	2.16	4.55	4.35	4.42
3	0	2.16	4.55	4.35	4.42
4	0	2.16	4.55	4.35	4.42
5	0	2.16	4.55	4.35	4.42
6	0	2.16	4.55	4.35	4.42
7	0	2.16	4.55	4.35	4.42
8	0	2.16	4.55	4.35	4.42
9	0	2.16	4.55	4.35	4.42
10	0	2.16	4.55	4.35	4.42
Total	**0**	**21.63**	**45.53**	**43.46**	**44.21**
	Graphite				
1 (OTTO)	40.71	18.62	0	0	0

As indicated above, only in channel 2 does both graphite and fuel pebbles reside, with fuel outnumbering graphite slightly. Also, the number of fuel pebbles in a channel does not change with pass number, a characteristic of burnup-independent recirculation patterns.

A full description of the PEBBED computational model of the PBMR-DIR, including partition coefficients, is given in Appendix E. A detailed description of the PBMR fuel element is given in Appendix F.

4.2.3 Analytical Results

4.2.3.1 Effect of the Size of the Inner Reflector

In the actual PBMR-DIR design, fuel pebbles comprise about 75% of the total pebble flow while graphite makes up the remainder in the central column. Before taking a detailed look at this particular configuration, a study was conducted of the effect of varying this ratio on the core multiplication factor. As indicated above, only one parameter, α^o, must be varied in the input deck to model the change in the size of the inner reflector. The other partition coefficients are automatically computed from this and the velocity profile. Figure **4-2** shows a plot of the result.

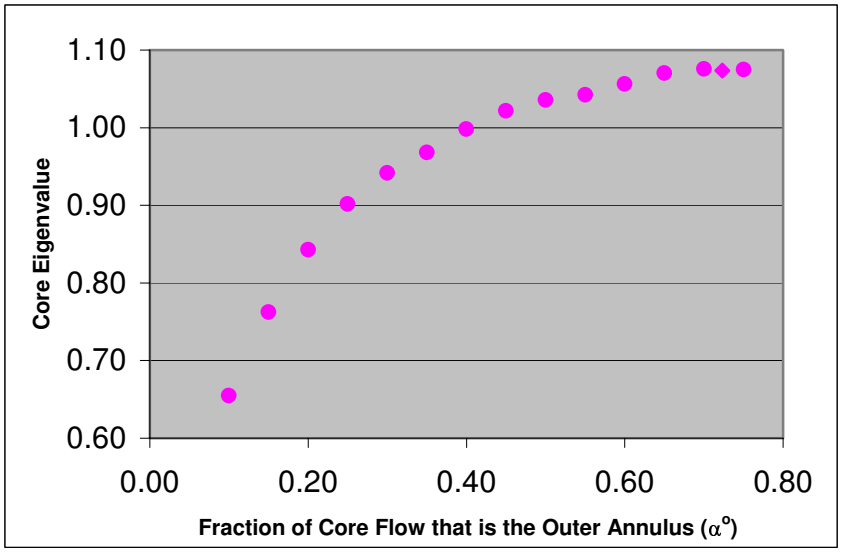

Figure **4-2**: Effect of inner reflector size on core multiplication factor.

A low value for α^o implies a very narrow annulus and a very thick inner reflector column. Other than the size of the inner reflector the other parameters (core outer boundary, height, pebble size) were held constant. The overall pebble flow rate was

automatically adjusted to maintain the discharge burnup at 80 MWD/kg_{ihm}. The plot indicates poor neutron economy for cores in which the inner reflector graphite comprises more than 50% of the pebble flow. The core eigenvalue appears to be approach an asymptotic value for outer flow fractions above α^o = 0.70. Increasing the size of the fuel annulus (decreasing the size of the inner reflector) beyond this yields little neutronic benefit.

4.2.3.2 Neutronic and Thermal Characteristics of the Asymptotic Core

For the nominal PBMR core, a value of α^o = 0.723 was computed based upon the flow characteristics obtained from the literature, Cross sections for this core model were computed using both COMBINE [86], [87] and MICROX-2. PEBBED produced the results shown in Table **4-7**. The INEEL COMBINE code differs from MICROX-2 in that its resonance treatment does not extend into the thermal spectrum. Furthermore, upscattering is only allowed in the thermal spectrum. This presents a problem when modeling graphite-moderated reactors with high burnup fuel. Plutonium isotopes build up to significant quantities and Pu-240 has a very high capture resonance at about 1 eV, well within the upscatter region. Partial compensation was achieved by generating a infinite lattice neutron spectrum with a 1.86 eV thermal energy upper limit. Most of the cross-sections were generated with this thermal energy cutoff. A separate 'cell' calculation using this spectrum but with the thermal energy set at 0.876 eV was run to generate the cross-sections for Pu-240 with a more accurate treatment of the low-lying resonance.

Designed for coated particle gas reactor fuel, MICROX does not share this energy barrier limitation and also has a more advanced treatment of the shadowing effects of the particles.

Table **4-7** was generated using the MICROX cross-sections.

Table **4-7**: Neutronic features of the PBMR-DIR.

Core Multiplication Factor (k_{eff})	1.0732
Mean Power Density (W/cm^3)	3.28 (3.28)
Peak Power Density (W/cm^3)	6.77 (6.56)
Peak Pebble Temperature (°C)	1,040 (1,063)
Mean Pebble Temperature (°C)	804 (760)
Fresh Fuel Rate (pebbles/day)	372
Total Pebble Flow Rate (pebbles/day)	5,140
Discharge Quantities (g/pebble)	
U-235	0.141
U-238	7.84
Pu-239	0.053
Pu-240	0.032
Pu-241	0.026

Correspondence with PBMR personnel yielded some VSOP data for comparison [88]. These are shown in parenthesis in the table. The peak power density and mean temperature computed by PEBBED are somewhat higher than those computed by VSOP. The peak fuel temperature is slightly lower than the VSOP value. The validity of the temperature comparison is rather limited because of the way these parameters are computed. For peak temperature, PEBBED computes a weighted average of the peak values achieved by pebbles in different flow zones (more on this in Section 4.5) while VSOP computes an average temperature of pebbles in the *batch* that has the overall

highest temperature. Given these different methods, complete agreement cannot be expected.

4.2.3.3 Enveloping Calculations and Pebble Histories

The recirculation matrix can be exploited to yield pebble history information for a specific trajectory rather than a weighted average of all trajectories. To do this, one or more new pebble types are specified in the input deck. The new pebbles have the same composition as the nominal fuel type but the partition coefficients describing their trajectories are altered. The type partition coefficients for the new pebble types are set to extremely low values ($<10^{-4}$) so that their presence does not significantly alter the neutronic characteristics of the core. The model is run and the pebble histories for these special types are generated along with the nominal types.

This approach has been exploited to generate bounding scenarios for fuel conditions in the PBMR-DIR. In addition to the nominal fuel and graphite pebble types described in the previous sections, four other pebble types were modeled corresponding to the cases in which pebbles are *confined to a single flow channel for their entire core trajectory* (the *pebble channeling* scheme briefly described in the previous chapter). The set of transfer partition coefficients for a given pass *m* for such channeled pebbles just form the identity matrix; i.e., all pebbles discharged from channel 3 are reintroduced into channel 3, etc. For example, the second radial channel in the PBMR is the so-called *mixing zone* containing roughly equal parts fuel and graphite spheres. Because of its proximity to the inner zone of pure graphite pebbles, the fuel in the mixing zone (channel 2) is exposed to a relatively pronounced thermal flux. Fuel pebbles thus generate much more power than pebbles with the same entry burnup passing through a

different flow channel, and consequently accrue more burnup on this pass. Pebbles that are confined to the mixing zone (channel 2) for their entire core lives are like candles that burn intensely and quickly. The next set of figures illustrate the pebble histories for the "average" pebble as well as pebbles that are channeled into each of the four fueled zones in the PBMR-DIR.

Figure **4-3** shows pebble power as a function of time for the channel-averaged pebble and for those restricted to channels 2 and 3. Each loop in a curve corresponds to a pass through the core.

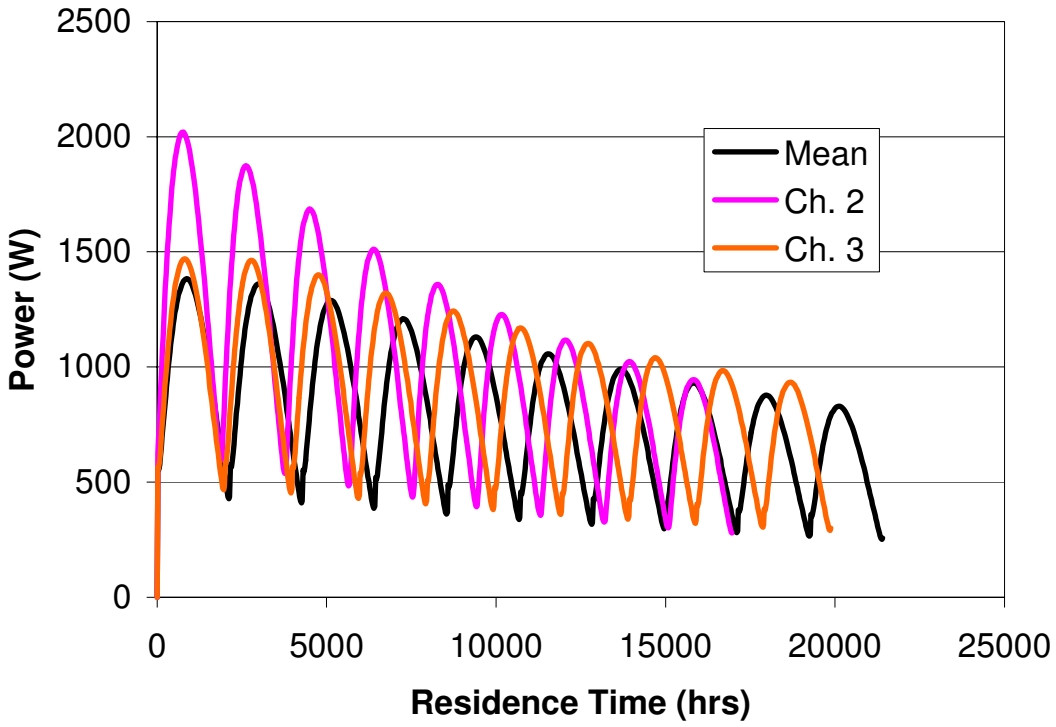

Figure **4-3**: Pebble power for average and channeled trajectories.

The "wavelengths" of the channel 2 and channel 3 trajectories are shorter than that of the mean and other channel trajectories because the axial pebble velocity is higher for the inner radial zones. The decrease in the amplitude over time corresponds

to the decrease in the fissile content of the pebbles. As stated previously, pebbles in channel 2 are exposed to a greater thermal flux and thus produce considerably more power than those in other trajectories. Careful examination of the figure also reveals that pebbles confined to channel 2 undergo only nine passes while all others undergo ten, another consequence of the higher thermal flux. These pebbles reach the discharge burnup value (80 MWD/kg_{ihm}) in one less pass through the core.

Figure **4-4** is a plot of the PEBBED-computed fuel temperature for the same set of trajectories.

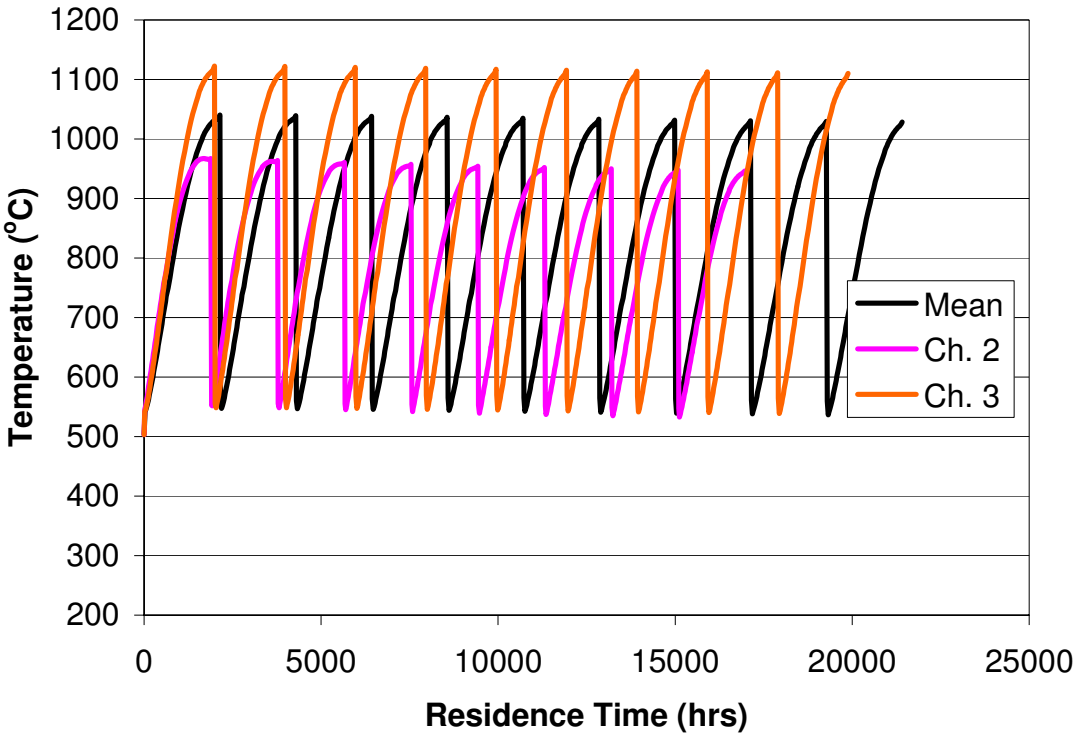

Figure **4-4**: Centerpoint fuel temperature for various trajectories.

During a single pass, the mean temperature varies roughly between 600°C and 1,030°C. Note that the peak temperature during each pass through the core occurs at the exit plane. Unlike LWR fuel, the higher conductivity of pebble fuel elements allows

heat to pass more quickly out of the pebble. As a consequence, the pebble fuel temperature profile tracks the surrounding coolant temperature profile rather than the power profile. The coolant enters the top of the core at about 500°C and exits the core at 900°C. The temperature difference between the surface and center of a pebble varies between 50° and 100°C. Pebbles in channels 4 and 5 exhibit similar temperature profiles.

Pebbles in channel 3 experience the greatest temperature variation and a peak temperature of 1,122°C, considerably higher than the trajectory-averaged peak of 1,040°C. This peak is attained for a trajectory that has a very low probability of occurring. Channel 3 carries 29.5% of the fuel flow through the core. The probability that an individual pebble is randomly dropped in channel 3 on all 10 passes of its trajectory is approximately 0.295^{10} or 1 chance in 500,000. There are roughly 330,000 fuel pebbles in the PBMR-DIR core. The product of these two numbers is 1.6, indicating that it is very likely that at least one pebble in the PBMR is following this trajectory. In fact, the number of pebbles attaining 1,122°C is about 30% of the total in the core. This is because this peak value occurs on the first pass through the core and 30% of all pebbles go through channel 3 on their first pass, regardless of the trajectories taken on subsequent passes. Thus for purposes of establishing the fuel temperature envelope, the 1,122°C value is appropriate.

Note that the pebbles in channel 2, while producing much more power than those in other channels, do not run at the highest temperature. As mentioned previously, the fuel temperature profile tracks the coolant temperature more closely than it tracks pebble power. Although the power produced is highest in this channel, only about half of the pebbles in this channel actually contain fuel and thus the local power density is lower

than that found in other channels. The coolant temperatures are lower and thus so are the fuel temperatures.

The analysis described above was used in the design of a PBMR fuel testing and qualification program proposed by the INEEL.

4.2.3.4 Isotopic Characteristics of the Spent Fuel

Also of interest in fuel cycle analysis is the buildup of plutonium and other minor actinides in pebble-bed fuel. Studies of plutonium content have been conducted using different code packages and methods [89]. These include:

1. An MIT study using VSOP (4-group)
2. An INEEL study using MCNP and ORIGEN (continuous, unit cell)
3. A PBMR Pty, Ltd. study using VSOP (4 group)
4. An INEEL study using COMBINE-6 and PEBBED (4 group)
5. An INEEL study using MICROX-2 and PEBBED (6 group).

Table **4-8** lists the amount of plutonium-239 per discharged pebble calculated in these studies.

Table **4-8**: Pu-239 content in discharged pebbles.

Study	**Pu-239 Mass (mg) in Pebble at 80MWD/kg$_{hm}$**
MIT-VSOP	11
INEEL-MCNP/ORIGEN	79
PBMR VSOP	86
COMBINE/PEBBED (4)	67
MICROX/PEBBED (6)	53

Clearly there is ample disagreement between the modeling methods. Each method has strengths and weaknesses. The MCNP-ORIGEN model uses continuous energy cross-sections but the model is only of a unit cell, not an entire recirculating core with its regionally varying spectra. VSOP updates its cross-sections (using the GAM-THERMOS libraries) for spectral and temperature changes but is limited to four energy groups with no upscattering. PEBBED can use more energy groups and treat upscattering but currently uses only a single set of constant cross-sections for each composition in the core. The cross-sections are computed in an iterative manner for a pebble of average burnup (see Chapter 5), which is an advantage over the other methods. Still, these results indicate the need for further development and benchmarking in the area of pebble-bed cross-section generation.

In another comparison, the total discharge plutonium vector was compared between some of these methods (Table **4-9**).

Table **4-9**: PBMR discharge Plutonium vector (% of total Pu mass).

Isotope	MCNP-ORIGEN	PBMR VSOP	COMBINE/PEBBED (4)	MICROX/PEBBED (6)
Pu-238	1	2	1	2
Pu-239	46	39	39	40
Pu-240	28	34	34	24
Pu-241	16	16	16	20
Pu-242	9	10	10	15

The four-group PEBBED and VSOP models agree well on a relative basis although the total amount of plutonium differs between the two. The Pu-240 content predicted by these models is much higher than the others; probably the result of the treatment of the 1 eV resonance. The six-group MICROX-PEBBED model shows a

significantly lower Pu-240 yield. Clearly, more development and benchmarking is needed to generate PBR isotopic data with certainty.

Figure **4-5** shows a plot of the thermal flux in the PBMR. The graphite inner reflector is rich with thermal neutrons but there is a thermal peak near the outer reflector as well.

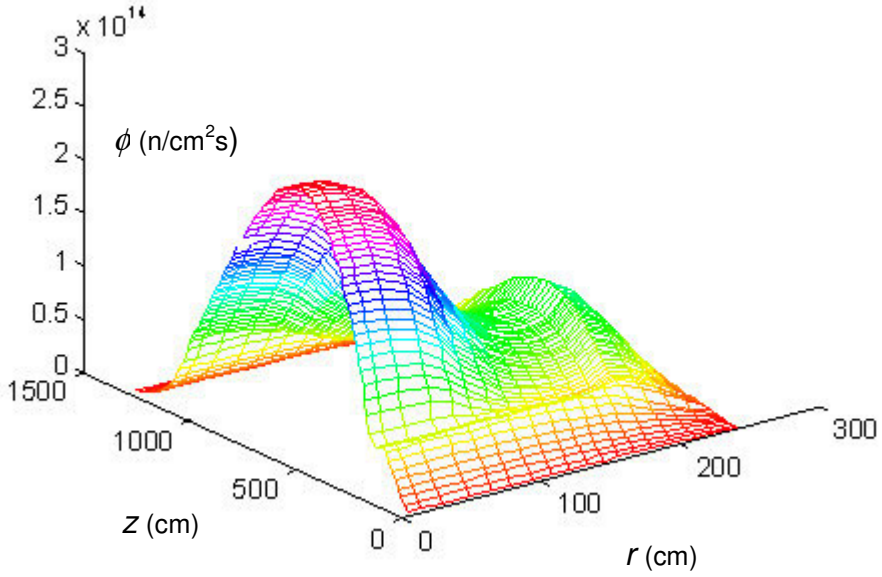

Figure **4-5**: Thermal (<1.86 eV) flux in the PBMR-DIR.

4.2.3.5 Depressurized Conduction Cooldown Transient

Assuming the successful operation of a surface cooler system, PEBBED's DCC module computes a peak accident temperature of 1,420℃ occurring 45 hours after accident initiation. Calculations by PBMR, Ltd. using THERMIX indicate a peak value of about 1,450℃ occurring about 55 hours after accident initiation [48]. A model of the core

was constructed at the INEEL using the safety analysis MELCOR. This model will be discussed in more detail in Chapter 6. The MELCOR model predicts a peak temperature of 1,406°C at 45 hours. The THERMIX and MELCOR models are two-dimensional and include convective heat transfer. The agreement with the PEBBED one-dimensional conduction-radiation model confirms the assumption that most heat transfer during this transient is radial and very little is convective.

The peak temperature value also suggests that the total core power can be raised to some extent without violating the 1,600°C limit. Indeed, the current PBMR design [48] is rated at 400 MWt.

4.3 GE MPBR with an OUT-IN Fuel Management Policy

In early 1982, the Department of Energy commissioned General Electric to conduct study of the use of a modular pebble-bed reactor to drive a steam reforming plant for process heat application [82]. Like the PBMR, this General Electric design featured a two-zone core, however, it used only a single pebble type that was loaded into the outer, annular zone for the first half of its residence time then transferred to the inner zone for the remainder. This *burnup-dependent*, or 'OUT-IN', loading scheme has been used extensively in batch-loaded LWR cores to limit power peaking.

4.3.1 Model of the GE MPBR

The GE MPBR features a 250 MWt core that has a radius of 1.45 meters and an approximate height of 9.3 meters. The fuel is a mixture of thorium and 20%-enriched

uranium. Thorium is fertile and is converted to uranium-233 while in the core. Helium coolant enters at 400°C and 4.6 MPa and exits at 950°C.

4.3.2 Recirculation Matrix

In an 'OUT-IN' or 'IN-OUT' PBR fuel management system, the core is divided into two zones, each of which contains one or more flow channels. One of the flow channels may be split between the two zones. A single type of fuel pebble is loaded into only one of the zones (the entry zone) and recirculated until an intermediate (transfer) threshold is attained. The pebbles are then transferred into the second (exit) zone and recirculated until the discharge burnup level is exceeded.

As with the PBMR, the radius of the boundary between the zones is determined by the relative rates of flow into these zones. For a *burnup-dependent* scheme, of which the OUT-IN is an example, the relative zone loading rate also fixes the transfer burnup threshold value, B_T, and the number of passes each pebble undergoes before being transferred, M_T.

The rate of flow between the zones must equate to the fresh fuel injection rate in order to maintain flow conservation. Because the entry zone flow rate is not likely to be an integer multiple of the fresh fuel injection rate, only a fraction of the pebbles on pass M_T can be transferred. The remainder will be transferred on the following pass, $M_T + 1$.

These parameters and the transfer coefficients are derived as follows for the single pebble type case (the p superscript is omitted for clarity as only one pebble type is used in this core design). The formulation is easily generalized to the multiple pebble type case.

As with the PBMR-DIR core, all but one of the flow channels resides within either the inner column or outer annulus. Define α_j^o as the fraction of the flow in flow channel *j* that is in the entry zone. The subscript *o* is used to indicate that the entry zone is the outer fuel annulus rather than the inner column but the equations are also valid for the reverse case. In fact, the values of these zone coefficients are numerically equal to the values of the type coefficients in the PBMR and thus are computed in the same way using Eq. **4.5**. In this case, however, the pebbles are all of one type (fuel). The superscript indicates the flow stream (inner or outer) of which the pebble is a member. Let α_T be the fraction of the pebbles on pass M_T that are transferred from the entry zone to the exit zone. This number is the same for all flow channels in the entry zone if there is only one discharge tube.

The flow rate of pebbles being transferred from the entry zone to the exit zone, F^T, is given by Eq. **4.8**.

$$F^T = F\sum_{j=1}^{J} {}^{M_T}\alpha_j \cdot \alpha_j \cdot \alpha_T \cdot \alpha_j^o + {}^{M_T+1}\alpha_j \cdot \alpha_j \cdot \alpha_j^o \qquad \textbf{4.8}$$

This can be simplified as follows.

$$= F\sum_{j=1}^{J} \alpha_j \cdot \alpha_j^o \left({}^{M_T}\alpha_j \cdot \alpha_T + {}^{M_T+1}\alpha_j \right) \qquad \textbf{4.9}$$

$$= F\sum_{j=1}^{J} \alpha_j \cdot \alpha_j^o \left({}^{M_T}\alpha_j \cdot \alpha_T + (1-\alpha_T)\cdot {}^{M_T}\alpha_j \right) \qquad \textbf{4.10}$$

$$= F\sum_{j=1}^{J} \alpha_j \cdot \alpha_j^o \cdot {}^{M_T}\alpha_j \qquad \textbf{4.11}$$

In fact, the transfer flow rate (rate at which pebbles are transferred from the outer to the inner zone) is simply equal to the flow rate of pebbles on any pass *m*, including *m* = 1 (the fresh fuel injection rate), because pebbles are introduced to the core only when they are fresh and discharged only after pass *M*.

The total flow rate in the entry zone can be computed from Eq. **4.12**.

$$F^o = \left[M_T \sum_{j=1}^{J} {}^{M_T}\alpha_j \cdot \alpha_j \cdot \alpha_j^o + \sum_{j=1}^{J} {}^{M_T+1}\alpha_j \cdot \alpha_j \cdot \alpha_j^o \right] F \qquad \textbf{4.12}$$

This simplifies to

$$F^o = F\left(M_T + 1 - \alpha^T\right) \sum_{j=1}^{J} {}^{M_T}\alpha_j \cdot \alpha_j \cdot \alpha_j^o \qquad \textbf{4.13}$$

$$= F\left(M_T + 1 - \alpha^T\right) \sum_{j=1}^{J} {}^{1}\alpha_j \cdot \alpha_j \cdot \alpha_j^o \qquad \textbf{4.14}$$

$$= \left(M_T + 1 - \alpha^T\right) {}^{1}F \,. \qquad \textbf{4.15}$$

${}^{1}F$ is the fresh fuel injection rate.

Eq. **4.15** can be solved for α^T to yield:

$$\alpha^T = M_T + 1 - \frac{F^o}{{}^{1}F} \qquad \textbf{4.16}$$

By the definition of a partition coefficient, $0 \le \alpha^T \le 1$, so that the transfer pass number M_T is fixed as the integer part of the quotient of the entry zone flow and fresh fuel flow, Eq. **4.17**,

$$M_T = \mathrm{int}\left(\frac{F^o}{{}^1F} \right) \qquad \textbf{4.17}$$

Thus, the transfer pass number and fraction of flow transferred in a two-zone simple transfer scheme are easily computed from the core flow distribution and fresh fuel injection rate. The fresh fuel injection rate is obtained from the total core flow and the number of passes computed for that pebble type.

These parameters are now used to derive the actual transfer coefficients for this fuel cycle.

For pre-transfer flow, the pebbles in channel *j* are distributed according to the partition of the entry zone among the flow channels *I*:

$$^m\alpha_{ij} = \frac{\alpha_i^o \alpha_i}{\sum_{\text{all } i} \alpha_i^o \alpha_i} \qquad m < M_T \qquad \textbf{4.18}$$

For each channel *j* completing transfer pass M_T, there are two flow paths: recirculation back into the entry zone channels or transfer to an exit zone channel. The transfer coefficient is the sum of the probabilities of these outcomes:

$$^m\alpha_{ij} = (1-\alpha_T)\frac{\alpha_i^o \alpha_i}{\sum_{\text{all } i} \alpha_i^o \alpha_i} + \alpha_T \frac{(1-\alpha_i^o)\alpha_i}{1-\sum_{\text{all } i} \alpha_i^o \alpha_i} \qquad m = M_T \qquad \textbf{4.19}$$

Finally, for post-transfer flow, all of the pebbles are equivalently distributed among the exit zone flow channels,

$$^m\alpha_{ij} = \frac{(1-\alpha_j^o)\alpha_i}{1-\sum_{\text{all } i} \alpha_i^o \alpha_i} \qquad m > M_T \qquad \textbf{4.20}$$

This expression can be obtained from Eq. **4.19** by setting $\alpha^T = 1$.

As in the PBMR-DIR case, all of the partition coefficients are thus easily computed from the pebble velocity profile, the discharge burnup, the core geometry, and the ratio of the outer annulus flow to the total pebble flow. In PEBBED, OUT-IN, or IN-OUT recirculation schemes can be specified easily and optimized by varying these quantities.

A full description of the PEBBED computational model of the GE-MPBR, including partition coefficients, is given in Appendix E. A detailed description of the GE-MPBR fuel element is given in Appendix F.

4.3.3 Analytical Results

4.3.3.1 Characteristics of the Asymptotic Core

An outer flow fraction (α^o) of 0.5 and a uniform velocity profile was specified for the GE-MPBR core. For simplicity, flow channel boundaries were adjusted slightly so that no channel contained a mixture of inner and outer zone pebbles. Solving for the recirculation matrix in PEBBED yielded the pebble flow pattern listed in Table **4-10**.

Table 4-10: Flow partition in the GE-MPBR (OUT-IN).

Fraction of Flow in Zone, a_i				
	Ch. 1	**Ch. 2**	**Ch. 3**	**Ch. 4**
	0.25515	0.24494	0.22852	0.27139
Number of Pebbles in Each Zone				
Pass				
1	0	0	8.45	10.04
2	0	0	8.45	10.04
3	0	0	8.45	10.04
4	0	0	8.45	10.04
5	0	0	8.45	10.04
6	9.44	9.1	0	0
7	9.44	9.1	0	0
8	9.44	9.1	0	0
9	9.44	9.1	0	0
10	9.44	9.1	0	0

For the GE study, VSOP was used to generate the cross-section, burnup, and thermal-hydraulic characteristics. The equilibrium nuclide distribution from VSOP was fed to a BOLD-VENTURE [52] model to generate power peaking factors. Table 4-11 shows a comparison of the VSOP-BOLD-VENTURE results vs. those produced by PEBBED for the equilibrium core.

Table 4-11: VSOP-BOLD-VENTURE vs. PEBBED physics results for the GE MPBR.

	VSOP-BOLD-VENTURE	PEBBED
Core Multiplication Factor	0.9980	1.045
Mean Fuel Residence Time (days)	737	741
Discharge Burnup (MWd/kg $_{ihm}$)	79.3	80.0
Overall Power Peaking Factor	2.1	1.6
Axial Distance of Power Peak below Top of Pebble Bed (cm)	278	329
Maximum Fuel Temperature (°C)	1,098	1,035
Mean Fuel Temperature (°C)	775	738
Fuel Inventory (kg)		
U-233	14.6	15.5
U-235	76.9	93.4
U-238	757	742
Th-232	1,304	1,322
Pu-239	3.4	6.0
Pu-240	2.0	2.6
Pu-241	.98	2.0
Pu-242	.77	0.995

The PEBBED-generated inventory indicates a higher buildup of plutonium relative to that produced by VSOP. Such a buildup is typical of thorium-fueled systems as the (n,γ) reaction in Th-232 eventually leads to Pu-238 and higher plutonium isotopes. Pu-238 was not listed in the GE study so comparison is difficult. The other differences in the way that cross-sections are generated in VSOP and for PEBBED may also be a significant source of the disagreement in nuclide densities, core multiplication factor, and power peaking. In particular, the temperature of the fuel pebbles varies significantly over the axial dimension of the core. The cross-sections computed using MICROX assumed

a proper average temperature but effect of variations was neglected. Coolant enters the top of the core so on average the fuel and moderator temperatures are much lower near the top, improving moderation. Local reactivity is thus underestimated in the upper part of the core and overestimated in the lower. As a result, the actual axial peak is probably higher than what is computed by PEBBED.

The cross-section libraries themselves may contribute to large differences. Most of the cross sections for the PEBBED model were taken from the PBMR-DIR set. Cross sections for the members of the thorium chain were computed in a separate cell calculation with no subsequent iteration (to be described in Chapter 5). This method yields quick results but does not capture the effect of the thorium-derived nuclides on the neutron spectrum.

Isotopic data for direct comparison is rare but a study of thorium-uranium fuel for light water reactors was recently completed at the INEEL [91]. Table **4-12** shows a comparison of the plutonium content of these fuels and the results obtained for the GE-MPBR computed by VSOP and PEBBED.

Table **4-12**: Plutonium isotopics for various Th-U fuel types.

	Th/U Ratio	**Burnup (MWd/kg$_{ihm}$)**	**Pu Content (kg/tonne$_{ihm}$)**	**Pu Vector % 238-239-240-241-242**
MOCUP LWR	25:75	56	4.9	7-50-17-18-8
MOCUP LWR	30:70	73	5.7	8-47-18-17-10
MOCUP LWR	35:65	85	6.8	9-46-18-17-10
VSOP GE-MPBR	58:42	80	4.5	NA-38-27-15-21
PEBBED-MICROX GE-MPBR	58:42	80	7.9	3-40-21-20-16

LWR and HTGR spectra are sufficiently different to prevent firm conclusions. Yet the LWR data does support the higher Pu content of the PEBBED results to some extent.

4.3.3.2 Accident Fuel Temperature

A peak fuel temperature attained during a depressurized conduction cooldown (DCC) in the GE-MPBR was computed by Lutz to be 1,644℃ using the two-dimensional THERMIX code [82]. The power and temperature distribution in the core at steady state was obtained by feeding the nuclide distribution from VSOP into a BURNER-VENTURE calculation. The peak temperature was achieved 27 hours after accident initiation.

Savage used the power and temperature distributions obtained in this study as a test of the one-dimensional (radial) conduction-radiation code SHERLOC [83]. Mentioned in the previous chapter, the methods and material properties employed in SHERLOC were adapted with minor modifications to produce the DCC fuel temperature module in PEBBED. PEBBED provides its own steady-state power and temperature distribution, which was shown above to be rather different that those produced by VSOP-BURNER-VENTURE. As a check on the DCC module, the steady-state radial temperature and power density distributions used by Savage were hard-wired into PEBBED to replace the PEBBED computed profiles in a test case. The results are shown in Table **4-13**.

Table 4-13: DCC peak temperature results for the GE-MPBR.

	Peak Fuel Temperature (°C)	Time of Peak (hours after shutdown)	Radial Location of Peak (cm below top of core)
BOLD-VENTURE-THERMIX	1,644	27	278
THERMIX steady-state SHERLOC transient	1,648	26	185
THERMIX steady-state PEBBED transient	1,643	25	185
PEBBED steady state and transient	1,507	19	329

The small differences between the SHERLOC and PEBBED calculation with the same initial conditions can be explained by the minor differences between the algorithms. The differences between the THERMIX and full PEBBED calculation are clearly the result of the flatter (axial and radial) power distribution computed by PEBBED. The peak power density predicted by PEBBED (6.6 W/cm^3) is significantly lower than predicted by BOLD-VENTURE (8.6 W/cm^3), perhaps a consequence of the lower axial peak resulting from the lack of temperature dependence in the cross-sections.

4.4 Summary

The recirculation matrix is derived for pebble-bed reactors with three different fuel-loading patterns. For each, it is shown that the elements of the recirculation matrices describing their flow are easily computed from a few general core parameters. Neutronic characteristics (eigenvalues, power peaking factors) are generated and, for the PBMR

and HTR Modul – 200, yield reasonable agreement with results obtained from the literature. Large differences, particularly with the GE-MPBR, are likely the result of the significant differences in the way that cross-sections are computed in the various models.

Peak fuel temperatures attained during depressurized conduction cooldown transients are computed using a one-dimensional, radial convection-radiation model. The DCC model was validated against a code (SHERLOC) employing the same method, correlations, and initial conditions. When using the boundary and initial conditions generated by PEBBED, the model yields satisfactory results for the PBMR-DIR. The peak DCC temperatures computed for the HTR Modul and GE-MPBR are somewhat lower than reported in the literature; a result that can be largely attributed to the lower power peaking computed by the current PEBBED/MICROX method of cross-sections.

The next chapter examines the application of PEBBED and the recirculation matrix to generic MPBR issues, i.e., not tied to a specific design. The topic of each section in Chapter 5 is the subject of already or soon-to-be published papers co-authored by the author of this work.

Chapter 5

Other Applications

In this chapter, applications of PEBBED and the recirculation matrix to generic MPBR issues, i.e., not tied to a specific design, are examined. The topic of each section is the subject of already or soon-to-be published papers co-authored by the author of this work.

5.1 Achieving Optimal Moderation using PEBBED and MICROX

5.1.1 Optimal Moderation

The concept of optimal moderation in a pebble-bed reactor was first proposed by Ougouag, et al. [92] In batch-loaded cores, such as the LWR and prismatic HTGR, the fuel within the core is replenished at periodic intervals of one year to eighteen months. In the time between refueling outages, the fuel itself is not expected to be mobile. In such reactors, after a number of refueling events, the core configuration is said to attain a state known as the “asymptotic loading pattern” or the “asymptotic equilibrium” core. However, despite this nomenclature, the core keeps changing between reloading events. Thus, the asymptotic loading pattern is not really a steady state; rather it merely indicates that subsequent reloading configurations will be essentially the same as this “asymptotic” pattern. During operation, even in the asymptotic pattern, the state of the core continues to change. This continuing change of the core makes the realization of certain optimization objectives difficult if not outright impossible. One particular objective

that cannot be met *continuously* with fixed fuel cores, such as LWRs, is that of optimal moderation. Here optimal moderation is meant as the moderation state that would exist exactly between over- and under-moderation (the concept is described further below). Here it is shown how optimal moderation can be achieved and maintained for the bulk of the operating life of a pebble bed reactor (or for any reactor with continuous refueling and defueling). Some of the safety and economic benefits of operating in the optimal moderation state are also described.

5.1.2 Temporary Optimal Moderation in Batch-loaded Cores

Light water power reactors are commonly built, by design, to be undermoderated. The purpose is to ensure negative reactivity feedback if the coolant density were to decrease, a necessary safety requirement. The level of undermoderation shifts during a cycle, but not enough to result in overmoderation. This condition is complicated to some extent by the presence of burnable poisons and, in the boiling water reactor (BWR), the normal presence of operational levels of boiling. Undermoderation and overmoderation are not the ideal state for the most efficient use of the neutrons generated in operation as is described below.

The ideal use of neutrons is in producing further fission events. Such a use would correspond to a fuel, moderator, and other material configuration that ensures the highest possible effective multiplication factor. One could envision a fixed-core reactor that is constructed to be thus optimally moderated. For example, this could be the case at the beginning of a cycle, i.e., just after refueling. In such a reactor, fuel depletion (and other composition changes that result from neutron interactions) would result in a nearly immediate departure from the optimal moderation once the reactor is operated. Such

departure may even result in an overmoderated configuration, which is prone to positive void reactivity feedback, an undesirable feature from the safety standpoint. Similarly, if optimal moderation were to arise later than immediately upon refueling, further depletion would again result in immediate departure from the desired state. From these considerations, it is apparent that optimal moderation in a fixed-fuel reactor cannot be maintained once the reactor is operated and therefore cannot be relied on as the normal operating mode. This conclusion applies to LWRs as well as to other fixed-fuel reactors such as the prismatic gas-cooled high temperature reactor. The foregoing conclusions apply even to the asymptotic equilibrium cycle described in the introduction. Furthermore, for light water reactor, once the reactor departs from optimal moderation, the expected ensuing overmoderation is undesirable. For fixed-core gas-cooled, graphite-moderated reactors the positive void reactivity feedback is not an issue since the coolant has very little reactivity impact. However both under and overmoderation may have a detrimental effect on the neutron economy.

In contrast to the LWR, graphite-moderated reactors are designed, when possible, in such a way as to allow the effective control of the positive reactivity insertion that would result from potential (though hypothetical they may be) water or hydrogen ingress events. For example, in the design of the HTR-Modul 200, the moderation level (i.e., fuel to moderator ratio) is chosen such that the negative reactivity worth of available control rods is sufficient to offset the positive reactivity insertion expected from a water ingress event [10]. In continuously refueled and defueled reactors, the moderating ratio need not be tied to control rod worth. In fact, because of the very low level of excess reactivity that can be achieved for a PBR and because of the existence of a true asymptotic fuel loading and burnup distribution pattern, the core can be designed to

remain continuously ideally moderated. The remainder of this section explores one approach to building optimal moderation into the design of a pebble bed reactor.

In a continuously fueled and defueled pebble bed reactor, an equilibrium asymptotic fuel loading and burnup distribution pattern arises relatively soon after initial loading and persists for the bulk of the operating life of the reactor. As explained in Chapter 3, this asymptotic loading pattern is determined uniquely by a small set of design and operational parameters such as fresh fuel enrichment, fuel discharge burnup, or pebble flow rate and pattern. Because of this uniqueness, and the small number of determining parameters, it is possible to optimize the design of a PBR for any specific objective by varying only that small number of parameters. These parameters are listed in Table 5-1.

Table 5-1: Optimization parameters for PBR core design and fuel management.

Core Power
Core Geometry (radius and height)
Reflector Geometry
Discharge Burnup
Total Pebble Flow Rate
Relative Zone Pebble Flow Rate (multiple zone cores)

5.1.3 Optimal Moderation in Static Cores

The fuel itself possesses numerous degrees of freedom that affect the characteristics of the core, including the moderation state. These include: total heavy metal loading per pebble, enrichment, moderator-fuel ratio, and moderator composition. Ougouag, et al., describe a study involving a set of MCNP [93] models that provide proof

that optimal moderation can be achieved merely by varying one or more fuel design parameters [92].

The MCNP model assumes a core geometry similar to that of the HTR Modul 200. The enrichment and particle density are held constant but the radius of the inner-fueled zone of the pebble is varied with a corresponding effect on the core multiplication factor. The results of these changes are shown in Figure **5-1**. It is clear that optimal moderation is achievable with fuel and materials typical of PBR designs. It is also clear that for this static reactor configuration (i.e., no fuel motion and no depletion) the location of the fueled/unfueled zones interface at a radius of 2.5 cm is not optimal.

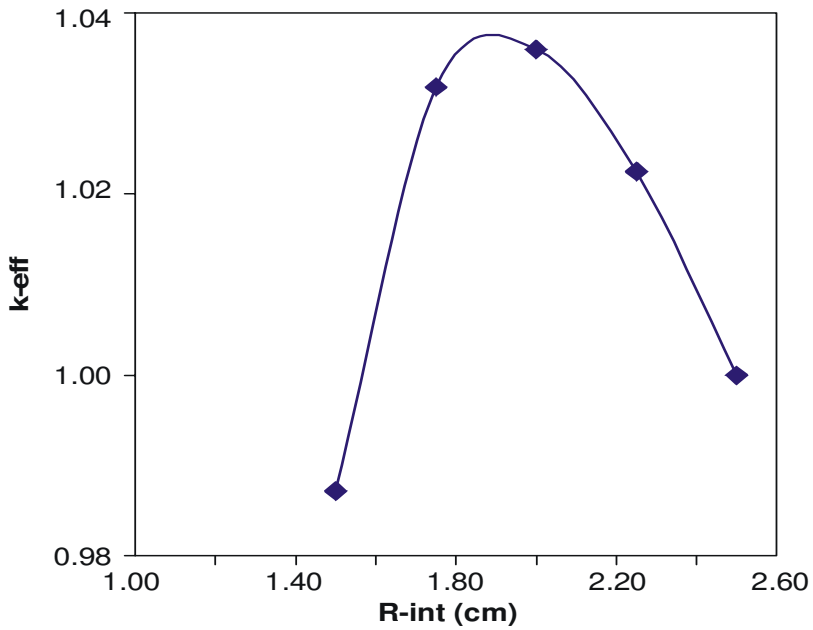

Figure **5-1**: Infinite core multiplication factor vs. fuel region radius (MCNP).

If a reactor is constructed using a pebble with fueled/nonfueled interface at about 1.9 cm, then the maximum neutron multiplication is achieved. In such a reactor the neutron economy is the most efficient and moderation is at its peak.

These results demonstrate that material compositions, including fuel, that constitute the core of a gas-cooled graphite-moderated pebble bed reactor can be adjusted to produce an optimally moderated core. Yet these results pertained to a static core and ignored the effects of operation (and hence depletion) that would terminate the optimally moderated state. To demonstrate optimal moderation in a recirculating PBR, an equilibrium cycle code such as PEBBED must be employed.

5.1.4 Asymptotic Pattern Iterations and Cross-Section Generation

The computation of the effective multiplication factor for a reactor core pre-supposes the availability of diffusion theory nuclear data that are compatible with the ultimately sought asymptotic state. That is, the neutron spectrum used in generating the data (multigroup cross section and diffusion coefficients) must be the neutron spectrum that would exist when the reactor core is in the asymptotic state. A priori, that spectrum is not known and therefore the corresponding nuclear data are not available. Two approaches are possible for producing the needed data.

In the first possible approach to diffusion theory preparation, a library of data is generated using a model assuming an infinite domain of fresh pebbles and gradually depleting them to the cutoff discharge burnup. A data library is thus generated for all possible depletion states of a pebble. Since the pebble bed reactor includes pebbles at various stages of depletion at every layer, the average state of depletion of any given level (and leakage in and out of adjacent layers) determines the neutron spectrum in the layer under consideration. One possibility (in the first approach) is to use data from the library directly, using data from pebbles at a depletion level (i.e., exposure in MWd) equal to the average depletion level of the core layer under consideration. A second

alternative (still in the first approach) is to generate macroscopic data using a mix of data from the library, at the various levels of depletion, in proportion to the number of pebbles present in the core layer (or modeling zone) under consideration that are at the corresponding levels of depletion.

In the second approach to diffusion data preparation, adopted in this work, an iterative scheme is followed. Microscopic nuclear data corresponding to the average burnup level (or any reasonable arbitrary burnup level, including fresh fuel data) of the entire core are initially assumed. The data are prepared using both MICROX-2 and COMBINE. The data are then used in the PEBBED code to determine the corresponding asymptotic loading and burnup pattern and the corresponding nuclide number densities and their respective distributions. The newly determined nuclide number densities are then input into the MICROX-2 code and the spectrum computation repeated and an updated set of diffusion theory microscopic data generated. The process is then repeated until convergence.

The product of the iterative process just described is a plausible design for a PBR asymptotic core, including the nuclides distribution, and the corresponding set of nuclear data based on a consistent spectrum. Each time the design of the fuel pebble or core is varied there results a different outcome of the iterative process. The search for an optimally moderated core consists in systematically varying the design of the fresh fuel pebble and logging the characteristics of the resulting asymptotic core. The optimal moderation fresh fuel pebble is the one that yields the asymptotic core design with the highest value of the effective multiplication factor. That core is the optimally moderated core given for the fuel enrichment, moderator choice, and core parameters listed in the previous section.

Once an optimally moderated core design is obtained, its properties are studied via further models. For example, the response of the core to water ingress is investigated by assuming the gradual addition of water vapor into the coolant phase (or the gradual substitution of water vapor for portions of the coolant). The sequence of required computations starts with an evaluation of the nuclear data (e.g., using MICROX-2). Input to this evaluation is the nuclides number densities of the optimally moderated asymptotic core augmented with the relevant concentration of water vapor and helium coolant. The resulting nuclear data are then used in a criticality calculation (without further depletion). The process is repeated as needed for increased water inventory in the core region. This method was applied to obtain the cross-sections for most of the models described in this work.

The nature of the asymptotic fuel loading and burnup distributions can be affected by, among other things, the design of the fresh fuel pebbles. As explained above, any changes to the pebble design were subjected to the constraint that all hardware of previous designs remain applicable. Thus the size of the pebbles is unchanged. A further simplifying choice is the assumption that the only parameter in the pebble design that is allowed to vary is the radius of the interface between the fueled and the nonfueled zones within the pebble and consequently the amount of fuel kernels present. The first result shown below is the demonstration of a continuously optimally moderated core. It followed by results that illustrate the property of such a core.

In Figure **5-2**, the change in the effective multiplication factor is shown for two possible pebble bed reactor as the radius of the fueled zone in fresh pebbles is varied.

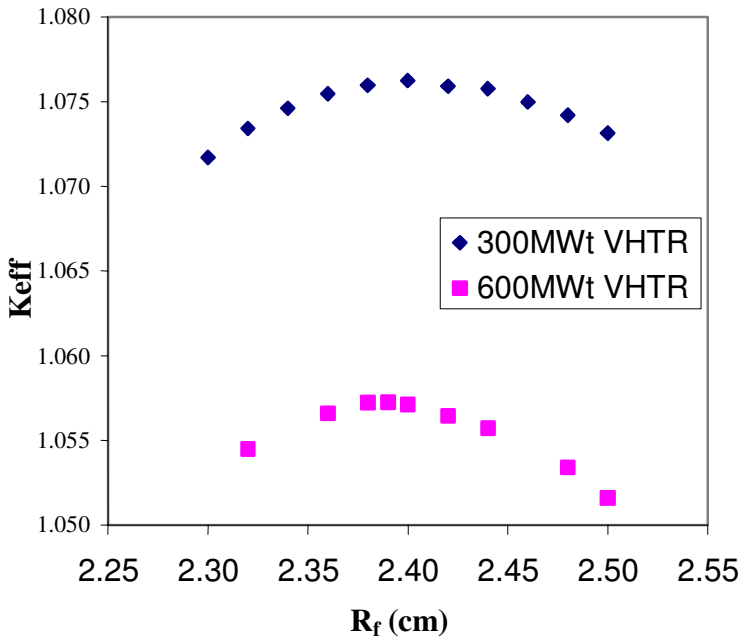

Figure 5-2: Effective multiplication factor dependence on the radius of the pebble fueled zone.

The two reactors addressed in the figure are a 300 MWth and a 600 MWth versions of a Very High Temperature Reactor (VHTR) to be discussed in Chapter 5. Each of the points on the figure corresponds to a converged PEBBED/MICROX-2 solution of the combined search for the asymptotic equilibrium fuel loading and burnup pattern and the corresponding consistent nuclear data.

The 300 MWt core displays peak moderation at a fuel region radius of 2.4 cm while the 600 MWt core peak is shifted slightly to 2.39 cm. As expected, the optimal pebble design depends on the size and power of the reactor. Though not demonstrated here, the optimal pebble design may also depend on other core design parameters. Since the same particle packing fraction is assumed within the fueled zone, the fuel region radius numbers correspond to a particle loading of about 13,271 particles per pebble for the 300 MWt core and 13,106 particles per pebble for the 600 MWt design. The performance and safety aspects of these designs will be discussed in later sections.

Since each point in Figure 5-2 corresponds to an asymptotic equilibrium pattern, the possibility of continuously optimally moderated operating reactor is demonstrated.

5.1.4.1 Consequences of Optimal Moderation on Water Ingress Reactivity Insertion

At least one modular gas-cooled reactor design, the GT-MHR, employs a shutdown cooling system in which decay heat carried by the helium in the core during periods when the reactor is shut down is passed to a water loop in a heat exchanger near the core [94]. Therefore, the potential exists for water to enter the core. It is possible that a similar system will be required for the pebble-bed VHTR, so an analysis of water ingress into the pebble-bed core is presented below.

Initial studies of the effect of water ingress into the coolant spaces between the pebbles were performed using COMBINE-generated cross-sections. The “Dry” peak corresponding to optimally moderated fuel was found to occur at a fuel region radius of 2.33 cm, substantially different from that computed using MICROX cross-sections. However, the results of the water ingress calculations qualitatively agree with subsequent MICROX runs and the previous MCNP study and thus are discussed here.

Figure 5-3 displays the effect of water ingress on core multiplication factor as computed with a full-core MCNP model.

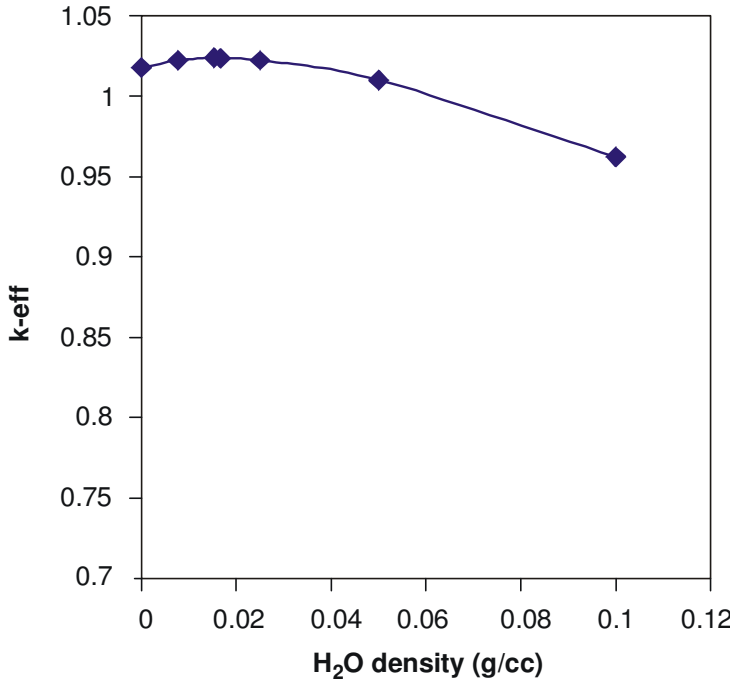

Figure 5-3: Core multiplication factor vs. density of steam in VHTR-300 coolant (MCNP).

In the figure it can be seen that a moderate rise in the multiplication factor occurs followed by a subsequent drop. The reactivity insertion is modest, even at its maximum. The concentration of water at this maximum reactivity insertion corresponds to a water inventory in the core region of approximately 500 kg. Such an amount of water can penetrate the core region only gradually, and only under the assumption of a major malfunction. In the early stages of the insertion only smaller amounts of water, and thus only smaller reactivity insertions are plausible. The consequence of this gradual insertion of reactivity is discussed below in conjunction with feedback effects. The MCNP results of Figure 4-2 do not account for the motion or the depletion of the fuel. For these effects, the PEBBED/COMBINE or the PEBBED/MICROX-2 combinations of codes must be used. Figure 5-4 shows the effect of water ingress for various pebble designs (i.e., various fueled zone radii).

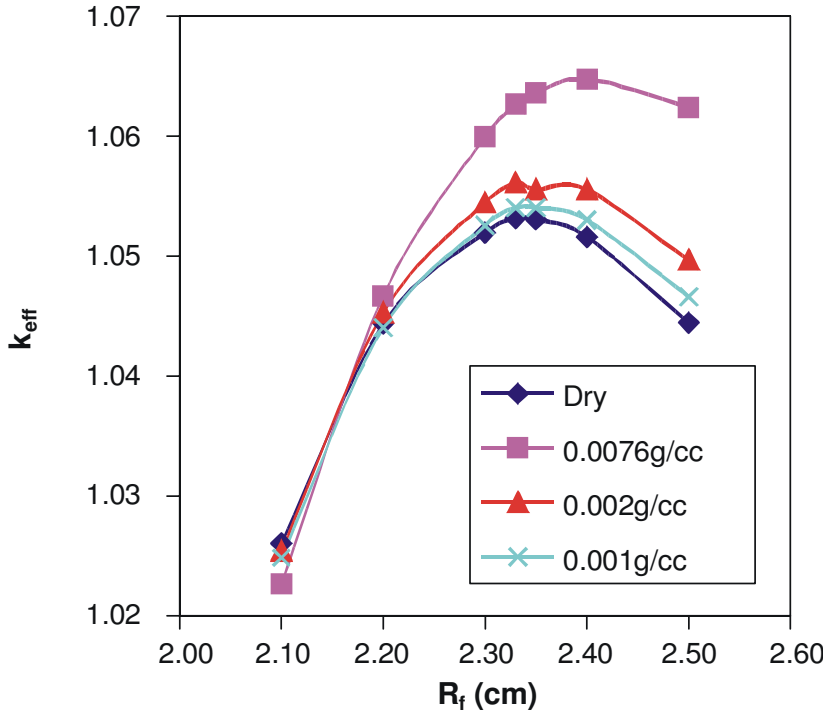

Figure 5-4: Multiplication factor versus fuel zone radius (PEBBED/COMBINE model).

The curve labeled “dry” pertains to cores with no water present. The rise then fall in the curve represent the change in core reactivity as the radius of the fueled region within the pebble is changed. In the modeling, the overall core size and other characteristics (including core dimensions, fuel circulation patterns etc. remain unchanged). Each point on the “dry” curve is the result of a converged iteration process using the PEBBED and the COMBINE codes. The other curves correspond to various steam densities in the coolant. All of the curves indicate a positive reactivity insertion for steam ingress for pebbles with fueled region radii of 2.20 cm or greater. Water has completely negative reactivity effect for small (R_f <2.1 cm) pebble designs.

The steam ingress performance of the ‘optimal’ pebble, i.e., one the design of which corresponds to the dry peak in Figure 5-2, was compared to that of the standard PBMR pebble design with a fuel region radius of 2.5 cm. Figure 5-5 shows the core

multiplication factor as a function of steam density for each case. Clearly water has a less severe reactivity effect for optimized pebbles. The peak characteristics are summarized in Table 5-2.

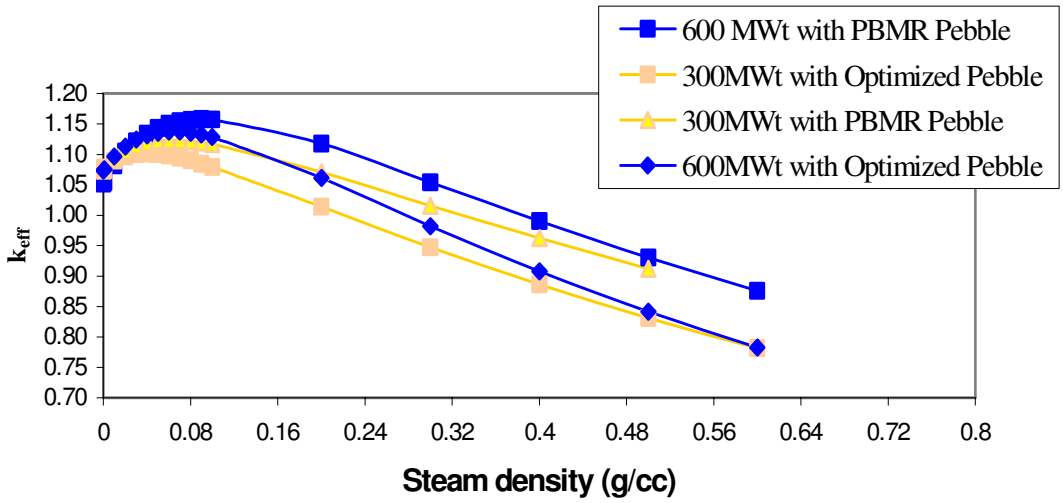

Figure 5-5: Core multiplication factor as a function of coolant steam density.

Table 5-2: Peak water ingress reactivity insertion for various VHTR core and fuel designs.

		Peak Insertion ($)	Water Density (g/cm^3)
300 MWt	Standard Fuel	7.74	0.06
300 MWt	Optimized Fuel	3.89	0.04
600 MWt	Standard Fuel	16.34	0.09
600 MWt	Optimized Fuel	9.49	0.06

The peak reactivity insertions from steam ingress for the optimized pebbles are roughly half as great as those for the standard pebbles.

Any insertion of reactivity will result in an increase in power and core temperature (assuming that coolant flow is held constant). Such power excursions are inherently

self-limiting because of the strong negative temperature coefficient of the graphite-moderated fuel.

Figure 5-6 illustrates the effect of temperature on the core multiplication factor. The data were generated using various graphite scattering kernels available in the COMBINE code.

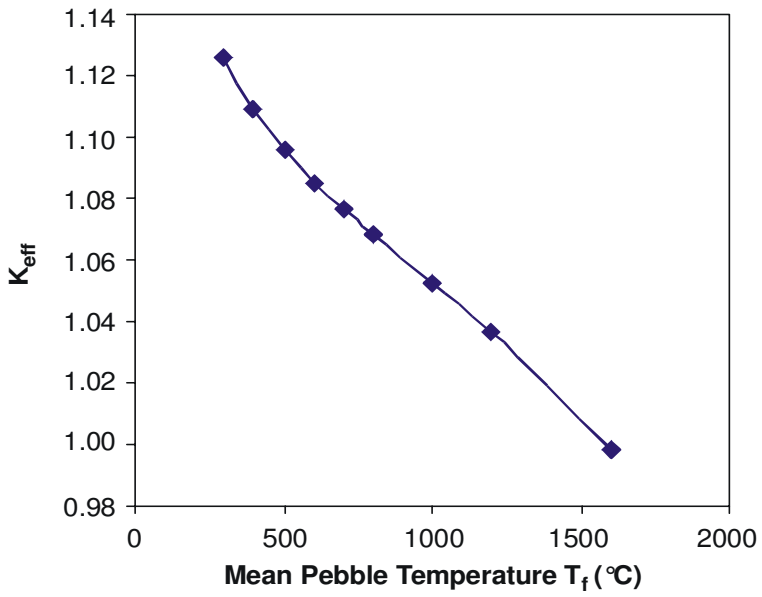

Figure 5-6: Core multiplication factor vs. fuel temperature.

Figure 5-7 compares four operating conditions for cores with pebbles of different fuel region radii. Recall that the COMBINE-optimized pebble has a fuel radius of 2.33 cm and the standard pebble has a fuel radius of 2.5 cm. The thick dark curve shows the nominal VHTR with a core-wide average pebble temperature of 1,100 K. The uppermost curve corresponds to this temperature but with a steam ingress of 0.0076g/cm^3, indicating a reactivity insertion of $1.39 for the optimized pebble and $2.66 for the standard PBMR pebble. (This steam density corresponds to the replacement of half the helium atoms by water molecules.)

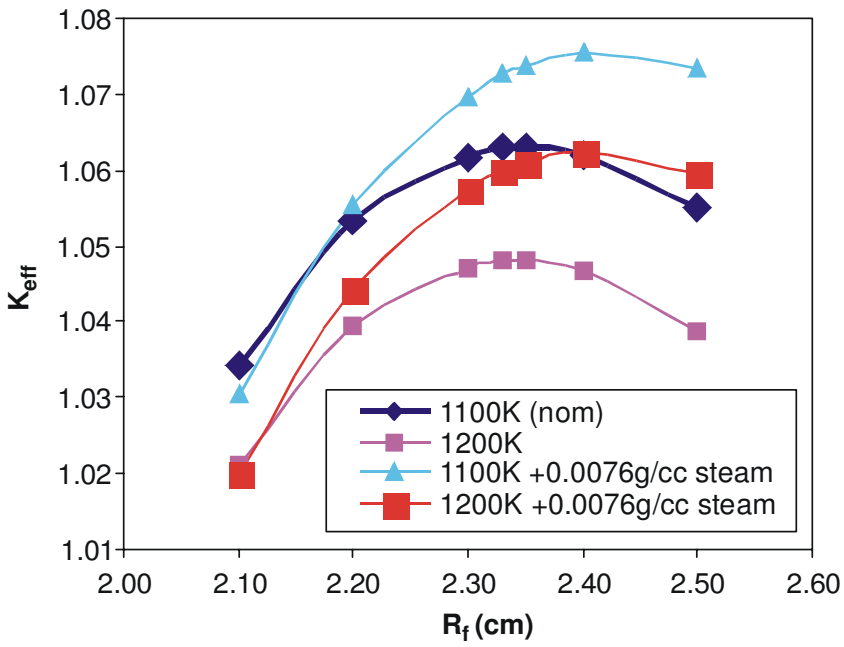

Figure 5-7: Core multiplication factor vs. fuel region radius.

The lowermost curve corresponds to a dry core at 1,200 K, a 100-degree increase above the nominal case. The curve just above it shows the combined reactivity effect of a 100 K increase in core-wide average temperature and the steam ingress. The core-optimized pebble is \$0.43 *less* reactive than the nominal core while the core fueled with the standard PBMR pebble is \$0.63 *more* reactive. Fission product energy is deposited almost instantaneously, while the time scale for reactivity insertion is the transit time of coolant through the core, so thermal feedback will occur faster than the reactivity insertion. Clearly, a VHTR core can be designed that is largely immune to water ingress events.

All of the foregoing analyses were performed with a fuel enrichment of 8%. The results may be different if enrichment is allowed to vary. The PEBBED studies also assume recirculation of the pebbles until they reach the maximum allowed burnup. Top

layer fueling with fresh and recirculated pebbles is assumed random. Additional optimization of the core could be possible if specific circulation schemes are assumed with deliberate placing of pebbles in preferred zones.

These preliminary results indicate that pebble fuel can be made much more resistant to ingress events. The PBR core fueled with an optimized pebble, while still exhibiting a significant reactivity insertion for a sufficiently high steam density, is superior to the nominal PBMR design in this regard. The higher moderating ratio of properly designed pebble fuel results in a significantly lower core excess reactivity that decreases the effect of water ingress. Furthermore, Figure **5-4** indicates that for certain pebble designs, steam ingress reactivity will be negative under all circumstances; a feature not attainable in batch reload high temperature gas reactor designs. Finally, as shown in Figure **5-7**, temperature feedback can be expected to mitigate the steam ingress reactivity insertion for the dry optimized pebble.

5.1.5 Effect of Pebble Optimization on Fuel Economy

As implied in the previous sections, an optimally-moderated pebble should yield a neutron economy superior to that of a non-optimized pebble. Specifications for PBMR and optimized pebbles were incorporated into the model of the PBMR (with dynamic inner reflector) and burned to the same discharge level of 80 MWd/kg_{hm}, The optimized pebble yielded a core with a noticeably higher core multiplication factor, confirming the prediction (see Table **5-3**).

Table 5-3: Core multiplication factor of the PBMR with nominal and optimized pebbles.

	k_{eff}
PBMR-DIR with Nominal Pebble	1.0737
PBMR-DIR with Optimal Pebble	1.0764

A reactor operating at a steady state has a core multiplication factor of 1.0 regardless of the pebble design so a second calculation was performed in which the discharge burnup of the core with optimized pebble was adjusted to yield the same core multiplication factor as that computed for the PBMR with standard pebble (Table 5-4).

Table 5-4: Fuel performance of optimal vs. nominal PBMR pebble.

k_{eff}	**1.074**		**1.073**	
Discharge Burnup (MWD/Kg_{hm})	**80**		**81.4**	
Enrichment	**8%**		**8%**	
HM loading (g)	**9**		**7.962**	
# Particles per pebble	**15,000**		**13,271**	
Pebble Injection Rate (peb/day)	**371.6**		**413**	
# Passes per pebble	**10**		**9**	
Residence Time (days)	**885**		**764**	
Discharge Concentration	(g/day)	total change (g/pebble)	(g/day)	total change (g/pebble)
U-235	**53**	-215	**43**	-221
U-238	**2,913**	-162	**2,872**	-152
Pu-239	**20**	20	**16**	16
Pu-240	**12**	12	**11**	11
Pu-241	**10**	10	**8**	8
Pu-242	**7**	7	**7**	7
Fuel Utilization (g/MWD)		-1.23		-1.23
HM Mass Daily Throughput (g/day)	**3,344**		**3,288**	
HM Mass Daily Throughput per MWD	**12.5**		**12.3**	
Particles/MWD	**20,799**		**20,451**	

The pebble injection rate is 11% higher in the optimized fuel because there is 11% less heavy metal contained within each pebble. If all other parameters were held constant, the heavy metal requirements of the cores would be the same. However, the improved neutron economy of the core charged with optimized pebbles would also result in a higher core multiplication factor. This extra reactivity can be either held down with burnable poisons or control rods, or it can be exploited to reduce the fuel requirements of the power plant. One way to do this is to reduce the enrichment of the uranium in the particles. Another is to reduce the size of the core and increase neutron leakage. For this work, the discharge burnup level was raised a bit by slowing down the flow rate slightly. The increased core-averaged burnup level and poison content reduced the core eigenvalue as well as the fresh fuel requirements of the core, expressed as particles loaded per MWd of energy produced. The bottom row of the table reveals that the optimized pebble uses 2% less fuel than the standard PBMR pebble.

This same optimized pebble yielded a safety benefit as well. Although the peak power attained by the optimized pebble is higher than that of the standard pebble, the mean and peak pebble temperatures did not significantly change. The peak DCC temperature also remained at about the same value. However, the 0.001 g/cm^3 steam ingress reactivities computed by PEBBED for the cores fueled with standard and optimized pebbles are \$0.30 and \$0.21, respectively. This is consistent with the results plotted in Figure **5-7**. The core with optimally-moderated fuel is much more tolerant of steam in the coolant. Again, a proper transient analysis code should be used to fully confirm this feature but the initial results generated by PEBBED suggest that significant benefits can be obtained with a fuel-core optimization process.

5.2 Bounding Cases for Hotspot Analysis

In pebble-bed reactors, pebbles are dropped in at the top, and a cone develops below each drop point. The pebbles roll off the mounds until they reach stable positions, and they move downward in an essentially axial direction. However, some radial wandering is expected, and the stable position on the top from which any pebble begins its downward course is somewhat randomly determined. These stochastic processes generate concern about the possibility of the development of hot spots, where clusters of highly reactive pebbles may form in regions of high thermal neutron flux, so that excessive heat generation may occur locally. To explore the possibility and consequences of such hot spot formation, the model of the PBMR-DIR analyzed in the previous chapter was modified to use various off-normal pebble recirculation patterns. Once again, the capability of the recirculation matrix to easily describe such patterns was exploited to obtain low-probability bounding operating conditions.

5.2.1 Modeling and Probability of Hot Channel Formation in the PBMR-DIR

The PBMR-DIR is characterized by a central column of graphite pebbles surrounding by an annulus of fueled pebbles. The graphite pebbles are loaded via a central loading tube while the fueled pebbles are loaded via a number of azimuthally-distributed tubes located some distance between the central axis and outer reflector. All pebbles exit the core through the same centrally-located discharge tube where they are separated by type and their burnup levels are measured. Pebble storage and fuel handling mechanism can easily be made to insure, with virtually complete certainty, that only fuel pebbles are forwarded to the annulus loading tubes while only

graphite pebbles are directed to the central loading tube. Nonetheless, it is an interesting exercise to conceive a *beyond-design-basis* situation in which the fresh and partially-burned fuel handling mechanisms fail and allow the graphite and fuel pebbles to be loaded into the incorrect zones. Two general failure scenarios are investigated here and illustrated in Figure **5-8**. Keep in mind that these are asymptotic core calculations; at nominal pebble flow rates the reactor would need to operate for up to three years with the prescribed faulty fuel handling mechanisms in order to achieve these core conditions. If the fuel handling mechanisms were to fail for much shorter periods of time, a small cluster of reactive pebbles may form but the remainder of the core would closely resemble the nominal case. In the event of a depressurized loss of coolant flow, pebbles in the cluster may exceed failure temperatures for a short period of time but extensive core damage would not ensue.

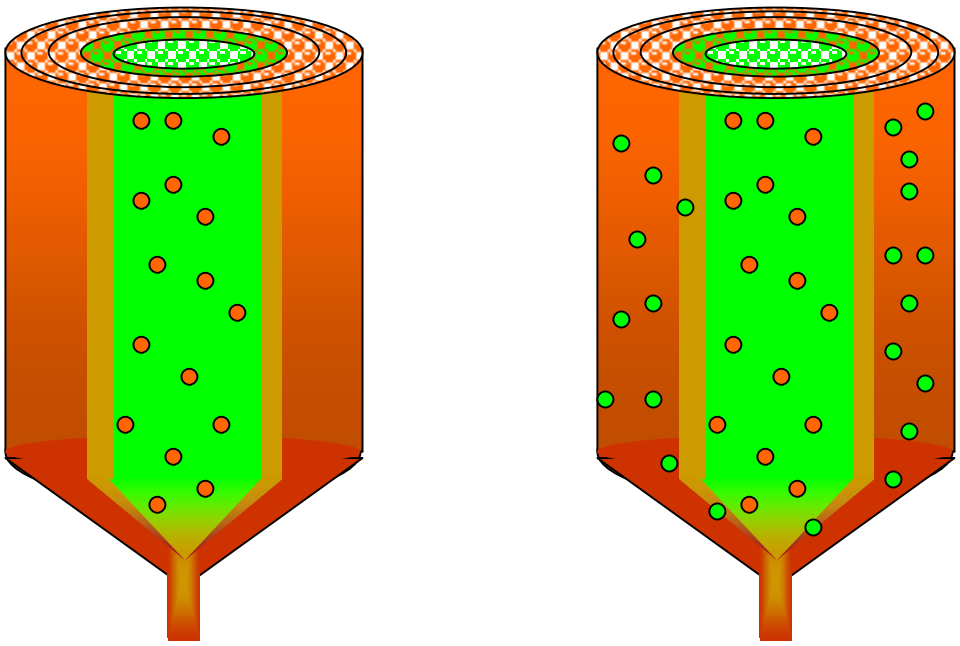

Figure **5-8**: Misdirected pebble scenarios in two-zone PBMR core.

In the first misdirection scenario (*replacement*), both the fresh fuel and recirculating fuel-sorting mechanisms are assumed to fail to various degrees. Fresh fuel pebbles are allowed into the central loading tube (along with graphite pebbles) so that very reactive pebbles are loaded into the central column with its high thermal flux. At the discharge tube, the sorting mechanism also fails in such a way that fueled pebbles may be routed back to either the central or annular loading tubes. Graphite pebbles, however, are properly loaded only in the central column. The net effect on the core is a replacement of some of the graphite pebbles with relatively fresh fuel pebbles (and an increase in the overall heavy metal inventory of the core). The fuel pebbles are transferred to the outer annulus after one or more passes through the central column. Table **5-5** shows the distribution by channel and pass of fuel and graphite pebbles in the a replacement scenario in which fresh fuel pebbles are loaded nominally into the outer annulus but also into the inner reflector region as well, replacing some of the graphite pebbles that are normally injected there. The misloaded fuel pebbles are transferred to the outer annulus after the first pass, as if the fuel recirculation system were functioning properly. For comparison, refer to the flow pattern of the nominal PBMR-DIR core shown in Table 4.2.

Table 5-5: Flow distribution in PBMR-DIR – addition of fuel to inner reflector for one pass (1st replacement scenario).

	Pebble Flow Rate (pebbles/hour)				
Channel	**1**	**2**	**3**	**4**	**5**
Pass			**FUEL**		
1	10.65	4.87	0	0	0
2	0	2.17	4.57	4.36	4.43
3	0	2.17	4.57	4.36	4.43
4	0	2.17	4.57	4.36	4.43
5	0	2.17	4.57	4.36	4.43
6	0	2.17	4.57	4.36	4.43
7	0	2.17	4.57	4.36	4.43
8	0	2.17	4.57	4.36	4.43
9	0	2.17	4.57	4.36	4.43
10	0	2.17	4.57	4.36	4.43
Total	10.65	26.56	45.65	43.58	44.33
			GRAPHITE		
1 (OTTO)	30.17	13.79	0	0	0

In the second misdirection scenario (*transposition*), there is a one-for-one transposition of graphite and fuel pebbles, i.e., whenever a fuel pebble is improperly loaded into the central column, a graphite pebble is also improperly loaded into the annulus. The overall core heavy metal inventory of the nominal PBMR-DIR is preserved. Table 5-6 shows the flow pattern for such a scenario in which fuel pebbles are inappropriately loaded into the central column while graphite pebbles are loaded into the annulus. After the first pass, the pebbles are sorted and loaded properly.

Table 5-6: Flow distribution in PBMR-DIR – switching of fuel and graphite for one pass (1st transposition scenario).

Channel	1	2	3	4	5
Pass			**FUEL**		
1	10.62	4.86	0	0	0
2	0	2.16	4.55	4.35	4.42
3	0	2.16	4.55	4.35	4.42
4	0	2.16	4.55	4.35	4.42
5	0	2.16	4.55	4.35	4.42
6	0	2.16	4.55	4.35	4.42
7	0	2.16	4.55	4.35	4.42
8	0	2.16	4.55	4.35	4.42
9	0	2.16	4.55	4.35	4.42
10	0	2.16	4.55	4.35	4.42
Total	10.62	24.33	40.98	39.12	39.37
			GRAPHITE		
1 (OTTO)	30.08	15.92	4.55	4.35	4.42

The number of variations on these two failure scenarios is extremely large because of the number of pebbles that can be misdirected. A few representative cases can be used to capture the general effect. Specifically investigated are the situations in which all fresh fuel pebbles loaded into the central column are transferred to the outer annulus after one, two, or three passes. To model these cases, an IN-OUT recirculation mode is specified for fuel pebbles loaded into the central column. The fraction of fuel pebbles loaded into the two fueling zones is adjusted to obtain transfer of all fuel pebbles after the specified number of passes through the central column. The geometry of the core and flow conservation require that all fuel pebbles are transferred out in three passes or less.

5.2.2 Consequences of a Combined Hot Channel Formation-DCC Event

Shown in Table 5-7 is the effect of these off-normal situations on the core eigenvalue, peak nominal fuel temperature (trajectory-averaged), and peak accident (DCC) fuel temperature.

Table 5-7: Effect of fuel handling failure modes on core parameters.

Case	K_{eff}	Peak Operating Fuel Temperature (°C)	Peak DCC Fuel Temperature (°C)
Nominal PBMR-DIR	1.074	1040	1452
Replacement			
Transfer after 1 pass	1.110	950	1,613
Transfer after 2 passes	1.116	1,078	1,696
Transfer after 3 passes	1.102	1,127	1,712
Transfer after 4 passes	1.085	1,133	1,676
Transposition			
Transfer after 1 pass	1.115	968	1,613
Transfer after 2 passes	1.127	1,268	1,736
Transfer after 3 passes	1.121	1,209	1,776
Transfer after 4 passes	1.109	1,243	1,784

The core multiplication factors (k_{eff}) reflect the fact that the distribution of fuel toward the central column yields better neutron economy. This effect diminishes if the pebbles are kept in the central column for more than one pass and their fissile content decreases. In actual operation, the extra reactivity would force the insertion of control rods or a reduction in the fresh fuel injection rate to keep the core critical. Peak fuel temperatures during normal operation are significantly higher than the nominal case but not so high as to lead to fuel failure. Peak accident (DCC) fuel temperatures do exceed the 1,600°C threshold so some particles would be expected to fail (see Figure 2-5) with

a small release of fission product inventory to the coolant. In none of the cases does this peak temperature exceed 1,800°C much less 2,000°C, the value at which extensive fuel failure would begin to occur. Furthermore, this is the peak value for the entire core, meaning that the bulk of the core never even reaches this peak temperature.

This type of analysis further reflects the robustness of the core and fuel. Even in a vanishingly low probability event in which the reactor is operated for years with a failed (or sabotaged) fuel handling mechanism, followed by a sudden and complete loss of coolant pressure and flow, large release of the fuel inventory would not be expected to occur.

In Chapter 6, a similar analysis is performed on a 300 MWt Very High Temperature Reactor design.

5.2.3 Accumulated Stress on Pebbles

The motion of the pebbles confers a unique benefit not shared by nuclear reactors with static cores. Although the pebbles move slowly downward, the locations of radial and axial temperature and power density peaks are essentially constant once the core reaches the asymptotic state. Pebbles flow through these hot spots and then move on to cooler areas. Figure **5-9** is a plot of the pebble center point temperature of a 600 MWt VHTR, to be described in more detail in Chapter 6. The curves correspond to the different passes the average pebble makes through the core and the number at the left end of each curve is the burnup accumulated before the start of the pass.

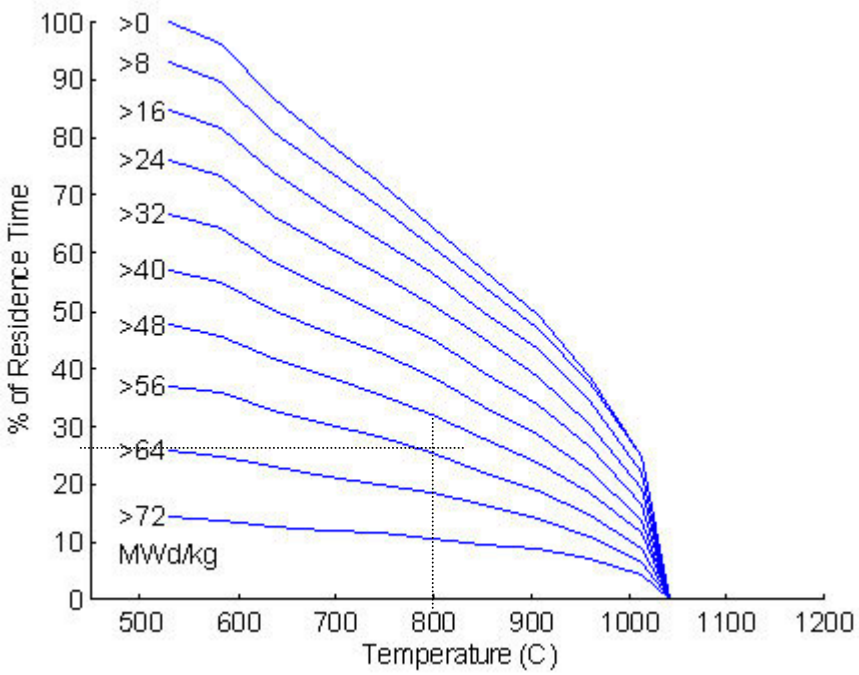

Figure **5-9**: Percent of residence time that the average pebble is above temperature.

For example, the dotted lines indicate that a pebble spends about 26% of its total core life above a temperature of 800°C and above 56 MWd/kg. The residence time for pebbles in this design is about 885 days.

The probability of fuel failure increases with temperature and burnup. The top curve indicates that a pebble is above 1,000°C for about 1/3 of its core life. The bottom curve indicates that the pebble is above 1,000°C *and* 72 MWd/kg for only about 7% of its residence time. The integrated stress on fuel particles is substantially lower than that of batch-loaded cores, in which certain fuel elements reside at hot spots throughout the cycle. In the pebble bed, thermal, and irradiation–induced stresses are shared almost equally among all pebbles, thus reducing the likelihood of fuel failure.

5.3 Considerations for Proliferation Resistance

The routine recirculation of the fuel pebbles and the online de-fueling and refueling of these reactors raises questions about their potential use as production facilities for weapons materials. However, this feature also allows the reactors to operate with very little excess reactivity. In this section the dual use of a PBR (simultaneous production of power and weapons materials) is investigated. This subject and analytical approach were conceived by Ougouag in 2001 as an application of the capabilities of PEBBED and published in papers by Ougouag, Gougar, and Terry [35],[36].

5.3.1 Dual Use of a PBR for Electricity and Weapons Production

The PEBBED code computes directly the asymptotic (equilibrium) fuel-loading pattern of a PBR, given the fresh fuel composition. This asymptotic core profile is that which is established well after (>3 years) the initial loading and persists for the remainder of the operating life of the reactor as long as the fuel composition and recirculation scheme are held constant. The profile is highly predictable. Presumably the result of extensive optimization, it is expected that this core will be maintained to the benefit of and by the operator. Departures from this pattern could be viewed as suspicious and as possible attempts at diversion of fuel for dual use. Any departure from the pattern will result in noticeable changes in fresh fuel requirements, power production, and/or discharge isotopics. All three attributes could easily be monitored via an instituted safeguards regime and via spent fuel re-purchase. As continuous burnup monitoring of discharged pebbles is part of the fuel management policy, the information on the isotopics could also be made available on-line or via the transmission of recorded data

sets to the safeguards authority. Uninterrupted fuel supply would be contingent upon acceptable reactor use.

The PBR owner is assumed to be a low technology country without front-end fuel cycle facilities (i.e., enrichment capability) and thus dependent on a supplier country for its fresh fuel needs. The supplier country is party to a non-proliferation regime and agrees to enforce safeguards on its fuel customers. Either the spent fuel is re-claimed or information on discharged pebbles average isotopics is required. Finally, it is assumed that for economic reasons the on-hand fresh fuel inventory of the PBR owner is maintained as low as practical. For this study, it is assumed that after the initial loading the fuel supplier periodically provides ninety days of fresh fuel to the PBR owner, just prior to stock exhaustion.

Three principal scenarios were investigated in the Ougouag studies: (i) the covert dual use of the facility, (ii) the overt diversion of the facility as built, and (iii) the construction of an alternate facility using equipment diverted from the original facility ("cannibalization"). Only the first of these will be discussed here, as it requires the most use of the recirculation matrix.

5.3.2 Covert Dual Use

In this scenario, a small number of *production* pebbles are covertly introduced into the reactor to produce weapons materials while still producing power. The goal of the reactor owner would be to produce weapons material at the maximum rate possible at which the effects on the legitimate fuel cycle use would be undetectable. The reactor owner expects to continue receiving replacement fresh fuel from the supplier. The maximum dissimulation case of this first scenario was considered in the first Ougouag

study [35] in which it was assumed that illicit fuel pebbles were manufactured by the reactor owner and used as production targets in the reactor. Those illicit pebbles were assumed identical to legitimate fuel pebbles in all respects except uranium enrichment. Thus, they included the same physical features and compositions, save for the replacement of enriched uranium with natural uranium. In that earlier study, it was shown that this scenario was very impractical for the production of weapons materials and that it resulted in very early detection because of shortfalls in power production and an unjustified increase in fresh fuel needs. The production pebbles were “optimized” to resemble the legitimate ones as much as possible. In this study, a variant of the first scenario is considered in which the illicit pebbles are optimized to *minimize the perturbation on the multiplication factor* that they cause (and thus minimize their impact on neutron economy).

This study shows that a PBR fueled only by natural uranium pebbles would be large enough to be detectable by reconnaissance satellites. It also shows that adding natural-uranium production pebbles to the regular fuel pebble flow stream at undetectable rates would not only lead to slow production of weapons material but would also produce plutonium of very marginal quality. If higher quality plutonium is sought, the time to accumulation of sufficient materials for practical weapons use is shown to be extremely large, and not compatible with the speedy production of even a modest arsenal.

5.3.2.1 Methods and Computational Models

There exist many ways by which covert production of weapons materials could be detected; here, it is assumed that a decrease in fuel utilization of more than 5% (or a

commensurate increase in fuel requirements) would cause suspicion. Similarly, a discrepancy between energy production and fuel consumption or fuel requirements would raise suspicion. Furthermore, a departure of discharged fuel pebbles isotopics from the nominal values that correspond to optimal plant operation would also be reasons for suspicion, as the isotopic distribution in an optimally operated PBR, a consequence of the asymptotic loading pattern, is likely unique and accurately predictable. The models developed in this study, as in the preceding one, rely on these measures to demonstrate the PBR is not a good choice for production of weapon materials. The models developed in these studies are conservative. That is, they are devised so that their predictions are consistently more pessimistic than reality. For example, the quantity of concern [95] is taken as the lower range of a mass of weapons-grade Pu-239 that could conceivably be fashioned into a weapon regardless of the actual quality expected from the mode of production. This would assume a very sophisticated design and access to advanced technologies. Thus, in this study, about 5 kg of Pu-239 is the quantity of concern, regardless of the presence of additional Pu isotopes. Note that the information presented in this work contains a large number of approximations and thus imply a certain degree of uncertainty is inherent in the results presented. However, the orders of magnitude, the trends, and the conclusions of the study are to be regarded as correct. The constraints on the various scenarios to weapons-material production were explored by constructing numerical models for analysis by the Monte Carlo code MCNP [93] and PEBBED. These models are described in turn below.

5.3.3.2 Optimized Natural Uranium Production Pebbles

The model results for the pebble design optimization study are only summarized here. The variation of the infinite multiplication factor, k_∞, with the uranium-graphite ratio was studied for several values of void radius of the fuel sphere. The greatest maximum value was shown to occur when the void radius is zero – i.e., when the fuel sphere is solid. The same conclusions were reached for pebbles with a 2 cm overall radius. The uranium-to-graphite volume ratio at which k_∞ is greatest for each value of the void radius was compiled for both pebble sizes considered. It was observed that the most successful production of Pu-239 would be achieved by using a pebble with a volume ratio of 0.00564, an average of all the values found for different trials. This corresponds to a solid uranium inner sphere radius of 0.533 cm, or only 17% of the radius of the pebble.

Production pebbles of the optimized design (i.e., natural uranium spheres 0.533 cm in radius within graphite shells 3 cm in external radius) were introduced into the PEBBED model of the two aforementioned PBR designs. In this study, the “driver” legitimate fuel pebbles were recirculated as in the legitimate cores, but the illicit production pebbles were removed after their first pass through the reactor for optimal plutonium isotopics. Introducing natural uranium into the core reduces the core reactivity. Thus, in order to maintain criticality the legitimate fuel pebble injection rate was increased with a corresponding decrease in discharge burnup of the driver fuel.

5.3.4 Effect of Introduction of Production Pebbles on Core Neutronics

The fuel utilization characteristics of the nominal and dual use (5% production pebbles) reactors are listed in Table 5-8.

Table 5-8: Operational parameters for nominal and dual use PBRs.

		Driver		Production		
Case	**k_{eff}**	**Injection Rate (peb/day)**	**Discharge Burnup (MWd/kg_{ihm})**	**Injection Rate (peb/day)**	**Pu-239 Content (mg/pebble)**	**5kg Accumulation Time (days)**
Nominal HTR	1.088718	356.1	80.0	NA	NA	NA
HTR with 5% NU	1.088736	397.4	70.5	271.9	31.4	586
Nominal PBMR	1.073666	371.6	80.0	NA	NA	NA
PBMR with 5% NU	1.073668	377.1	78.4	72.25	26.9	2,573

Not surprisingly, the higher number of production pebbles in the HTR Modul 200 core causes a much greater perturbation. The discharge burnup of the driver fuel had to be reduced by over 10% to maintain the same multiplication factor as the nominal core. Pu-239 was produced at such a rate that five kilograms is accumulated in a little over a year and a half. However, the fresh fuel requirement increased by 11% so a 90-day supply of driver fuel would last only 80 days at full power. A 10-day shutdown every three months would have considerable impact on the economics of the power plant and would be immediately noticeable to the safeguards authority.

The PBMR-DIR with 5% of its graphite pebbles replaced with production pebbles would be harder to detect. The discharge burnup need only be reduced by

1.6 MWD/kg_{ihm} to sustain Pu production. This may be easier to sustain if there is uncertainty in the burnup measurements and the reactivity loss may be recovered in other ways such as increasing the coolant flow rate and lowering the temperature of the core. However, the Pu-239 production rate is significantly lower than the previous case; a full seven years is required to accumulate five kg of weapons material.

Table 5-9 lists the plutonium content of discharged pebbles for the different cases.

Table 5-9: Isotopics of discharge pebbles (mg per pebble).

Case	Pu-239	Pu-240	Pu-241	Pu-242
Nominal HTR Driver	38.1	23.0	18.8	16.1
Dual Use HTR Driver	38.8	23.1	18.2	12.1
Dual Use HTR Production	31	3.0	0.3	.009
Nominal PBMR Driver	53.3	32.0	25.8	20.0
Dual Use PBMR Driver	54.0	32.4	25.9	19.1
Dual Use PBMR Production	26.9	5.6	1.4	0.10

The quality of the Pu-239 in the discharged HTR production pebbles is greater than that of the PBMR. 90% of the plutonium is Pu-239 while only 80% of the plutonium in the PBMR pebbles is Pu-239; very poor quality for weapons material and probably due to the relatively slow passage of the production pebbles through the core. The Dual Use HTR produces weapons material much more quickly and of higher quality but it does not do so covertly, a condition of this scenario. In both cases, extensive chemical processing of the indigenously produced production pebbles would be required to extract good quality weapons material.

5.3.5 Conclusion

Once again the utility of the PEBBED code is demonstrated in addressing an issue associated with pebble-bed reactors. The recirculation matrix allows various multiple-pebble recirculation schemes to be modeled and compared with ease. In this study, the code was used to show that the covert production of Pu-239 for weapons using standard fuel and core designs is difficult and time consuming.

The study ignored many issues of paramount importance to the safety and practicality of the various scenarios (dual use/cannibalization). For example, the design of the pebbles is likely to be improper for the retention of fission products and generated gases. Ensuing releases could cause health and safety concerns and would most likely make the facility easier to detect. The study could also be used for the identification of safeguard steps and procedures and for the identification of sensitive equipment. Such an extended study should be conducted.

Chapter 6

Design of a Very High Temperature Reactor

In this chapter the conceptual design method of a Very High Temperature Reactor (VHTR) using a recirculating pebble-bed core is presented. The approach exploits the unique neutronic and thermal-hydraulic capabilities to generate key parameters for a range of candidate designs. The ability of the code to estimate passive safety characteristics is confirmed using a more sophisticated accident analysis code and model. The uniqueness of the asymptotic pattern and the small number of independent parameters that define it suggest that the PBR fuel cycle can be efficiently optimized given a specified objective. In this paper, candidate core geometries are evaluated primarily on the basis of core multiplication factor and peak accident fuel temperature. Pumping power, pressure vessel fast fluence, and maximum particle power are considered as well. A design that achieves the criticality and passive safety objectives can be analyzed and further optimized with more detailed and sophisticated models. For this study, 300 MWt and 600 MWt designs were generated.

6.1 Background and Approach

6.1.1 VHTR – Characteristics and Design Objectives

The Very High Temperature Reactor is one of six advanced concepts chosen by the Department of Energy for further research and development under the Generation IV program [5]. Of the six concepts, the VHTR offers the greatest potential for economical

production of hydrogen as well as electricity because of the high outlet temperature of the helium coolant (1,000°C). This outlet temperature is one of only two absolute requirements for the candidate designs in this study. The other requirement is that the VHTR be passively safe, i.e., no active safety systems or operator action are required to prevent damage to the core and subsequent release of radionuclides during design basis events. The worst such event, the depressurized loss of forced cooling scenario (D-LOFC), is bounded by a depressurized conduction cooldown (DCC) transient in which helium pressure and flow are lost. During a DCC, the negative temperature reactivity shuts down the chain reaction. However, passive safety also requires that the subsequent decay heat be removed from the core by conduction and radiation before the fuel reaches failure temperatures. For TRISO-particle-based gas reactor fuel, a conservative limit on fuel temperatures is the widely accepted value of 1,600°C.

Other desirable objectives of a VHTR design include acceptable operating peak fuel temperature (<1,250°C), lifetime pressure vessel fluence (<$3x10^{18}$ n/cm^2), minimal pumping power, and peak particle power (<0.2 W). Of course, criticality is assumed. Therefore a range of acceptable core multiplication factors (k_{eff}) was identified that allows sufficient margin to offset the negative reactivity of minor fission products not modeled in the code. In all the designs considered here, the fuel is assumed composed of 8% enriched UO_2 in coated particles embedded in a graphite matrix. Other enrichment values are possible but were not considered in this study.

In the event of ingress, the hot graphite in the core would react with air and water in exothermic reactions. This could in turn result in core damage. This is compounded by the fact that ingress may also inject positive reactivity at a rate that could result in fuel failure, before said failure could be pre-empted by the negative reactivity feedback from

the subsequent temperature increase. Proper design must include an assessment of water and air ingress reactivity.

A parameter unique to the recirculating pebble-bed reactor is the rate at which pebbles flow through the core. During normal operation, pebbles trickle through the core and drop out of discharge tube at the bottom of the core vessel. Typically three or four pebbles are released every minute. The burnup of each pebble is measured to determine if it is to be reloaded at the top or delivered to a spent fuel container for subsequent processing to disposal. The total pebble flow rate is limited by considerations on the physical integrity of the pebbles. In addition, the speed at which pebbles flow affects the design of the burnup measurement system. For this study, pebble flow was limited to 4,500 pebbles per day (about 1 every 20 seconds) for every 300 MWt of core power to allow for adequate burnup measurement time using two parallel fuel measurement channels. This limitation on the pebble discharge rate (and consequently on in-core flow rate) can of course be relaxed to allow higher pebble throughput merely by providing a larger number of fuel measurement channels. The limitations stemming from physical considerations on the pebbles' integrity would remain, however. As with those described in previous chapters, the models used in the VHTR design search did not include control elements.

6.1.2 Passive Safety Confirmation with MELCOR

For confirmation of passive safety, the thermal-hydraulics code MELCOR is used. MELCOR is an integrated systems-level code developed at Sandia National Laboratory to analyze severe accidents [100]. It has been used extensively to analyze LWR severe accidents for the Nuclear Regulatory Commission. However, because of

the general and flexible nature of the code, other concepts such as the pebble-bed reactor can be modeled. For the analysis presented in this report a modified version of MELCOR 1.8.2 was used. The INEEL modifications to MELCOR 1.8.2 were the implementation of multi-fluid capabilities and the incorporation of the ability to model carbon oxidation [101]. The multi-fluid capabilities allow MELCOR to use other fluids, such as helium, as the primary coolant.

The power profile of a core computed by PEBBED calculations is used to establish the initial steady state distribution in a MELCOR full transient analysis.All the PEBBED/MELCOR models include a stainless steel core barrel, a 30 cm gas gap between the outer reflector and core barrel, a 5 cm gap between barrel and steel pressure vessel, and a 30 cm gap between the vessel and the concrete containment. A natural circulation (air) reactor cavity cooling system (RCCS) is assumed to function as designed during design basis events. This allows the use of a constant outer wall temperature boundary condition. The PEBBED model uses a finer radial mesh than the one used in MELCOR but the MELCOR model is two-dimensional (R-Z) and allows for axial heat removal. Figure **6-1** shows the layout of the heat structures in the MELCOR model.

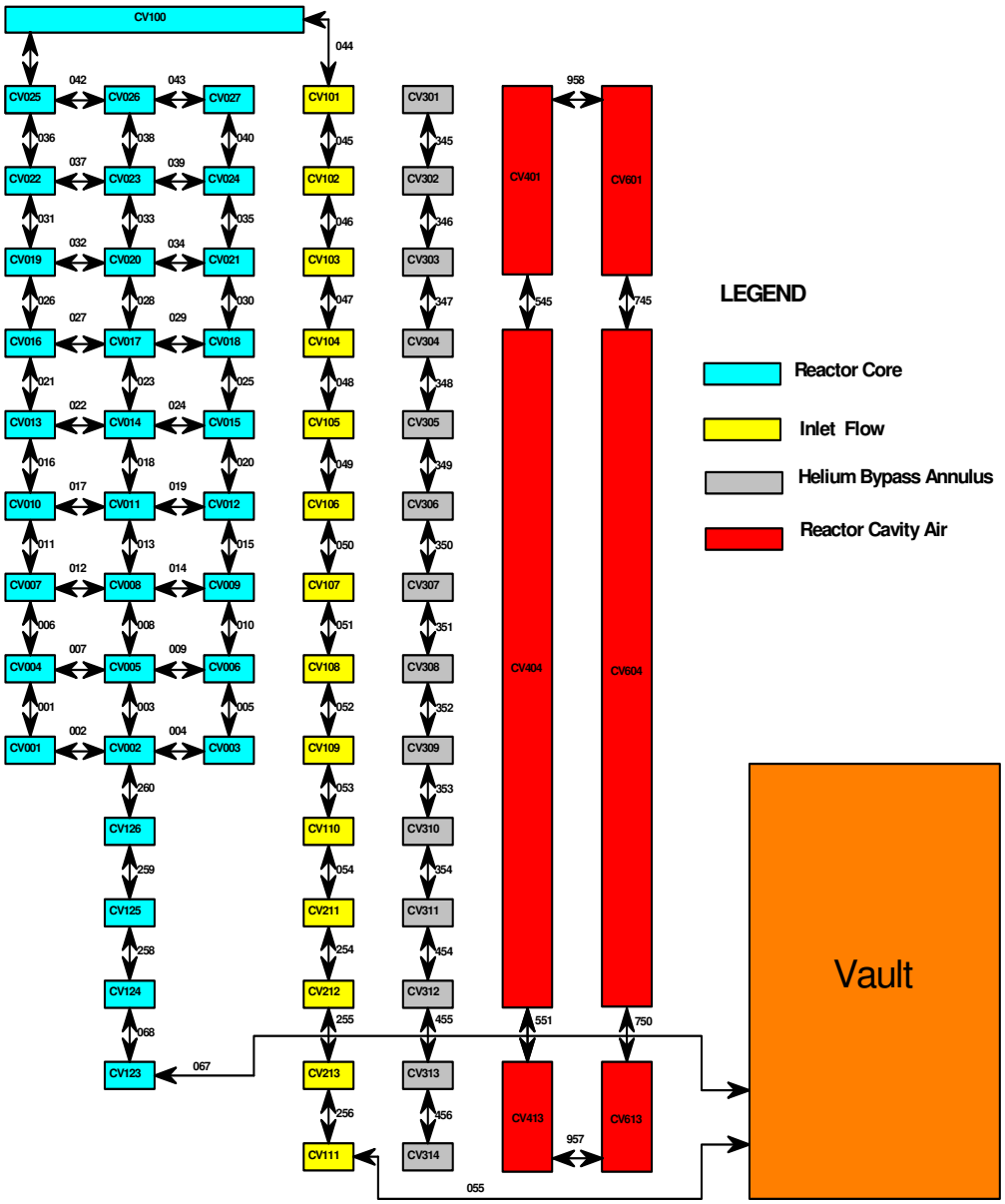

Figure **6-1**: MELCOR model of the VHTR.

The two-dimensional nature of the model is clearly indicated. The arrows between structures represent the heat flow between them and are specified by suitable heat transfer correlations.

6.1.3 Confirmation of PEBBED Accident Temperature Calculations

The one-dimensional radial conduction radiation model in PEBBED incorporates a number of material properties and physical effects but ignores or simplifies a number of features in the geometry of a PBR. This allows for rapid estimation of peak accident temperature. A PEBBED DCC calculation takes minutes on a PC while the execution of the MELCOR model shown above takes hours or days depending on the length of the transient. It is necessary then to confirm the PEBBED approach using a comparable MELCOR model.

A simple VHTR design, based loosely upon the PBMR, was employed for this purpose. The annular core is 9.4 meters high with a solid inner graphite reflector with a radius of 40 cm. The fuel annulus has an outer radius of 175 cm. The recirculation scheme is type- and pass-independent; the pebbles are dropped randomly into the top and recirculated 10 times before discharge at 80 MWD/kg_{ihm}. The fuel pebbles were optimized using the method described in Section 5.1. The COMBINE code was used to generate the cross-sections and the optimal fuel region radius was found to be 2.33 cm. This core geometry and fuel design resulted in very high neutron economy; a core multiplication factor of 1.104 was calculated.

The PEBBED and MELCOR models used the same material properties including a correlation for heat transfer in a pebble-bed and a constant thermal conductivity in graphite of 35.55 W/mK. PEBBED's thermal module contains a graphite conductivity

correlation that is temperature and fluence dependent but this was not used for this calculation. A constant inner containment wall temperature of 35°C was used as an outer boundary condition. The core barrel was assumed to be made of solid graphite; the pressure vessel was assumed to be made of type 304 stainless steel. The gas gaps were filled will stagnant helium. MELCOR allows natural convection of this gas while PEBBED does not. The MELCOR model used a maximum time step of 0.5 seconds while the PEBBED model used a time step size of 30 seconds.

PEBBED and MELCOR models of the depressurized conduction cooldown accident yielded the following results obtained from a design study performed at the INEEL [102]. Figure **6-2** shows the progression of the peak fuel temperature as computed by MELCOR.

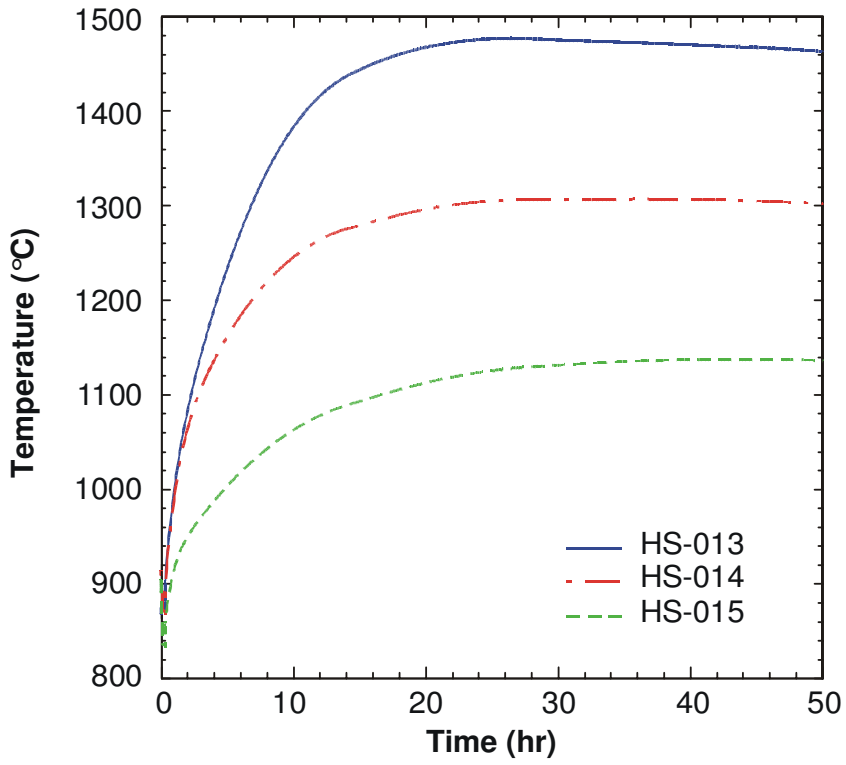

Figure **6-2**: Peak fuel temperature in a depressurized conduction cooldown of the 300 MWt test VHTR – MELCOR.

As shown in Figure 6-1, the core is divided into three radial zones and the curves in the above figure correspond to those zones. MELCOR computes a peak fuel temperature of 1,473°C occurring 27 hours after accident initiation.

The PEBBED model is one-dimensional and is shown in Figure 6-3.

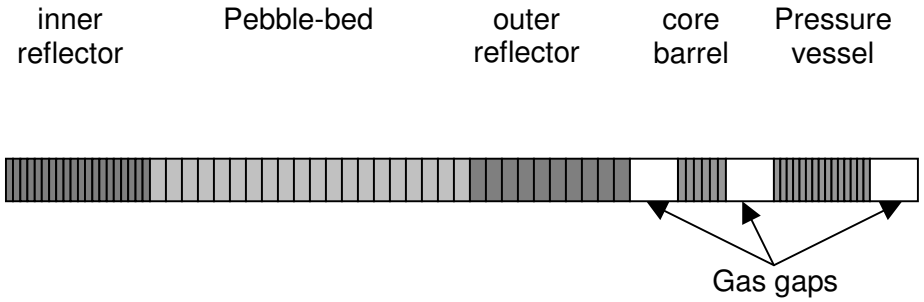

Figure 6-3: PEBBED radial model of the 300 MWt test VHTR.

The progression of the transient as calculated by PEBBED is shown in Figure 6-4.

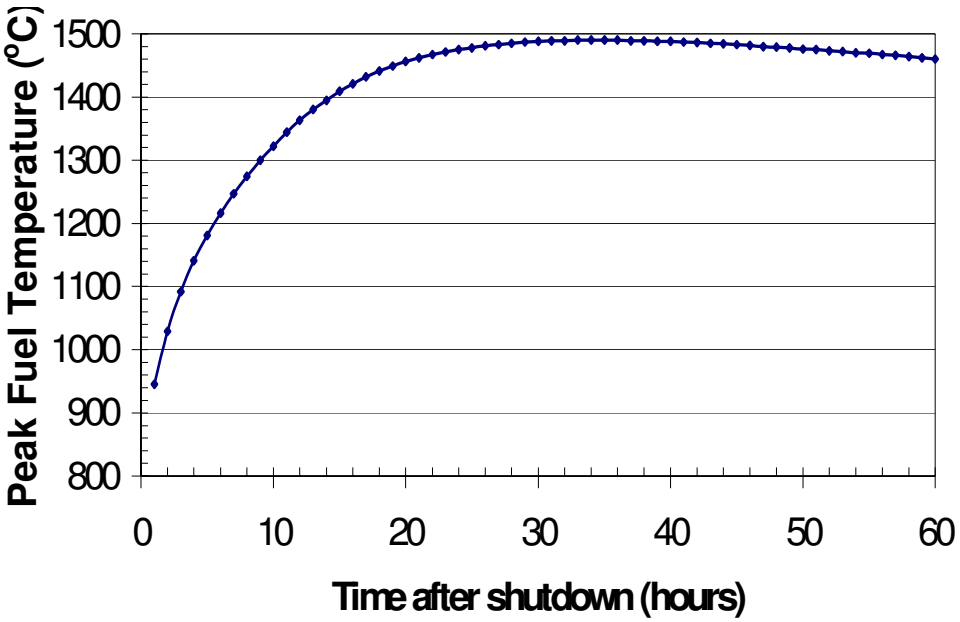

Figure 6-4: Peak fuel temperature in a depressurized conduction cooldown of the 300 MWt test VHTR – PEBBED.

PEBBED computes a peak temperature of 1,490°C at 34 hours after accident initiation. The peak temperature is slightly higher and can easily be explained by the lack of axial heat removal in this model. Although the MELCOR model used the power density distribution computed by PEBBED, it computes its own initial steady-state temperature distribution, another source of difference. As in the previously discussed cases (Chapter 4), the simpler and faster PEBBED model estimates peak accident fuel temperatures with reasonable accuracy for design purposes.

A similar comparison was conducted for a 600 MWt VHTR design. The higher power output requires a larger core so the fuel inner and outer radii of the VHTR-300 were increased. The MELCOR and PEBBED thermal-hydraulic models were otherwise the same.

As one more test, a MELCOR model of the PBMR-DIR was also constructed and run to generate results for the DCC transient. Selected characteristics of the test candidates are shown in Table 6-1.

Table 6-1: Features of VHTR test systems.

Design	VHTR-300	VHTR-600	PBMR-DIR
Inner Reflector/Fuel Annulus/Outer Reflector Radius (cm)	40/175/251	110/225/301	~87/175/251
Height (cm)	940	900	840
Power dDnsity (W/cc)			
Mean	3.5	5.5	3.3
Peak	6.1	8.8	6.8
Peak Fuel Temperature (℃)			
Normal	1,039	1,053	1,040
DCC (*PEBBED*)	1,490 (34 hrs)	1,773 (74 hrs)	1,419 (42 hrs)
DCC (*MELCOR*)	1,476 (27 hrs)	1,772 (62 hrs)	1,406 (45 hrs)
Peak Vessel Fast Fluence after 60 years (n/cm2)	3.2E19	2.8E19	4.5E19

Given the differences in the geometries of the models, the differences in the predicted peak accident fuel temperatures are plausible. The PEBBED peak temperature values are conservatively higher than those predicted by MELCOR. The time-to-peak computed by PEBBED is longer, a non-conservative error, so any subsequent analysis should pay close attention to this value. For design and scoping purposes, however, the simple, one-dimensional transient model used in PEBBED is considered adequate.

As for passive safety, the 600 MWt test design does not satisfy the requirement, coming in at well over 1,700℃ and staying above that temperature for at least 80 hours according to PEBBED. The data plotted in Figure 2-5 suggests that properly designed

fuel may be able to withstand this event with modest particle failure. Moreover, only a small fraction of the core actually attains this temperature so, even with this design, significant release of the core inventory is very unlikely. Nonetheless, lower peak accident temperatures should be pursued in design efforts to provide an adequate margin of safety.

6.2 Approach and Results

6.2.1 Basic Design Approach

The design process for the VHTR began by choosing an established PBR concept and making subsequent adjustments. For this work, the PBMR-DIR vessel and internals was chosen as the starting point. The first departure from this model was the addition of a solid inner reflector rather than a dynamic pebble reflector. The fuel pebbles were designed using the optimization process described in Chapter 5 but using MICROX rather than COMBINE for generating cross-sections. From there, candidate VHTR designs were obtained by changing the core and inner reflector radii and evaluating the results. The thicknesses of the ex-core components (outer reflector, core barrel, pressure vessel, and gas gaps) were held constant. A significant, though limited, number of candidate designs for 300 and 600 MWt reactors were analyzed.

The PEBBED models include neither the bulk of the minor fission products nor control rods that may be partially inserted during nominal operation. Both of these reduce core reactivity. The PBMR-DIR model is computed to have a core eigenvalue of about 1.073. This leaves enough excess reactivity to allow for the addition of these features later on yet still keep a critical core. For the VHTR design runs, an eigenvalue of

1.073 was therefore adopted as a reasonable target for good designs. The 1,600℃ limit for fuel temperature during a depressurized conduction cooldown was also a design target.

The flow rate of pebbles in the core offers a degree of freedom not available to batch-loaded reactors. To achieve a certain discharge burnup, there are an infinite number of flow rate values that will suffice, each corresponding to a certain number of passes through the core. The slowest flow rate corresponds to an OTTO core (one pass per pebble). At twice this rate, pebbles will pass through the core twice before the discharge burnup is attained. Higher flow rates are advantageous in that they reduce the mean burnup differential across the core and thus reduce axial power peaking. To understand this, consider a core with a specified discharge burnup of 80 MWd/kg_{ihm}. For the OTTO cycle (M = 1), the average burnup at the entry plane is zero while the average burnup at the exit plane is 80 MWd/kg_{ihm}. The burnup differential is 80 MWd/kg_{ihm}, quite high for a PBR. Doubling the flow rate means that half the pebbles at the entry plane are fresh (0 MWd/kg_{ihm}) while the other half are roughly half-burned (~40 MWd/kg_{ihm}). The mean entry plane burnup is about 20 MWd/kg_{ihm} Likewise at the exit plane, half the pebbles are half-burned while the remainder are full burned. The mean exit plane burnup is thus roughly 60 MWd/kg_{ihm}. The mean burnup differential across the core is about 40 MWd/kg_{ihm}, about half that of the OTTO case. Adjusting the flow rate to yield ever higher numbers of passes for the fuel will result in an ever-decreasing burnup gradient, going to zero in the limit of infinite pebble speed.

Of course, practical limits are imposed on the flow rate. The recirculating fuel cycle requires that each pebble have its burnup measured at the exit plane to decide if is to be put back in or discharge. Current pebble burnup measurement technology means that about 20 to 30 seconds per pebble is required for such a measurement. A single

burnup measurement stream can thus handle about 5,000 pebbles per day. Advanced measurement techniques have been proposed that may significantly reduce the measurement time [103]; nonetheless, for this study pebble flow rates were limited to about 5,000 pebbles per day per 300 MW of thermal power produced. This allows high-powered VHTR cores to use parallel measurement streams.

Other core characteristics were considered desirable but not at the expense of good core eigenvalue and DCC peak fuel temperature values. These other characteristics include: pressure vessel diameter and core height (smaller is better), flux at the pressure vessel (less is better), peak fuel temperature during normal operation, and steam ingress reactivity. These and other parameters will be compared with the PBMR-DIR values.

6.2.2 The Search for the Feasible 300 MWt and 600 MWt Designs

The first core modification consisted of varying the size of the inner reflector until the core multiplication factor attained a maximum. Figure **6-5** shows the PEBBED-computed effective core multiplication factor for a VHTR-300 as a function of the radius of the inner reflector. Equivalent cases were run using COMBINE and MICROX cross-sections. The fuel annulus outer radius was kept at 175 cm, the same as the PBMR.

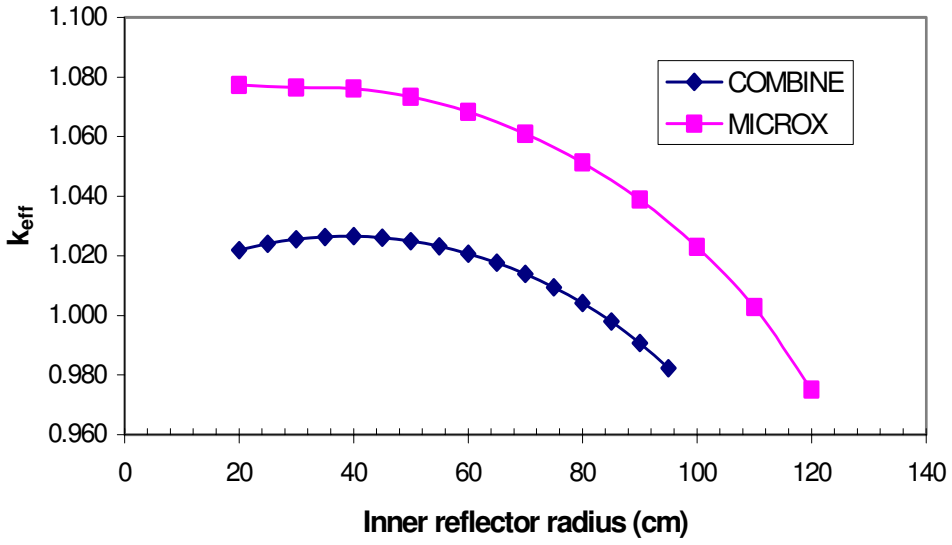

Figure **6-5**: Asymptotic core eigenvalue vs. radius of inner eeflector – VHTR-300.

The COMBINE cross-section indicates a much less reactive core. It also indicates a neutronically optimal inner reflector radius of 40 cm. Below and above this value, the core is not optimally moderated. The optimal radius of the fuel region in the COMBINE-based optimization is 2.33 cm. The MICROX results show that the core multiplication factor continues to increase as the inner reflector is reduced and there is no peak value in the range considered. Both sets of data indicate that an inner reflector size near 40 cm yields a core with good neutron economy. However, this geometry does not *necessarily* yield a core that is passively safe, and when it does, it may not necessarily be (and indeed is not expected to be) the core design with the largest passive safety margin. The temperature calculation may indicate the need to compromise neutron economy in the interest of core safety.

In light of the superior neutron economy of the 300 MWt core, the target discharge burnup was raised to 94.3 MWd/kg_{ihm} (10% FIMA) for the VHTR-300 design search. This lowered the core eigenvalue to the PBMR target and improved fuel

utilization. Another approach would be to lower the fuel enrichment. A proper economic analysis would need to be conducted to determine the best approach.

In the 600 MWt case, the inner reflector dimensions that allowed a passively safe core did not bracket the core eigenvalue peak so a neutronically optimal inner reflector had to be abandoned. The neutron economy of the VHTR-600 was inferior to that of the VHTR-300; the discharge burnup of 83 MWd/kg_{ihm} was found to yield the target core eigenvalue. This is a slight improvement over the PBMR result.

Table **6-2** lists some of the candidate VHTR-300 systems analyzed.

Table 6-2: Attributes of some candidate 300 MWt VHTR reactors.

Height (cm)		**Power Density**		**Fuel Temperature**		**Peak ΔT**	**Peak Part.**	**Peak**	**Peak Fast Flux**
850	k_{eff}	Mean	Peak	Mean	Peak	Across Pebble	Power	DCC Temp	At RPV
		W/cm^3	W/cm^3	℃	℃	℃	W	℃	n/cm^2-s
Inner Reflector Radius (cm)									
				Fuel Annulus Radius (cm) = 175cm					
30	1.0760	3.78	7.90	862	1030	69	0.1	1670	9.80E+09
40	*1.0733*	*3.87*	*8.05*	*862*	*1029*	*69*	*0.1*	*1631*	*1.00E+10*
50	1.0683	3.99	8.14	863	1029	69	0.1	1592	1.10E+10
60	1.0609	4.16	8.24	863	1029	69	0.11	1547	1.10E+10
70	1.0513	4.37	8.40	863	1029	70	0.12	1504	1.20E+10
80	1.0388	4.64	8.65	864	1030	71	0.13	1458	1.30E+10
90	1.0229	4.99	9.02	865	1032	79	0.14	1416	1.50E+10
100	1.0027	5.45	9.56	866	1036	89	0.16	1372	1.70E+10
110	0.9751	6.06	10.34	869	1044	104	0.18	1329	2.00E+10
120	0.0938	6.92	11.47	874	1057	125	0.22	1289	2.30E+10
				Fuel Annulus Radius (cm) = 195 cm					
120	1.0383	4.01	7.31	861	1028	66	0.11	1368	1.20E+10
130	1.0214	4.33	7.69	862	1030	73	0.12	1328	1.30E+10
140	1.0003	4.76	8.22	864	1033	83	0.14	1289	1.50E+10
150	0.9726621\0.9352723	5.32	8.95	867	1040	97	0.16	1254	1.80E+10
160	0.9353	6.1	10.0	871	1052	117	0.19	1218	2.10E+10
				Fuel Annulus Radius (cm) = 215 cm					
120	1.0383	3.53	6.31	858	1026	58	0.1	1291	1.10E+10
130	1.0214	3.83	6.68	859	1027	64	0.11	1256	1.20E+10
140	1.0003	4.22	7.19	861	1029	73	0.12	1223	1.40E+10
150	0.9727	4.74	7.88	864	1034	86	0.14	1190	1.60E+10
160	0.9353	5.45	8.86	868	1044	104	0.17	1158	1.90E+10

Of the candidate designs listed in Table **6-2**, the design with the 175 cm fuel annulus and 40 cm inner reflector (shown in italics) possesses high neutron economy and adequately low DCC peak temperature. The core eigenvalue is high enough to allow for a decrease in enrichment or higher discharge burnup. The design with the 30 cm reflector may also work but the safety margin is narrower. The larger designs show less neutron economy. Because a smaller pressure vessel is preferable, there is no reason to consider these further.

The chosen design shows promise but the peak accident fuel temperature is still over the prescribed limit of 1,600°C. This was addressed by increasing the core height from 850 cm to 875 cm and lowering the overall power density. A modest increase in core height would not be expected to significantly raise the cost of the plant. Increasing the core diameter would also lower the power density but at a higher cost. Hoop stresses on a pressure vessel increase with the diameter, not the height. Increasing the diameter would require a thicker vessel.

The PEBBED model was run with the 875 cm core height. As expected, the DCC peak temperature dropped to about 1,608°C without significantly perturbing the other parameters of interest. This value is better and could probably be lowered even further with subtle changes to the core geometry. Per the previous discussion of flow rates, however, an attempt was made to lower the axial power peaking by increasing the flow rate so that the pebbles pass through the core more quickly and more often. Indeed, doing so lowered the peak DCC fuel temperature to 1,597°C, under the limit. The flow rate required to achieve this however was computed to be 5,600 pebbles per day, higher than what can be handled by a single burnup measurement system using today's technology. A detailed analysis of the effect of these variables should be part of future design efforts.

A 600 MWt core will be larger to keep the core power density to a safe level. However, a thick fuel annulus also means a longer conduction path during a DCC transient. The VHTR-300 discussed in the previous section was used as a starting point for the search for a 600 MWt core. The height was raised to 900 cm and the inner and outer boundaries of the fuel annulus were varied to produce a set of candidate designs for PEBBED analysis. An upper limit on the core size was set at five meters. This is roughly the dimension of the prismatic GT-MHR [94], which is also designed to run at 600 MWt. For comparison, some dimensions of the GT-MHR are provided in Table **6-3**.

Table **6-3**: Dimensions of the prismatic GT-MHR.

Inner reflector effective outer diameter (m)	2.96
Fuel annulus effective outer diameter (m)	4.83
Pressure vessel outer diameter (m)	7.66
Height of active core (m)	7.93

Table **6-4** lists some of the candidate VHTR-600 systems analyzed. Of the candidate designs listed in, the one with the 250 cm fuel annulus and 150 cm inner reflector is worthy of further study. It displays a peak DCC temperature well near 1,600℃ and enough excess reactivity to account for other fission products and shutdown margin.

Table 6-4: Attributes of some candidate 600 MWt VHTR reactors.

Height (cm)		**Power Density**		**Fuel Temperature**		**Peak ΔT**	**Peak Part.**	**Peak**	**Peak Fast Flux**
950	k_{eff}	Mean W/cm^3	Peak W/cm^3	Mean °C	Peak °C	Across Pebble °C	Power W	DCC Temp °C	At RPV n/cm^2-s
Inner reflector radius (cm)									
					Fuel Annulus Radius = 215 cm				
130	1.0599	6.86	12.6	870	1039	104	0.19	1680	2.00E+10
140	1.0408	7.55	13.54	873	1046	118	0.21	1634	1.80E+10
150	1.0159	8.47	14.82	877	1058	137	0.24	1591	1.60E+10
					Fuel Annulus Radius = 220 cm				
130	1.0675	6.38	11.82	868	1035	96	0.17	1643	1.80E+10
140	1.0505	6.98	12.62	870	1041	108	0.19	1597	2.00E+10
150	1.0289	7.76	13.71	874	1049	123	0.22	1554	2.40E+10
					Fuel Annulus Radius = 225 cm				
120	1.0870	5.55	10.61	864	1030	82	0.15	1684	1.50E+10
130	1.0746	5.96	11.13	866	1031	89	0.16	1642	1.70E+10
140	1.0593	6.48	11.82	868	1036	99	0.18	1599	1.90E+10
150	1.0401	7.15	12.74	871	1043	112	0.20	1555	2.10E+10
					Fuel Annulus Radius = 230 cm				
130	1.0798	5.89	10.90	867	1030	86	0.15	1722	1.60E+10
140	1.0659	6.37	11.52	869	1031	95	0.17	1661	1.80E+10
150	1.0488	6.98	12.34	872	1036	106	0.19	1618	2.00E+10
					Fuel Annulus Radius = 250 cm				
120	1.1089	4.18	8.25	859	1026	60	0.11	1704	1.10E+10
130	1.1008	4.41	8.51	859	1026	64	0.11	1662	1.20E+10
140	1.0913	4.69	8.85	860	1027	68	0.12	1623	1.30E+10
150	*1.0800*	*5.03*	*9.30*	*862*	*1028*	*74*	*0.13*	*1582*	*1.40E+10*

The eigenvalue for the selected core was slightly higher than the PBMR-DIR value. It was found that by increasing the discharge burnup to 82.6 MWd/kg_{ihm} the target value could be achieved. The slightly larger burnup gradient pushed the DCC peak fuel temperature up to 1,584℃. There were no significant changes to the other listed parameters either.

6.2.3 Selected Performance Characteristics of the VHTR

All the designs used in the VHTR search used pebbles optimized according the method described in Chapter 5. Presumably, they should exhibit improved performance over core designs that use a pebble that is not so optimized. In this section, fuel utilization and response to steam ingress are two measures by which the chosen VHTRs are compared to the PBMR-DIR.

A fuel utilization calculation like the one conducted in Section 5.1 was performed. Again, fuel utilization is expressed in terms of the number of *fuel particles consumed per net unit of thermal energy* produced. Both the standard and optimized pebbles use the same particle design; only the number of particles per pebble varies. Net thermal energy is the thermal output of the core less the power required to pump the coolant. The pressure drop through pebble-bed reactors is greater than a prismatic HTGR of the same thermal power rating and coolant profile. At high power and taller cores, the power required to pump helium through the core can become very significant.

Table **6-5** lists these performance parameters for the PBMR-DIR with standard fuel and the two VHTR designs with their optimized pebbles.

Table 6-5: Performance characteristics of PBMR vs. VHTR designs.

Design	PBMR-DIR	VHTR-300	VHTR-600
Thermal Power (MW)	268	300	600
Pumping Power (MW)	2.9	6.4	26.5
0.001g/cm^3 Steam Ingress Reactivity ($)	0.30	0.41	0.09
Discharge Burnup (MWd/Kg$_{hm}$)	80	94.3	82.6
Fuel Utilization (particles/ net MWd)	21,024	18,047	21,084

The results indicate a 14% improvement in fuel utilization by the VHTR-300 as compared to the PBMR-DIR. Interestingly, the response to a 0.001 g/cm^3 steam ingress condition was worse ($0.41 for the VHTR-300 compared to $0.30 for the PBMR-DIR). Further study should be performed to discover what drives the increase.

The VHTR-600 displays a fuel utilization rate comparable to that of the PBMR. In terms of gross thermal power, the design is more efficient but the considerable pumping power (26 MW vs. about 3 MW for the PBMR) takes a toll on the overall plant efficiency. Clearly, high-powered pebble-bed cores cooled in this fashion may have some difficulty competing with prismatic gas-cooled reactors of comparable power. This may limit the PBR to small markets. On the other hand, if the economics permit, clusters of 300 MWt VHTRs may prove to be the preferred alternative.

Recently, a design innovation has been proposed that may address the issue of large pressure drops in the PBR. Muto [104] proposed that helium be blown in radially through the outer reflector, through the fuel annulus, and into an exit channel in the inner reflector. The coolant is forced through the narrow dimension of the pebble-bed rather than through the entire axial length of the core, thus reducing the pressure drop. This concept should be explored in future VHTR design efforts.

6.2.4 Conclusion

For the two power levels studied here, potential VHTR designs have been identified using PEBBED and a simple direct search method. Success was achieved in producing a core design that has sufficiently high neutron economy to account for possible control elements and is tolerant of the extreme loss of coolant accidents. The calculation of peak temperatures during such an accident was confirmed for three cases against results obtained using the accident analysis code MELCOR. A 300 MWt VHTR conceptual design was generated that displays superior fuel economy compared to an established design. A 600 MWt core was also designed to be passively safe. Improved fuel utilization in this design is offset by the high pumping power required during operation.

Further optimization and design changes may yield improved results for secondary objectives vessel such as pressure vessel fluence values and pumping power. To achieve a 60-year vessel life, fluence levels must be reduced by an order of magnitude. Acceptable fluence levels may be obtained by increasing the width of the outer reflector (at the cost of a larger pressure vessel) and through the use of a borated shield. More accurate treatment (a transport calculation) of the shielding is required to assess how much the design must be modified to reduce the fluence. Pumping power can be reduced by changing the core geometry within the bounds of passive safety.

6.3 Hotspot Analysis of the VHTR-300

In Section 5.2, off-normal scenarios were modeled to study the effects of non-random distribution of pebbles on core temperatures. Some scenarios were

proposed wherein pebbles were made to pass through regions of high thermal flux while they were highly reactive, and then moved to regions of lower thermal flux when they had reached a burnup level that made them less reactive. A similar analysis was performed for the test VHTR-300 discussed in Section 6.2.1 in order to assess its vulnerability to 'hotspots'. The test core was modified by removing the inner reflector. A single central loading tube can thus provide fuel to the entire core. Also, the discharge burnup was raised to 94 MWD/kg_{ihm} to reduce core reactivity, as was done the design search. The larger core burnup gradient increases the power peaking in the core. This is evident in the larger DCC peak temperature computed for the nominal VHTR-300 model.

These off-normal recirculation scenarios were modeled using specially-constructed recirculation matrices that correspond to nonrandom distributions of fresh and depleted pebbles. The effect on the DCC peak fuel temperature is summarized and discussed in this section.

6.3.1 Non-random Flow Distributions

Four alternate pebble recirculation patterns are modeled:

5. OUT-IN – in which fresh pebbles are loaded into and kept in the outer fuel zone for eight passes then transferred to the inner zone for the remaining two passes,
6. IN-OUT – in which pebbles are loaded into the inner zone and kept for a number of passes before being transferred to the outer,
7. PEBBLE-CHANNELING – in which pebbles remain in their original channels throughout their life,
8. FULLY RANDOM – no deliberate zoning of pebbles occurs.

A variant on the IN-OUT scheme is also investigated in which a certain percentage (x) of fresh pebbles are loaded into the central channel and the remaining (100-x) percentage are distributed randomly over the outer zone. The pebbles are all recirculated randomly after the first pass. The four main types of pebble recirculation listed above are “hard-wired” into the PEBBED code and can easily be executed by setting the appropriate flags and variables in the input deck. This variant on the IN-OUT scheme however, requires that the transfer partition coefficients be computed separately and supplied in an auxiliary input file. These cases are labeled WARM in the subsequent discussion. The central channel constitutes 10% of the total pebble flow area in the core in all of these calculations.

The partition coefficients for the various hotspot models are listed in Appendix E along with the base model of the VHTR-300.

6.3.2 Results

Table 6-6 presents the results of the PEBBED thermal analysis of these scenarios during DCC events.

Table 6-6: Results of the VHTR-300 hot spot analyses.

Case	Peak Power Density (g/cm^3)	Peak LOFA Fuel Temp. (℃)	Peak Fuel Temp. (℃)	Peak k-eff
Nominal VHTR-300	6.2	1,699	1,037	1.0781
Out-In	5.6	1,598	1,049	1.0711
In-Out-1	10.3	1,680	1,403	1.0868
In-Out-2	10.3	1,805	1,354	1.0916
In-Out-3	9.6	1,848	1,283	1.0951
In-Out-4	9.0	1,835	1,226	1.0940
Pebble Channeling	FIX	FIX	FIX	FIX
Fully Random	6.2	1,731	1,024	1.0818
WARM1-20	7.8	1,742	1,123	1.0809
WARM1-30	7.4	1,731	1,089	1.0799
WARM1-40	7.0	1,720	1,061	1.0685
WARM1-50	6.6	1,709	1,039	1.0790

The index x in the IN-OUT-x case specification refers to the number of passes in which a fresh pebble is kept in the inner zone before being transferred to the outer annulus. The index in the WARM1-x case specification refers to the percentage of fresh pebbles that are dropped into the inner zone upon initial insertion into the core.

In the “IN-OUT” cases the peak LOCA fuel temperature exceeds 1,800℃. Fuel damage is to be expected in the region where this hot spot occurs (the central channel). In Figure 6-6, peak fuel temperatures are for various axial locations in the IN-OUT-1 model. The axial locations are somewhat evenly spaced so that each curve represents $1/9^{th}$ of the core.

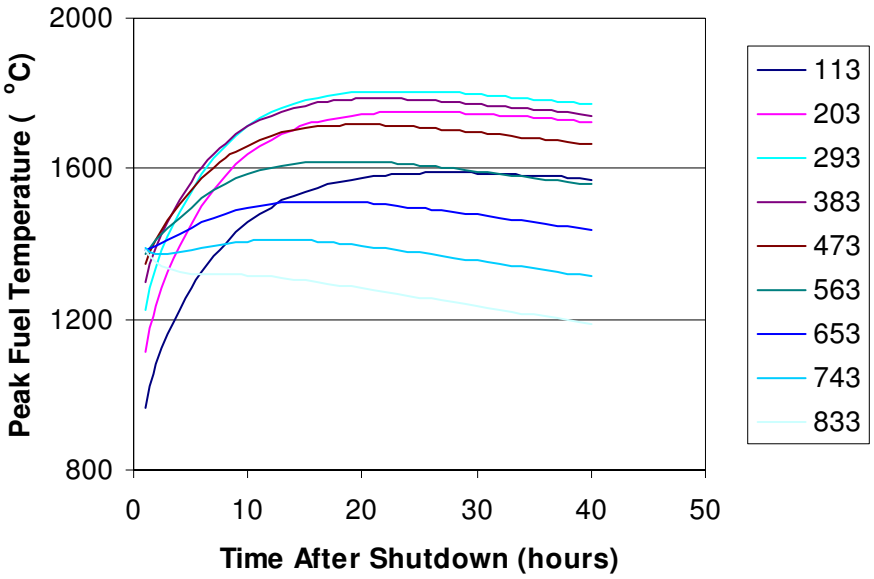

***Values in legend are distances (cm) from the top of the core**

Figure **6-6**: DCC fuel temperatures at different axial locations* – extreme IN-OUT event.

From the plot one can estimate that at least half of the core exceeds 1,600℃ for some time, while at least 40% exceeds this temperature for much more than 30 hours. Figure **2-5** indicates that 1 in 1,000 particles can be expected to fail under these conditions, or a total fuel failure of 0.04 % of the fuel inventory.

Probabilities for these events have not yet been calculated rigorously, but some general conclusions may be drawn. With only a single loading tube at the top, the only way in which these configurations can be achieved is by statistical deviation from a fully random loading process. The central channel comprises 10% of the flow in the core, therefore, 10% of the fresh pebbles should ordinarily fall into the sensitive “hot” zone. The pebbles make about 10 passes each during their lives; so about 10% of all the pebbles are fresh. Hence, if all of the fresh pebbles fell onto the hot-zone 10% of the surface area, they would cover that part of the surface. As each pebble fell onto the hot

zone, it would reduce the remaining available area for the remaining pebbles. Even if there are only 100 pebbles in each layer, ignoring competition from pebbles on passes after their first pass one can show that the probability of all of the fresh pebbles landing on the central 10% of the surface area is 5.78×10^{-13}. This is only the probability that all the fresh pebbles in a single layer will land in the central zone. For the feat to be repeated layer after layer until an entire column of fresh pebbles is established is so improbable that the typical scientific calculator does not store numbers small enough to quantify it. The probabilities of cases IN-OUT-2 through IN-OUT-4 are progressively smaller.

The WARM events are less severe; the temperatures do not exceed 1,800°C so fuel failure is less likely. The probability of these cases is higher; it is more probable that only a fraction of fresh pebbles will randomly clump in the central zone. However, to sustain this condition for the time needed to establish an equilibrium core still requires a statistical fluctuation the probability of which is infinitesimal.

6.3.3 Conclusion

The random nature of fuel loading in a pebble-bed reactor and its effects on core safety parameters is addressed to some degree through the analysis of extreme loading heterogeneities made possible using the recirculation matrix formulation in the PEBBED code. In these extreme cases, the peak accident fuel temperature is shown to exceed the threshold above which fuel failure can be expected to occur but not above the temperature at which the silicon carbide layers begin to decompose. Local pebble failure would be expected to occur but substantial core disassembly is not predicted.

It is noted that the probability of occurrence of any of the non-random pebble distributions described above is vanishingly small, orders of magnitude smaller than what is considered a design basis event.

Chapter 7

Automating PBR Design with PEBBED

A manual search for a reactor design as presented in the previous chapter is inefficient and unlikely to result in the best possible design. A much more sophisticated approach is desired. As part of this work, an optimization feature was added to PEBBED to perform design studies. The new tool was developed with funding from a DOE Nuclear Energy Research Initiative grant. Preliminary results of its application to the PBR are provided here. Three different core types were optimized using this tool: a simple type-independent, burnup-independent core based upon the HTR Modul 200, a VHTR 600 (as described in the previous chapter), and a 250 MWt cogenerator with an OUT-IN recirculation scheme like the GE-MPBR.

As discussed in Chapter 2, the advanced optimization component now available in PEBBED is based upon a genetic algorithm. A relatively simple algorithm is used without much “tuning” of parameters that may significantly improve the execution time. However, the method is shown to be more effective than the manual search employed in the previous chapter.

7.1 Genes, Traits, and Fitness

The *fitness* of an individual (candidate design) is a function of its traits, as specified by the user. Fitness specifications are developed for the three cases stated above, and the results of the optimization are presented. PEBBED allows the user to specify the variables (genes) over which the search is to be performed. For this design

study, variables included the inner reflector radius, the fuel annulus width, the core height, and the fraction of total pebble flow that is in the outer zone (of a two-zone core). These variables were allowed to vary over a range specified in an input file containing the optimization parameters.

The user then specifies the core characteristics or *traits* that determine fitness. For this study, traits included equilibrium core eigenvalue, maximum DCC fuel temperature, outer reflector radius, and ratio of required pumping power to total thermal power. Peak operating fuel temperature, maximum particle power, and reactivity can also be selected as traits in PEBBED but were neglected in this study.

The way in which these traits are factored into the overall fitness is specified by the user in a 4-point interpolation scheme. As an example, the maximum accident fuel temperature fitness is illustrated in Figure **7-1**.

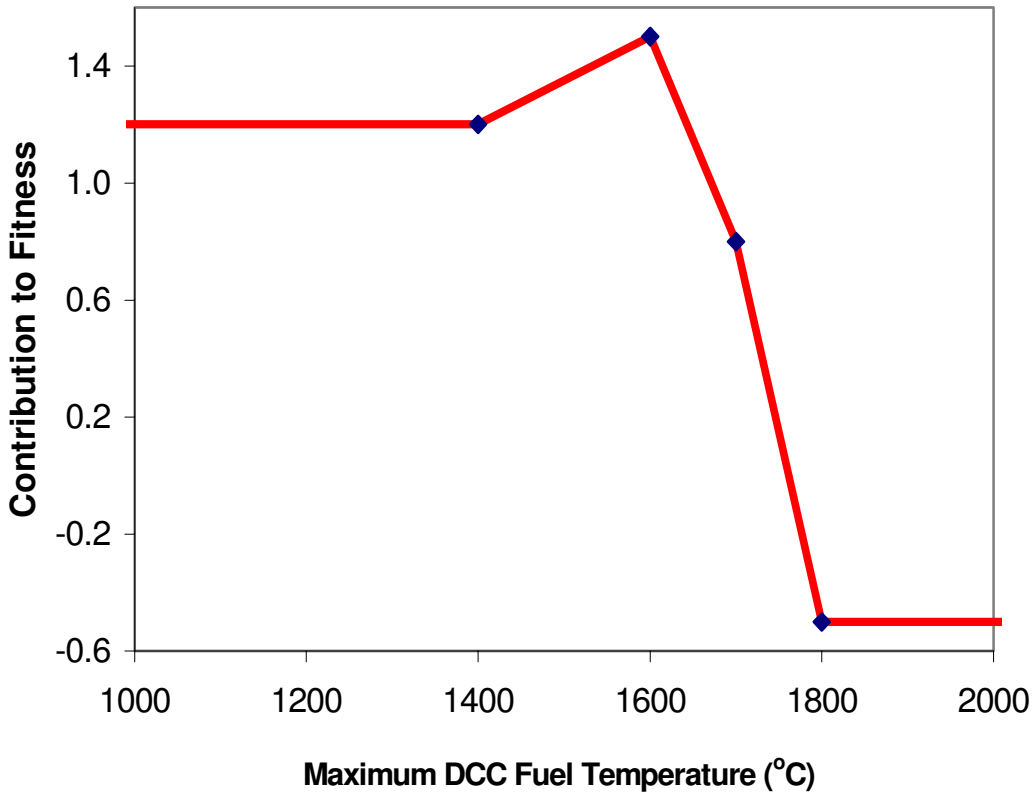

Figure 7-1: Example of a four-point peak fuel temperature contribution to the fitness specification.

If this trait were the only one to be specified in an optimization run, the algorithm would be driven toward a set of genes that yield a peak accident fuel temperature of 1,600℃. Above this value, the fitness value drops and even goes negative as a value of 1,800℃ is approached. Negative values can be used to strongly penalize designs that exhibit completely unacceptable traits such as exceeding fuel failure temperatures during a DCC transient.

The contributions from all selected traits are summed to yield the overall fitness of the individual. For example, in the VHTR-600 MWt design study to be discussed later in the chapter, core eigenvalue, maximum DCC fuel temperature, outer reflector radius,

and height were the selected traits. The specifications for these traits are shown in the following plots. Figure 7-2 illustrates how core multiplication factor is weighted.

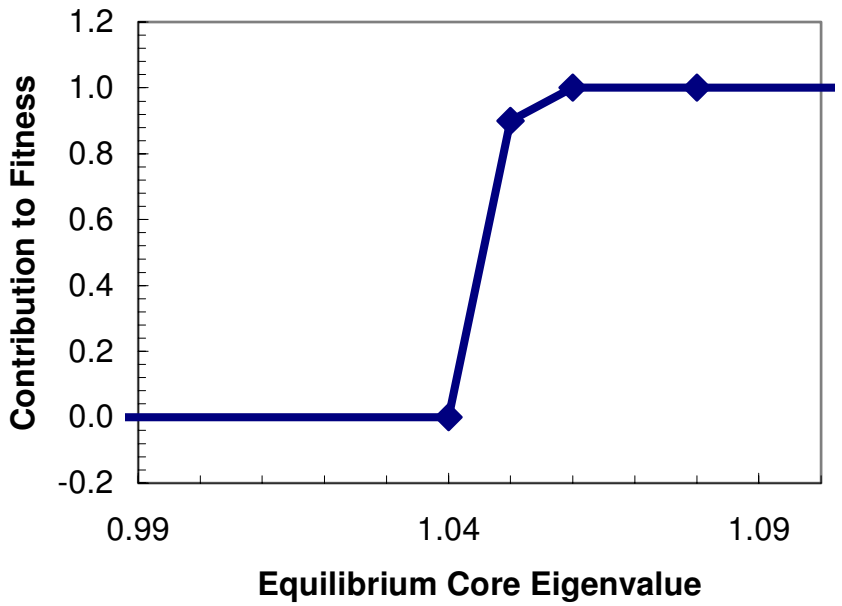

Figure 7-2: Core eigenvalue contribution to fitness.

The plot achieves its maximum at 1.06 (3rd point) and then is constant for higher eigenvalues. This allows for the negative reactivity of fission products not currently modeled in PEBBED and control rods that may be used to hold down any excess reactivity that is used for power manipulation. Holding it constant above that value means that cores with higher eigenvalues will be considered neither better nor worse. The algorithm may drive the solution to k_{eff} = 1.06 if reducing it helps raise the fitness contribution of another trait.

Figure 7-3 illustrates the fitness contribution from the size of the outer reflector. The overall contribution does not go above 0.3, a somewhat arbitrarily chosen number. The radius of the outer reflector is minimized for economic reasons: to keep the size of

the pressure vessel down. The pressure vessels of proposed gas-cooled reactors are very large compared to their LWR counterparts and present a manufacturing challenge.

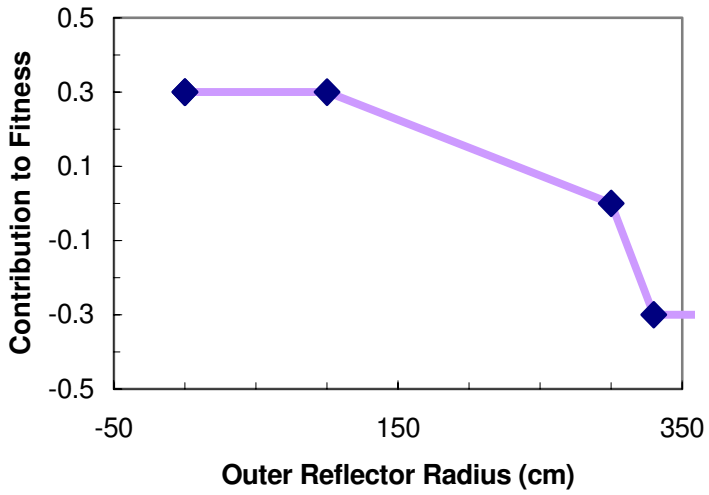

Figure **7-3**: Outer reflector radius contribution to fitness.

Penalizing large diameters can help to avoid impractical designs even if they are passively safe. However, the overall magnitude of this fitness contribution is less than that from the core eigenvalue and maximum DCC fuel temperature because (so the author assumes in this work) it is more important to make a critical, passively safe reactor than a small one.

For small modular PBRs such as the PBMR and the VHTR-300, pumping power is not significant (1-3 MW) even though it is still larger than a comparable prismatic core. Pumping power rises with the cube of the mass flow rate so that for high power pebble-bed reactors the required pumping power can be a significant fraction of the total thermal power output (see Table 6-5). For this reason, pumping power was added as a trait and chosen for the VHTR-600 MW optimization. Figure **7-4** illustrates the fitness contribution from the ratio of pumping power to core power.

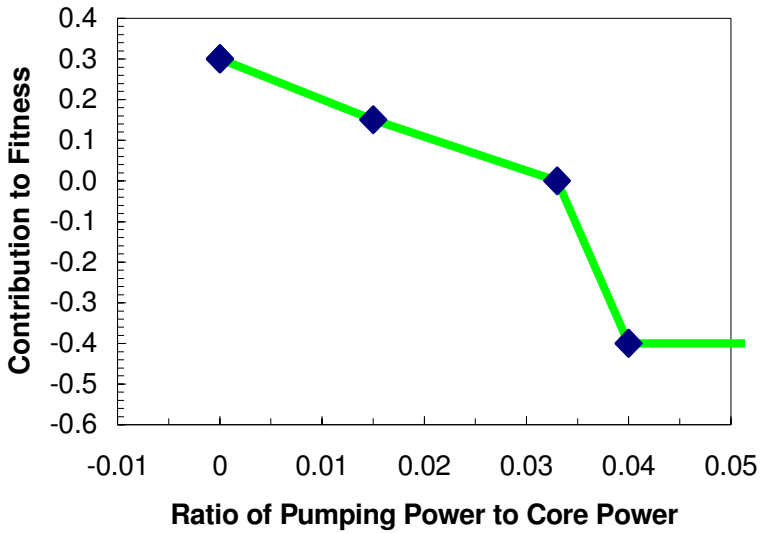

Figure 7-4: Pumping power contribution to fitness.

The solution will be driven toward lower ratios (i.e., shorter cores) with a heavy penalty above 0.03.

There is a complex interplay between the variables that specify core geometry and the traits that result. Core fitness specification itself is an art that can take considerable study. A full core design involves some testing and tweaking of the fitness functions until a fully satisfactory design is obtained. However, even the early attempts discussed in the following sections show that the method is powerful and flexible.

7.2 Description of the Operators

As discussed in Chapter 2, genetic algorithms apply three operations to a set of individuals: selection, crossover, and mutation. Variations on each of these have been applied to many different problems with varying degrees of success. For this work, no effort was made to experiment with different operators, a considerable effort in itself.

Rather, a set was chosen that the author judged to be adequate for the type of problem being solved. This set was successful in producing satisfactory designs in a reasonable amount of time. They are discussed in this section. Future development will likely lead to more efficient algorithms.

7.2.1 Selection

Individuals that exhibit superior traits “survive” into the next generation. Superiority in this algorithm simply means a higher overall fitness value as described above. The user specifies *which* traits are to contribute to the fitness and how they are to be weighted. The user also specifies the number of individuals in a population as well as the number of individuals that are allowed to survive and populate the next generation. Grefenstette [69] observed that a population size of 80 yielded an efficient algorithm. Goldberg [70] quotes studies performed with population sizes of between 16 and 100 with satisfactory results for sizes of 30 and above. For the efforts described in the next section, a population size of 40 was chosen. Of these, the 10 individuals in a generation that displayed the highest fitness were deemed the survivors.

7.2.2 Cross-over

The variables available for selection as “genes” in PEBBED (inner reflector radius, fuel annulus width, outer reflector width, active core height, fraction of core pebble flow that is in the outer zone) are all real-valued and are coded as such. The crossover operation involved taking weighted averages of the genes of two parent

individuals to form two new individuals. The “parents” are selected randomly from the “survivors” of the selection operation.

The weights used in determining the genes of the offspring are computed from the fitness of the selected parents according to the following formula. Let g_1 and F_1 be the values of the gene and overall fitness, respectively, of parent 1. Likewise the subscript 2 denotes the properties of parent 2. The hybrid gene computed for the first offspring, g_1', is given by Eq. **7.1**.

$$g_1' = g_1 + \frac{F_1}{F + F_{21}}(g_2 - g_1) \; . \qquad \textbf{7.1}$$

The value of the gene computed for the other offspring is obtained from the complementary weight, Eq. **7.2**.

$$g_1' = g_1 + \frac{F_2}{F + F_{21}}(g_2 - g_1) \qquad \textbf{7.2}$$

A user-specified crossover probability value determines whether the crossover operation occurs for a given gene in a match. For the cases performed in the next section, a crossover probability of 85% was used. In other words, for each gene pair processed, there was an 85% chance that the corresponding genes of the offspring were computed in this fashion, and a 15% chance that no mixing occurred. In these cases, offspring #1 took the gene of parent 1 and offspring #2 took the gene of parent 2.

This process takes place until the population is replenished to the user-specified level.

7.2.3 Mutation

After the new population is formed, a mutation operation may be performed on all but the fittest individual in the population. The algorithm loops through each gene of each individual (except the fittest) and generates a random number between 0 and 1 for each. If the number is less than or equal to a user-specified mutation probability, that gene is changed to a new value. The new value is itself a randomly chosen member on the interval (gene domain) specified in the input file and thus is correlated neither to the genes of the parents nor the original value of the individual.

The three operations described above are performed on each generation. The number of generations computed in a design process is specified by the user.

7.3 Results

7.3.1 Search for a Better HTR Modul 200

The first application of the PEBBED genetic algorithm tool was the HTR Modul 200. Recall from Section 4.1 that PEBBED computed a core eigenvalue of 1.0885 and a peak DCC fuel temperature of 1,455°C. This suggests (within the accuracy of the PEBBED model) that there is some margin for varying the core geometry that would allow for better performance while still preserving passive safety features. A simple optimization was performed in which the only ‘gene’ was the radius of the fuel annulus. The height was kept at the original design value (940 cm) and there is no inner reflector. As a single zone core, there is no outer zone flow fraction to be varied. The selected traits included the core eigenvalue, the peak DCC fuel temperature, and the outer reflector radius.

The four-point fitness specification for this run is given in Table 7-1.

Table 7-1: Four point fitness specification for the simple 200 MWt core design.

Point	k_{eff}	F_k	DCC Peak Temp ℃	F_t	Outer Reflector Radius (cm)	F_r
1	1.04	0	1,400	1.2	0	0.3
2	1.05	1	1,600	1.5	100	0.3
3	1.07	1.1	1,700	0.8	300	0
4	1.08	1	1,800	-0.5	330	-0.3

The genotype in this problem consisted only of the fuel annulus width. The HTR Modul 200 design has a fuel annulus width of 150 cm (there is no inner reflector so this is also the core radius). The range of acceptable values (gene domain) is specified in Table 7-2.

Table 7-2: Nominal values and gene domain for the 200 MWt simple core optimization.

Gene	HTR Modul 200 Value	Minimum Value	Maximum Value
Fuel Annulus Width (cm)	150	120	170

The trait specifications strongly favor a peak DCC fuel temperature of 1,600℃ and a core eigenvalue (k_{eff}) of 1.07. The weight on the DCC fuel temperature was set to be greater than that of the eigenvalue (1.5 vs. 1.1) so that passive safety would not be trumped by fuel economy. Small outer reflector radii were rewarded to some extent but the fitness contribution of this trait is small compared to the other traits.

After 10 generations and, the algorithm produced the results shown in Table 7-3.

Table 7-3: Selected results of HTR Modul 200 and optimized version.

Trait	HTR Modul 200	PEBBED Design
k_{eff}	1.0885	1.09470
DCC Peak Temperature (°C)	1,424	1,599
Outer Reflector Radius (cm)	245	251.6

As expected, the solution was driven toward a peak DCC temperature of 1,600°C. Evidently, the fitness advantage of this temperature outweighed that of both the optimal eigenvalue and a smaller radius because the computed eigenvalue is much higher than the optimal and the outer reflector radius is slightly larger than the HTR Modul 200. At this point, a core designer may choose to try again with a lower DCC temperature fitness specification to drive the solution toward a smaller vessel size. Alternatively, the fuel enrichment may be lowered to take advantage of the improved neutron economy of this core.

Once an optimal design is identified (either this one or the result of further iterations), confirmation of passive safety should be confirmed using a multi-dimensional safety analysis code. Given the agreement shown in the previous chapter between the PEBBED and MELCOR estimates of peak accident temperature, MELCOR modeling was not performed on this design.

7.3.2 Search for a Better GE-MPBR

The second application of the optimization tool was the GE-MPBR. Recall from Section 4.2 that this 250 MWt core features an “OUT-IN” refueling policy in which fresh pebbles are loaded into the outer zone, recirculated four more times, then transferred to the inner zone for five passes before discharge. The parameter that is used to generate

the partition coefficients is the fraction of pebble flow that is in the outer zone, α^o. The nominal value that yields the five OUT-five IN pattern was found to be 0.5.

For the nominal GEMPBR, PEBBED computed a core eigenvalue of 1.045 and a peak DCC fuel temperature of 1,507℃. As with the HTR Modul 200, there is no inner reflector. The selected traits once again included the core eigenvalue, the peak DCC fuel temperature, and the outer reflector radius.

The four-point fitness specification for this run is given in Table 7-4.

Table 7-4: Four point fitness specification for an optimized GE-MPBR.

Point	k_{eff}	F_k	DCC Peak Temp ℃	F_t	Outer Reflector Radius (cm)	F_r
1	1.04	0	1,400	1.2	0	0.3
2	1.05	1	1,575	1.3	100	0.3
3	1.07	1.1	1,700	0.6	300	0
4	1.08	1	1,800	-0.5	330	-0.3

The core eigenvalue and outer reflector radius fitness specifications are the same as those set for the previous optimization. The DCC fuel temperature peak weight was relaxed a bit to 1.3 (from 1.5) but the abscissa was decreased from 1,600℃ to 1,575℃ to provide a safety margin.

The genotype in this problem consisted of the fuel annulus width, the height, and the outer flow fraction, α^o. The nominal GE-MPBR values and the gene domain for this problem are included in Table 7-5.

Table 7-5: Nominal values and gene domain for the GE-MPBR optimization.

Gene	GE-MPBR value	Minimum Value	Maximum Value
Fuel Annulus Width (cm)	145	80	120
Height (cm)	926	750	1,000
Outer Flow Fraction	0.5	0.05	0.95

By changing the fraction of outer flow, the transfer burnup threshold is adjusted, i.e., pebbles may be moved from the outer to the inner flow zone after something other than five passes.

After ten generations and seven hours on a Dell Precision 650 Workstation, the algorithm produced the results shown in Table 7-6.

Table 7-6: Selected results of GE-MPBR and optimized version.

Trait	GE-MPBR	PEBBED Design
k_{eff}	1.045	1.05271
Outer Flow Fraction	0.5	0.14
Outer Reflector Radius (cm)	245	250
Height (cm)	926	861
Diameter of Active Core (cm)	145	150
DCC Peak Temperature (°C)	1,424	1,569
Peak Operating Fuel Temperature (°C)	1,035	1,002
Peak Power Density (W/cm^3)	6.51	6.16

As expected, the solution was driven toward a peak DCC temperature of 1,575°C but other traits and limits kept the temperature at a slightly lower value. The core diameter was pushed to the upper limit of 150 cm. This increased the neutron economy somewhat but not as high as the 1.07 target eigenvalue. Relaxing the limit on the core

diameter may yield better results but this particular core is the same diameter as that of the HTR Modul 200 and thus can use the vessel designed for that reactor.

The stress on the fuel temperature was decreased slightly from 1,035℃ to 1,002℃, probably the result of the lower overall power density of the larger core as is indicated by the peak power density value. The peak temperature during a DCC transient was increased considerably but is still comfortably below the 1,600℃ limit.

Interestingly, PEBBED produces an optimized core with a significantly smaller outer annulus. The outer flow fraction drops from 50% to 14%. This means that fresh fuel pebbles are circulated in the periphery of the core for only a couple of passes before being transferred to the inner zone. The flow distribution is shown in Table 7-7. The flow distribution of the nominal GE-MPBR is shown in Table 4-10.

Table 7-7: Flow distribution of optimized GE-MPBR.

	Fraction of Flow in Zone, a_i			
	Ch. 1	**Ch. 2**	**Ch. 3**	**Ch. 4**
	0.25515	0.24496	0.22850	0.27137
	Number of Pebbles in Each Zone			
Pass				
1	0	0	0.0	18.49
2	3.19	3.06	2.86	9.38
3	5.50	5.28	4.92	2.79
4	5.50	5.28	4.92	2.79
5	5.50	5.28	4.92	2.79
6	5.50	5.28	4.92	2.79
7	5.50	5.28	4.92	2.79
8	5.50	5.28	4.92	2.79
9	5.50	5.28	4.92	2.79
10	5.50	5.28	4.92	2.79

The table indicates that almost two-thirds of the pebbles are transferred to the inner zone after one pass and the remaining are transferred after the second. After the second pass, a few pebbles still appear in channel 4. These are actually inner zone pebbles; channel 4 contains 27% of the total core flow but the outer zone only makes up 14% of the total. Therefore, (100-14/27) = 48% of the outer channel is in the inner flow zone of the two-zone core.

Recall that the fuel for the GE-MPBR is a 50/50 mixture of 20% enriched uranium and fertile thorium. Thorium is converted to fissile U-233 within the core. The buildup of U-233 is shown in Table 7-8.

Table 7-8: Mass of U-233 in pebbles at exit plane after each pass.

	Mass of U233 (grams/pebble)	
Pass	**Nominal GE-MPBR**	**Optimized GE-MPBR**
0*	0.0	0.0000
1	0.00974	0.00868
2	0.02285	0.02165
3	0.03441	0.03443
4	0.04409	0.04555
5	0.05210	0.05474
6	0.05944	0.06224
7	0.06626	0.06835
8	0.07186	0.07331
9	0.07637	0.07731
10	0.07996	0.08054

* pass #0 indicates the fresh pebble content

The buildup of U-233 is slightly slower in the optimized core but it achieves a slightly higher discharge value. The differences in this case are not neutronically significant and are not likely related to the differences in the computed temperature.

Once again, to complete the design study, passive safety should be confirmed using a multi-dimensional safety analysis code.

7.3.3 Search for a Better VHTR-600

The 600 MWt pebble-bed VHTR identified in the previous chapter was used as a reference point for a genetic algorithm optimization. This reactor contains a solid inner reflector and a simple burnup-independent recirculation scheme. The discharge burnup was kept at a nominal 80 MWd/kg_{ihm}. Once again a population size of 40 was chosen, from which 10 survivors were propagated to next generation.

The four point fitness specification for this run is given in Table 7-9.

Table 7-9: Four point fitness specification for VHTR-600.

Point	k_{eff}	F_k	DCC Peak Temp. ℃	F_t	Outer Reflector Radius (cm)	F_r	Pumping Power/Core Power	F_p
1	1.04	0	1,400	1.2	0	0.3	0	0.3
2	1.05	0.9	1,575	1.3	100	0.3	0.05	0.15
3	1.073	1.0	1,700	0.5	305.5	0	0.10	0
4	1.08	1	1,800	-0.5	330	0	0.15	-0.4

The contribution from the core eigenvalue peaks at 1.073, the target eigenvalue from the previous search. The DCC peak fuel temperature contribution peaks at 1,575℃, somewhat lower than the limit to provide an extra margin for safety. These two specifications dominate the fitness function but lower reflector radii is also rewarded to a

lesser extent. Another gene was added to cause the fitness function to favor low pumping power. Table 7-10 shows the reference gene values from the VHTR-600 designed in the previous chapter as well as the range chosen for the genetic algorithm search.

Table 7-10: Nominal values and gene domain for the VHTR-600 optimization.

Gene	Reference VHTR-600 Value	Minimum Value	Maximum Value
Inner Reflector Radius (cm)	150	1	150
Fuel Annulus Width (cm)	100	80	120
Height (cm)	950	750	1,050

Table 7-11 lists the results of the manual search from the previous chapter and the one obtained using the genetic algorithm. This GA result was obtained after eight generations of a population of 40 individuals. It required 29 hours of CPU time on a Dell Precision 650 workstation.

Table 7-11: Selected results of VHTR-600 manual and automated design runs.

	VHTPBR-600 (Manual Search)	VHTPBR-600 GA search
Inner Reflector Radius (cm)	150	147.8
Fuel Annulus Radius (cm)	250	246.6
Outer Reflector Radius (cm)	326	322.6
Height (cm)	950	991.9
K_{eff}	1.073	1.073
Maximum DLOCA Fuel Temperature (°C)	1,584	1,573
Pumping Power (MW)	26	28
Maximum Operating Fuel Temperature (°C)	1,028	1,025
Peak Particle Power (W)	0.14	0.14

The GA-designed core is slightly thinner than the reference design. The accident temperature fitness specification peak of 1,575°C is slightly smaller than the reference design value of 1,584°C. To achieve the more stringent criterion, the core width was narrowed to provide a shorter conduction length to the reflectors. To re-capture the desired core eigenvalue, the height of the core was raised by 42 cm. The fitness benefit of achieving the target eigenvalue was somewhat offset by an increase in the required pumping power (2 MW more than the reference design).

The outer diameter of the pressure vessel is 7.45 meters, smaller than the prismatic GT-MHR by 21 cm. The active core is two meters taller than the GA design. A proper sensitivity study should be performed to find the optimal tradeoff between diameter and height. This specification could then be incorporated directly or indirectly into the fitness specification in future design efforts.

The major downside of a large pebble-bed, compared to the prismatic HTGR, is the tremendous pumping power requirement, 26-28 MW for a 600 MWt core. This requirement effectively makes the VHTR-600 a VHTR-570 and undercuts much of the advantages derived from the optimization of the fuel. One way to compensate may be to implement the cross flow scheme of Muto [104] and have the coolant pass radially through the bed rather than axially. This improvement alone may make the difference in economic viability. PEBBED's temperature correlations are not currently able to handle cross flow so this is an option that cannot yet be explored.

7.4 Conclusions

A simple genetic algorithm is shown to yield improved designs for various types of pebble-bed reactors. A four-point fitness specification allows the user to specify with

great flexibility which core characteristics determine a good design and how the fitness varies with these traits. The requisite genetic operators of selection, crossover, and mutation that have been devised for this work do yield improvements over reference designs; further study of these and other operators may result in improved computational efficiency.

The technique was applied to three reactor designs with different core configurations. The first is a simple burnup-independent core with no inner reflector based upon the HTR Modul 200. The code exploited a margin in the peak accident fuel temperature to increase the size of the core and improve neutron economy. In the second application, the OUT-IN scheme of the GE-MPBR 250 MWt base design was modified to yield a core with a 150 cm radius and an 861 cm height; shorter and fatter than the nominal GE-MPBR but still passively safe and with a higher core multiplication factor. Finally, the code generated was used to generate a 600 MWt Very High Temperature Reactor. The new design is slightly thinner and taller than the one that was obtained in the manual search, largely because of a more stringent accident fuel temperature specification.

Considerable improvement in computational efficiency may result from a study of different algorithm parameters and operators.

Chapter 8

Conclusions and Further Work

The purpose of this research was the development of a method and tool for analyzing, designing, and optimizing the pebble-bed reactor with recirculating fuel. While a few codes and methods have been created for the PBR, this work shows how PBR core design and fuel cycle optimization reduce to the manipulation of a handful of key parameters that are readily manipulated using simple or advanced techniques.

8.1 Fuel Management and Neutronics Analysis in Pebble-Bed Reactors

A pebble-bed reactor is able to operate with what is effectively continuous refueling. Fuel, in the form of pebbles, is added to the top of the core at intervals measured in minutes. Pebbles drop out of the bottom of the core. If a pebble has not achieved the specified discharge burnup, it is dropped back into the core for another pass. If this mode of operation is continued, the core will achieve an asymptotic state in which pebbles constantly circulate through the core but the core-wide flux and nuclide distributions are essentially constant.

Pebble flow studies performed in Germany decades ago indicate that, for vessel geometries typical of pebble-bed reactors, pebbles follow well-behaved and largely vertical streamlines. (These studies have recently been accurately simulated using sophisticated discrete element codes that calculate the motion of individual pebbles.) This flow behavior can be modeled using a conservation law that treats burnup as an incompressible fluid. With knowledge of the pebble velocity profile, a variable

transformation (time to axial dimension) is applied to the nuclide depletion equations. The depletion equations are solved simultaneously with the neutron diffusion equation in an iterative fashion.

The radial burnup distribution at the entry plane is a boundary condition of this system. However, this distribution can be determined from the composition of the fresh fuel and the nature in which partially burned pebbles are reintroduced into the core. In this work it is shown how the flow of pebbles in the core can be parameterized in a way that links the entry plane burnup distribution to the composition of pebbles at the exit plane. Thus, the complete burnup profile of the core can be solved in a self-consistent manner with the neutron flux. Furthermore, it is shown that this parameterization of pebble flow (described in terms of a *recirculation matrix*) can be completely determined in terms of a few variables that are computed in advance of the neutronics calculation. As a result, pebble-bed core design and fuel management become readily amenable to simple and advanced optimization techniques.

8.2 Passive Safety in Pebble-Bed Reactors

For the foreseeable future, new nuclear power plant must demonstrate an exceptional degree of safe operation. While this can be achieved with engineered active safety systems, such systems add considerably to the capital cost of the plant. There is considerable interest in designing reactors that are passively safe, i.e., for all design basis events, core integrity is maintained using passive heat removal mechanisms. The modular pebble-bed reactor achieves this standard through the use of a robust coated particle fuel form and a tall, thin core with a low power density. In the event of a complete loss of coolant pressure and flow, the resulting core temperature increase

terminates the fission reaction through Doppler feedback. Decay heat is transported from the core via conduction and radiation at such a rate that fuel failure temperatures can be avoided. The fuel temperature design limit used in this work is the widely accepted 1,600°C.

By assuming that heat transfer under these conditions is exclusively radial and nonconvective, the transient heat transfer problem can be solved using a simple one-dimensional conduction equation. A finite difference solution to this equation has been added to PEBBED to quickly generate peak fuel temperatures during a depressurized conduction cooldown event. Comparison to results from two-dimensional analyses of pebble-bed reactor accidents reveals that this method is sufficiently accurate for conceptual design purposes.

8.3 Analysis of Existing PBR Designs

PEBBED was used to analyze three different types of recirculating pebble-bed cores. The PEBBED core models are rather simple in that neither control rods nor most minor fission products are included. Use of control rods in the modular PBR is generally limited to holding down core reactivity during shutdown; and then they are inserted only into the outer reflector, not into the core. For this reason, neglecting control rods is considered a reasonable assumption for most design purposes. Because of the online and semi-continuous refueling, excess reactivity can be kept to a minimum, also eliminating then need for burnable poisons. Minor fission products account for a few percent $\delta k/k$. Compensation for unmodeled reactivity effects in the PEBBED design models is achieved by setting target eigenvalues to high values (1.05 to 1.07).

Cross sections are generated for the asymptotic core in an iterative fashion using PEBBED and a cross-section code such as COMBINE or MICROX-2. Cross-sections for the fresh fuel composition are inserted into the PEBBED core model and depleted to generate the number densities of the fuel at the mean burnup level of the core. The new number densities are fed back to the cross-section generation code to produce improved values. This procedure is repeated until the core eigenvalues from successive PEBBED iterations differ by no more than \$0.10 (65 pcm). This method captures the spectral characteristics of the core that result from the burnup of the fuel. PEBBED currently does not adjust the cross-sections for variations in temperature. These variations can be many hundreds of degrees in the PBR. On the other hand, the PEBBED models use a six-group energy structure that captures resonance and upscattering effects better than the four-group VSOP code.

8.3.1 Results of Core Analysis

The HTR Modul 200 represents the first and simplest type of PBR modeled. It features a solid cylindrical core and a single type of pebble that is loaded randomly. PEBBED neutronic analysis of the core yields a core multiplication of 1.088 with cross-sections generated using the MICROX-2 code. DCC accident analysis of the 200 MWt core yields a peak fuel temperature of 1,424°C, considerably lower than the 1,530°C reported in the literature for this core. A likely reason is that PEBBED may underestimate the axial power peaking in the core that results from the fuel temperature distribution.

This reactor design may also be operated safely at a core power of 250 MWt. PEBBED confirms this with a peak accident temperature of 1,589°C for this core power.

The axial location of the power peak computed by PEBBED agrees well with that reported in an earlier study.

An early design of the South African Pebble Bed Modular Reactor uses a dynamic inner reflector made of graphite pebbles surrounded by a fuel pebble annulus. Fuel pebbles are loaded via peripheral loading tubes while the graphite pebbles are loaded via a central tube. The recirculation matrix for this scheme is generated from general core properties and the ratio of the flow of pebbles in the outer annulus to the total core flow.

PEBBED analysis of the PBMR-DIR yields a core multiplication factor of 1.073, sufficiently high to account for control rods, fission products, and required excess reactivity. The peak operating fuel temperature computed by PEBBED is 1,040°C, somewhat lower than that computed using VSOP (1,063°C) but reasonably close given the different definitions of fuel temperature used by the two codes. PEBBED computes a peak accident temperature of 1,419°C compared to the THERMIX (2D) computed value of 1,450°C. The PEBBED value compares favorably with one computed by the 2D accident analysis code MELCOR (1,406°C) using the core power densities supplied by PEBBED. Again, the differences between the PEBBED and literature values are likely the result of differences in power peaking that are attributable to the way in which cross sections are modeled.

An OUT-IN fuel recirculation scheme is demonstrated using a core design of a MPBR developed by General Electric. In the GE-MPBR, pebbles are loaded with a mixture of uranium and thorium oxides. The fresh pebbles are introduced in the outer radial region of the core, circulated for five passes, then transferred to the inner core zone for another five passes. The higher mean burnup of the inner zone reduces power peaking.

The PEBBED/MICROX combination yields a core eigenvalue of 1.045 compared to the VSOP-computed value of 0.998. VSOP tracks a larger number of fission products but it does not explicitly track Pu-238. A separate power profile was generated by GE using the BOLD/VENTURE code and nuclide densities from VSOP. This analysis also yields a higher power peaking factor than what is computed using PEBBED. Discharge isotopic composition of pebbles varies greatly between VSOP, PEBBED, and MCNP-ORIGEN models of the PBMR, indicating a need for cross-section methods development and benchmarking.

A depressurized conduction cooldown transient in the GE-MPBR was analyzed by both GE (using THERMIX) and Oak Ridge National Laboratory using the one-dimensional code SHERLOC. SHERLOC employs essentially the same method as is used in PEBBED and the results agree well when a common power and initial temperature profile is used. However, the BOLD-VENTURE-THERMIX value for the peak DCC temperature is 1,644°C while the PEBBED value is only 1,507°C. The difference is directly attributable to the lower power peaking computed by PEBBED, again a difference in the modeling of cross-sections.

8.4 Other Applications of PEBBED and the Recirculation Matrix

The ability to efficiently model the asymptotic fuel loading in a pebble-bed reactor for an arbitrary fuel recirculation scheme was exploited to study a handful of issues associated with pebble-bed reactors. Each of the topics addressed in this portion of the thesis were (or will be) presented in American Nuclear Society conference transactions.

Continuously fueled reactors offer the distinct advantage that an optimal ratio of fuel to moderator can be maintained indefinitely once the asymptotic core has been

reached. This feature was demonstrated by computing the core eigenvalue of a reactor for a number of pebble designs that differed in the amount of fuel particles they contain. Plotting the results yielded a definite peak corresponding to the *optimally moderated* core-fuel configuration. Comparisons between a PBMR-DIR reactor fueled with standard and optimized pebbles showed safety and performance benefits. The optimized pebble yielded a core that was more tolerant of steam ingress, i.e., the resulting reactivity insertion was less for the optimized pebble than for the standard. Reactors using optimized pebbles also used less fuel than those using standard pebbles although the difference in the PBMR-DIR design was slight.

The stochastic nature of pebble loading and motion has led to concerns that hot spots could develop in a PBR core with subsequent fuel failure. To address this issue, the fuel-loading pattern in the PBMR-DIR model was adjusted to correspond with extreme cases of pebble misdirection. Simulations of fresh fuel pebbles being loaded into the central reflector region were performed by generating special recirculation matrices. Under these circumstances, the peak accident temperatures attained by the anomalous cores did achieve levels that would lead to mild fuel failure (up to 1,784℃ in the worst case) in a large portion of the core (less than 0.05% overall fuel inventory release). It is noted, however, that because such a core condition would take so long to develop (one to three years to develop an asymptotic core) the probability that such a configuration would develop in conjunction with a complete loss of coolant flow and pressure is certainly beyond design basis.

The possibility was addressed that an owner of a standard PBR would attempt to clandestinely produce weapons plutonium. Under the scenario addressed in this work, indigenously produced production pebble fueled with natural uranium would be introduced into the core without the knowledge of the reactor or fuel vendor. One case

modeled with PEBBED involved replacing 5% of the fuel pebbles in an HTR Modul-like reactor with these production pebbles. The other case involved replacing 5% of the *graphite* pebbles in the PBMR-DIR with such production pebbles. In the first case, the absorption of neutrons by the illicit material led to a 12% increase in the required refueling rate. In the second, there was only a slight increase in the required fueling rate (about 1.4%) which conceivably be compensated through other means. However, to acquire enough Pu-239 for a weapon would require seven years at this rate of production. It is concluded that the low excess reactivity inherent in a properly fueled PBR does not allow for both secret and fast accumulation of quality weapons material.

8.5 Design of a Very High Temperature Pebble-bed Reactor

The efficiency with which PEBBED can model a wide variety of PBRs was exploited in the design of the Generation IV reactor concept, the Very High Temperature Reactor or VHTR. The VHTR is a high temperature, gas-cooled reactor that can produce an outlet temperature of 1,000℃ yet still demonstrate passive safety features.

PEBBED can quickly generate peak accident (DCC) fuel temperatures by solving a simple one-dimensional conduction problem. The accuracy of this approach was tested using the safety analysis code MELCOR. Two-dimensional MELCOR models of three different reactors were constructed using the power profiles generated in PEBBED. The peak accident temperatures computed by MELCOR and PEBBED showed remarkable agreement given the nature of the two calculations. With this result in hand, a search for 300 and 600 MWt VHTR designs was initiated.

The pebbles used in the VHTR design search were optimized per the method described in Chapter 5. Then, starting with a familiar base design (the PBMR-DIR),

modifications to the core geometry were made until reasonable values for core eigenvalue and DCC peak temperature were obtained. The pebble-based graphite inner reflector of the PBMR-DIR was replaced with a solid graphite cylinder. The inner reflector and fuel annulus radius were then varied. When values close to the targets were achieved, the core height and discharge burnup were adjusted to home in on the final design.

A 300 MWt VHTR was generated that fits inside the PBMR-DIR vessel. The peak accident fuel temperature fell slightly above the 1,600°C limit so a slight downward adjustment was effected by increase the flow rate of pebbles. The completed design displayed a 14% improvement in fuel economy over the PBMR-DIR.

A 600 MWt VHTR was generated that fits inside the radial dimension of the pressure vessel of the 600 MWt prismatic GT-MHR designed by General Atomics. The pebble-bed VHTR is considerably taller than the GT-MHR (950 cm vs. 793 cm). The improved fuel economy of the optimized pebble is offset by the considerable pumping power requirements of this tall reactor so that the fuel requirements of the VHTR-600 are comparable to that of the PBMR-DIR.

This design process provides the starting point for more detailed design studies and optimization. Complex neutronic and thermal-hydraulic modeling can take place with some confidence that a satisfactory design will emerge.

8.6 Automated Design of Pebble-bed Reactors

The direct search method described in the previous section yielded a design that satisfied the basic requirements of the VHTR. Yet it is likely that the resulting designs are not the best that can be obtained. An automated search tool, based upon a genetic

algorithm, was shown to produce user-specified core characteristics with minimal user intervention.

8.6.1 Genetic Algorithm Search

A genetic algorithm is a type of stochastic optimization technique in which favorable attributes of the members of a randomly generated population are used to direct the search toward promising regions of the solution space. In a direct analogy to biological reproduction, selection, crossover, and mutation operations are performed on specified parameters shared by the member of the population to generate new members with ever improving characteristics.

In this work, an individual is a specific core design. The parameters varied by the algorithm may include: inner and outer reflector width, fuel annulus width, height, and fraction of pebble flow that composes the outer flow zone. The user specifies which of these “genes” will be varied and the upper and lower bounds on the values. A PEBBED analysis is conducted on each individual to generate a “fitness” value. The fitness is a function of characteristics of the PEBBED solution which currently may include: core eigenvalue, peak operating fuel temperature, peak accident fuel temperature, outer reflector radius, reactivity (as measured against the previous case), required pumping power, and peak particle power.

The user specifies which of these “traits” are to contribute to the fitness function. For each chosen trait, the contribution to the overall fitness is determined by a four-point interpolation scheme. This allows the user great flexibility in directing the solution toward particular core characteristics. It also requires the user to exercise some engineering judgment in specifying the fitness function.

Once the genes and trait functions are established the user chooses the size of the population and the number of survivors, i.e., the number of solutions that will be propagated to the next generation. Those with the highest fitness values survive (*selection*). The genes of the survivors are used to reconstruct the population. Genes of new members are generated by mixing the genes of randomly chosen survivors (*crossover*). Finally, there is a small probability that one or more genes of randomly chosen individuals will be arbitrarily changed to new values (mutation). This allows the algorithm to explore previously untested regions of the solution space.

8.6.2 Design Results

This method was used to optimize the design of existing PBR concepts. In the first case, the core diameter of the HTR Modul 200 was varied to produce a passively safe version with improved neutron economy. After 10 generations, the resulting design was slightly larger in diameter and possessed a higher eigenvalue. The peak accident fuel temperature settled at 1,599℃, very close to the target specified by the fitness function.

In the second case, a core with an OUT-IN fueling scheme was optimized by varying the core radius, the height, and the fraction of flow composing the outer flow zone. Compared to the original design, the resulting core yielded higher core eigenvalue and a much smaller outer fuel zone.

In the third case, a 600 MWt Very High Temperature pebble-bed Reactor was designed from scratch and compared to the one obtained from the previous manual search (reference design). The genes varied in this search included the inner reflector radius, the fuel annulus width, and the height. The traits contributing to the fitness

function included the core eigenvalue, the peak accident fuel temperature, the outer reflector radius, and the required pumping power.

After eight generations, the algorithm produced a design that exhibited an eigenvalue comparable to the reference design. The peak accident fuel temperature was slightly lower than the reference design and matched closely the target value specified in the fitness function. The algorithm achieved this by narrowing the core annulus and increasing the height of the core. The required pumping power was also increased slightly. However, the outer diameter of the pressure vessel is small than both the reference design and the prismatic GT-MHR.

The genetic algorithm employed in this work is not the product of a detailed study of computational parameters and sensitivity studies. Improvements on the scheme can probably be discovered with a modicum of effort. Nonetheless, this inaugural algorithm did produce satisfactory designs and amply demonstrates the effectiveness of this approach.

8.7 Future Work

This research was meant to be introductory. The state of core design and fuel management in pebble-bed reactors is decades behind that of light water reactors. Advanced methods and tools have yet to be developed, largely because of the lack of interest in PBR development since the closure of the THTR. With the operation of the HTR-10 and the imminent construction of the PBMR, an ever-increasing need for such advanced tools will be observed.

The current state of PEBBED and its recirculation matrix formulation addresses the key need for an efficient and accurate design tool. However, the results obtained

from this effort also point to other developments that will be required for this technology to mature.

The generation of *accurate cross-sections* is the next major step. The results shown in this work indicate a large discrepancy among the different codes and techniques available for this task. These discrepancies lead directly to large uncertainties in power peaking factors, discharge isotopics, critical dimensions, etc. While the fundamental conclusions and trends observed in this work are sound, large error bars must be attached to any numerical results until improved methods and benchmarks are developed.

In particular, parametric variations in cross sections must be implemented to account for the wide range of temperatures and material compositions in the core. The single set of values currently employed in PEBBED models are generated about the mean temperature and composition of fuel pebbles. However, neutron scattering in graphite and absorption in heavy metals may be strongly dependent on local conditions. Work is underway at the INEEL in conjunction with the Pennsylvania State University and the Georgia Institute of Technology to develop advanced cross section generation methods.

The current diffusion equation solver in PEBBED is a standard finite difference treatment (albeit in three-dimensional cylindrical coordinates). Small computational mesh sizes are needed to achieve high accuracy but they also lead to long calculation times. To retain accuracy while lowering execution times, a modern *diffusion equation solver* should be implemented. At the INEEL, a coarse, mesh finite difference nodal solution in being implemented and tested. This type of nodal solution fits easily into the existing algorithm and will allow larger mesh sizes with no loss of accuracy.

An analytical solution to the cylindrical nodal equations has been developed at the INEEL. Mathematical singularities have thwarted earlier attempts at obtaining an analytical solution but an ingenious workaround was discovered and developed by Ougouag and Terry. This will eventually be the default solver in PEBBED.

Future reactor models will also need to be more sophisticated. As previously indicated, most *minor fission products* are neglected. The structure of PEBBED allows a large number of decay chains to be included once an improved method for generating cross sections is developed. In many cases, however, large groups of fission products can be treated as one or more lumped fission products to adequately capture the reactivity effects. Development of lumped fission products appropriate for high burnup HTGR fuel will require then application of suitable depletion codes and techniques.

Although *control rods* have a minimal role to play during normal operation, they are required to shut down the reactor and keep it subcritical when the reactor is cold. One important consideration for pebble-bed reactors is that, unlike cores with stationary fuel, control rods cannot be inserted into the active core. They must be inserted into the outer reflector (or the inner reflector if it is solid). Generating cross sections requires the use of transport codes to adequately treat the high absorption properties of the rods and to generate the proper spectrum in the reflector regions.

Because the rods are limited to reflector positions, the reactivity worth is not as great as if they could be inserted into the core. This fact poses a limitation on the radial size of the reactor core. If the core is too large, radial neutron leakage and thus rod worth may be too small to provide adequate cold shutdown margin. Future design efforts must incorporate rod worth calculations to avoid this serious deficiency.

On a related note, a potential drawback of large graphite-moderated reactors is the possibility of large spatial *xenon transients*. MPBR cores are sufficiently narrow to

prevent large radial and azimuthal distributions in xenon concentration but axial transients are possible. Like control rod worth, these may limit the size that can be achieved and should be explored with a proper transient analysis code.

Radial pebble flow is not currently modeled in PEBBED. This is not a serious deficiency because radial flow is largely restricted to the low flux region of the bottom conus. However, neglect of this radial flow does introduce error that can be avoided with a little development. The burnup equation is currently solved along axial streamlines but this can be generalized to non-axial streamlines if the geometry of those lines is properly specified. The non-axial flow error may be particularly important with fast spectrum reactors.

The first few years of operation in a PBR core are not optimal. The core takes some time to achieve the asymptotic state for which it would presumably have been optimized. The so-called *running-in period* requires modified fuel pebbles or different core configurations to achieve safe and economic operation. The coupled diffusion-depletion equations currently solved in PEBBED assume that the reactor has achieved a steady state core configuration, i.e., the partial derivative of the burnup with respect to time in the left hand side of Eq. **2.4** vanishes. However, a poorly designed transition core may adversely affect the overall economics of the plant. Furthermore, startup is not the only time in which the core may be in transition. Over the 60-year life of a plant, a number of advances in fuel design would be expected to occur. Switching to a new fuel design entails a long transition time until a new asymptotic state is achieved.

The time-dependent burnup equations will need to be incorporated into PEBBED to treat these cases. The input specification will need to be modified to accommodate a time-dependent fresh fuel injection description.

Light water reactor fuel management has been the subject of many advances in optimization of which genetic algorithms are but one type. The algorithm in PEBBED has not been optimized and probably can benefit greatly from various parametric studies and testing of different operators.

Other optimization methods may prove very effective as well. Simulated annealing and neural networks are two methods that have been applied with success to LWR fuel management. Some studies have suggested that the genetic algorithm is very good at locating the region in which a global optimum exists but not so well at converging to that optimum. Hybrid solution techniques have been proposed in which a stochastic technique is augmented with a neural network or traditional linear optimization method that performs a faster local search. All of these approaches can be used with the recirculation matrix formulation in PEBBED and are worthy of further study.

Bibliography

1. Goodjohn, A. J., 1991, "Summary of Gas-Cooled Reactor Programs," *Energy*, Vol. 16, No. ½, pp. 79-106.

2. Zhong, Z. and Z. Qin, 2001, "Overview of the 10MW High-Temperature Gas-Cooled Reactor Test Module," *Proceedings of the Seminar on HTGR Application and Development, Beijing, China (PRC), March 2001.*

3. 2001, "Critical Experiments and Reactor Physics Calculations for Low-Enriched High Temperature Gas Cooled Reactors," *IAEA TECDOC 1249*, 2001.

4. Magwood, W., 2000, "Roadmap to the Next Generation Nuclear Power Systems: A Vision for a Powerful Future," *Nuclear News*, American Nuclear Society, November 2000.

5. Ryskamp, J. (Idaho National Engineering and Environmental Laboratory), 2003, *Next Generation Nuclear Plant – High-Level Functions and Requirements*, INEEL/EXT-03-01163, September 2003.

6. Terry, W. K., H. D. Gougar, and O. M. Ougouag, 2001, "Novel Method for the Deterministic Design, Analysis, and Optimization of the In-Core Fuel Cycle of a Recirculating Pebble-Bed Reactor," *Annals of Nuclear Energy*, Vol. 29, pp. 1345-1364.

7. Schulten, R., 1978, "Pebble-bed HTRs," *Annals of Nuclear Energy*, Vol. 5 (8-10): pp. 357-374.

8. Schulten, R., 1989, "Twenty Years of AVR High-Temperature Reactor Operation," *Atomwirtschaft-Atomtechnnik*, Vol. 34 (4), pp. 166-168, April 1989.

9. Frewer, H., W. Keller, and R. Pruschek, 1985, "The Modular High-Temperature Reactor," *Nuclear Science and Engineering*, Vol. 90, p. 411-426.

10. Lohnert, G. H. and H. Reutler, 1983, "The Modular HTR – A New Design of High-Temperature Pebble-Bed Reactor," *Nuclear Energy*, Vol. 22, No. 3, June 1983.

11. Zgliczynski, J., A. Neylan, and D. Kapich, 1993, "The Gas-Turbine Modular Helium Reactor (GT-MHR) Offers Potential for Stretch Capability to 300Mwe per Reactor Module," *The 1993 International Joint Power Generation Conference and* Exposition*, Kansas City, MO, October 1993*.

12. Simnad, M., 1991, "The Modular HTGR: Its Possible Role in the Use of Safe and Benign Nuclear Power," *Proceedings of the International Conference on Global*

Climate Change: Its Mitigation Through Improved Production and Use of Energy, *American Institute of Physics, Los Alamos, NM, October 1991*.

13. Ball, S., 2001, "Status of the Gas-Turbine Modular Helium Reactor for Plutonium Disposition," *Proceedings of the Seminar on HTGR Application and* Development*, Beijing, China (PRC), March 2001*.

14. Gouge, M. J., 1995, "Closed Cycle Gas Turbine Nuclear Power Plant for Submarine Propulsion," *Naval Engineers Journal*, November 1995.

15. Petti, D. A. (ed.), 2002, *Annual Report of the Modular Pebble-bed Reactor Project*, University Research Consortium, INEEL-EXT-02-01545, November 2002.

16. Drüke, V. and D. Filges, 1987, "The Critical HTR Test Facility KAHTER – An Experimental Program for Verification of Theoretical Models, Codes, and Nuclear Data Bases." *Nuclear Science and Engineering*, Vol. 97, No. 1, September 1987.

17. Naidoo, D., 2000, "ASTRA Critical Facility Configuration Report," PBMR, 003402-34 (Rev. A), May 2000.

18. Fujikawa, S., O. Baba, M. Ohkubo, H. Ando, T. Iyoku, and T. Nakazawa, 2001, "Present Status of the HTTR and Topics from Operation," *Proceedings of the Seminar on HTGR Application and Development, Beijing, China, March 2001*.

19. Van Heek, A. I., 2001, "The Pebble-bed HTR, the Nuclear Option in the Netherlands," *Proceedings of the Seminar on HTGR Application and Development, Beijing, China (PRC), March 2001*.

20. Van Heek, A. I., 2002, "ACACIA, A Small Scale Nuclear Power Plant with Cogeneration Capabilities," *Proceedings of the American Society of Mechanical Engineers (ASME) Turbo* Conference*, June 2002*.

21. Crommelin, G., 1999, "The NEREUS Installation," *Proceedings of the International Gas Turbine and Aeroengine Congress and Exhibition, ASME*, *Indianapolis, IN, June 1999*.

22. 2001, "China's First High Temperature Reactor Goes Critical," *Nuclear News*, American Nuclear Society, February 2001.

23. 2003, "Pebble Rolls On," *Professional Engineering*, Institution of Mechanical Engineers, July 9, 2003.

24. 2003, "As Technology is Fine-tuned, PBMR Design Takes Final Shape," *Nucleonics Week,* Vol. 44, No. 39, September 25, 2003.

25. Breitbach, G. and H. Barthels, 1980, "The Radiant Heat Transfer in the High Temperature Reactor Core after Failure of the Afterheat Removal Systems," *Nuclear Technology*, Vol. 49, pp. 392-399, August 1980.

26. Petersen, K., 1983, “The Safety Concept of HTRs with Natural Heat Removal for the Core in Accidents, Juel-1872, October 1983.

27. Rehm, W., 1980, “Unterschungen uber die Verzogerte Nachwarmeabfuhr bein einem Kugelhaufen-Hochtemperaturreaktor-Konzept grosber Leistung als Beitrag zu den Moglichkeiten der Begreenzung Hypothetischer Unfalle,” Juel-1647, February 1980.

28. Wolters, J. and W. Kröger et al, 1984, “Zum Störfallverhalten des HTR Modul; eine Trendanalyse,” KFA Report Jül-Spez-260, June 1984.

29. Mertens, J., 1985, “Sicherheittechnische Untersuchungen zum Störfallverhalten des HTR-Modul,” KFA Report Jül-Spez-335, November 1985.

30. Scherer, W., H. Gerwin, T. Kindt, and W. Patscher, 1987, “Analysis of Reactivity and Temperature Transient Experiments at the AVR High-Temperature Reactor,” *Nuclear Science and Engineering*, Vol. 97, pp. 58-63.

31. Nickel, H., 2002, “HTR Coated Particles and Fuel Elements,” *presented at the HTR/RCS 2002 High Temperature Reactor School, Cadarache, France, November 2002*.

32. Petti, D., J. Buongiorno, J. Maki, R. Hobbins, and G. Miller, 2003, “Key Differences in the Fabrication, Irradiation, and High Temperature Accident Testing of US and German TRISO-Coated Particle Fuel, and Their Implications on Fuel Performance,” *Nuclear Engineering and Design*, 222, pp. 281-297.

33. Teuchert, E., H. Rütten, B. Worley, and D. Vondy, 1979, ”US/FRG/Joint Report on the Pebble bed High Temperature Reactor Resource Conservation Potential and Associated Fuel Cycle Costs,” ORNL-5582, November 1979.

34. Werner, H., 1997, "Build-up of Plutonium Isotopes in HTR Fuel Elements – A Comparison Between Computed Prediction and Chemical Analysis," *Nuclear Engineering and Design*, 170, pp. 147-164.

35. Ougouag, A. M. and H. D. Gougar, 2001, “Preliminary Assessment of the Ease of Detection of Attempts at Dual Use of a Pebble Bed Reactor,” *Trans. Am. Nucl. Soc.*, 85.

36. Ougouag, A. M., H. D. Gougar, and W. K. Terry, 2002, “Examination of the Potential for Diversion or Clandestine Dual Use of a Pebble-Bed Reactor to Produce Plutonium,” *Proceedings of HTR 2002, 1st International Topical Meeting on High Temperature Reactor Technology (HTR), Petten, Netherlands, April 22-24, 2002*.

37. Ougouag, A. M., M. Modro, W. K. Terry, and H. D. Gougar, 2002, “Rational Basis for a Systematic Identification of Critical Components and Safeguards Measures for a Pebble-Bed Reactor," *Trans. Am. Nucl. Soc.*, 87.

38. Massimo, L., 1976, *The Physics of High-Temperature Reactors*, Oxford, Pergamon Press.

39. Schulten, R., K. Kugeler, and W. Frohling, 1984, "Applications of Nuclear Process Heat," *Progress in Nuclear Engineering*, Vol. 14 (3), pp. 227-268.

40. Yan, X. L. and L. Lidsky, 1991, "Design Study for an MHTGR Gas Turbine Power Plant," *Proceedings of the 53rd American Power Conference, Chicago, IL, April 1991*.

41. Verkerk, E. C., 1996, "Helium Storage and Control System for the PBMR," *Proceedings of HTGR Technology Development, Johannesburg, SA, November 1996*, IAEA TECDOC-988, pp. 195-203.

42. Plukiene, R. and D. Ridikas, 2003, "Modeling of HTRs with Monte Carlo: From a Homogeneous to an Exact Heterogeneous Core with Microparticles," *Annals of Nuclear Energy*, 30, pp. 1573-1585.

43. Bell, G. I., 1959, "A Simple Treatment for Effective Resonance Absorption in Dense Lattices," *Nuclear Science and Engineering,* Vol. 5, No. 2, pp. 158-159.

44. Valko, J., P. Tsvetkov, and J. Hoogenboom, 2000, "Calculation of the Dancoff Factor for Pebble-bed Reactors," *Nuclear Science and Engineering*, Vol. 135, pp. 304-307.

45. Rahnema, F., 2003, *Homegenized Cross Section Development for the Pebble Bed Reactor Core*, INEEL LDRD Progress Report, June 23, 2003.

46. Bedenig, D., W. Rausch, and G. Schmidt, "Parameter Studies Concerning the Flow Behavior of a Pebble with Reference to the Fuel Element Movement in the Core of the THTR 300MWe Prototype Reactor," *Nuclear Engineering and Design*.

47. Bedenig, D., 1967, "Ein Theoretisches Model Zur Beschreibung Des Kugelhaufen-Fliessverhaltens Im Core Eines Kugelhaufen-Reaktors," *Nuclear Engineering and Design*, Vol. 6, pp. 479-488.

48. Mulder, E., 2003, "PBMR Almost Current Status," *Presentation given to the ANS Gas Reactor Technology Course by M. Feltus, PBMR Pty, Ltd, San Diego, CA*, June 2003.

49. Reitsma, F., "Nuclear Energy Corporation of South Africa," Private Correspondence, October 2003.

50. Teuchert, E., U. Hansen, and K. Haas, 1980, "VSOP – Computer Code System for Reactor Physics and Fuel Cycle Simulation," Kernforschunsanslage Jülich, JÜL-1649, March 1980.

51. Leithner, D. and S. Brandes, 1988, "Improved Fuel Utilization by Optimization of High-Temperature Reactor Core Design," *Kerntechnik*, Vol. 52, No. 4.

52. Vondy, D. and B. Worley, 1979 (Oak Ridge National Laboratory), "Pebble-bed Reactor Core Physics and Fuel Cycle Analysis," ORNL-5484, October 1979.

53. Jung, H., 1981, "Simultanlösung des Abbrand- und Durchlaufproblems der Kugeln bei Kugelhaufenreaktoren" (Simultaneous solution of the burn-up and fuel-movement problems in pebble-bed reactors), Atomkernenergie-Kerntechnik Bd. 38 (1981) Lfg.2, p. 141.

54. Oppe, J., J. Kuijper, J. de Haas, E. Verkerk, and H. Klippel, 2001, "Modeling of Continuous Reload HTR Systems by the PANTHERMIX Code System," *Transactions of the American Nuclear Society Topical Meeting on Mathematics and Computation, Salt Lake City, UT, September 2001*.

55. Massimo, L., 1968, "KUGEL, ein Programm, um das raumabhängige Gleichgewicht-Isotopengemisch in einem Kugelhaufenreaktor zu berechnen-Nucleonik" (KUGEL, a program to compute the spatially-dependent neutronics in a pebble-bed reactor with [pebbles of initially] equal isotopic composition), 11Bd., Heft 2, pp. 72-76.

56. Gießer, W., H. Jung, and L. Massimo, 1969, "Fuel Management Methods for Pebble-bed Reactors and their Applications to the AVR," Atomkernenergie, Vol. 14., No. 10, pp. 43-46.

57. Izenson, M., 1986, *Effects of Fuel Particle and Reactor Core Design on Modular HTGR Source Terms*, Doctoral Dissertation, Massachusetts Institute of Technology, September 1986.

58. Sekimoto, H., Obara, T., Yukinori, S., and Suetomi, E., "New Method to Analyze Equilibrium Cycle of Pebble-Bed Reactors," J. Nucl. Sci. and Tech., 24[10], pp. 765-772, October 1987.

59. Obara, T. and H. Sekimoto, 1991, "New Numerical Method for Equilibrium Cycles of High Conversion Pebble-bed Reactors," *Journal of Nuclear Science and Technology*, 28[10], pp. 947-957, October 1991.

60. Liem, P. H., 1994 "BATAN-MPASS: A General Fuel Management Code for Pebble-Bed High-Temperature Reactors," *Annals of Nuclear Energy*, Vol. 21, No. 5, 290.

61. Liem, P. H., 1994, "Design Procedures for Small Pebble-Bed High Temperature Reactors," *Annals of Nuclear Energy*, Vol. 23, No. 3, pp. 207-215.

62. Nabielek, H. et al, 1989, "The Performance of High Temperature Reactor Fuel Particles at Extreme Temperatures," *Nuclear Technology*, 84, 62.

63. Martin, David G., 2002, "Considerations Pertaining to the Achievement of High Burn-ups in HTR Fuel," *Nuclear Engineering and Design,* Vol. 213, pp. 241-258.

64. Hansen, U., R. Schulten, and E. Teuchert, 1972, “Physical Properties of the ‘Once Through Then Out’ Pebble-Bed Reactor”, *Nuclear Science and Engineering*, 47, pp. 132-139.

65. Holland, J., 1992, ”Genetic Algorithms,” *Scientific American*, Vol. 66, July 1992.

66. Parks, G. T., 1993, ”An Intelligent Stochastic Optimization Routine for Nuclear Fuel Design,” *Nuclear Technology*, Vol. 89, p. 233.

67. Mahlers, Y., 1995, “Core Loading Pattern Optimization Based on Simulated Annealing and Successive Linear Programming,” *Annals of Nuclear Energy*, Vol. 22, No. 1, pp. 29-37.

68. Kropaczek, D. and P. Turinsky, 1991, ”In-Core Nuclear Fuel Management Optimization for Pressurized Water Reactors Utilizing Simulated Annealing,” *Nuclear Technology*, Vol. 95, July 1991.

69. Grefenstette, J. J., 1986, “Optimization of the Control Parameters for Genetic Algorithms,” IEEE Trans Syst., Man,Cyber., SMC-16.

70. Goldberg, David E., 1989, *Genetic Algorithms in Search, Optimization, and Machine Learning*, Addison-Wesley, Reading, MA.

71. Poon, P. and G. Parks, 1993, “Application of Genetic Algorithms to In-Core Nuclear Fuel Management Optimization,” *Proceedings of the Joint International Conference on Mathematical Models and Supercomputing in Nuclear Applications, Karlsruhe, Germany, April 1993*.

72. DeChaine, M. and M. Feltus, 1995, ”Nuclear Fuel Management Optimization Using Genetic Algorithms,” *Nuclear Technology*, Vol. 111, pp. 109-114, July 1995.

73. DeChaine, M. and M. Feltus, 1996,”Fuel Management Optimization Using Genetic Algorithms and Expert Knowledge,” *Nuclear Sciecne and Engineering*, Vol. 124, pp. 188-196.

74. Yamamoto, A., 1996, “Loading Pattern optimization Using Genetic Algorithms,” *Proceedings of the ANS Conference on the Physics of Reactors (PHYSOR)*, *Mito, Japan, 1996*, Vol., 3, pp. 1-48.

75. Martín del Campo, C., and H. López François, 2001, “AXIAL: a System for Boiling Water Reactor Fuel Assembly Axial Optimization Using Genetic Algorithms,” *Annals of Nuclear Energy*, Vol. 28, pp. 1667-1682.

76. Stamm’ler, R. J. J. and M. J. Abbate, 1983, *Methods of Steady-State Reactor Physics in Nuclear Design*, New York, Academic Press.

77. Ougouag, A. M. and W. K. Terry (Idaho National Engineering and Environmental Laboratory), 2002, *Development of a Novel Method for the Solution of the*

Neutron Diffusion Equation in General Cylindrical Geometry, INEEL/EXT-2002-489, April 2002.

78. Benedict, M., T. Pigford, and H. W. Levi, 1981, *Nuclear Chemical Engineering*, New York, McGraw-Hill.

79. Gougar, H. D., W. K. Terry, A. M. Ougouag, and C. B. Neill, 2002, "Matrix Formulation for Pebble Circulation in the PEBBED Code", *Proceedings of the 1st International Topical Meeting on High Temperature Reactor Technology, Petten, The Netherlands, April 22-24, 2002*.

80. Incropera, F. P. and D. P. DeWitt, 1990, *Fundamentals of Heat and Mass Transfer,* 3rd. Ed.*,* Wiley and Sons.

81. Gnielinski, V., 1978, "Gleichungen zur Berechnung des Wärme- und Stoffaustausches in durchströmten ruhenden Kugelschütten bei mittleren und großen Peclet-Zahlen," *Verfahrenstechnik* 12, No. 6, pp. 363-366.

82. Lutz, D. E., C. Cowan, C. Davis, K. El Sheik, M. Hui, A. Lipps, and T. Wu, 1982, *Modular Pebble-Bed Reactor Reforming Plant Design for Process Heat*, GEFR-00630, General Electric Company, September 1982.

83. Savage, M. G. (Oak Ridge National Laboratory), 1981, "A One-Dimensional Modeling of Radial Heat Removal During Depressurized Heatup Transients in Modular High Temperature Gas-Cooled Reactors," ORNL/TM009215, DE84016746, July 1981.

84. Gruen, G. E., 1985, "Passive Cooling Model for Pebble Bed Reactor," INEL Report SE-A-85-004, EG&G Idaho, February 1985. Stamm'ler, R. J. J., and M. J. Abbate, 1983, *Methods of Steady-State Reactor Physics in Nuclear Design*, New York, Academic Press.

85. Matthews, D., 1997, *An Improved Version of the MICROX-2 Code*, PSI Bericht Nr. 97-11, Paul Scherrer Institut, Switzerland, November 1997.

86. Grimesey, R. A., D. Nigg, and R. Curtis (Idaho National Engineering Laboratory), 1991, "COMBINE/PC-A Portable ENDF/B Version 5 Neutron Spectrum and Cross-Section Generation Code," EGG-2589, April 1991.

87. Yoon, W. Y., 1994, "COMBINE-6 Cycle 1," WYY-01-94, Idaho National Engineering Laboratory Internal Memo, January 17, 1994.

88. Mulder, E., 2000, PBMR Pty, Ltd., Private Correspondence, Cambridge, MA, November 2000.

89. Terry, W. (ed.) (Idaho National Engineering and Environmental Laboratory), 2001, *Modular Pebble Bed Reactor Project 2001 Annual Report*, INEEL/EXT-2001-1623, December 2001.

90. MacLachlan, A., 2003, "As Technology is Fine-Tuned, PBMR Design Takes Final Shape," *Nucleonics Week* 10, Vol. 44, No. 39, September 25, 2003.

91. MacDonald, P. and J. S. Herring (Idaho National Engineering and Environmental Laboratory), 2000, "Advanced Proliferation Resistant, Lower Cost, Uranium-Thorium Dioxide Fuels for Light Water Reactors", 1st Annual Report, INEEL/EXT-2000-01217.

92. Ougouag, A. M., H. D. Gougar, W. K. Terry, R. Mphahlele, and K. N. Ivanov, 2004, "Optimal Moderation in the Pebble-Bed Reactor for Enhanced Passive Safety and Improved Fuel Utilization," *to be published in the Proceedings of PHYSOR 2004, American Nuclear Society Topical on the Physics of Advanced Reactors, Chicago, IL, April 2004.*

93. J. Briesmeister (Editor) (Los Alamos National Laboratory), 1993, *MCNP – A General Monte Carlo N-Particle Transport Code*, Version 4B, LA-12625-M, Rev. 2.

94. Potter, R. C., 1996, *Gas Turbine-Modular Helium Reactor (GT-MHR) Conceptual Design Description Report*, General Atomics Project No. 7658, San Diego, CA, July 1996.

95 Mark, J. C., T. Taylor, E. Eyster, W. Maraman, and J. Wechsler, 1987, "Can Terrorists Build Nuclear Weapons?" pp. 55-65, *Preventing Nuclear Terrorism*, Paul Leventhal and Yonah Alexander, Editors, Lexington Books.

96 Benenati, R. F. and C. B. Brosilow, 1962, "Void Fraction Distribution in Beds of Spheres," *A.I. Ch.E.* Journal 8, No. 3, pp. 359-361.

97 Zainuddin Karriem, Coenie Stoker, and Frederik Reitsma, "MCNP Modeling of HTGR Pebble-Type Fuel," paper NG-VIII/04 in *proceedings of Advanced Monte Carlo for Radiation Physics, particle Transport Simulation, and Applications (Monte Carlo 2000), Lisbon, Portugal, October 23-26, 2000, sponsored by OECD/NEA and ANS*.

98. Lebenhaft, J. R. and M. J. Driscoll, 2001, "MCNP4B Analysis of the HTR-10 Startup Core," *Transactions of the American Nuclear Society*, Vol. 84, pp. 214-215.

99. Murata, I. and A. Takahashi, 1998, "Analysis of Critical Assembly Experiments by Continuous Energy Monte Carlo Method with Statistical Geometry Model," *Technology Reports of the Osaka University*, 48 (2304), pp. 19-31, April 1998.

100. Gauntt, R. O., R. K. Cole, S. H. Hodge, S. B. Rodriguez, R. L. Sanders, R. C. Smith, D. S. Stuart, R. M. Summers, and M. F. Young, 1997, *MELCOR Computer Code Manuals*, NUREG/CR-6119, Vol 1, Rev. 1, SAND97-2397-2398.

101. Merrill, B. J., R. L. Moore, S. T. Polkinghorne, and D. A. Petti, 2000 *Fusion Engineering and Design,* 51-52, 555-563.

102. MacDonald, P.E. (Idaho National Engineering and Environmental Laboratory), 2003, *NGNP Preliminary Point Design – Results of the Initial Neutronics and Thermal-Hydraulics Assessments*, INEEL/EXT-03-00870 Rev. 1, September 2003.

103. Hawari, A. I., Bingjing Su, Jianwei Chen, and Zhongxiang Zhao, 2001, *Investigation of On-Line Burnup Monitoring of Pebble Bed Reactor Fuel Using Passive Gamma-Ray and Neutron Detection Methods, Transactions of the Winter 2001 Annual Meeting of ANS, Reno, NV, November 2001*, Trans. ANS 85, pp. 98-99.

104. Muto, Y. and Y. Kato, 2003, A *New Pebble Bed Core Concept with Low Pressure Drop*, *Transactions of the Global 2003 Conference, American Nuclear Society, New Orleans, November 2003*.

105. Grefenstette, J. J., 1986, “Optimization of the Contro, Parameters for Genetic Algorithms,” *IEEE Trans. Syst., Man, Cyber.*, SMC-16.

Appendix A

PEBBED Solution to the Diffusion Equation

Finite Difference Solution to the Diffusion Equation

Much of the following material was obtained from reference [76].

The diffusion equation for energy group *g* is given by

$$-\vec{\nabla}\bullet D_g(\vec{r})\vec{\nabla}\phi_g(\vec{r})+\Sigma_{r,g}(\vec{r})\phi_g(\vec{r})=\sum_{g'\neq g}\Sigma_{s,g'\to g}(\vec{r})\phi_{g'}(\vec{r})+\frac{1}{k}\chi_g\sum_{g'}\nu_{g'}\Sigma_{f,g'}(\vec{r})\phi_{g'}(\vec{r}) \quad . \qquad \textbf{(A1)}$$

The corresponding neutron current is given by

$$\vec{J}_g(\vec{r})=-D_g(\vec{r})\vec{\nabla}\phi_g(\vec{r}) \quad . \qquad \textbf{(A2)}$$

Each term in (A1) is integrated over the volume of the mesh cell in which the material properties and flux are assumed constant.

The integrated leakage term is then converted into a surface integral using the Divergence Theorem. In the finite difference (FD) approximation, the leakage through a surface is equal to the product of the current across each surface and the magnitude of the corresponding surface element. The sum over all surfaces bounding the mesh cell yields the total leakage from the cell.

$$\int -\vec{\nabla}\bullet D_g\vec{\nabla}\phi_g\,dV=\int -\left(D_g\vec{\nabla}\phi_g\right)\bullet\vec{n}\,dS=\int\left(-D_g\frac{\partial\phi_g}{\partial\vec{n}}\right)dS=\sum_j J_{kj}\Delta S_{kj} \qquad \textbf{(A3)}$$

The neutron balance equation for mesh cell k bordered by J mesh cells can thus be expressed as

$$\sum_{j=1}^{J}J_{kj}\Delta S_{kj}+\Sigma_{r,k}\phi_k\Delta V_k=Q_k\Delta V_k \qquad \textbf{(A4)}$$

Define a dimensionless (except for the azimuthal direction) diffusion coefficient as

$$d_{x,k} \equiv \frac{D_k}{\Delta_{x,k}} \qquad \textbf{(A5)}$$

Assuming that one direction is considered at a time then spatial index subscript is dropped, and define the following:

$$\phi_{kj} \equiv \frac{d_k\phi_k + d_j\phi_j}{d_k + d_j}$$: flux at surface between cells j and k, **(A6)**

$$d_{kj} \equiv \frac{2d_k d_j}{d_k + d_j}$$: mean dimensionless diffusion coefficient at boundary, **(A7)**

$$J_{kj} \cong d_{kj}\left(\phi_k - \phi_j\right)$$: approximate current across boundary (R-Z or X-Z). **(A8)**

For the azimuthal direction in cylindrical coordinates, the current is given by

$$J_{kj} \cong \frac{2d_{kj}\left(\phi_k - \phi_j\right)}{r_i + r_{i+1}}$$: approximate current across boundary **(A9)**

in which *k* and *j* denote the azimuthal mesh point of the cell and its azimuthal neighbor and *i* denotes the radial mesh point of the cell.

For non-azimuthal systems, Equation (A4) can be expressed as

$$\sum_{j=1}^{J} \Delta S_{kj} d_{kj}\left(\phi_k - \phi_j\right) + \Sigma_{r,k}\phi_k \Delta V_k = Q_k \Delta V_k \qquad \textbf{(A10)}$$

This expression can be expanded to include the azimuthal current contributions if those terms include the appropriate radius in the denominator ($J_\theta = -D\frac{1}{r}\frac{\partial\phi}{\partial\theta}$).

The source term Q has contributions from fission and in-scattering.

$$Q_k = \sum_{g' \neq g} \Sigma_{s,g' \to g,k} \phi_{g',k} + \chi_g \sum_{g'} \nu_{g'} \Sigma_{f,g',k} \phi_{g',k} \qquad \textbf{(A11)}$$

Surface and Volume Elements

In the one or two-dimensional solvers, the delta term(s) representing the mesh intervals along the un-modeled dimension(s) appear in every term in Equation (A4). The effective volume and surface elements in these 'reduced' geometries are thus computed from the non-redundant terms only. The expressions for the effective mesh cell surface areas (ΔS) and volume (ΔV) in the 1D, 2D, and 3D are as follows (the 3D terms are not reduced):

Cartesian	**Volume Element**	**Surface Elements**	
1D:	$\Delta V = \Delta x_i$, Δy_j, or Δz_k	$\Delta S = 1$	
2D:	y-z: $\Delta V = \Delta y_j \Delta z_k$	$\hat{y} \bullet dS = \Delta z_k$	$\hat{z} \bullet dS = \Delta y_j$
	x-z: $\Delta V = \Delta x_i \Delta z_k$	$\hat{x} \bullet dS = \Delta z_k$	$\hat{z} \bullet dS = \Delta x_i$
	x-y: $\Delta V = \Delta x_i \Delta y_j$	$\hat{x} \bullet dS = \Delta y_j$	$\hat{y} \bullet dS = \Delta x_i$
3D:	$\Delta V = \Delta x_i \Delta y_j \Delta z_k$	$\hat{x} \bullet dS = \Delta x_i \Delta y_y$	
		$\hat{y} \bullet dS = \Delta x_i \Delta z_k$	
		$\hat{z} \bullet dS = \Delta x_i \Delta y_j$	

Cylindrical	**Volume Element**	**Surface Elements**
1D:	r: $dV = 0.5(r_i + r_{i+1}) \Delta r_i$	$dS_i = r_i$
	θ: $dV = r_1 \Delta \theta_j$	$dS_j = 1$
	z: $dV = \Delta z_k$	$dS_k = 1$

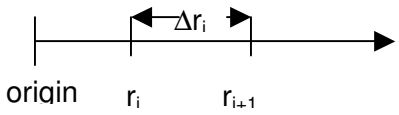

2D:	r-z: $dV = 0.5(r_i + r_{i+1})\,\Delta r_i \Delta z_k$	$\hat{r} \bullet dS = r_i \Delta z_k$
		$\hat{z} \bullet d\vec{S} = 0.5(r_i + r_{i+1})\Delta r_i$
	r-θ: $dV = 0.5(r_i + r_{i+1})\,\Delta r_i\ \Delta\theta_j$	$\hat{r} \bullet d\vec{S} = r_i \Delta\theta_j$
		$\hat{\theta} \bullet dS = 0.5(r_i + r_{i+1})\Delta r_i$
3D:	$dV = 0.5(r_i + r_{i+1})\,\Delta r_i\ \Delta\theta_j \Delta z_k$	$\hat{r} \bullet d\vec{S} = r_i \Delta\theta_j \Delta z_k$
		$\hat{\theta} \bullet d\vec{S} = \Delta r_i \Delta z_k$
		$\hat{z} \bullet d\vec{S} = 0.5(r_i + r_{i+1})\Delta\theta_j \Delta r_i$

Boundary Conditions

Stamm'ler and Abbate [76] provide a straightforward treatment of boundary conditions for cartesian and *rz* geometries. The partial currents across a boundary can be expressed as:

$$j^{\pm} = \frac{\phi}{4} \pm \frac{J}{2} \qquad \textbf{(A12)}$$

The positive and negative partial currents are related by the albedo, α, according to

$$j^{-} = \alpha j^{+} + j^{ext} \qquad \textbf{(A13)}$$

in which j^{ext} is an arbitrary external current. Substituting (A13) into (A12) and solving for J yields

$$J = \frac{1}{2}\phi\left(\frac{1-\alpha}{1+\alpha}\right) - \frac{2j^{ext}}{1+\alpha} \qquad \textbf{(A14)}$$

Assume a fictitious 'reflector' mesh cell *r* opposite the actual boundary mesh *k* and apply

$$J_{kr} = d_{kr}(\phi_k - \phi_r) = \frac{2d_k d_r}{d_k + d_r}\phi_k - \frac{2d_k d_r}{d_k + d_r}\phi_r \qquad \textbf{(A15)}$$

In this notation, the subscript *k* is generic; it can be applied to any dimension. Substitute (A6) into (A14) to get another expression for the current at the boundary.

$$\begin{aligned} J &= \frac{1}{2}\phi_{kr}\left(\frac{1-\alpha}{1+\alpha}\right) - \frac{2j^{ext}}{1+\alpha} \\ &= \frac{1}{2}\left(\frac{1-\alpha}{1+\alpha}\right)\frac{d_k\phi_k}{d_k + d_r} + \frac{1}{2}\left(\frac{1-\alpha}{1+\alpha}\right)\left[\frac{d_r\phi_r}{d_k + d_r} - \frac{4j^{ext}}{1-\alpha}\right] \end{aligned} \qquad \textbf{(A16)}$$

Equate flux terms in (A15) and (A16) to get the following expressions for the dimensionless diffusion coefficient and flux for the reflector mesh cell.

$$d_r = \frac{1}{4}\left(\frac{1-\alpha}{1+\alpha}\right) \qquad \textbf{(A17)}$$

$$\phi_{\mathrm{r}} = \frac{4j^{ext}}{1-\alpha} \qquad \textbf{(A18)}$$

Assuming that the external current is zero, the second term in (A15) vanishes. The first term yields the current, which can be expressed in terms of the boundary cell flux and albedo.

$$J_{kr} = \frac{2d_k\left(\frac{1}{4}\left(\frac{1-\alpha}{1+\alpha}\right)\right)}{d_k + \frac{1}{4}\left(\frac{1-\alpha}{1+\alpha}\right)}\phi_k$$

$$= \frac{2d_k d_r}{d_k + d_r}\phi_k \qquad \text{if} \quad d_r = \frac{1}{4}\left(\frac{1-\alpha}{1+\alpha}\right) \qquad \textbf{(A19)}$$

For azimuthal geometries, a 'wrap-around' condition is assumed, i.e. the inner and outer azimuthal mesh points are coincident.

Coefficient Matrix (Coupling coefficients)

From Equation (A6) one can determine the coupling coefficients that relate the flux in a mesh cell with that of its neighbors and the source term. $A_{i,j,k}$ is the diagonal term. The axial cell neighbors (k-1 and k+1) are not shown in this 2D representation. The k in the following expressions specifically denotes the axial mesh index.

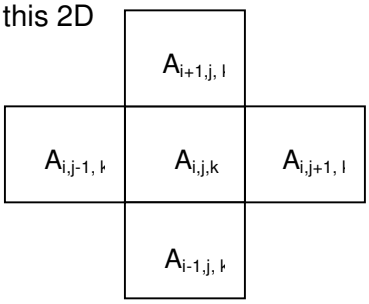

$$\begin{aligned} &A_{i,j,k}\phi_{i,j,k} + A_{i,j,k-1}\phi_{i,j,k} + A_{i,j,k+1}\phi_{i,j,k+1} \\ &+ A_{i,j-1,k}\phi_{i,j-1,k} + A_{i,j+1,k}\phi_{i,j+1,k} \\ &+ A_{i-1,j,k}\phi_{i-1,j,k} + A_{i+1,j,k}\phi_{i+1,j,k} = Q_{i,j,k}\Delta V_{i,j,k} \end{aligned} \qquad \text{(A20)}$$

Non-boundary mesh cell coupling coefficients are given by

$$A_{i,j,k} = \Sigma_{r,i,j,k}\Delta V_{i,j,k} + d_{i,i-1}\Delta S_{i,i-1} + d_{i,i+1}\Delta S_{i,i+1} + \frac{2d_{j,j-1}\Delta S_{j,j-1}}{r_i + r_{i+1}} + \ldots$$

$$\ldots + \frac{2d_{j,j+1}\Delta S_{j,j+1}}{r_i + r_{i+1}} + d_{k,k-1}\Delta S_{k,k-1} + d_{k,k+1}\Delta S_{k,k+1}$$

$$A_{i-1,j,k} = -d_{i,i-1}\Delta S_{i,i-1}$$

$$A_{i+1,j,k} = -d_{i,i+1}\Delta S_{i,i+1}$$

$$A_{i,j-1,k} = \frac{-d_{j,j-1}\Delta S_{j,j-1}}{0.5(r_i + r_{i-1})}$$

$$A_{i,j+1,k} = \frac{-d_{j,j+1}\Delta S_{j,j+1}}{0.5(r_i + r_{i+1})}$$

$$A_{i,j,k-1} = -d_{k,k-1}\Delta S_{k,k-1}$$

$$A_{i,j,k+1} = -d_{k,k+1}\Delta S_{k,k+1}$$

(A21 a-g)

For non-azimuthal boundary cells, one of the off-diagonal coefficients vanishes and the diagonal coefficient includes an albedo term, d_r, as defined in (A19). The following expressions are for the axial dimension. Identical expressions hold for the radial dimension and the y-dimension in XYZ geometry.

Coupling coefficients for inner and outer axial boundary mesh cells

$$A_{i,j,k-1} = 0$$

$$A_{i,j,k+1} = -d_{k,k+1}\Delta S_{k,k+1}$$

$$A_{i,j,k} = \Sigma_{r,i,jk}\Delta V_k + d_{k,k+1}\Delta S_{k,k+1} + \Delta S_{k,k-1}\frac{2d_k d_r}{d_k + d_r}$$

(A22)

(inner)

$$A_{i,j,k-1} = -d_{k,k-1}\Delta S_{k,k-1}$$

$$A_{i,j,k+1} = 0$$

$$A_{i,j,k} = \Sigma_{r,i,j,k}\Delta V_{i,j,k} + d_{k,k-1}\Delta S_{k,k-1} + \Delta S_{k,k+1}\frac{2d_k d_r}{d_k + d_r} \quad \textbf{(A23)}$$

(outer)

For three-dimensional cylindrical systems, an inner radial boundary condition may not be specified. The geometry of the system is altered by merging the azimuthal cells at $i = 1$ (inner radial) into one fully-cylindrical node. The neutron balance in this node is the sum of the leakage terms from the J nodes at $i = 2$ and the neighboring axial nodes and the removal and source terms:

$$\sum_{j=1}^{J} d_{1,j}\Delta S_{1,j}\left(\phi_{1,k} - \phi_{1,j,k}\right) + d_{k,k-1}\Delta S_{k,k-1}\left(\phi_{1,k-1} - \phi_{1,k}\right) + d_{k,k+1}\Delta S_{k,k+1}\left(\phi_{1,k+1} - \phi_{1,k}\right) + \ldots$$
$$\ldots + \Sigma_{r,1,k}\phi_{1,k}\Delta V_{1,k} = Q_{1,k}\Delta V_{1,k} \quad \textbf{(A24)}$$

The central cell is not subdivided azimuthally so the j subscript is dropped from the variables assigned to that cell. The matrix equation for the inner cells is thus given by

$$A_{1,k}\phi_{1,k} + A_{1,k-1}\phi_{1,k-1} + A_{1,k+1}\phi_{i,k+1} + \sum_{j=1}^{J} A_{2,j,k}\phi_{2,j,k} = Q_{1,k}\Delta V_{1,k} \quad \textbf{(A25)}$$

The neighbor cell coupling coefficients are defined as in Equation 18 (without the j subscript) or Equations A22 and A23 for the axial boundary cells. However, the central cell coupling coefficient, $A_{1,k}$, for this cell is given by

$$A_{1,k} = \sum_{j=1}^{J}\Delta S_{1,j}d_{1,j} + \Delta S_{k,k+1}d_{k,k+1} + \Delta S_{k,k-1}d_{k,k-1} + \Sigma_{r,1,k}\Delta V_{1,k} \quad \textbf{(A26)}$$

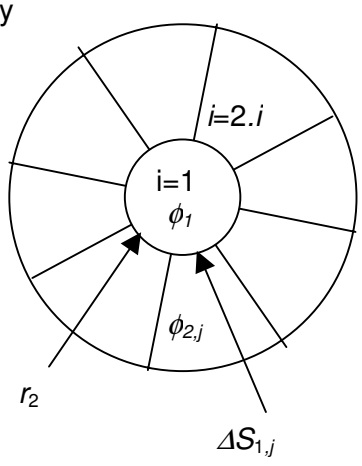

One can maintain the standard matrix structure by accepting a degeneracy in the azimuthal nodes (*j*) of the inner radial node (*i* = 1). The banded matrixOne must also be careful not to count more than one of these nodes in the fission power and power normalization calculations if the volume of the cell is πr_2^2.

The resulting coefficient matrix is banded with 3, 5, or 7 adjacent bands depending on the number of dimensions modeled. If the azimuthal direction is among them, there will also be off-diagonal terms coupling the 1st and last nodes in the θ–direction. Finally, for *R*-θ-*Z* systems, the *i* = 1 rows will include contributions from all *i* = 2 terms for a given axial node *k* to account for the geometry illustrated at the right.

The system of N equations for each dimension is solved iteratively using Successive Over-relaxation (SOR) acceleration of the flux according to

$$\phi_{i,j,k}^{m+1} = \frac{\omega}{A_{i,j,k}}\left[Q_{i,j,k}\Delta V_{i,j,k} - \sum_{n=1}^{n\,\dim} A_{d_n,d_n-1}\phi_{d_n-1}^{m+1} - \sum_{n=1}^{n\,\dim} A_{d_n,d_n+1}\phi_{d_n+1}^{m}\right] + (1-\omega)\phi_{i,j,k}^{m} \qquad \textbf{(A27)}$$

in which *m* represents the current iterate and d_n is the dimension (*r*,θ, or *z*). The acceleration parameter, ω, is found by trial and error. Starting with an initial flux guess (unity or solution from previous source iteration), Equation (A27) is solved twice for all mesh cells: a forward sweep followed by a backward sweep, until the maximum difference between successive flux values differs by less than the user-specified tolerance. This is the inner or flux iteration.

Once the flux has converged for a given source term, the integrated source term is re-computed according to

$$\int_V Q dV =$$

$$= \sum_{i=1}^{I} \sum_{j=1}^{J} \sum_{k=1}^{K} \left[\sum_{g' \neq g} \Sigma_{s,g' \to g,i,j,k} \phi_{g',i,j,k} + \frac{1}{\lambda} \chi_g \sum_{g'} \nu_{g'} \Sigma_{f,g',i,j,k} \phi_{g',i,j,k} \right] \quad \textbf{(A28)}$$

or, in operator notation

$$\int_V Q dV = \underline{\underline{F}} \underline{\phi} \quad \textbf{(A29)}$$

in which *F* is the source term operator (all groups and meshes). The new eigenvalue,λ, is computed from

$$\lambda^{n+1} = \lambda^n \frac{\left\langle \underline{\underline{F}} \underline{\phi}^{n+1}, \underline{\underline{F}} \underline{\phi}^{n+1} \right\rangle}{\left\langle \underline{\underline{F}} \underline{\phi}^{n}, \underline{\underline{F}} \underline{\phi}^{n+1} \right\rangle} \quad \textbf{(A30)}$$

This last calculation is repeated (outer loop) until the eigenvalue convergence criterion is satisfied.

Finally, after the outer loop has converged, the fluxes for all groups are scaled by the same factor to yield the user-specified power level.

Appendix B

Solution to the Depletion Equations in PEBBED

Burnup and Nuclide Density

Equation **2.4** describes the *flow* or accumulation of burnup in a computational cell over time. Burnup accumulation, however, is a consequence of the fission process and thus is inherently tied to nuclide depletion as follows.

The burnup accrued by the fuel contained within the cell is the amount energy released by the atoms fissioned within the cell per unit of initial heavy metal. A number, call it *I*, of fissionable isotopes are likely to exist within the cell so the energy released is computed by summing over these,

$$B = \frac{1}{m_{ihm}} \sum_{i=1}^{I} \kappa_i \sigma_{f,i} \left(N_{i,f}(t) - N_{i,o} \right) \Phi \Delta V \quad , \qquad \textbf{(B1)}$$

in which

m_{ihm} = the initial mass of heavy metal in the cell,

κ_I = energy released during the fission of an atom if isotope *I*

$\sigma_{f,I}$ = fission cross section of isotope *I,*

$N_{i,f}(t)$ = number density of isotope *i* in the cell after depletion

$N_{i,o}$ = number density of isotope *i* in the cell before depletion

Φ = mean fluence in the cell (assumed constant)

ΔV = volume of cell.

For an asymptotic core, the mean number density does not change with time but varies along the direction of pebble flow. Assuming that this flow is axial with speed

$v = dz/dt$, the final number density is the value at the downstream boundary of the cell and is a function of the height of the cell and the flow rate.

The rate of burnup accumulation is related to the rate of change of the number density of the fissionable isotopes:

$$\frac{\partial B}{\partial t} = \frac{1}{m_{ihm}} \frac{\partial}{\partial t} \left[\sum_{i=1}^{I} \kappa_i \sigma_{f,i} \left(N_{i,f}(t) - N_{i,o} \right) \Phi \Delta V \right] . \quad \textbf{(B2)}$$

Only the final number density varies so that

$$\frac{\partial B}{\partial t} = \frac{1}{m_{ihm}} \left[\sum_{i=1}^{I} \kappa_i \sigma_{f,i} \left(\frac{\partial \left(N_{i,f}(t) - N_{i,o} \right)}{\partial t} \right) \Phi \Delta V \right] . \quad \textbf{(B3)}$$

Thus, the rate of change of burnup can be computed from the rate of change of nuclide density. The nuclide density (depletion) equations form a system of first order linear differential equations the solution to which is described in the next section.

Simple Batch Decay

Nuclear Chemical Engineering [78] provides the derivation of the Batch decay equation for a system of isotopes. In the example used in the reference, Lead-211 decays to Lead-207 in three steps as follows.

$$^{211}_{82}Pb \xrightarrow{\beta^-} {}^{211}_{83}Bi \xrightarrow{\alpha} {}^{207}_{81}Tl \xrightarrow{\beta^-} {}^{207}_{82}Pb \quad \textbf{(B4)}$$

Lead-211 (Pb-211) is the chain precursor (1st nuclide in the chain) and its net rate of change is given by:

$$\frac{dN_1}{dt} = -\lambda_1 N_1 \quad \textbf{(B5)}$$

The rates of change of Bi-211, Tl-207, and stable Pb-207 are functions of the concentrations of their respective precursors:

(Bi211) $$\frac{dN_2}{dt} = \lambda_1 N_1 - \lambda_2 N_2 \quad \textbf{(B6)}$$

(Tl207) $$\frac{dN_3}{dt} = \lambda_2 N_2 - \lambda_3 N_3 \quad \textbf{(B7)}$$

(Pb207) $$\frac{dN_4}{dt} = \lambda_3 N_3 \quad \textbf{(B8)}$$

The solutions to these equations, subject to initial condition $N(t=0) = N^o$, are

$$N_1 = N_1^0 e^{\lambda_1 t} \quad \textbf{(B9)}$$

$$N_2 = \frac{\lambda_1}{\lambda_2 - \lambda_1} N_1^0 \left(e^{-\lambda_1 t} - e^{-\lambda_2 t} \right) \quad \textbf{(B10)}$$

$$N_3 = \lambda_2 \lambda_1 N_1^0 \left[\frac{e^{-\lambda_1 t}}{(\lambda_2 - \lambda_1)(\lambda_3 - \lambda_1)} + \frac{e^{-\lambda_2 t}}{(\lambda_1 - \lambda_2)(\lambda_3 - \lambda_2)} + \frac{e^{-\lambda_3 t}}{(\lambda_1 - \lambda_3)(\lambda_2 - \lambda_3)} \right] \quad \textbf{(B11)}$$

The amount of the last and stable member of the chain can be obtained from a material balance,

$$N_4 = N_1^0 \left(1 - e^{-\lambda_1 t} \right) - (N_2 + N_3) . \quad \textbf{(B12)}$$

The above formulation can be generalized to obtain an expression for the number density of the ith member of an arbitrary linear decay chain,

$$N_i = \lambda_{i-1} \ldots \lambda_2 \lambda_1 N_1^0 \sum_{j=1}^{i} \left[\frac{e^{-\lambda_j t}}{\prod_{\substack{k=1 \\ k \neq j}}^{i} (\lambda_k - \lambda_j)} \right] \quad (i > 1) . \quad \textbf{(B13)}$$

The above equation assumes zero initial concentration of chain members. Non-zero initial concentrations can be accommodated via superposition,

$$N_i = \sum_{l=1}^{i\text{-}1} \lambda_{i-1} \ldots \lambda_2 \lambda_1 N_1^0 \sum_{j=1}^{i} \left[\frac{e^{-\lambda_j t}}{\prod_{\substack{k=l \\ k \neq j}}^{i} (\lambda_k - \lambda_j)} \right] + N_i^0 e^{-\lambda_j t} \qquad \textbf{(B14)}$$

Batch Decay and Capture

This equation is only valid for simple radioactive decay. In the presence of a constant neutron flux ϕ, gain and loss of an isotope may also occur as a result of neutron capture. Fortunately, this formulation is easily generalized to account for both. First, define a *removal* rate constant, μ_i, for the *i*th isotope in the chain as

$$\mu_i = \lambda_i + \phi \sigma_i \quad . \qquad \text{(B15)}$$

Also define the *link* constant, ξ_i ,between the *i*th and *i+1*th isotope as

$$\xi_i = \begin{cases} \lambda_i & \text{if } i \text{ forms } i+1 \text{ by radioactive decay} \\ \phi \sigma_i & \text{if } i \text{ forms } i+1 \text{ by neutron capture} \end{cases}$$

Then it can be shown that Equation B14 becomes

$$N_i = \sum_{l=1}^{i\text{-}1} \xi_{i-1} \ldots \xi_2 \xi_1 N_1^0 \sum_{j=1}^{i} \left[\frac{e^{-\mu_j t}}{\prod_{\substack{k=l \\ k \neq j}}^{i} (\mu_k - \mu_j)} \right] + N_i^0 e^{-\mu_i t} \qquad \textbf{(B16)}$$

to account for the growth and decay of isotopes in the presence of a neutron flux.

Decay, Capture, and Fission

One must then account for the production of isotopes due to fission (the formation of fission products and their subsequent removal products).

Define a production rate, *P*, of a chain precursor directly formed from the splitting of *M* fissionable isotopes as

$$P \equiv \sum_{m=1}^{M} \gamma_m \sigma_m^f \phi \qquad \textbf{(B17)}$$

in which γ_m is the fission yield of fission product from the splitting of *m* and σ_m^f is the fission cross-section of isotope *m*. Then the change in number density $dN_i(t',t)$ of chain isotope *i* resulting from the decay of *Pdt'* atoms of the chain precursor during time interval *dt'* is given by

$$dN_i(t,t') = \xi_{i-1}\ldots\xi_2\xi_1 P dt' \sum_{j=1}^{i} \left[\frac{e^{-\mu_j (t-t')}}{\prod_{\substack{k=l \\ k\neq j}}^{i} (\mu_k - \mu_j)} \right] \qquad \textbf{(B18)}$$

Integrate the above over the interval (0,*dt'*) to obtain

$$N_i(t) = \xi_{i-1}\ldots\xi_2\xi_1 P dt' \sum_{j=1}^{i} \left[\frac{1-e^{-\mu_j t}}{\mu_j \prod_{\substack{k=l \\ k\neq j}} (\mu_k - \mu_j)} \right] \quad (i>1) \qquad \textbf{(B19)}$$

Finally, a given chain isotope itself may be formed by fission with a rate given by

$$P_j = \sum_{m=1}^{M} \gamma_{jm} \sigma_m^f \phi \qquad \textbf{(B20)}$$

so that the general expression for the production of isotopes in a chain due only to fission is given by

$$N_i = \sum_{l=1}^{i-1} \left\{ \xi_{i-1} \ldots \xi_2 \xi_1 P_l \sum_{j=1}^{i} \left[\frac{1 - e^{-\mu_j t}}{\mu_j \prod_{\substack{k=l \\ k \neq j}}^{i} (\mu_k - \mu_j)} \right] \right\} + P_i \frac{e^{-\mu_i t}}{\mu_i} \qquad \textbf{(B21)}$$

This equation assumes zero initial nuclide densities ($N_i^o = 0$ for all i). The production of isotopes due to fission is independent of the production of isotopes due to decay or capture and therefore these processes can be superimposed. The complete expression for the number of isotopes formed from decay, neutron capture, and fission is the sum of Equations B16 and B21,

$$N_i = \underbrace{\sum_{l=1}^{i-1} \left\{ \xi_{i-1} \ldots \xi_2 \xi_1 P_l \sum_{j=1}^{i} \left[\frac{1 - e^{-\mu_j t}}{\mu_j \prod_{\substack{k=l \\ k \neq j}}^{i} (\mu_k - \mu_j)} \right] \right\} + P_i \frac{e^{-\mu_i t}}{\mu_i} + \ldots}_{\textit{Fission product contribution}}$$

$$\underbrace{\ldots + \sum_{l=1}^{i-1} \xi_{i-1} \ldots \xi_2 \xi_1 N_1^0 \sum_{j=1}^{i} \left[\frac{e^{-\mu_j t}}{\prod_{\substack{k=l \\ k \neq j}}^{i} (\mu_k - \mu_j)} \right]}_{\textit{Batch decay/capture contribution}} + N_i^0 e^{-\mu_i t} \qquad \textbf{(B22)}$$

Linearization of Chains

This formulation is valid for properly linearized chains. An example of the linearization of chains is given here.

Thorium-232 is a fertile isotope that is converted to fissile uranium-233 via Protactinium-233. U-233 fissions but also may capture a neutron and convert to U-234

and then again to U-235. U-234 may also be formed by the neutron capture from Pa-233. The split and merged chain can be presented in the following diagram:

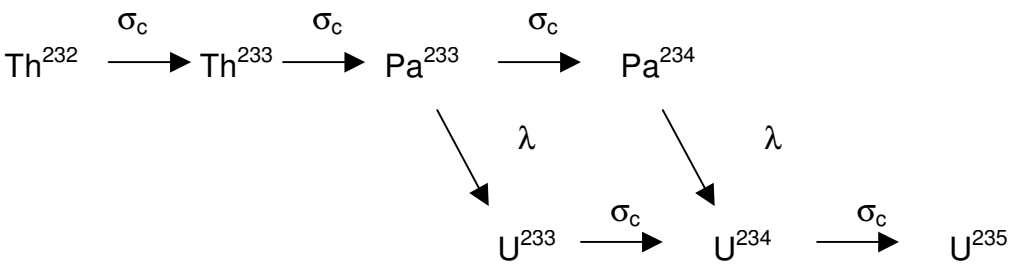

To be amenable to the depletion formulation derived above, it must be split into two linear chains with a few common members, namely,

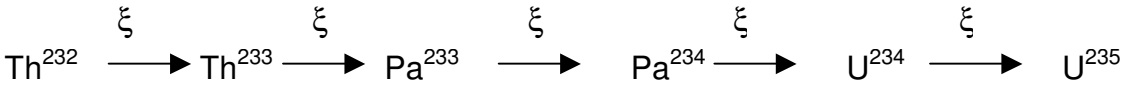

and

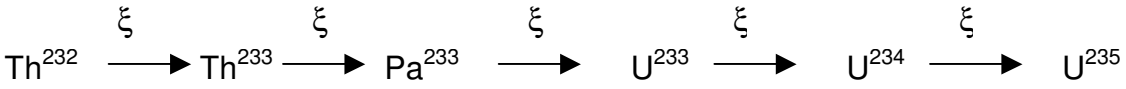

The production of U-234 and U-235 is the sum of the contributions from the two chains. In PEBBED, individual chains are identified by their precursor isotopes but a given chain may have multiple branches to accommodate situations as described above.

Time Intervals in PEBBED

In PEBBED, the time interval over which a depletion occurs is computed directly from the channel axial velocity, v_i, and the axial mesh width Δ_k,

$$t = \frac{\Delta_k}{v_i} \qquad \textbf{(B23)}$$

in which *k* is the index counting the axial mesh intervals and *i* is the index counting the radial mesh intervals. Pebbles flow downward, so the initial nuclide densities are those at the upper boundary of a mesh cell.

In the current version of PEBBED, the spatial mesh over which the diffusion theory is solved is also the same as that over which the depletion equations are solved. This allows for direct coupling of the flux profile to the depletion mesh. Also, the small mesh size required for accurate diffusion theory results also means that the constant flux assumption used in the depletion equations is reasonably valid.

(A nodal approach to the solution of the diffusion equation is being developed for PEBBED and would allow much larger mesh intervals. The depletion formulation will have to be generalized to incorporate a spatially varying flux.)

Round-off Error

Implementation of this depletion formulation on a digital computer introduces the possibility of significant error in long chains. The decay and fission production terms in Equation B19 both contain summations of exponential functions with alternating positive and negative coefficients. Each term in the sum is the contribution from a predecessor of the nuclide in question. The farther back in the nuclide's lineage, the less of a contribution will be made by a predecessor. Yet the coefficient of the exponential term may not be small so that small precision errors in the density may result in very large errors in the final result. The remedy proposed by England and described in Stamm'ler and Abbate is commonly used. It requires the evaluation of the following inequality,

$$\sum_{j=l}^{i} c_{jl}^{i} e^{-\mu_i t} < \left(\max_{j=l \to i} \left| c_{jl}^{i} e^{-\mu_i t} \right| \right) \cdot 10^{-N} \quad . \qquad \textbf{(B24)}$$

in which

$$c_{jl}^{i} = \frac{\prod_{k=l}^{i} \xi_k}{\prod_{\substack{k=l \\ k \neq j}}^{i} \left(\mu_k - \mu_j\right)} \quad . \tag{B25}$$

and *N* is the maximum number of significant digits stored in computer memory. This expression evaluated for each branch in a chain. Contributions from decay/capture predecessors for which the inequality holds true are discarded. For the fission yield term, the following inequality is evaluated with the same consequence,

$$\beta_l^i - \sum_{j=l}^{i} \frac{c_{jl}^{i}}{\mu_j} e^{-\mu_i t} < \left(\max_{j=l \to i} \left| \beta_l^i - \frac{c_{jl}^{i}}{\mu_j} e^{-\mu_i t} \right| \right) \cdot 10^{-N} \tag{B26}$$

in which

$$\beta_l^i = \frac{\prod_{k=l}^{i} \xi_k}{\prod_{k=l}^{i} \mu_k} \tag{B27}$$

.

Appendix C

Transient, Non-Convective Radial Heat Transfer in PEBBED

One-Dimensional Radial Conductive Heat Transport

The one-dimensional, transient conduction in cylindrical coordinates can be expressed as

$$\rho(T)C_p(T)\frac{\partial T(r,t))}{\partial t} = \nabla \bullet k(T)\nabla T(r,t) + q(r,t) = \frac{1}{r}\frac{\partial}{\partial r}\left(k(T)r\frac{\partial T(r,t)}{\partial r} \right) + q(r,t) \quad \text{(C1)}$$

This equation is solved using a standard finite-difference approach described here. The approach is loosely based upon that used in the SHERLOC code [83] but there are a few key differences. SHERLOC uses a mesh-centered control volume while PEBBED uses a boundary-centered approach. SHERLOC assumes constant mesh width while PEBBED allows variable mesh spacing. Being a stand-alone conduction-radiation code, the steady-state core power density must be supplied to SHERLOC. PEBBED computes its own.

Consider the discretization of the radial dimension in a pebble-bed reactor ($r = 0$ corresponds to the core centerline) with the left and right boundaries of cell i at distances r_i and r_{i+1} from the core centerline (Figure C-1).

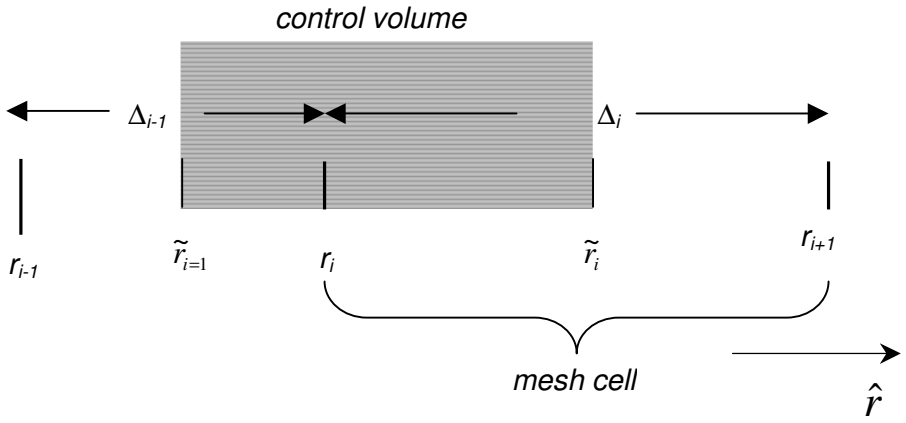

Figure **C-1**: Radial mesh interval in PEBBED transient calculation.

This is applied as follows to the control volume shown in the diagram with boundaries at $\tilde{r}_i$ and $\tilde{r}_{i-1}$. Assume that the material properties are constant across a cell but may change discontinuously at the cell boundaries. These material properties include:

cell heat generation rate (W/cm^3)	q_i
cell density (g/ cm^3)	ρ_i
cell specific heat (J/gC°)	C_i^p
cell thermal conductivity (W/cmC°)	k_i

Fourier's Law for the heat current across the boundaries yields

$$\frac{1}{r}\frac{\partial}{\partial r}\left(k(T)r\frac{\partial T(r,t)}{\partial r}\right) = k(T)A\frac{\partial T(r,t)}{\partial r}\bigg|_{\tilde{r}_{i-1}} + k(T)A\frac{\partial T(r,t)}{\partial r}\bigg|_{\tilde{r}_i} . \qquad \textbf{(C2)}$$

Denote the midpoint of cell *i* as

$$\tilde{r}_i \equiv \frac{r_i + r_{i+1}}{2} \qquad \textbf{(C3)}$$

and the mean temperature of the control volume as $\tilde{T}_i$.

The heat balance for the control volume becomes

$$\tilde{\rho}_i\left(\tilde{T}\right)\tilde{C}_i^p\left(\tilde{T}\right)\frac{\partial \tilde{T}_i(t))}{\partial t} = k_{i-1}A_{\tilde{r}_{i-1}}\left.\frac{\partial T(t)}{\partial r}\right|_{\tilde{r}_{i-1}} + k_i A_{\tilde{r}_i}\left.\frac{\partial T(t)}{\partial r}\right|_{\tilde{r}_i} + \tilde{q}_i(t) \quad . \tag{C4}$$

The control volume, illustrated by the shaded region in the figure, may be composed of two different materials and has a volume given by

$$\tilde{V}_i = h_i\pi\left(\tilde{r}_i^{\,2} - \tilde{r}_{i-1}^2\right) \tag{C5}$$

Assuming that the height of the cells are equal ($h_i = h$), one may compute the following thermal parameters for the control volume:

$$\tilde{q}_i \equiv \frac{q_{i-1}\tilde{r}_{i-1}\Delta_{i-1} + q_i\tilde{r}_i\Delta_i}{\tilde{r}_{i-1}\Delta_{i-1} + \tilde{r}_i\Delta_i} \tag{C6}$$

volume-averaged volumetric specific heat (J/cm^{3}C^o)

$$\tilde{C}_i \equiv \frac{\rho_{i-1}C_{i-1}^p\tilde{r}_{i-1}\Delta_{i-1} + \rho_i C_i^p\tilde{r}_i\Delta_i}{\tilde{r}_{i-1}\Delta_{i-1} + \tilde{r}_i\Delta_i} \tag{C7}$$

volume-averaged heat generation rate (W/cm^3)

The change in the quantity of thermal energy in the control volume is the sum of the heat generated within the volume and the flow of heat into the volume across the boundaries.

$$\frac{d\tilde{Q}_i}{dt} = \tilde{C}_i\frac{dT_i}{dt} = \tilde{q}_i\tilde{V}_i + \tilde{A}_{i-1}k_{i-1}\left.\frac{d\tilde{T}}{dr}\right|_{r=\tilde{r}_{i-1}} - \tilde{A}_i k_i\left.\frac{d\tilde{T}}{dr}\right|_{r=\tilde{r}_i} \tag{C8}$$

in which T_i is the temperature at r_i that is assumed to be equal to the average temperature of the control volume and the cross-sectional area of the heat transfer surface at the boundary is defined as

$$\tilde{A}_i = 2\pi\tilde{r}_i h \quad . \tag{C9}$$

A difference equation is used to approximate the derivative of the temperature at the cell boundaries,

$$\frac{d\tilde{T}_i}{dt} \cong \frac{T_{i+1} - T_i}{\Delta_i} \quad , \tag{C10}$$

and this leads to an approximation of the time derivative,

$$\frac{d\tilde{Q}_i}{dt} \cong \tilde{q}_i \tilde{V}_i + \tilde{A}_{i-1} k_{i-1} \frac{\tilde{T}_{i-1} - \tilde{T}_i}{\Delta_{i-1}} + \tilde{A}_i k_i \frac{\tilde{T}_{i+1} - \tilde{T}_i}{\Delta_i} \quad . \tag{C11}$$

Substituting in the expressions for the control volume and surface areas yields

$$\frac{d\tilde{Q}_i}{dt} \cong \tilde{q}_i h\pi\left(\tilde{r}_i^2 - \tilde{r}_{i-1}^2\right) + h2\pi\tilde{r}_{i-1} k_{i-1} \frac{\tilde{T}_{i-1} - \tilde{T}_i}{\Delta_{i-1}} + h2\pi\tilde{r}_i k_i \frac{\tilde{T}_{i+1} - \tilde{T}_i}{\Delta_i} \quad . \tag{C12}$$

To discretize the time variable, a superscript is introduced to denote the temperature and other thermal properties at a specific time step *n*, and the forward-difference approximation is applied to yield

$$\frac{d\tilde{Q}_i^n}{dt} \cong \frac{\tilde{Q}_i^{n+1} - \tilde{Q}_i^n}{t^{n+1} - t^n} = \frac{\tilde{C}_i \tilde{V}_i \left(T_i^{n+1} - T_i^n\right)}{t^{n+1} - t^n} = \frac{\tilde{C}_i h\pi\left(\tilde{r}^2{}_i - \tilde{r}_{i-1}{}^2\right)\left(T_i^{n+1} - T_i^n\right)}{t^{n+1} - t^n} \quad . \tag{C13}$$

Substituting this expression into Equation C13 and dropping the common $h\pi$ term yields the difference equation for transient radial conduction in the control volume, assuming constant material properties and heat generation:

$$\frac{\tilde{C}_i\left(\tilde{r}_i^2 - \tilde{r}_{i-1}^2\right)\left(T_i^{n+1} - T_i^n\right)}{t^{n+1} - t^n} = \tilde{q}_i\left(\tilde{r}_i^2 - \tilde{r}_{i-1}^2\right) + 2\tilde{r}_{i-1} k_{i-1} \frac{\tilde{T}_{i-1} - \tilde{T}_i}{\Delta_{i-1}} + 2\tilde{r}_i k_i \frac{\tilde{T}_{i+1} - \tilde{T}_i}{\Delta_i} \tag{C14}$$

In fact, for the types of problems to which this equation is applied, the heat generation rate is a function of time, following a decay heat curve. The material properties change as well because they are often temperature-dependent and the temperature changes over time. A *theta-differencing* technique is thus used to accommodate variations in the parameters. Define an intermediate temperature

$$T_i^\theta \equiv \theta T_i^{n+1} + (1-\theta) T_i^n \qquad 0 \le \theta \le 1 \tag{C15}$$

as a weighted average of the temperatures at successive time steps. The material properties are then evaluated at this time step. Of course, T_i^{n+1}, is the quantity to be computed in a transient calculation and is thus not known in advance. A solution scheme is employed that starts by assuming that $T_i^{n+1} = T_i^n$ and iterating to convergence.

In the theta-differencing algorithm, the finite difference formulation in Equation C14 is generalized to

$$\frac{\tilde{C}_i^{n+\theta}\left(\tilde{r}_i^2 - \tilde{r}_{i-1}^2\right)\left(T_i^{n+1} - T_i^n\right)}{t^{n+1} - t^n} = \tilde{q}_i\left(\tilde{r}_i^2 - \tilde{r}_{i-1}^2\right) + \theta\left[\frac{2\tilde{r}_{i-1}k_{i-1}^{n+\theta}}{\Delta_{i-1}}\left(\tilde{T}_{i-1}^{n+1} - \tilde{T}_i^{n+1}\right) + \frac{2\tilde{r}_i k_i^{n+\theta}}{\Delta_i}\left(\tilde{T}_{i+1}^{n+1} - \tilde{T}_i^{n+1}\right)\right] + \ldots$$
$$\ldots + \quad (1-\theta)\left[\frac{2\tilde{r}_{i-1}k_{i-1}^{n+\theta}}{\Delta_{i-1}}\left(\tilde{T}_{i-1}^{n} - \tilde{T}_i^{n}\right) + \frac{2\tilde{r}_i k_i^{n+\theta}}{\Delta_i}\left(\tilde{T}_{i+1}^{n} - \tilde{T}_i^{n}\right)\right] \qquad \textbf{(C16)}$$

To obtain a form that is readily implemented in a computer program, the (n+1) terms are moved to the left-hand-side,

$$\frac{\tilde{C}_i^{n+\theta}\left(\tilde{r}_i^2 - \tilde{r}_{i-1}^2\right)T_i^{n+1}}{t^{n+1} - t^n} - \theta\left[\frac{2\tilde{r}_{i-1}k_{i-1}^{n+\theta}}{\Delta_{i-1}}\left(\tilde{T}_{i-1}^{n+1} - \tilde{T}_i^{n+1}\right) + \frac{2\tilde{r}_i k_i^{n+\theta}}{\Delta_i}\left(\tilde{T}_{i+1}^{n+1} - \tilde{T}_i^{n+1}\right)\right] =$$
$$\frac{\tilde{C}_i^{n+\theta}\left(\tilde{r}_i^2 - \tilde{r}_{i-1}^2\right)T_i^{n}}{t^{n+1} - t^n} + \tilde{q}_i\left(\tilde{r}_i^2 - \tilde{r}_{i-1}^2\right) + \ldots$$
$$\ldots + (1-\theta)\left[\frac{2\tilde{r}_{i-1}k_{i-1}^{n+\theta}}{\Delta_{i-1}}\left(\tilde{T}_{i-1}^{n} - \tilde{T}_i^{n}\right) + \frac{2\tilde{r}_i k_i^{n+\theta}}{\Delta_i}\left(\tilde{T}_{i+1}^{n} - \tilde{T}_i^{n}\right)\right] \qquad \textbf{(C17)}$$

Define H_i as the quantity on the right-hand-side,

$$H_i \equiv \frac{\tilde{C}_i^{n+\theta}\left(\tilde{r}_i^2 - \tilde{r}_{i-1}^2\right)T_i^{n}}{t^{n+1} - t^n} + \tilde{q}_i\left(\tilde{r}_i^2 - \tilde{r}_{i-1}^2\right) + \ldots$$
$$\ldots + \quad (1-\theta)\left[\frac{2\tilde{r}_{i-1}k_{i-1}^{n+\theta}}{\Delta_{i-1}}\left(\tilde{T}_{i-1}^{n} - \tilde{T}_i^{n}\right) + \frac{2\tilde{r}_i k_i^{n+\theta}}{\Delta_i}\left(\tilde{T}_{i+1}^{n} - \tilde{T}_i^{n}\right)\right]. \qquad \textbf{(C18)}$$

On the left-hand-side of (C17), collect the $\tilde{T}_i^{n+1}$ terms,

$$\frac{\tilde{C}_i^{n+\theta}\left(\tilde{r}_i^2-\tilde{r}_{i-1}^2\right)T_i^{n+1}}{t^{n+1}-t^n}-\theta\left[\frac{2\tilde{r}_{i-1}k_{i-1}^{n+\theta}}{\Delta_{i-1}}\left(\tilde{T}_{i-1}^{n+1}-\tilde{T}_i^{n+1}\right)+\frac{2\tilde{r}_i k_i^{n+\theta}}{\Delta_i}\left(\tilde{T}_{i+1}^{n+1}-\tilde{T}_i^{n+1}\right)\right]=$$

$$\theta\left[\frac{2\tilde{r}_{i-1}k_{i-1}^{n+\theta}}{\Delta_{i-1}}+\frac{2\tilde{r}_i k_i^{n+\theta}}{\Delta_i}\right]\tilde{T}_i^{n+1}\ -\ \theta\left[\frac{2\tilde{r}_{i-1}k_{i-1}^{n+\theta}}{\Delta_{i-1}}\tilde{T}_{i-1}^{n+1}+\frac{2\tilde{r}_i k_i^{n+\theta}}{\Delta_i}\tilde{T}_{i+1}^{n+1}\right] \quad \textbf{(C19)}$$

and define

$$D_i\equiv\ \theta\left[\frac{2\tilde{r}_{i-1}k_{i-1}^{n+\theta}}{\Delta_{i-1}}+\frac{2\tilde{r}_i k_i^{n+\theta}}{\Delta_i}\right]+\frac{\tilde{C}_i^{n+6}\left(\tilde{r}_i^2-\tilde{r}_{i-1}^2\right)}{t^{n+1}-t^n} \quad \textbf{(C20)}$$

$$P_i\equiv\ \theta\left[\frac{2\tilde{r}_{i-1}k_{i-1}^{n+\theta}}{\Delta_{i-1}}\tilde{T}_{i-1}^{n+1}+\frac{2\tilde{r}_i k_i^{n+\theta}}{\Delta_i}\tilde{T}_{i+1}^{n+1}\right]\ . \quad \textbf{(C21)}$$

So one may write

$$\tilde{T}_i^{n+1}=\frac{H_i+P_i}{D_i}\ . \quad \textbf{(C22)}$$

Again, there is one unknown term, $\tilde{T}_{i+1}^{n+1}$, that must be assigned an assumed value and then updated until a convergence specification is met.

The value of θ is specified by the user. For $\theta = 0$, the material properties are evaluated at the starting point of the time interval and $\tilde{P}_i$ vanishes. There are no assumed values in this *fully explicit* algorithm so no iteration is required. However, it is not guaranteed to be stable for all time steps. For $\theta = 1$, the material properties are evaluated at the end point of the time interval. This fully implicit algorithm is stable for all time steps but one must iterate to obtain the solution. For $0.5 \le \theta < 1$, the *semi-implicit* solution scheme is also stable. The default value in PEBBED is 0.5.

The temperature-dependent material properties are provided in look-up tables and are updated after the algorithm has converged on the new temperature.

Initial Conditions

Before the transient calculation may begin, however, an initial temperature distribution must be computed. This is obtained from a steady-state solution to Equation C14, i.e.,

$$0 \cong \tilde{q}_i \tilde{V}_i + \tilde{A}_{i-1} k_{i-1} \frac{\tilde{T}_{i-1} - \tilde{T}_i}{\Delta_{i-1}} + \tilde{A}_i k_i \frac{\tilde{T}_{i+1} - \tilde{T}_i}{\Delta_i} \quad . \tag{C23}$$

The steady-state temperature distribution in the core is computed by PEBBED using an appropriate convective heat transfer correlation. Outside of the active core, one may assume that the heat generation rate in the mesh cells is zero so that

$$0 = \tilde{A}_{i-1} k_{i-1} \frac{\tilde{T}_{i-1} - \tilde{T}_i}{\Delta_{i-1}} + \tilde{A}_i k_i \frac{\tilde{T}_{i+1} - \tilde{T}_i}{\Delta_i} \quad . \tag{C24}$$

This is a simple system of linear equations easily solved with a standard matrix inversion routine. It requires known boundary conditions: the temperatures at the core-reflector interface and outer model boundary. The first is supplied by the steady-state core temperature calculation; the second is supplied by the user. Because the thermal conductivity is temperature-dependent, some iterations are required to obtain a consistent steady-state solution.

Material Properties

For thermal conductivity calculations, there are currently seven materials available for model construction: void, pebble-bed, graphite, stainless steel-304, 2.25Cr:1Mo steel, concrete, and carbon brick. Some of the material properties used in PEBBED were taken from reference [83] and incorporated as look-up tables. Some are illustrated here.

Concrete properties are assumed to be temperature-independent. The thermal conductivity for concrete is 0.9344 W/mC° and the specific heat is 837.3 J/kgC°.

Graphite

Graphite conductivity exhibits a strong dependence on temperature and fluence. A correlation developed at Oak Ridge [33] captures this dependence.

$$K_g(\Phi, T_\Phi) = RG_1(T_g) \tag{C25}$$

in which

K_g = graphite thermal conductivity (*W/cmK*)

Φ = fluence of irradiated graphite (n/cm^2)

T_Φ = temperature at which graphite was irradiated (K)

T_g = temperature of graphite (K)

and

$$R(T_g, T_\Phi) = \{1 + F(T_g, T_\Phi)G_1(T)[G_2(T_\Phi)G_4(T_g) + (1 - G_2(T_\Phi))G_3(T_g)]\}^{-1} \tag{C26}$$

$$F(T_g, T_\Phi) = \alpha(T_\Phi)8.8H(T_\Phi, T_g)\{1 - \exp(-\beta(T_\Phi)\cdot 10^{21}\Phi)\} \tag{C27}$$

$$\beta(T_\Phi) = 1.116 - 0.000269T_\Phi \qquad \beta \geq 0 \tag{C28}$$

$$H(T_{g,}T_\Phi) = [1 - 8.45\cdot 10^{-8}T_g(420 + 1.65T_g)]\alpha(T_\Phi) \tag{C29}$$

$$\alpha(T_\Phi) = 1.055 - 0.00057T_\Phi \qquad \alpha \geq 0 \tag{C30}$$

The temperature-dependent quantities, G_n, are obtained by linear interpolation from the data sets shown in Table C-1.

Table C-1: Temperature-dependent parameters in graphite conductivity correlation.

Temperature (*K*)	G_1	G_2	G_3	G_4
300	1.10	1.0	1.12	74.2
350	1.05	1.0	0.905	71.0
400	1.00	1.0	0.766	68.2
500	0.90	1.0	0.605	63.5
600	0.84	0.7	0.518	60.5
700	0.78	0.7	0.467	58.4
800	0.72	0.7	0.431	56.4
900	0.67	0.7	0.410	55.5
1,000	0.62	0.7	0.394	55.0
1,100	0.58	0.7	0.384	54.9
1,200	0.54	0.7	0.375	54.3
1,300	0.50	0.2	0.368	54.1
1,600	0.46	0.2	0.355	54.3

Figure C-2 illustrates the conductivity as a function of temperature and fluence. Assumed in this plot is that the graphite temperature is the same as the temperature at which the graphite was irradiated.

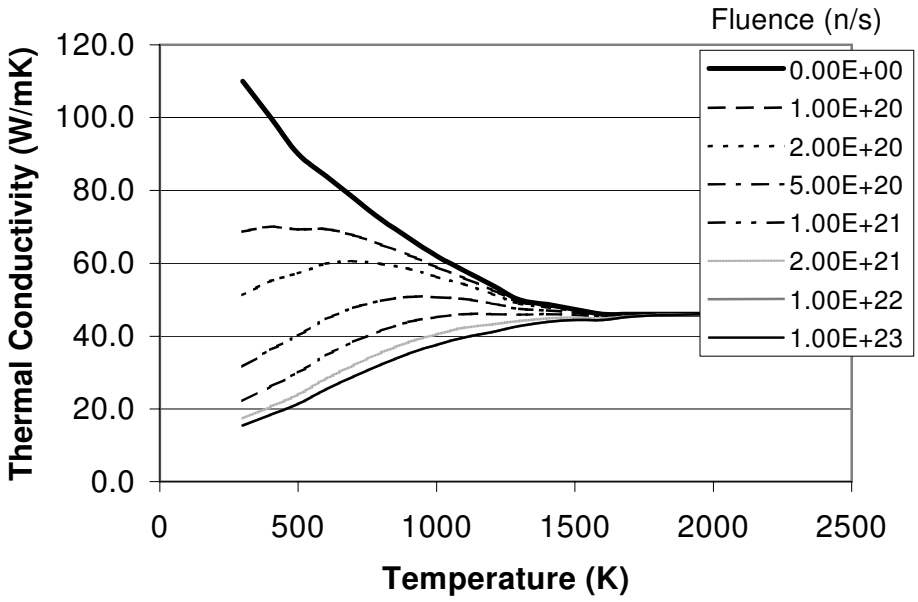

Figure C-2: Graphite thermal conductivity.

For the graphite in pebbles, the fluence and irradiation temperature are obtained from the pebble history computed by PEBBED. For reflector graphite, fluence and irradiation temperature are user-supplied quantities.

For most pebble designs, graphite makes up the bulk of the mass so that for the purpose of determining pebble temperature, the conductivity and specific heat are considered to be that of pure graphite. The user also has the option of specifying a fixed value for graphite conductivity in the fuel and graphite shell regions.

Because the core is not composed of solid graphite but of graphite sphere, an effective thermal conductivity is used which accounts for the contact between adjacent pebbles and the radiative heat transfer between them. Breitbach and Barthels proposed a modification to a model initially created by Zehner and Schlunder. The details are not provided here but are available from reference [83]. The modified Zehner-Schlunder model is given by:

$$K_{pb} = 4\sigma T^3 D_p \left\{ \left[1 - p^{0.5}\right](1-p) + \frac{p^{0.5}}{\frac{2}{\varepsilon} - 1}\left(\frac{B_z + 1}{B_z}\right)\left[1 + \frac{1}{\left(\frac{2}{\varepsilon} - 1\right)K_g}\right]^{-1} \right\} \qquad \textbf{(C31)}$$

in which

σ = the Stefan-Boltzmann constant =5.669x10-8 W/m^{2}K^4,

T = pebble temperature (K),

ε = emmissivity of graphite,

K_g = thermal conductivity of graphite (W/mK),

B_z = 1.25*(p/(1-p))$^{10/9}$

p = pebble bed packing fraction, and

D_p = pebble diameter (cm).

The specific heat of graphite is obtained by interpolation from the following plot.

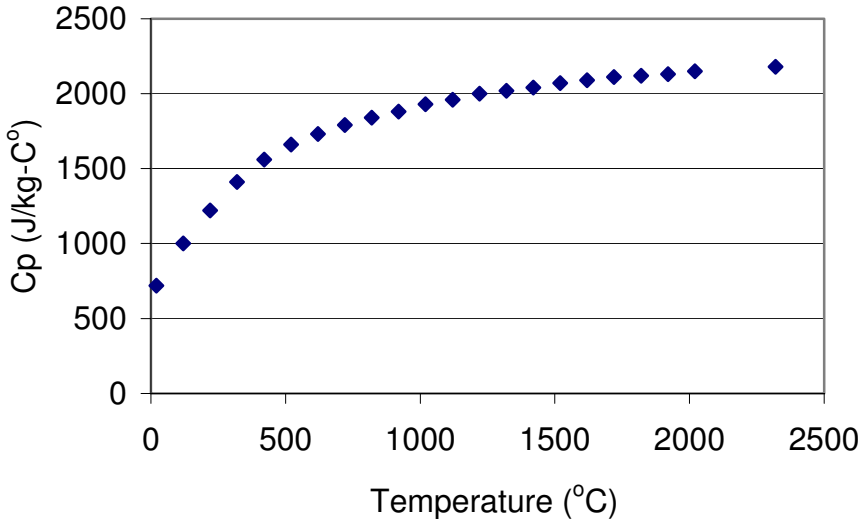

Figure **C-3**: Graphite specific heat.

Other Solids

Temperature-dependent thermal properties are also provided as lookup tables for stainless steel type 304 (SSTL-304) and 2.25 Chromium – 1 Molybdenum carbon steel (2.25Cr-1Mo Steel). Their properties are plotted below.

SSTL-304

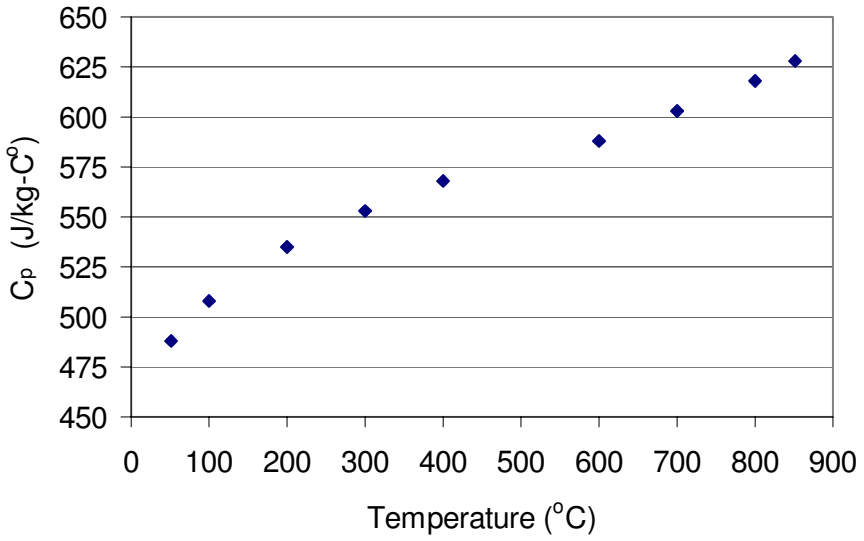

Figure **C-4**: SSTL-304 specific heat.

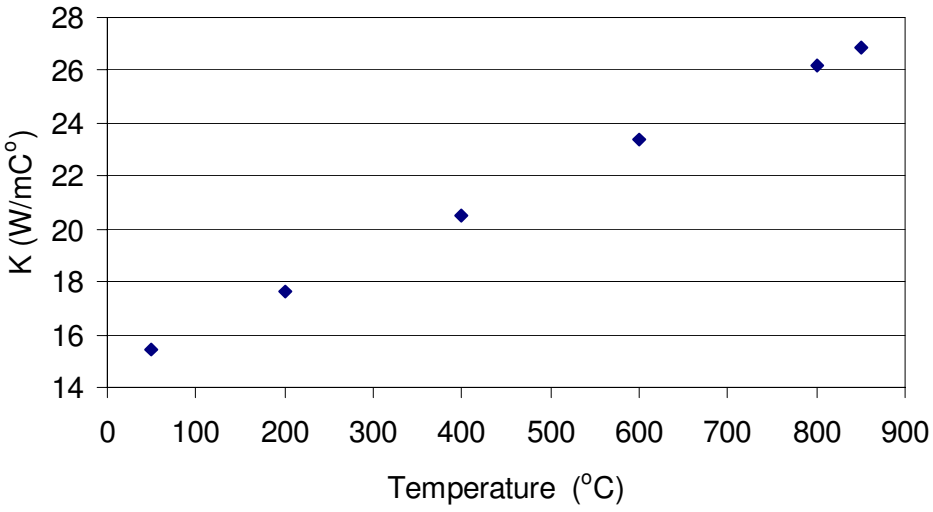

Figure **C-5**: SSTL-3-4 thermal conductivity.

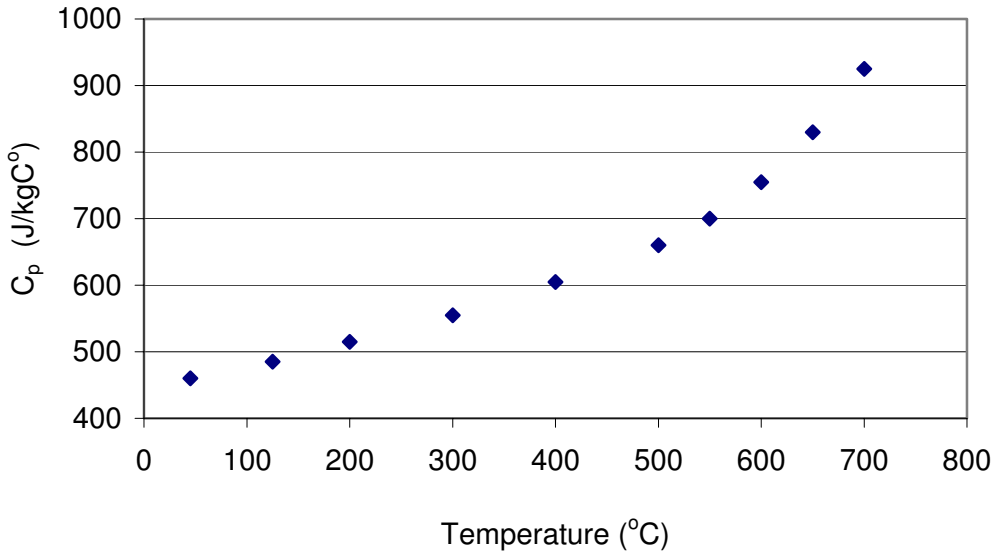

Figure C-6: 2.25Cr-1Mo specific heat.

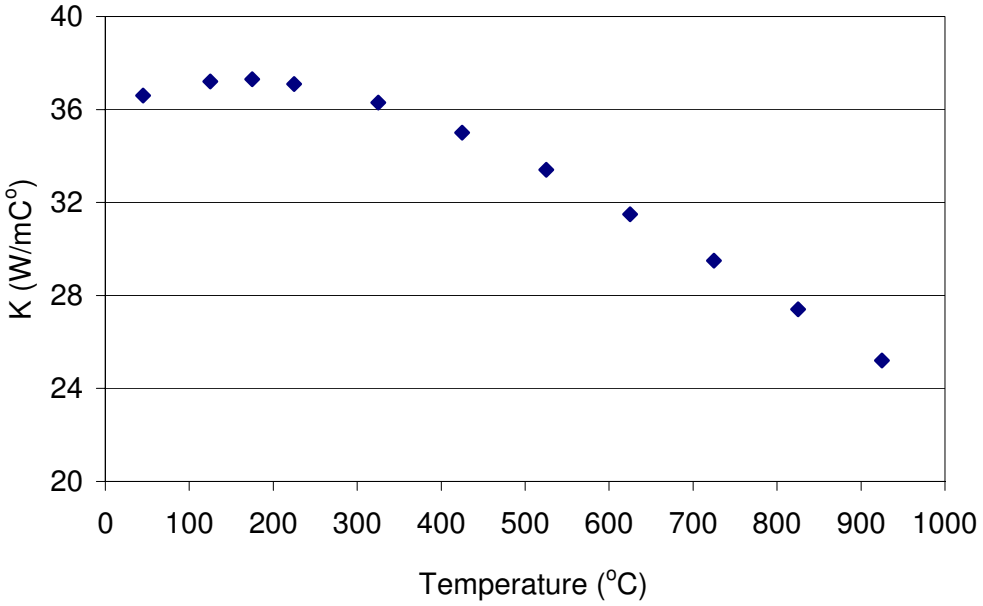

Figure C-7: 2.25Cr-1Mo thermal conductivity.

The remaining materials available in the PEBBED code have the properties shown in Table C-2.

Table C-2: Thermal properties of non-temperature dependent materials.

Material	Specific Heat, C_p, (J/kgK)	Thermal Conductivity, K, (W/mK)
Concrete	837.3	0.9344
Carbon Brick	709	6

Baked carbon brick is a graphite pre-product used for furnace insulation and other applications. Many early HTGR designs used carbon brick to line the outer radial surface of the outer graphite reflector. The low thermal conductivity inhibits radial heat transfer and decreases parasitic heat loss during normal operation, thereby improving cycle efficiency. Carbon brick is not used in today's modular HTGR cores *because* it inhibits radial heat transfer and thus increases peak fuel temperature during a depressurized conduction cooldown event.

The user has the option of specifying a substitute material into a region. The user-supplied constant density, specific heat, thermal conductivity, and emissivity are added on a special line in the input deck.

Gas Gaps

For gas channels such as exist between the core barrel and pressure vessel or pressure vessel and cavity cooling channels, heat transfer is assumed to occur by radiation and conduction through helium. For a sufficiently high temperature difference, the predominant heat transfer mechanism is radiation. An effective conductivity of a gas gap is the sum of the helium conduction contribution and radiation. The radiative heat transfer rate can be expressed in terms of a heat transfer coefficient as follows.

The heat flux between two surfaces at temperatures T_1 and T_2 is given by the thermal radiation law:

$$q''(T_1,T_2)=\sigma\varepsilon_{12}\left(T_1^4-T_2^4\right)=h_r\left(T_1-T_2\right) \tag{C32}$$

in which

ε_{12} = the effective emissivity between the surface,

σ= the Stefan-Boltzmann constant (defined above), and

h_r= radiation heat transfer coefficient across the gap (W/m^{2}K).

Solving the above for h_r, one obtains

$$\begin{aligned} h_r\left(T_1,T_2\right) &= \sigma\varepsilon_{12}\frac{\left(T_1^4-T_2^4\right)}{T_1-T_2} \\ &= \sigma\varepsilon_{12}\frac{\left(T_1^2+T_2^2\right)\left(T_1^2-T_2^2\right)}{T_1-T_2} \\ &= \sigma\varepsilon_{12}\frac{\left(T_1^2+T_2^2\right)\left(T_1-T_2\right)\left(T_1+T_2\right)}{T_1-T_2} \\ &= \sigma\varepsilon_{12}\left(T_1^2+T_2^2\right)\left(T_1+T_2\right) \end{aligned} \tag{C33}$$

The effective emissivity, ε_{12}, is given by:

$$\varepsilon_{12}=\left[\frac{1-\varepsilon_1}{\varepsilon_2}+F_{12}+\frac{A_1}{A_2}\frac{1-\varepsilon_2}{\varepsilon_1}\right]^{-1} \tag{C34}$$

in which ε_1 and ε_2 are the emissivities of the respective surface materials.

For infinite concentric cylinders, F_{12} = 1.0, so the above becomes,

$$\varepsilon_{12}=\left[\frac{1}{\varepsilon_1}+\frac{A_1}{A_2}\left(\frac{1}{\varepsilon_2}-1\right)\right]^{-1} \tag{C35}$$

Substituting this expression into the above yields the radiative heat transfer coefficient at surface 1. The value of the coefficient at surface 2 is obtained by using

$$\varepsilon_{21} = \frac{A_1}{A_2}\varepsilon_{12} \quad . \tag{C36}$$

Thus, defining the effective conductivity of a gas gap of width Δ_g due to radiation as

$$K_{rad} = \Delta_g h_r \tag{C37}$$

one obtains the total effective conductivity of the gas gap as

$$K_{gap} = K_{He} + K_{rad} \tag{C38}$$

$$\begin{aligned} K_{gap} &= K_{He} + K_{rad} \\ &= K_{He} + \Delta_g \sigma \varepsilon_{12} \left(T_1^2 + T_2^2\right)\left(T_1 + T_2\right) \end{aligned} \tag{C39}$$

The heat capacity of the gap is assumed to be zero.

Appendix D

Validation of PEBBED Neutronics Solver

Benchmarks for PBR equilibrium cycle calculations have not yet been established. The stand-alone diffusion equation solver can be validated however and is done so in this appendix with simple cases for which analytical solutions exist.

CRITICALITY

Criticality conditions and flux profiles can be obtained analytically for simple reactor configurations. Most analytical treatments assume a boundary condition of zero flux at an extrapolated boundary. PEBBED assumes a zero reentrant current boundary condition (except for pure reflected cases) so these analytical solutions must be re-worked. The zero reentrant current boundary condition leads to a criticality condition that must be evaluated using a numerical search, as closed form solutions do not exist. MATLAB routines were written to generate critical dimensions given number densities and cross-sections. PEBBED models were constructed using the computed geometry (critical dimension) and material specifications. Computed eigenvalue ($k_{eff} = 1$) and flux profiles must match the analytical solution to validate the code.

Analytical solutions for a number of simple reactors are developed in the following discussion. From these solutions, critical geometries can be determined. Corresponding PEBBED models with these geometries were then constructed and run. Accuracy is measured by how closely the PEBBED-computed eigenvalue matches unity.

Shown below are the analytical solutions of simple cases for which PEBBED models were constructed. A table of analytical vs. PEBBED computed eigenvalues follows this section.

ANALYTICAL SOLUTIONS

1.0 1-Group Treatment of Reactors

Some Definitions:

$$B_m^2 = \frac{k_\infty - 1}{L^2} \qquad k_\infty = \frac{\nu\Sigma_f^f}{\Sigma_a^t} \qquad L^2 = \frac{D}{\Sigma_a^t}$$

1.1 1D, 1 Group Bare Homogeneous Slab (-a/2 ≤≤ a/2)

Boundary Conditions:

$$\left.\frac{d\phi(x)}{dx}\right|_{x=0} = 0$$

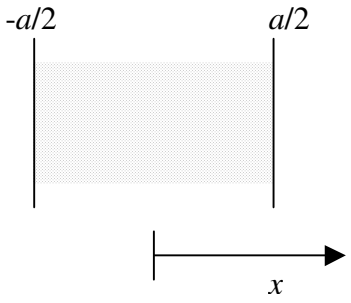

$$J_-\left(\frac{a}{2}\right) = 0$$

Criticality Condition:

$$a = \frac{2}{B_m}\cot^{-1}\left(2DB_{m)}\right)$$

Flux:

$$A = \frac{B_m P}{2\gamma\Sigma_f \sin\left(\frac{B_m a}{2}\right)} \qquad \phi(x) = A\cos(B_m x)$$

1.2 1D, 1 Group Bare Homogenous Infinite Cylinder of Radius *R*

Boundary Conditions:

$$\left.\frac{d\phi(r)}{dr}\right|_{r=0} = 0 \qquad J_-(R) = 0$$

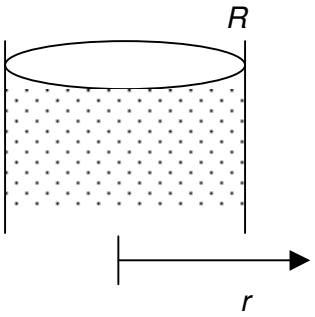

Criticality Condition:

$$2DB_m = \frac{J_o(B_m R)}{J_1(B_m R)}$$

There is no closed form solution for *R*. It can be obtained to any sufficient precision using a numerical search.

Flux:

$$\phi(r) = AJ_o(B_m r) \qquad A = \frac{B_m P}{\gamma\Sigma_f R J_1(B_m R)}$$

1.3 1D, 1 Group Reflected Slab

Boundary Conditions:

$$J^c\left(\frac{a}{2}\right) = J^R\left(\frac{a}{2}\right)$$

$$\phi^c\left(\frac{a}{2}\right) = \phi^R\left(\frac{a}{2}\right)$$

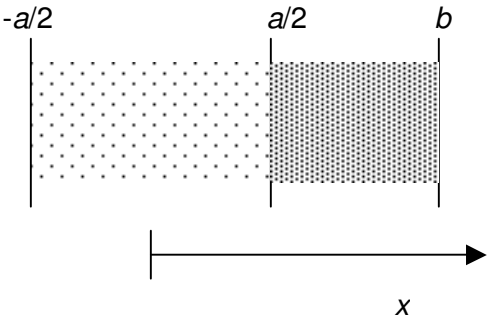

$$J_-(b) = 0 \qquad \left.\frac{d\phi(x)}{dx}\right|_{x=0} = 0$$

Criticality Condition:

$$B_m^c D^c \tan\left(\frac{B_m^c a}{2}\right) = \left(\frac{D^R}{2L^R}\right)\left[\frac{F\exp\left(\frac{-a}{2L^R}\right)+\exp\left(\frac{a}{2L^R}\right)}{-F\exp\left(\frac{-a}{2L^R}\right)+\exp\left(\frac{a}{2L^R}\right)}\right]$$

in which

$$F = \exp\left(\frac{2b}{L^R}\right)\left[\frac{\frac{1}{4}+\frac{D^R}{2L^R}}{\frac{1}{4}-\frac{D^R}{2L^R}}\right]$$

Flux:

$$\phi(x) = A^c \cos\left(B_m x\right) \qquad |x| \le a/2$$

$$\phi(x) = C^R\left(-F\exp\left(\frac{-x}{L^R}\right)+\exp\left(\frac{x}{L^R}\right)\right) \qquad a/2 \le |x| \le b$$

in which

$$A^c = \frac{B_m P}{2\gamma\Sigma_f \sin\left(\frac{B_m a}{2}\right)}$$

$$C^R = \frac{A^c \cos\left(0.5 B_m^c a\right)}{-F\exp\left(-\frac{a}{2L^R}\right)+\exp\left(\frac{a}{2L^R}\right)}$$

1.4 2D, 1 Group Bare Homogeneous Square

One assumes that the Helmholtz equation for this system is separable in **x** and **y**.

$$\phi(r,z) = X(x)Y(y)$$

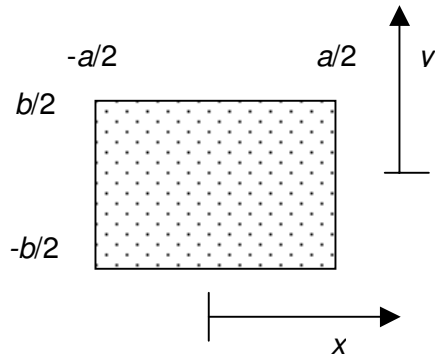

Boundary Conditions:

$$J_{y-}\left(\frac{b}{2}\right) = 0 \qquad J_{x-}\left(\frac{a}{2}\right) = 0$$

$$\left.\frac{\partial\phi(x,y)}{\partial x}\right|_{x=0} = 0 \qquad \left.\frac{\partial\phi(x,y)}{\partial y}\right|_{y=0} = 0$$

Criticality Condition:

$$a = b = \frac{2}{B_m}\cot^{-1}\left(2DB_{m)}\right)$$

Flux:

$$\phi(x,y) = A\cos\left(B_m^x x\right)\cos\left(B_m^y y\right)$$

1.5 2D, 1 Group Bare Homogeneous Finite

1.6 Cylinder (R-Z)

$$A = \frac{B_m^x B_m^y P}{4\gamma\Sigma_f \sin\left(\frac{B_m^x a}{2}\right)\sin\left(\frac{B_m^y b}{2}\right)}$$

One assumes that the Helmholtz equation for this system is separable in **r** and **z**.

$$\phi(r,z) = \mathrm{R}(r)\,\mathrm{Z}(r)$$

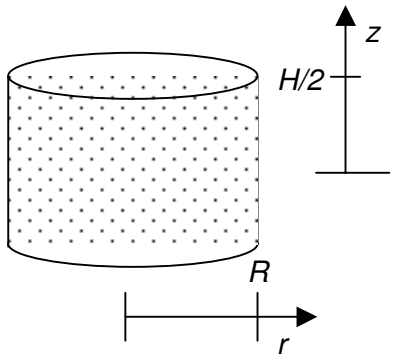

The two components are solved separately in the manner shown above for the 1D cases to yield:

$$\phi(r,z) = AJ_o(B_m r)\cos\left(B_m^z z\right)$$

$$A = \frac{B_m^r B_m^z}{4\gamma\Sigma_f R J_1\left(B_m^r R\right)\sin\left(0.5 B_m^z H\right)}$$

For a reactor that is azimuthally uniform, this solution is valid for any azimuthal location θ.

$$\phi(r,\theta,z) = AJ_o(B_m r)\cos\left(B_m^z z\right) \quad \text{for all } \theta$$

1.6 3D, 1 Group Bare Homogenous Cube

One assumes that the Helmholtz equation for this system is separable in **x**, **y**, and **z**.

$$\phi(r,z) = X(x)Y(y)Z(z)$$

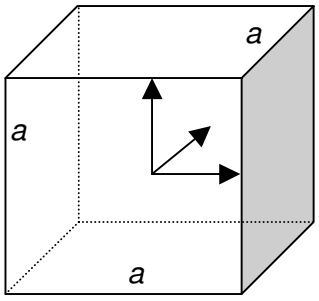

Boundary Conditions:

$$\left.\frac{\partial\phi(x,y,z)}{\partial x}\right|_{x=0} = \left.\frac{\partial\phi(x,y,z)}{\partial y}\right|_{y=0} = \left.\frac{\partial\phi(x,y,z)}{\partial z}\right|_{z=0} = 0$$

$$J_{-x}\left(\frac{a}{2}\right) = J_{-y}\left(\frac{a}{2}\right) = J_{-z}\left(\frac{a}{2}\right) = 0$$

Criticality Condition:

$$a = \frac{2}{B_m}\cot^{-1}\left(2DB_{m)}\right)$$

Flux:

$$\phi(x,y) = A\cos\left(B_m^x x\right)\cos\left(B_m^y y\right)\cos\left(B_m^z z\right)$$

$$A = \frac{B_m^x B_m^y B_m^z P}{8\gamma\Sigma_f \sin\left(\frac{B_m^x a}{2}\right)\sin\left(\frac{B_m^y a}{2}\right)\sin\left(\frac{B_m^z a}{2}\right)}$$

2.0 2-Group Treatment

For bare reactors, the group fluxes all share the same spatial dependence. This allows the derivation of a criticality condition in terms of a single buckling. The flux shapes are the same as the one-group cases.

2.1 1D, Bare Slab of width *a*

$$k_\infty = \frac{\nu\Sigma_f^f}{\Sigma_a^t} \qquad L_T^2 = \frac{D_2}{\Sigma_{a2}}$$

$$B_m^2 = \frac{k_\infty - 1}{L_T^2} \qquad \tau_T = \frac{D_1}{\Sigma_{a1} + \Sigma_{s1\to 2}}$$

Criticality Condition:

The boundary conditions specified for the 1-group treatment apply here. The reactor is critical for a slab of width *a*, such that the following expressions are satisfied.

$$a = \frac{2}{B_m}\cot^{-1}\left(2DB_m\right) \qquad \frac{k_\infty}{\left(1 + B_m^2 L_T^2\right)\left(1 + B_m^2 \tau_T\right)} = 1$$

2.2 2D Rectangle (length *b* may not equal width *a*)

Criticality Condition:

$$a = \frac{2}{B_x}\cot^{-1}\left(2DB_x\right) \qquad \frac{k_\infty}{\left(1 + B_m^2 L_T^2\right)\left(1 + B_m^2 \tau_T\right)} = 1$$

$$b = \frac{2}{B_y}\cot^{-1}\left(2DB_y\right) \qquad B_m^2 = B_x^2 + B_y^2$$

2.3 2D Cylinder

$$H = \frac{2}{B_z}\cot^{-1}\left(2DB_z\right) \qquad B_m^2 = B_r^2 + B_z^2$$

$$2DB_r = \frac{J_o\left(B_r R\right)}{J_1\left(B_r R\right)}$$

3.0 Numerical Results

For the 1-group cases, material properties from Example 6.3 in the *Introduction to Nuclear Engineering, 2nd Edition*, by J. Lamarsh were used. These material properties were used to compute critical dimensions (using bisection search routines coded in MATLAB). PEBBED models were constructed using these materials and dimensions. For the 2-group cases, material properties from Example 6.6 of Lamarsh were used.

Table **D-1**: Analytical vs. PEBBED-calculated core eigenvalues.

Case Geometry	# of Energy Groups	Analytical Eigenvalue	Computed Critical Dimensions	PEBBED Eigenvalue
Bare Critical One-Dimensional Cylinder	1	1	a = 30.47 cm	1.00002
Bare Critical One-Dimensional Slab	1	1	a =36.38 cm	1.00002
Bare Critical Two-Dimensional Square	1	1	a =56.165 b = 56.165 cm	
Bare Critical Two-Dimensional Cylinder	1	1	R = 35 cm H = 94.343 cm	1.00001
Bare Critical Three-Dimensional Cylinder	1	1	R = 35 cm H = 94.343 cm	1.00001
Infinite Two-Dimensional Slab	1	2.6069 (k_∞)	N/A	2.6069
Reflected Critical One-Dimensional Cylinder	1	1	Core R = 25 cm Reflector Width = 38.121 cm	.00002
Reflected Critical One-Dimensional Slab	1	1	Core R = 20 cm Reflector Width = 18.931 cm	1.00018
Bare Critical One-Dimensional Slab	2	1	a =54.474cm	1.00043
Bare Critical Two-Dimensional Square	2	1	a =60.0 b = 136.50 cm	0.99980
Bare Critical Two-Dimensional Cylinder	2	1	R = 60.0 cm H = 80.217 cm	1.00019

Appendix E

Reactor Models

Table E-1: HTR Modul 200.

Core Geometry	
Core (pebble-bed)	radius = 150 cm, height = 940 cm
Top reflector	radius = 240 cm, height = 135 cm
Radial reflector	width = 95 cm, height = 940 cm
Bottom reflector	radius = 240 cm, height = 260 cm
Gas plenum between core and top reflector	height = 80 cm
Pebble Flow	
Pebble packing fraction	0.613
Mean pebble flow rate (pebbles/day)	5300
Normalized axial velocity profile $v_z(r)$ *(v_o = velocity at inner flow boundary)*	$v(r) = v_o$
Number of flow channels	1
Number of flow zones	1
Pebble Data Ex-Core Decay Time	
Composition (see below)	FUEL
Discharge burnup (MWD/kg_{ihm})	80
Ex-core decay time (hours)	40
Recirculation mode	Random (1 flow zone)
Nuclear Data	
Energy Group	Max. Energy (eV)
1	1.6905E7
2	1.1109E5
3	7102.
4	29.023
5	2.3823
6	1.8554
Fuel isotopes (that produce fission products)	U-235, Pu-239, Pu-241
Depletion chains	
U-235	U-235 U-236 U-237 Np-237 Np238 Pu-238 Pu-239
U-238	U-238 Np-239 Pu-239 Pu-240 Pu-241 Pu-242
Xe	I-135 Xe-135
Sm	Pm-149 Sm-149

Table E-1: HTR Modul 200 (continued).

Composition Specification	**BOL Homogenized Atom Density (atoms/barn-cm)**
FUEL isotopes	
C-12	0.05302
U-235	7.603E-06
U-238	8.874E-05
O-16	1.927E-4
Si-28	2.119E-4
He-4	1.964-4
REFLECTOR isotopes	
C-12	0.07671
VOID isotopes	
He-4	5.076E-04
Thermal-Hydraulic Data	
Core power (MW)	200
Helium temperature (°C) - inlet/outlet	250/700
He flow rate (kg/s)	86
He specific heat (J/kg-K)	5196
He inlet pressure (Mpa)	6.0

Depressurized Conduction Cooldown Model			
Region	**Composition**	**Outer Radius (cm)**	**Density (g/cm^3)**
1	Pebble-bed	150	1.06
2	Reflector	230	1.53
3	Carbon brick	250	6.0
4	Void (He)	265	0.0
5	SSTL-304	270	7.8
6	Void (He)	295	0.0
7	2.25Cr-1Mo Steel	310	7.675
8	Void (He)	430	0.0
9*	Concrete	480	1.75
* Used in models in with no reactor cavity cooling system			
Outer boundary temperature (°C)		35	
Mean reflector fluence (n/cm^2)		0	

Table **E-2**: PBMR-DIR.

Core Geometry		
Core (pebble-bed)	radius = 175m, height = 850 cm	
Top reflector	radius = 250 cm, height = 135 cm	
Radial reflector	width = 75 cm, height = 850 cm	
Bottom reflector	radius = 250 cm, height = 260 cm	
Gas plenum between core and top reflector	height = 50 cm	
Pebble Flow		
Pebble packing fraction	0.613	
Mean pebble flow rate (pebbles/day)	5140	
Normalized axial velocity profile $v_z(r)$ *(v_o = velocity at inner flow boundary)*	$v(r) = v_o(-2.302E\text{-}5r^2 + 2.750E\text{-}3r + 1)$	
Number of flow channels	5	
Outer radii of flow channels (cm)	72.5-102.5-129.5-152.5-175.0	
Number of flow zones	2	
Radius of zone boundary (cm)	87.5	
Pebble Data Ex-Core Decay Time		
Composition (see below)	**FUEL**	**GRAPHITE**
Discharge burnup (MWD/kg_{ihm})	80	0
Ex-core decay time (hours)	40	0
Recirculation mode	Type-dependent, Burnup-independent (outer zone only)	Type-dependent, Burnup-independent (inner zone only)
Nuclear Data		
Energy Group	Max. Energy (eV)	
1	1.6905E7	
2	1.1109E5	
3	7102.	
4	29.023	
5	2.3823	
6	1.8554	
Fuel isotopes (that produce fission products)	U-235, Pu-239, Pu-241	
Depletion chains		
U-235	U-235 U-236 U-237 Np-237 Np238 Pu-238 Pu-239	
U-238	U-238 Np-239 Pu-239 Pu-240 Pu-241 Pu-242	
Xe	I-135 Xe-135	
Sm	Pm-149 Sm-149	

Table E-2: PBMR-DIR (continued).

Composition Specification	**BOL Homogenized Atom Density (atoms/barn-cm)**
FUEL isotopes	
C-12	0.05290
U-235	9,998E-06
U-238	1.135E-04
O-16	2.470E-4
Si-28	2.700E-4
He-4	1.964-4
REFLECTOR isotopes	
C-12	0.07671
VOID isotopes	
He-4	5.076E-04
GRAPHITE isotopes	
C-12	0.05379
He-4	1.964E-04
Thermal-Hydraulic Data	
Core power (MW)	268
Helium temperature (°C) - inlet/outlet	503/900
He flow rate (kg/s)	125.74
He specific heat (J/kg-K)	5196
He inlet pressure (Mpa)	7.0

Depressurized Conduction Cooldown Model			
Region	**Composition**	**Outer Radius (cm)**	**Density (g/cm^3)**
1	Pebble-bed	175	1.06
2	Graphite	251	1.53
3	Void (He)	281	0.0
4	Graphite	284	1.53
5	Void (He)	291	0.0
6	2.25Cr-1Mo Steel	301	7.675
7	Void (He)	364.5	0.0
8*	Concrete	370	1.75
* Used in models in with no reactor cavity cooling system			
Outer boundary temperature (°C)		50	
Mean reflector fluence (n/cm^2)		5.7E20	

Partition Coefficients for the PBMR-DIR

flow partition coefficients (α_j)

	j->	1	2	3	4	5
		0.19008	0.18793	0.21260	0.20294	0.20645

type partition coefficients (α_j^p)

	j->	1	2	3	4	5
	1 (fuel)	0.000000	0.53748	0.99998	0.99998	0.99998
	2 (graphite)	1.000000	0.46251	0.00000	0 00000	0.00000

transfer partition coefficients ($^m\alpha_j^p$) for all *m*, $p = 1$

	j->	1	2	3	4	5
	1	0.000000	0.000000	0.000000	0.000000	0.000000
	2	0.139711	0.139711	0.139711	0.139711	0.139711
i	3	0.294048	0.294048	0.294048	0.294048	0.294048
	4	0.280697	0.280697	0.280697	0.280697	0.280697
	5	0.285544	0.285544	0.285544	0.285544	0.285544

Transfer partition coefficients ($^m\alpha_j^p$) for $p = 2$ (graphite) are not defined since graphite pebbles are assumed to be non-recirculating.

Table **E-3**: GE-MPBR.

Core Geometry	
Core (pebble-bed)	radius = 144.8 cm, height = 926 cm
Top reflector	radius = 344.8 cm, height = 100 cm
Radial reflector	width = 100 cm, height = 926 cm
Bottom reflector	radius = 344.8 cm, height = 100 cm
Gas plenum between core and top reflector	none
Pebble Flow	
Pebble packing fraction	0.613
Mean pebble flow rate (pebbles/day)	4438
Normalized axial velocity profile $v_z(r)$ *(v_o = velocity at inner flow boundary)*	$v(r) = v_o$
Number of flow channels	4
Outer radii of flow channels (cm)	73.1 102.4 123.6 144.8
Number of flow zones	2
Pebble Data Ex-Core Decay Time	
Composition (see below)	FUEL
Discharge burnup (MWD/kg_{ihm})	80
Ex-core decay time (hours)	5
Recirculation mode	Burnup-dependent (OUT-IN)
Nuclear Data	
Energy Group	Max. Energy (eV)
1	1.6905E7
2	1.1109E5
3	7102.
4	29.023
5	2.3823
6	1.8554
Fuel isotopes (that produce fission products)	U-235, Pu-239, U-233
Depletion chains	
U-235	U-235 U-236 U-237 Np-237 Np238 Pu-238 Pu-239
U-238	U-238 Np-239 Pu-239 Pu-240 Pu-241 Pu-242
Xe	I-135 Xe-135
Sm	Pm-149 Sm-149
Th-232a	Th-232 Pa-233 U-233 U-234 U-235
Th-232b	Th-232 Pa-233 (Pa-234) U-234 U-235

Table E-3: GE-MPBR (continued).

Composition Specification	**BOL Homogenized Atom Density (atoms/barn-cm)**
FUEL isotopes	
C-12	0.05043
U-235	8.107E-06
U-238	3.202-05
O-16	1.953E-4
Si-28	1.069E-3
He-4	1.427E-4
Th-232	5.752E-05
REFLECTOR isotopes	
C-12	0.08022
Thermal-Hydraulic Data	
Core power (MW)	250
Helium temperature (℃) - inlet/outlet	400/950
He flow rate (kg/s)	87.4
He specific heat (J/kg-K)	5196
He inlet pressure (Mpa)	4.0

Depressurized Conduction Cooldown Model			
Region	**Composition**	**Outer Radius (cm)**	**Density (g/cm^3)**
1	Pebble-bed	144.7	1.04
2	Reflector	220	1.6
3	Reflector	245	1.6
4	SSTL-304	248	7.8
5	Void (He)	266	0.0
6	2.25Cr-1Mo Steel	282	7.675
7	Void (He)	382	0.0
8*	Concrete	422	1.75
* Used in models in with no reactor cavity cooling system			
Outer boundary temperature (℃)		50	
Mean reflector fluence (n/cm^2)		0	

Partition Coefficients for the GE-MPBR

flow partition coefficients (α_j)

	j->	1	2	3	4
		0.25515	0.24494	0.22852	0.27139

type partition coefficients (α_j^p)

	j->	1	2	3	4
p	1 (fuel)	1.000000	1.000000	1.000000	1.000000

transfer partition coefficients ($^m\alpha_j^p$) for $m < 5$, $p = 1$

	j->	1	2	3	4
	1	0.000000	0.000000	0.000000	0.000000
	2	0.000000	0.000188	0.000188	0.000188
i	3	0.000000	0.457032	0.457032	0.457032
	4	0.000000	0.542780	0.542780	0.542780

transfer partition coefficients ($^m\alpha_j^p$) for $m > 4$, $p = 1$

	j->	1	2	3	4
	1	0.510300	0.510300	0.510300	0.510300
	2	0.489700	0.489700	0.489700	0.489700
i	3	0.000000	0.000000	0.000000	0.000000
	4	0.000000	0.000000	0.000000	0.000000

Table **E-4**: VHTR-300.

Core Geometry	
Inner reflector	radius = 40 cm, height = 875 cm
Core (pebble-bed)	radius = 175 cm, height = 875 cm
Top reflector	radius = 225 cm, height = 140 cm
Radial reflector	width = 75 cm, height = 875 cm
Bottom reflector	radius = 225 cm, height = 260 cm
Gas plenum between core and top reflector	height = 50 cm
Pebble Flow	
Pebble packing fraction	0.613
Mean pebble flow rate (pebbles/day)	5599
Normalized axial velocity profile $v_z(r)$ *(v_o = velocity at inner flow boundary)*	*$v(r) = v_o(-2.302E\text{-}5r^2 + 2.750E\text{-}3r + 1)$*
Number of flow channels	5
Outer radii of flow channels (cm)	75.5 96.8 132.4 153.7 175.0
Number of flow zones	1
Pebble Data Ex-Core Decay Time	
Composition (see below)	FUEL
Discharge burnup (MWD/kg_{ihm})	93.9
Ex-core decay time (hours)	40
Recirculation mode	Random (1 flow zone)
Nuclear Data	
Energy Group	Max. Energy (eV)
1	1.6905E7
2	1.1109E5
3	7102.
4	29.023
5	2.3823
6	1.8554
Fuel isotopes (that produce fission products)	U-235, Pu-239, Pu-241
Depletion chains	
U-235	U-235 U-236 U-237 Np-237 Np238 Pu-238 Pu-239
U-238	U-238 Np-239 Pu-239 Pu-240 Pu-241 Pu-242
Xe	I-135 Xe-135
Sm	Pm-149 Sm-149

Table E-4: VHTR-300 (continued).

Composition Specification		**BOL Homogenized Atom Density (atoms/barn-cm)**	
FUEL isotopes			
C-12		0.05300	
U-235		8.845E-06	
U-238		1.004E-04	
O-16		2.186E-4	
Si-28		2.389E-4	
He-4		1.964-4	
REFLECTOR isotopes			
C-12		0.07671	
VOID isotopes			
He-4		5.076E-04	
Thermal-Hydraulic Data			
Core power (MW)		300	
Helium temperature (°C) - inlet/outlet		600/1,000	
He flow rate (kg/s)		144.4	
He specific heat (J/kg-K)		5196	
He inlet pressure (Mpa)		7.0	
Depressurized Conduction Cooldown Model			
Region	**Composition**	**Outer Radius (cm)**	**Density (g/cm^3)**
1	Reflector (inner)	40	1.8
2	Pebble-bed	175	1.10
3	Reflector	251	1.8
4	Void (He)	281	0.0
5	Reflector (core barrel)	284	1.8
6	Void (He)	291	0.0
7	2.25Cr-1Mo Steel	301	7.675
8	Void (He)	428	0.0
Outer boundary temperature (°C)		35	
Mean reflector fluence (n/cm^2)		0	

Partition Coefficients for the Manually Optimized VHTR-300

flow partition coefficients (α_j)

	j->	1	2	3	4	5
		0.14167	0.13104	0.28952	0.20944	0.22834

type partition coefficients (α_j^p)

	j->	1	2	3	4	5
p	1 (fuel)	1.000000	1.000000	1.000000	1.000000	1.000000

transfer partition coefficients (${}^m\alpha_j^p$) for all *m, p* = 1

	j->	1	2	3	4	5
	1	0.14167	0.14167	0.14167	0.14167	0.14167
	2	0.13104	0.13104	0.13104	0.13104	0.13104
i	3	0.28952	0.28952	0.28952	0.28952	0.28952
	4	0.20944	0.20944	0.20944	0.20944	0.20944
	5	0.22834	0.22834	0.22834	0.22834	0.22834

Partition Coefficients for the VHTR-300 used in the Hotspot Analysis

flow partition coefficients (α_j)

	j->	1	2	3	4	5
		0.10000	0.29755	0.20056	0.18983	0.21203

type partition coefficients (α_j^p)

	j->	1	2	3	4	5
p	1 (fuel)	1.000000	1.000000	1.000000	1.000000	1.000000

transfer partition coefficients (${}^{m}\alpha_j^p$) for all *m, p* = 1 – nominal case

	j->	1	2	3	4	5
	1	0.100001	0.100001	0.100001	0.100001	0.100001
	2	0.297548	0.297548	0.297548	0.297548	0.297548
i	3	0.200555	0.200555	0.200555	0.200555	0.200555
	4	0.189832	0.189832	0.189832	0.189832	0.189832
	5	0.212065	0.212065	0.212065	0.212065	0.212065

transfer partition coefficients (${}^{m}\alpha_j^p$) for *m=1, p* = 1 – InOut 1

	j->	1	2	3	4	5
	1	0.000001	0.000000	0.000000	0.000000	0.000000
	2	0.330609	0.000000	0.000000	0.000000	0.000000
i	3	0.222839	0.000000	0.000000	0.000000	0.000000
	4	0.210924	0.000000	0.000000	0.000000	0.000000
	5	0.235628	0.000000	0.000000	0.000000	0.000000

transfer partition coefficients (${}^{m}\alpha_j^p$) for *m>1, p* = 1 – InOut 1

	j->	1	2	3	4	5
	1	0.000001	0.000001	0.000001	0.000001	0.000001
	2	0.330609	0.330609	0.330609	0.330609	0.330609
i	3	0.222839	0.222839	0.222839	0.222839	0.222839
	4	0.210924	0.210924	0.210924	0.210924	0.210924
	5	0.235628	0.235628	0.235628	0.235628	0.235628

flow partition coefficients (α_j) – hot2

	j->	1	2	3	4	5
		0.11098	0.08921	0.25678	0.31040	0.23262

transfer partition coefficients (${}^{m}\alpha_{j}^{p}$) for *m=1, p* = 1 – InOut 2

	j->	1	2	3	4	5
	1	0.554921	0.554921	0.000000	0.000000	0.000000
	2	0.445079	0.445079	0.000000	0.000000	0.000000
i	3	0.000000	0.000000	0.000000	0.000000	0.000000
	4	0.000000	0.000000	0.000000	0.000000	0.000000
	5	0.000000	0.000000	0.000000	0.000000	0.000000

transfer partition coefficients (${}^{m}\alpha_{j}^{p}$) for *m>1, p* = 1 – InOut 2

	j->	1	2	3	4	5
	1	0.000000	0.000240	0.000240	0.000240	0.000240
	2	0.000240	0.320980	0.320980	0.320980	0.320980
i	3	0.320980	0.388000	0.388000	0.388000	0.388000
	4	0.388000	0.290780	0.290780	0.290780	0.290780
	5	0.290780	0.000240	0.000240	0.000240	0.000240

flow partition coefficients (α_j) – hot3

	j->	1	2	3	4	5
		0.15755	0.13541	0.23231	0.25851	0.21622

transfer partition coefficients (${}^{m}\alpha_{j}^{p}$) for *m=1,2, p* = 1 – InOut 3

	j->	1	2	3	4	5
	1	0.525155	0.525155	0.525155	0.525155	0.525155
	2	0.451373	0.451373	0.451373	0.451373	0.451373
i	3	0.023473	0.023473	0.023473	0.023473	0.023473
	4	0.000000	0.000000	0.000000	0.000000	0.000000
	5	0.000000	0.000000	0.000000	0.000000	0.000000

transfer partition coefficients (${}^{m}\alpha_j^{p}$) for *m>2, p* = 1 – InOut 3

	j->	1	2	3	4	5
	1	0.000000	0.000000	0.000000	0.000000	0.000000
	2	0.000000	0.000000	0.000000	0.000000	0.000000
i	3	0.321811	0.321811	0.321811	0.321811	0.321811
	4	0.369304	0.369304	0.369304	0.369304	0.369304
	5	0.308884	0.308884	0.308884	0.308884	0.308884

flow partition coefficients (α_j) – hot4

	j->	1	2	3	4	5
		0.16906	0.23108	0.16995	0.19995	0.22995

transfer partition coefficients (${}^{m}\alpha_j^{p}$) for *m<4, p* = 1 – InOut 4

	j->	1	2	3	4	5
	1	0.422655	0.422655	0.422655	0.422655	0.422655
	2	0.577345	0.577345	0.577345	0.577345	0.577345
i	3	0.000000	0.000000	0.000000	0.000000	0.000000
	4	0.000000	0.000000	0.000000	0.000000	0.000000
	5	0.000000	0.000000	0.000000	0.000000	0.000000

transfer partition coefficients (${}^{m}\alpha_j^{p}$) for *m>3, p* = 1 – InOut4

	j->	1	2	3	4	5
	1	0.000000	0.000000	0.000000	0.000000	0.000000
	2	0.000244	0.000244	0.000244	0.000244	0.000244
i	3	0.283250	0.283250	0.283250	0.283250	0.283250
	4	0.333252	0.333252	0.333252	0.333252	0.333252
	5	0.383253	0.383253	0.383253	0.383253	0.383253

flow partition coefficients (α_j) – warm1-20 through warm1-50

	j->	1	2	3	4	5
		0.10000	0.29755	0.20056	0.18983	0.21206

transfer partition coefficients (${}^{m}\alpha_{j}^{p}$) for all *m, p* = 1 – warm1-20

	j->	1	2	3	4	5
	1	0.088889	0.088889	0.088889	0.088889	0.088889
	2	0.301223	0.301223	0.301223	0.301223	0.301223
i	3	0.203036	0.203036	0.203036	0.203036	0.203036
	4	0.192174	0.192174	0.192174	0.192174	0.192174
	5	0.214678	0.214678	0.214678	0.214678	0.214678

transfer partition coefficients (${}^{m}\alpha_{j}^{p}$) for all *m, p* = 1 – warm1-30

	j->	1	2	3	4	5
	1	0.077778	0.077778	0.077778	0.077778	0.077778
	2	0.304897	0.304897	0.304897	0.304897	0.304897
i	3	0.205512	0.205512	0.205512	0.205512	0.205512
	4	0.194517	0.194517	0.194517	0.194517	0.194517
	5	0.217296	0.217296	0.217296	0.217296	0.217296

transfer partition coefficients (${}^{m}\alpha_{j}^{p}$) for all *m, p* = 1 – warm1-40

	j->	1	2	3	4	5
	1	0.066667	0.066667	0.066667	0.066667	0.066667
	2	0.308570	0.308570	0.308570	0.308570	0.308570
i	3	0.207988	0.207988	0.207988	0.207988	0.207988
	4	0.196861	0.196861	0.196861	0.196861	0.196861
	5	0.219914	0.219914	0.219914	0.219914	0.219914

transfer partition coefficients (${}^{m}\alpha_{j}^{p}$) for all *m, p* = 1 – warm1-50

	j->	1	2	3	4	5
	1	0.055560	0.055560	0.055560	0.055560	0.055560
	2	0.312242	0.312242	0.312242	0.312242	0.312242
i	3	0.210463	0.210463	0.210463	0.210463	0.210463
	4	0.199203	0.199203	0.199203	0.199203	0.199203
	5	0.222531	0.222531	0.222531	0.222531	0.222531

Table **E-5**: VHTR-600.

Core Geometry	
Inner reflector	radius = 150 cm, height = 950 cm
Core (pebble-bed)	radius = 250 cm, height = 950 cm
Top reflector	radius = 326 cm, height = 140 cm
Radial reflector	width = 76 cm, height = 950 cm
Bottom reflector	radius = 326 cm, height = 260 cm
Gas plenum between core and top reflector	height = 50 cm
Pebble Flow	
Pebble packing fraction	0.613
Mean pebble flow rate (pebbles/day)	8314
Normalized axial velocity profile $v_z(r)$ *(v_o = velocity at inner flow boundary)*	*$v(r) = v_o(-2.302E\text{-}5r^2 + 2.750E\text{-}3r + 1)$*
Number of flow channels	5
Outer radii of flow channels (cm)	171.1 192.1 213.2 234.2 250.0
Number of flow zones	1
Pebble Data Ex-Core Decay Time	
Composition (see below)	FUEL
Discharge burnup (MWD/kg_{ihm})	80.0
Ex-core decay time (hours)	5
Recirculation mode	Random (1 flow zone)
Nuclear Data	
Energy Group	Max. Energy (eV)
1	1.6905E7
2	1.1109E5
3	7102.
4	29.023
5	2.3823
6	1.8554
Fuel isotopes (that produce fission products)	U-235, Pu-239, Pu-241
Depletion chains	
U-235	U-235 U-236 U-237 Np-237 Np238 Pu-238 Pu-239
U-238	U-238 Np-239 Pu-239 Pu-240 Pu-241 Pu-242
Xe	I-135 Xe-135
Sm	Pm-149 Sm-149

Table E-5: VHTR-600 (continued).

Composition Specification		**BOL Homogenized Atom Density (atoms/barn-cm)**	
FUEL isotopes			
C-12		0.05300	
U-235		8.735E-06	
U-238		9.919E-05	
O-16		2.158E-4	
Si-28		2.359E-4	
He-4		1.964-4	
REFLECTOR isotopes			
C-12		0.07671	
VOID isotopes			
He-4		5.076E-04	
Thermal-Hydraulic Data			
Core power (MW)		600	
Helium temperature (°C) - inlet/outlet		600/1,000	
He flow rate (kg/s)		288.4	
He specific heat (J/kg-K)		5,196	
He inlet pressure (Mpa)		7.0	
Depressurized Conduction Cooldown Model			
Region	**Composition**	**Outer Radius (cm)**	**Density (g/cm^3)**
1	Reflector (inner)	150	1.8
2	Pebble-bed	250	1.10
3	Reflector	326	1.8
4	Void (He)	356	0.0
5	Reflector (core barrel)	360	1.8
6	Void (He)	366	0.0
7	2.25Cr-1Mo Steel	376	7.675
8	Void (He)	503	0.0
Outer boundary temperature (°C)		35	
Mean reflector fluence (n/cm^2)		0	

Partition Coefficients for the VHTR-600

flow partition coefficients (α_j)

	j->	1	2	3	4	5
		0.16316	0.19126	0.21682	0.23857	0.19019

type partition coefficients (α_j^p)

	j->	1	2	3	4	5
p	1 (fuel)	1.000000	1.000000	1.000000	1.000000	1.000000

transfer partition coefficients ($^m\alpha_j^p$) for all *m, p* = 1

	j->	1	2	3	4	5
	1	0.16316	0.16316	0.16316	0.16316	0.16316
	2	0.19126	0.19126	0.19126	0.19126	0.19126
i	3	0.21682	0.21682	0.21682	0.21682	0.21682
	4	0.23857	0.23857	0.23857	0.23857	0.23857
	5	0.19019	0.19019	0.19019	0.19019	0.19019

Appendix F

Fuel Pebble Models

Table F-1: HTR Modul 200 pebble.

Element	At. Wt.
U-235	235.0439
U-238	238.0508
oxygen	15.9994
carbon	12.011
silicon	28.0855

Fuel Kernel

Enrichment (%) = 7.8 N_A = 6.0220E+23

	Atom %
U-235	7.8919
U-238	92.1081

Particle Layer		Mol. Fraction	Outer Dia. (mm)	Radius (cm)	Thickness (μm)	Volume (cm^3)	Density (g/cm^3)	Mol. Wt (g/mol)	No. Density ($\#/cm^3$)	Particle Mass (g)
PPyC			0.900	0.0450	0	0.000E+00	1.06	12.011	5.315E+22	0.000E+00
PyC seal			0.900	0.0450	0	0.000E+00	1.95	12.011	9.777E+22	0.000E+00
OPyC			0.900	0.0450	35	8.232E-05	1.85	12.011	9.275E+22	1.523E-04
SiC			0.830	0.0415	35	6.954E-05	3.20	40.0965	4.806E+22	2.225E-04
	Carbon	1						12.011	4.806E+22	6.666E-05
	Silicon	1						28.0855	4.806E+22	1.559E-04
IPyC			0.760	0.0380	40	6.521E-05	1.85	12.011	9.275E+22	1.206E-04
PyC seal			0.680	0.0340	0	0.000E+00	1.95	12.011	9.777E+22	0.000E+00
C Buffer			0.680	0.0340	90	9.919E-05	0.90	12.011	4.512E+22	8.927E-05
Kernel (UO2)			0.500	0.0250	500	6.545E-05	10.40	269.812291	2.321E+22	6.807E-04
	U-235	0.079						235.04393	1.832E+21	4.680E-05
	U-238	0.921						238.05079	2.138E+22	5.532E-04
	Oxygen	2						15.9994	4.642E+22	8.073E-05
	Carbon	0						12.011	0.000E+00	0.000E+00

Table F-1. HTR Modul 200 pebble (continued).

	Density (g/cm^3)	Mol. Wt (g/mol)	No. Density ($\#/cm^3$)
C matrix	1.75	12.011	8.774E+22
C cover	1.75	12.011	8.774E+22
Reflector	1.53	12.011	7.671E+22

Pebble	**o. d. (mm)**	**Volume (cm^3)**	**# Particles**	**Total Particle Volume**	**Pack Factor**	**C Matrix Volume**
Fuel Core	50	65.4	11,700	4.5	0.068	61.0
Graphite Cover	60	47.6	0			
Total Volume		113.1				

Reactor Core	**# Pebbles**	**Diameter (m)**	**Volume (m^3)**	**Vol/Pebble (cm^3)**	**Pack Factor**	**Eff p.f.**	
		3.0	66.4	184.5	0.613	0.613	
Fuel	3.60E+05						
Graphite	0.00E+00	**height (m)**	**eff H (m)**	**eff V m^3)**	**void/peb (cm^3)**	**eff vd/pb (cm^3)**	**Eff. Vd r (cm)**
Total	360,000	9.40	9.40	66.4	71.4	71.4	3.532

Material Densities	**w/o of part.**	**Mass per particle (g)**	**Mass (g) per fuel zone**	**N (p. core) $\#/cm^3$**	**Mass per pebble (g)**	**N (pebble) $\#/cm^3$**	**N (cell) $\#/cm^3$**
U-235	3.7%	4.68E-05	5.475E-01	2.143E+19	5.475E-01	1.240E+19	7.603E+18
U-238	43.7%	5.53E-04	6.472E+00	2.501E+20	6.472E+00	1.448E+20	8.874E+19
Oxygen	6.4%	8.07E-05	9.445E-01	5.432E+20	9.445E-01	3.143E+20	1.927E+20
Carbon	33.9%	4.29E-04	7.375E+02	5.650E+23	1.310E+03	5.806E+23	3.559E+23
Silicon	12.3%	1.56E-04	1.824E+00	5.974E+20	1.824E+00	3.457E+20	2.119E+20
Helium						5.754E+20	2.227E+20

Table F-2: PBMR pebble.

Element	At. Wt.	Fuel Kernel		
U-235	235.0439	Enrichment (%) = 8	N_A = 6.0220E+23	
U-238	238.0508			
oxygen	15.9994		**Atom %**	
carbon	12.011	U-235	8.0941	
silicon	28.0855	U-238	91.9059	

Particle Layer		Mol. Fraction	Outer Dia. (mm)	Radius (cm)	Thickness (mm)	Volume (cm^3)	Density (g/cm^3)	Mol. Wt (g/mol)	No. Density ($\#/cm^3$)
PPyC			0.962	0.048	0	0.000E+00	1.06	12.011	5.315E+22
PyC seal			0.962	0.048	0	0.000E+00	1.95	12.011	9.777E+22
OPyC			0.962	0.048	43	1.142E-04	1.86	12.011	9.326E+22
SiC			0.876	0.044	35	7.781E-05	3.20	40.0965	4.806E+22
	Carbon	1						12.011	4.806E+22
	Silicon	1						28.0855	4.806E+22
IPyC			0.806	0.040	53	9.457E-05	1.90	12.011	9.526E+22
PyC seal			0.700	0.035	0	0.000E+00	1.95	12.011	9.777E+22
C Buffer			0.700	0.035	100	1.141E-04	0.96	12.011	4.813E+22
Kernel (UO2)			0.500	0.025	500	6.545E-05	10.50	269.806213	2.344E+22
	U-235	0.081						235.04393	1.897E+21
	U-238	0.919						238.05079	2.154E+22
	Oxygen	2						15.9994	4.687E+22
	Carbon	0						12.011	0.000E+00
				Particle volume (cm^3) = 4.661E-04					

Table F-2. PMBR pebble (continued).

	Density (g/cm^3)	Mol. Wt (g/mol)	No. Density (#/cm^3)
C matrix	1.75	12.011	8.774E+22
C cover	1.75	12.011	8.774E+22
Reflector	1.53	12.011	7.671E+22

Pebble	**o. d. (mm)**	**Volume (cm^3)**	**# Particles**	**Total Particle Volume**	**Pack Factor**	**Volume (cm^3)**
Fuel Core	50	65.45	15,000	7.0	0.107	58.5
Graphite Cover	60	47.6	0			
Total Volume		113.1				
	Fuel Annulus					

Reactor Core	**# Pebbles**	**i. d. (m)**	**o. d. (m)**	**Volume (m^3)**	**Vol/Pebble (cm^3)**	**Pack Factor**	**Eff p.f.**
		1.75	3.50	61.3	184.5	0.613	0.613
Fuel	330,000						
Graphite	0	**height (m)**	**eff H (m)**	**eff V (m^3)**	**void/peb (cm^3)**	**eff vd/pb (cm^3)**	**Eff. Vd r (cm)**
Total	330,000	8.50	8.44	60.9	71.4	71.4	3.532

Material Densities	**w/o of part.**	**Mass per particle (g)**	**Mass (g) per fuel zone**	**N (p. core) #/cc**	**Mass per pebble (g)**	**N (pebble) #/cm^3**	**N (cell) #/cm^3**
U-235	3.4%	4.846E-05	7.269E-01	2.845E+19	7.269E-01	1.647E+19	1.009E+19
U-238	38.8%	5.573E-04	8.359E+00	3.231E+20	8.359E+00	1.870+20	1.146E+20
Oxygen	5.7%	8.150E-05	1.223E+00	7.031E+20	1.223E+00	4.069E+20	2.494E+20
Carbon	40.1%	5.762E-04	1.109E+02	8.4988E+22	1.9433E+02	8.615E+22	5.2809E+22
Silicon	12.1%	1.744E-04	2.616E+00	8.571E+20	2.616E+00	4.960E+20	3.0405E+20
Helium						5.331E+20	2.063E+20

Table **F-3**: GE-MPBR pebble

Element	At. Wt.
Th-232	232.038
U-235	235.0439
U-238	238.0508
oxygen	15.9994
carbon	12.011
silicon	28.0855

Fuel Kernel

U enrichment (%) = 20

N_a = 6.0220E+23

	Atom %		**Wt %**
Th-232	58.91%	Th	58.35%
U-235	8.3022%	U	41.65%
U-238	32.79%		

Particle Layer		**Mol. Fraction**	**Outer Dia.(mm)**	**Radius (cm)**	**Thickness (mm)**	**Volume (cm^3)**	**Density (g/cm^3)**	**Mol. Wt (g/mol)**	**No. Density (#/cm^3)**
PPyC			0.600	0.030	0	0.000E+00	1.06	12.011	5.315E+22
PyC seal			0.600	0.030	0	0.000E+00	1.95	12.011	9.777E+22
OPyC			0.600	0.030	40	3.948E-05	1.80	12.011	9.025E+22
SiC			0.520	0.026	30	2.266E-05	3.20	40.0965	4.806E+22
	Carbon	1						12.011	4.806E+22
	Silicon	1						28.0855	4.806E+22
IPyC			0.460	0.023	30	1.745E-05	1.90	12.011	9.526E+22
PyC seal			0.400	0.020	0	0.000E+00	1.95	12.011	9.777E+22
C Buffer			0.400	0.020	100	2.932E-05	1.00	12.011	5.014E+22
Kernel (UO2/ThO2)			0.200	0.010	200	4.189E-06	10.5	266.257908	2.375E+22
	Th-232	0.589						232.038	1.399E+22
	U-235	0.083						235.04393	1.972E+21
	U-238	0.328						238.05079	7.787E+21
	Oxygen	2						15.9994	4.750E+22
	Carbon	0						12.011	0.000E+00
					Particle volume (cm^3) = 1.131E-04				

Table **F-3**. GE-MPBR pebble (continued).

	Density (g/cm^3)	Mol. Wt (g/mol)	No. Density (#/cm^3)
C matrix	1.7	12.011	8.523E+22
C cover	1.7	12.011	8.523E+22
Reflector	1.6	12.011	8.022E+22
Top Reflector			

Pebble	**o. d. (mm)**	**Volume (cm^3)**	**# Particles**	**Total Particle Volume**	**Pack Factor**	**Volume (cm^3)**
Fuel Core	50	65.45	181,100	20.5	0.313	45.0
Graphite Cover	60	47.6				
Total Volume		113.1				
	Fuel Zone					

Reactor Core	**# Pebbles**	**i. d. (m)**	**o. d. (m)**	**Volume (m^3)**	**Vol/Pebble (cm^3)**	**Pack Factor**	**Eff p.f.**
		0	2.9	61.0	184.5	0.613	0.613
Fuel	367,920						
Graphite	0	**height (m)**	**eff H (m)**	**eff V (m^3)**	**void/peb (cm^3)**	**eff vd/pb (cc)**	**Eff. Vd r (cm)**
Total	367,920	9.26	10.31	67.9	71.4	71.4	3.532

Material Densities	**w/o of part.**	**Mass per particle (g)**	**Mass (g) per fuel zone**	**N (p. core) #/cc**	**Mass per pebble (g)**	**N (pebble) #/cm^3**	**N (cell) #/cm^3**
Th-232	9.0%	2.258E-05	4.089E+00	1.621E+20	4.089E+00	9.383E+19	5.752E+19
U-235	1.3%	3.223E-06	5.838E-01	2.285E+19	5.838E-01	1.322E+19	8.107E+18
U-238	5.2%	1.289E-05	2.335E+00	5.223E+19	2.335E+00	5.223E+19	3.202E+19
Oxygen	2.1%	5.286E-06	9.573E-01	5.505E+20	9.573E-01	3.186E+20	1.953E+20
Carbon	62.1%	1.553E-04	1.046E+02	8.010E+22	1.856E+02	8.226E+22	5.043E+22
Silicon	20.3%	5.078E-05	9.197E+00	3.013E+21	9.197E+00	1.744E+21	1.069E+21
Helium						3.688E+20	1.427E+20

Hans D. Gougar
Manager, Fission & Fusion Systems Department
Idaho National Engineering and Environmental Laboratory
P. O. Box 1625, Idaho Falls, ID 83415-3860
Phone: (208) 526-2760; Fax: (208) 526-4968; E-mail: goughd@inel.gov

GENERAL BACKGROUND

Dr. Gougar's research interests and experience meet in the fields of reactor physics and safety analysis. Gougar received a BS degree in physics from the University of Wisconsin and MS and Ph.D. degrees in Nuclear Engineering from Penn State University. At Penn State, Gougar conducted research in dynamics and multivariable control of the university's research reactor. His current research is in core neutronics and fuel management for high temperature gas reactors.

Other work at the INEEL includes reactor physics and managerial support for the Advanced Test Reactor (ATR). The ATR is a 250MW test reactor with unique neutronic and thermal-hydraulic characteristics. His responsibilities include core physics analysis in support of core safety. Gougar was recently named the Manager of the Fission and Fusion Systems Department of the Nuclear Science and Engineering Division of the INEEL.

Recent technical work includes the development the PEBBED computer code that models neutronics and fuel burnup for recirculating pebble-bed reactors. PEBBED is the first core physics and fuel management code to model pebble-bed reactors in three dimensions. In addition to writing the code, Gougar developed a unique pebble recirculation formulation that allows efficient modeling of virtually any recirculation pattern and then coupled this to a genetic algorithm for efficient pebble-bed reactor design optimization.

RELEVANT PUBLICATIONS

Gougar, H.D., "Development of Multivariable Control Capability of the Penn State Breazeale Reactor," A Master's Thesis in Nuclear Engineering, Pennsylvania State University, University Park, PA, May 1997.
H. D. Gougar, W. K. Terry, A. M. Ougouag, and C. B. Neill, "Matrix Formulation for Pebble Circulation in the PEBBED Code", Proceedings of the 1st International Topical Meeting on High Temperature eactor Technology, Petten, The Netherlands, April 22-24, 2002.
H. D. Gougar and A. M. Ougouag, "The Modular Pebble Bed Reactor as Power/Heat Supply for Remote Industrial Operations ", Proceedings of the Canadian Institute of Mining, Metallurgy, and Petroleum 2002 Conference, Vancouver, CAN, April 28-30, 2002.
GOUGAR, H. D., A. M. OUGOUAG, W. K. TERRY, and R. M. MOORE "*Conceptual Design of a Very High Temperature Pebble-bed Reactor*," , Transactions of Global 2003 Embedded ANS Topical Meeting, New Orleans, Nov. 20.